THÈSE / UNIVERSITÉ DE BRETAGNE OCCIDENTALE
sous le sceau de l'Université Bretagne Loire

pour obtenir le titre de
DOCTEUR DE L'UNIVERSITÉ DE BRETAGNE OCCIDENTALE
Mention : Géosciences Marines
École Doctorale des Sciences de la Mer

présentée par

Marta Payo Payo

Préparée à IFREMER, Unité Géosciences Marines, Laboratoire Environnement Sédimentaires

Modélisation du transport sédimentaire et des interactions morphodynamiques par les courants de turbidité dans les canyons sous-marins. Application à la Méditerranée Occidentale

Date de soutenance le 14 décembre 2016
devant le jury composé de :

Jaco H. BAAS
Université de Bangor, Royaume Uni /*Rapporteur*
Stefan M. LUTHI
Professeur, TUDelft, Pays Bas /*Rapporteur*
Nathalie BABONNEAU
Maitre de conférences, IUEM-UBO, Brest, France, / *Examinateur*
Florence CAYOCCA
Chef de service, AAMP / *Examinateur*
Robert LAFITE
Professeur, Université de Rouen / *Examinateur*
Nabil SULTAN
Chercheur, IFREMER, Brest /*Directeur de thèse*

Ricardo SILVA JACINTO
Chercheur, IFREMER, Brest /*Co-encadrant de thèse, invité*
Miquel CANALS
Professeur, Université de Barcelone / *Co-directeur de thèse, invité*
Marina RABINEAU
Chargé de Recherche CNRS, IUEM-UBO, Brest /*Co-encadrant, invité*

ABSTRACT

Turbidity currents in submarine canyons are the main contribution for sediment transfer across the continental margins. Geological studies of submarine canyons and associated turbiditic systems for more than 30 years led to an extraordinary breakthrough in the understanding of how turbidite systems evolve. However, these studies remain limited to *a posteriori* interpretations, based on the distribution of deposits and morphological evidences. The overarching aim of this thesis is to apply a 2DH process-based model to simulate large-scale turbidity currents on two different submarine canyons in the western Mediterranean coast.

The work in La Fonera canyon, in the Catalan margin, focuses on the modelling of sediment transport and accumulation resulting from trawling activities on the canyon flanks. The numerical process-based provides a 3D visualization of potential trawling impacts on sediment dynamics. The study represents a starting point for the assessment of the sedimentary impact of bottom trawling in deep continental margins. The present work can help in the identification of trawling areas with lesser impacts. The Var Sedimentary System, located in the vicinity of Nice (France), is connected to the Var River during both low and high-stands and it can be considered as a natural laboratory for the study of the climatic control on the turbiditic activity. The influence of Coriolis forces on the spatial evolution of the hyperpycnal flows and hence in the construction of the Var Sedimentary Ridge (VSR) is evidenced and supported for the first time.

The major drawback is the limited amount of information for the necessary initial and boundary conditions; hence modelling results might not be of predictive quality. However, modelling results provide a full-scale vision of the system allowing the identification of sediment pathways and deposition areas on the basis of physical processes and enlarge the present knowledge of the canyons studied. The results obtained may help in the identification of strategic mooring and coring sites to further advance the state of our knowledge on sediment dynamics of the different cases studies.

Keywords Coriolis forces, modelling, hydrodynamics, sedimentology, submarine canyons, trawling, turbidity current

RESUME

Les courants de turbidité dans les canyons sous-marins contribuent largement au transfert sédimentaire à travers des marges continentales. L'étude géologique des canyons sous-marins et des systèmes turbiditiques associés a permis des avancées fondamentales dans la compréhension de l'évolution des courants de turbidité. Ces études sont cependant limitées à des interprétations a posteriori, basées sur la répartition des dépôts et des évidences morphologiques. Cette thèse vise à l'application de la modélisation numérique des courants de turbidité, sur la base des processus physiques, à deux canyons sous-marins de la côte Méditerranée Occidentale.

Des courants de turbidité liés au chalutage de fond sont modélisés dans le canyon de La Fonera. Les résultats du modèle permettent de spatialiser ce transport; ainsi le modèle peut être un point de départ pour l'identification de zones de pêche au chalut avec un moindre impact.

L'absence d'un plateau continental au niveau de Nice a permis une alimentation continue du système turbiditique du Var indépendamment des variations du niveau marin. Ainsi ce système s'avère un laboratoire naturel pour l'étude du control climatique sur l'activité turbiditique. L'influence des forces de Coriolis dans l'évolution spatiale des courants de turbidité et dans la construction de la Ride sédimentaire du Var est modélisée et mise en évidence pour la première fois.

La modélisation numérique des courants de turbidité ne peut pas fournir à présent des résultats de qualité prédictive du fait de la quantité limitée d'information disponible pour établir les conditions initiales de l'écoulement qui impactent largement son évolution et dépôts. Malgré ce fait, la modélisation numérique permet d'élargir les interprétations du fonctionnement sédimentaire des canyons étudiés, d'identifier les chemins empruntés par les écoulements et leur dépôt final et de mieux préparer des cibles (mouillages et carottage) lors des campagnes à la mer.

Mots-clés canyons sous-marins, chalutage, courants de turbidité, forces de Coriolis, hydrodynamique, modélisation, sédimentologie

This work was supported by the Laboratoire d'Excellence‖ LabexMER and co-funded by a state grant from the French government through Agence Nationale de la Recherche (ANR) under the « Investissements d'Avenir » Programme, reference ANR-10-LABX-19-01, and by a grant from the Regional Council of Brittany. Additional support was also provided by Actions-Marges Program (Mediterranée Occidentale).

Remerciements, aknowledgements, agradecimientos.

Au terme de ces trois années, je tiens à exprimer ma gratitude à tous ceux qui ont rendu possible cette aventure. La navigation a été parfois houleuse mais toujours parsemée de belles rencontres professionnelles et amicales.

Tout d'abord, je voudrais te remercier Ricardo. Merci pour ta confiance mais aussi pour tout ce que tu m'as apporté tant du point de vue scientifique qu'humaine. Avec toi j'ai appris à repousser mes limites que sont bien plus loin que j'en avais cru. Merci aussi à toi Nabil, tu as toujours cru en moi et tu m'as toujours soutenu. Malgré tes nombreuses responsabilités tu as toujours été disponible pour de fructueuses discussions. Merci à vous deux d'avoir rassuré sur le cap à suivre quand le navire semblait chavirer. Merci Marina pour ton accueil dès mon arrivée et pour avoir toujours cru à ce projet de thèse. Moltes gràcies Miquel, por la acogida en Barcelona en la UB, por enseñarme a escribir *más grande* y por confiar en una ingeniera para una tesis de geología.

I would also like to thank my PhD committee: Jaco (Baas), Stefan (Luthi), Nathalie (Babonneau), Florence (Cayocca) and Robert (Lafite), for their healthy criticism and for their very constructive remarks. It was a real honour to defend my work in front of such a panel of experts and I really enjoyed the discussion that followed my presentation. I am particularly grateful to Jaco and Stefan for reviewing my thesis; your final reports were of great help to prepare the defence.

Je tiens également à remercier à Benoit (Waeles) et Nicolas (Le Dantec) d'avoir bien voulu être membres de mon comité de suivi de thèse et d'avoir suivi mes travaux au cours de ces trois dernières années. Merci pour votre aide et vos précieux conseils.

Arantza et Roland, vous êtes à l'origine de cette aventure française. Merci à Xavier (Bertin), mon parcours académique française a commencé à tes cotés au LIENNs. Merci à toi et aussi à toi Benoit, de m'avoir en parlé et encouragé à faire cette thèse.

Je voudrais remercier les membres del'unité « Geosciences Marines », et de l'UMR-6538 « Domaines Oceaniques », vous avez contribué à mes réflexions, mes galères et mes bons moments. Merci aussi au bureau de l'EDSM. Merci à Sylvia (Baronne), Corinne (Tarditi), Corinne (Floch-Laizet), Aurelie (François) et Elisabeth (Bondu) pour leur disponibilité et leur accueil dans les belles galères administratives.

Au cours de ces trois ans, j'ai eu la chance de pouvoir collaborer avec des chercheurs que m'ont beaucoup apporté et qui ont contribué à ma construction scientifique : Galderic (Lastras), Pere (Puig), Jacobo (Martin), Anna (Sanchez-Vidal), Lucille (Bonneau), Marie (Mauffrey) et Serge (Berné). Merci Serge et Maria-Angela pour votre accueil à Perpignan au CEFREM.

J'ai également eu la chance d'embarquer sur le Pourquoi Pas ? J'y ai beaucoup appris et je m'y suis très bien sentie. Merci à Vincent (Riboulot), tu m'as permis de participer à cette aventure à bord, merci encore ! Merci à Gwendoline (Gregoire) pour m'amener en merveilleuse balade en la Rade de Brest !

Merci aux thésards, post-docs et autres jeunes du GM et de l'IUEM mais aussi ceux en dehors des labos, vous avez été source de motivation et de détente et vous avez devenus excellents amis. Vous êtes si nombreux ! Merci à Olafur, Ludovico et Nils pour leur compagnie ces derniers mois. Merci à Marie, ton Barado a été refuge. Merci à mes copains d'ici et d'ailleurs, vous avez été bouée de sauvetage : merci Camille, Matthieu, Flo, Momo, Luc, Flo, Alice…Obrigada Caio e Mariana e até já ! Gracias Nis, Silvix, Noe, Vio, Arantza, Roland, Yanira, Chris… gracias por seguirme, aunque estemos lejos, y por estar ahí. Os echo de menos.

Gracias a mis Payitos. Somos casa, somos mucho más que cuatro. Gracias por la calma, por la crítica, por el reprís, por las ganas, por el tesón, por la chispa, por la curiosidad. Gracias por hacerme valiente y por cuidarme.

Gracias E, ¡tantas! Gracias por estar a mi lado y por hacerme grande. Thanks for making me smile and for keeping me sane. Thanks for all those *todo irá bien* and all those *worse things happen at sea*. Thanks for helping me fight my demons and for preventing me from sabotaging myself. El viaje empieza ahora.

TABLE OF CONTENTS

Introduction (English) :

THESIS INTRODUCTION

1. General background

Sediment gravity flows are mixtures of sediment and fluid that flow down a slope due to gravity forces acting on sediment grains (Middleton and Hampton, 1973). They drive the sediment transport in many parts of the deep ocean, freshwater lakes and reservoirs. On land, river systems are responsible for the transport of the majority of sediment from mountain ranges to the coastal line. In the ocean, turbidity currents, a particular type of the continuum of sediment gravity flows containing a relative low proportion of fine-grained sediment, are the most important process moving sediment from shallow areas to the deep ocean (Piper and Normark, 2009). Preferential pathways of turbidity currents are the deep incisions on the continental slope, the submarine canyons. Continuous turbidity current activity over geological time scales results in the largest sediment accumulations on our planet, the submarine fans. Since these deposits have been described in numerous locations worldwide, one might think that these flows are well understood. However, despite the large body of research on flow behaviour, the relationship between initiation processes, flow evolution and final deposit is still sometimes difficult to establish (Piper and Normark, 2009; Talling et al., 2012). Turbidity currents are generally unpredictable, often catastrophic, rare at observational scales and happen in relatively inaccessible environments. Measurements of marine turbidity currents are scarce, highly localised and usually biased towards shallow environments and frequent flows and are yet to be obtained for flows that reach and build submarine fans (Talling et al., 2013). As such there is still debate about the internal structure of turbidity currents, their interaction with underlying bedforms and the initiation processes and type of flows that produce the different types of seabed deposits.

2. Turbidity currents in submarine canyons in the Mediterranean

The Mediterranean Sea is a “hotspot” for canyons due to its geological history, the tectonics, and the sediments from rivers (Canals et al., 2013). A unique feature of the Mediterranean Sea is its desiccation and sea lowering during the late Miocene “Messinian Salinity Crisis” (Hsü, 1972; Hsü et al., 1977). The subaerial exposition and erosion of the continental margin during this period would have favoured the incision of the margin by rivers and the development of canyons (Lofi et al., 2005). Tectonic uplifting and margin progradation have masked and modified some of the canyons formed during the late Miocene (Bertoni and Cartwright, 2005; Ridente et al., 2007).

The oceanographic conditions of the Mediterranean are partly due to its semienclosed character: tides are very limited due to the narrow connection with the Atlantic Ocean and the water column is stratified in three different water masses in its western part. The Atlantic Water (AW) is the fresher water mass, covering the first 100-200m of the water column, that enters through the Strait of Gibraltar (Millot and Taupier-Letage, 2005). The Levantine Intermediate Water (LIW) is formed due to strong winter evaporation and lies between 200 and 600-1000 m. The Western Mediterranean Deep Water (WMDW) is formed due to strong surface cooling and evaporation due to cold and dry westerlies over the Gulf of Lions and occupies the deeper layers of the western Mediterranean Sea (MEDOC GROUP, 1970). The stratification of the water column has been shown to be more intense during sea level low-stands than during sea level high-stands (Cacho et al., 2000). Both limited tide and stratification of the water column ease the modelling of turbidity currents since processes such as internal waves can be omitted.

The study cases examined in this thesis (Fig. 0.1) are geographically close; however, the timescales and forcing mechanisms are different in each case. The relatively small spatial scales allow the modelling of the whole system in each case. As such each one of the cases can be considered as a

natural laboratory for its triggering mechanism. La Fonera submarine canyon, located in the Catalan margin between Barcelona and the French-Spanish border is a representative case of contemporary turbidity currents due to the anthropic action of trawling. The Var Sedimentary System, located in the vicinity of Nice (France), due to its continuous connection to the Var River during low and high-stands allows the study of the climatic control of hyperpycnal flows.

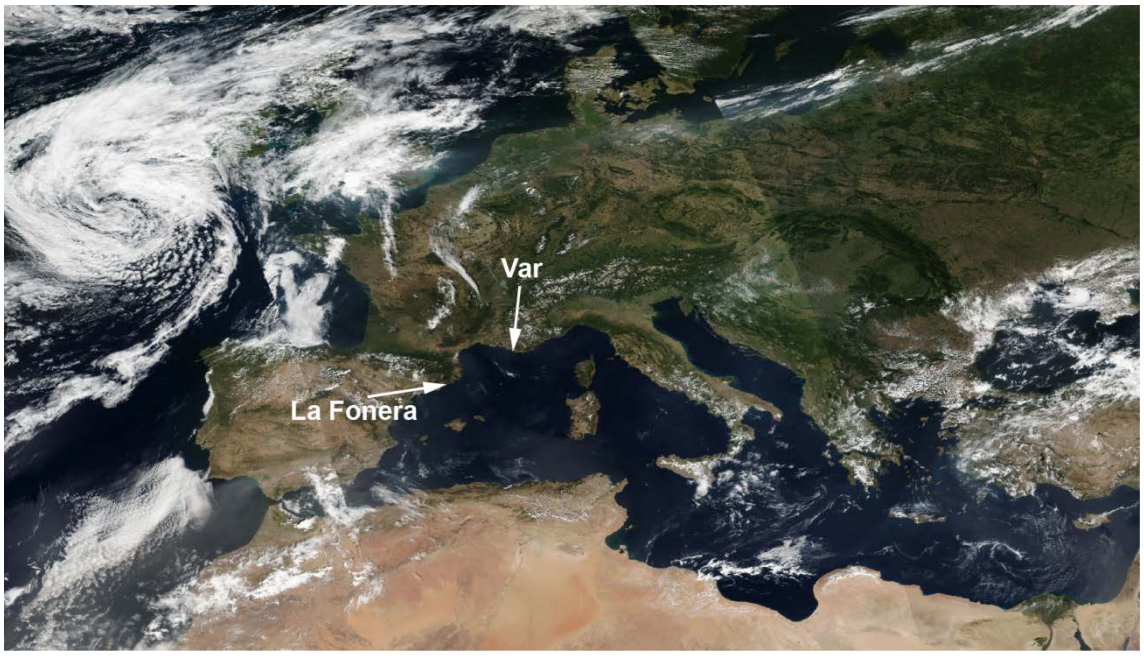

FIGURE 0. 1 SATELLITE IMAGE (27TH AUGUST 2016, WGS84) OF THE MEDITERRANEAN SEA FROM HTTPS://WORLDVIEW.EARTHDATA.NASA.GOV/.. THE FIGURE SHOWS THE LOCATION OF THE TWO CANYONS STUDIED IN THE PRESENT THESIS : LA FONERA SUBMARINE CANYON AND THE VAR SEDIMENTARY SYSTEM

3. Implications and relevance of turbidity currents

In addition to their importance in sediment transfer and in paleoclimate studies, turbidity currents have societal and economic relevance. In terrestrial systems, turbidity currents are responsible for much of the sedimentation in reservoirs and lakes and the consequent loss of water storage capacity (e.g. Cesare et al., 2001). In the deep ocean ancient deposits of turbidity currents such as submarine sandy fans form important hydrocarbon reservoirs (e.g. Stow and Mayall, 2000). Turbidity currents are a potential hazard for seafloor infrastructure such as oilfield pipelines and communication cables (e.g. Heezen and Ewing, 1952; Gennesseaux et al., 1980; Hsu et al., 2008; Cattaneo et al., 2012). Submarine cables that carry 95% of international data and voice traffic lie across the path of turbidity currents and are often interrupted by their passage (Carter et al., 2009). A better knowledge of these flows could help improve hazard assessment and mitigation for strategic deep-sea structures.

In order to understand the impact of these flows, it is also important to understand their potential to recur. Turbidite deposits provide a record for the frequency of triggering mechanisms such as hyperpycnal flows (e.g. Mulder et al., 2001; Bonneau et al., 2014), earthquakes (e.g. Goldfinger, 2010; Cattaneo et al., 2012; Ratzov et al., 2015), submarine landslides and tsunamis (e.g. Wynn and Masson, 2003; Hunt et al., 2011). A better understanding of turbidity currents can help in the determination of these potential hazards since to date there is no widespread and simple relationship between initiating process and type of deposit (Piper and Normark, 2009; Talling, 2014).

Turbidity currents funnel large quantities of sediment and organic matter to the deep where organic carbon it is partly consumed and buried (e.g. Canals et al., 2006; Sanchez-Vidal et al., 2012; Sparkes et al., 2015). They play a significant role in the supply of organic matter to deep-sea ecosystems and they modulate organic carbon burial and hence potentially pCO_2 levels in the atmosphere (Galy et al., 2007). In the context of increased liberation of CO_2 to the atmosphere and man-induced climate change, a better comprehension of turbidity current processes can also contribute to the quantification of this sequestration and its importance in the global carbon cycle.

For these reasons, a better understanding of turbidity currents is not only of scientific interest but also of societal relevance.

4. Numerical modelling approach

Much of the present knowledge on turbidity currents comes from their preserved deposits (e.g. Bouma, 1962). Triggering mechanisms, flow evolution and deceleration were primarily inferred from observations on the resulting deposits because in most cases the only information available from a submarine flow is its deposit. Laboratory-scale experiments and numerical modelling have provided insight into both the internal structure of turbidity currents and the characteristics of the deposits associated to a given type of flow (e.g. Kuenen, 1937; Felix, 2002; Baas et al., 2011).

The hydrodynamics of TC are difficult to study in natural environments and the data available is still scarce. Laboratory experiments are time consuming and measurement of flow properties and relationships between flow structure and transport and deposition remain difficult to establish. Numerical modelling can cope with some of the limitations of field data and experimental modelling; nonetheless the three different approaches are complementary and form an interlinked feedback system. Process-based models are preferred since they provide insight into the underlying physics of the phenomena. Today large scale computational power is available at low cost and advances in numerical methods and mathematical algorithms produce accurate solutions for physical problems. These improvements have led to the development of more complex dynamic models. Turbidity currents (like all other Earth Science processes) are multi-scale both in time and space; small scale mechanisms that are not yet well understood (i.e. erosion and resuspension) determine the large scale evolution of the flow. Numerical models are used with a wide range of purposes focused on different scales, from prediction of turbidite geometries and grain-size distribution (2DH models) to modelling of the vertical structure of turbulence (depth solving model). The choice of model to simulate a certain flow should be based on the scales of the processes to be simulated.

In the present thesis, Nixes-TC (Jacinto and Burel, 2003), a numerical process-based model developed to reproduce underwater sediment-laden flows, is applied to a set of Mediterranean canyons. The model simulates the spatial development of an unsteady TC flowing in deep ambient fluid and provides the deposition pattern produced by the simulated TC. The equations of the model are the depth integrated fluid, momentum and sediment conservation equations. The vertical scales of the current are not resolved but 2DH models can produce relatively accurate predictions of current evolution and deposit characteristics (Kneller and Buckee, 2000). Process based models are a useful tool to simulate hypotheses in turbidity systems, allowing the comprehension of the physics involved. They can bridge the gap between the large time scales of stratigraphy models and short time scales of hydrodynamic models with affordable computer resources.

5. Overarching thesis aim and thesis outline

Modelling can complete and enlarge current interpretations of the sedimentary functioning of the canyons studied since present knowledge is based on snapshots of field data limited in time and space. The overarching aim is to apply a 2DH process-based model to simulate large-scale turbidity currents of real-life modern and ancient turbiditic systems in an attempt to bridge the gap between short time scale hydrodynamic models and large time scale stratigraphic models. To do so, first we need to assess the reliability of large-scale simulations to reproduce sediment transport and deposition of real-life scenarios by comparing the model results with field observations. If the results are accurate enough, we can enlarge our current understanding of the systems. To achieve the main objective, **concrete questions are drawn up for the two study cases**: 1) **La Fonera**: Can we model turbidity currents on the basis of Vessel Monitoring System? What are the turbidity pathways and sedimentation patterns due to trawling-induced turbidity currents? How can this study help to define areas of bottom trawling less destructive and more environment friendly? 2) **The Var**: How are hyperpycnal flows triggered, and do they have a climatic control? Do Coriolis forces play a significant role in the construction of the Var Sedimentary Ridge? The two canyons present contrasting triggering mechanisms and time scales. In addition to these, the data available in each canyon differs: in La Fonera the source is known whilst the information available on the deposits is limited. On the contrary, in the Var, the deposit is largely known but information on the source is lacking.

The document is structured in 4 main chapters (Chapters 1 to 4) that are coherent and complete separately. **Chapter 1** provides an overview on submarine canyons and sediment gravity flows. It is a synthesis of background knowledge of the genesis and evolution of submarine canyons and the role that turbidity currents play in these environments. The second part of the chapter deals with the different types of sediment gravity flows, and the related controversies, and focuses on the physical processes that underlie the propagation of turbidity currents and the final result deposition. The numerical model implemented throughout this thesis is presented in **Chapter 2**. Prior to the discussion of the model from a physical and mathematical point of view, commonly used research methods and approaches to modelling turbidity currents and sediment transport are presented. Models aim to reproduce reality as accurate as possible, in the present thesis two real scenarios are evaluated and the model results are compared to field evidence. The two first canyons are explored in detail in their respective chapters. The present day turbidity currents triggered due to trawling activity in La Fonera canyon are presented in **Chapter 3**. This chapter is accepted in Marine Geology with the same title and was presented at several French and international conferences. Hyperpycnal flows at different climatic periods and the influence of Coriolis effects on these flows and in the construction of the Var Sedimentary Ridge are investigated in **Chapter 4**. Finally **Chapter 5** summarizes the conclusions of this thesis, discusses possible improvements and provides an outlook for future work. Each one of the chapters closes with a list of literature references.

References

Baas, J.H., Best, J.L., Peakall, J., 2011. Depositional processes, bedform development and hybrid bed formation in rapidly decelerated cohesive (mud–sand) sediment flows. Sedimentology 58, 1953–1987. doi:10.1111/j.1365-3091.2011.01247.x

Bonneau, L., Jorry, S.J., Toucanne, S., Jacinto, R.S., Emmanuel, L., 2014. Millennial-Scale Response of a Western Mediterranean River to Late Quaternary Climate Changes: A View from the Deep Sea. J. Geol. 122, 687–703. doi:10.1086/677844

Bouma, A.H., 1962. Sedimentology of Some Flysch Deposits. A Graphic Approach to Facies Interpretation. Amsterdam, Elsevier.

Cacho, I., Grimalt, J.O., Sierro, F.J., Shackleton, N., Canals, M., 2000. Evidence for enhanced Mediterranean thermohaline circulation during rapid climatic coolings. Earth Planet. Sci. Lett. 183, 417–429. doi:10.1016/S0012-821X(00)00296-X

Canals, M., Puig, P., de Madron, X.D., Heussner, S., Palanques, A., Fabres, J., 2006. Flushing submarine canyons. Nature 444, 354–357. doi:10.1038/nature05271

Canals, M., Company, J.B., Martín, D., Sànchez-Vidal, A., Ramírez-Llodrà, E., 2013. Integrated study of Mediterranean deep canyons: Novel results and future challenges. Prog. Oceanogr., Integrated study of a deep submarine canyon and adjacent open slopes in the Western Mediterranean Sea: an essential habitat 118, 1–27. doi:10.1016/j.pocean.2013.09.004

Carter, L., Burnett, D., Drew, S., Hagadorn, L., Marle, G., Bartlett-McNeil, D., Irvine, N., 2009. Submarine Cables and the Oceans: Connecting the World. The United Nations Environment Programme World Conservation Monitoring Centre Biodiversity Series (No. 31). ICPC/UNEP/UNEP-WCMCWCMC.

Cattaneo, A., Babonneau, N., Ratzov, G., Dan-Unterseh, G., Yelles, K., Bracène, R., Mercier de Lépinay, B., Boudiaf, A., Déverchère, J., 2012. Searching for the seafloor signature of the 21 May 2003 Boumerdès earthquake offshore central Algeria. Nat Hazards Earth Syst Sci 12, 2159–2172. doi:10.5194/nhess-12-2159-2012

Cesare, G., Schleiss, A., Hermann, F., 2001. Impact of Turbidity Currents on Reservoir Sedimentation. J. Hydraul. Eng. 127, 6–16. doi:10.1061/(ASCE)0733-9429(2001)127:1(6)

Felix, M., 2002. Flow structure of turbidity currents. Sedimentology 49, 397–419. doi:10.1046/j.1365-3091.2002.00449.x

Galy, V., France-Lanord, C., Beyssac, O., Faure, P., Kudrass, H., Palhol, F., 2007. Efficient organic carbon burial in the Bengal fan sustained by the Himalayan erosional system. Nature 450, 407–410. doi:10.1038/nature06273

Gennesseaux, M., Mauffret, A., Pautot, G., 1980. Les glissements sous-marins de la pente continentale niçoise et la rupture des câbles en mer Ligure (Méditerranée occidentale). C R Acad Sci Paris Série D, 959–962.

Goldfinger, C., 2010. Submarine Paleoseismology Based on Turbidite Records. Annu. Rev. Mar. Sci. 3, 35–66. doi:10.1146/annurev-marine-120709-142852

Heezen, B.., Ewing, M., 1952. Turbidity currents and submarine slumps, and the 1929 Grand Banks earthquake. Am. J. Sci. 250, 849–873.

Hsu, S.-K., Kuo, J., Lo, C.-L., Tsai, C.-H., Doo, W.-B., Ku, C.-Y., Sibuet, J.-C., 2008. Turbidity Currents, Submarine Landslides and the 2006 Pingtung Earthquake off SW Taiwan. Terr. Atmospheric Ocean. Sci. 19, 767. doi:10.3319/TAO.2008.19.6.767(PT)

Hunt, J.E., Wynn, R.B., Masson, D.G., Talling, P.J., Teagle, D.A.H., 2011. Sedimentological and geochemical evidence for multistage failure of volcanic island landslides: A case study from Icod landslide on north Tenerife, Canary Islands. Geochem. Geophys. Geosystems 12, Q12007. doi:10.1029/2011GC003740

Jacinto, R.S., Burel, D., 2003. Modélisation du devenir à court terme des boues de dragage rejetées par clapage. Rev. Fr. Génie Civ. 7, 1151–1166. doi:10.1080/12795119.2003.9692539

Kuenen, P.H., 1937. Experiments in connection with Daly's hypothesis on the formation of submarine canyons. Leidse Geol Meded 8, 327–335.

MEDOC GROUP, 1970. Observation of Formation of Deep Water in the Mediterranean Sea, 1969. Nature 227, 1037–1040. doi:10.1038/2271037a0

Middleton, G.V., Hampton, M.A., 1973. Part I. Sediment Gravity Flows: Mechanics of Flow and Deposition 1–38.

Millot, C., Taupier-Letage, I., 2005. Circulation in the Mediterranean Sea, in: Saliot, A. (Ed.), The Mediterranean Sea, Handbook of Environmental Chemistry. Springer Berlin Heidelberg, pp. 29–66.

Mulder, T., Migeon, S., Savoye, B., Faugères, J.-C., 2001. Inversely graded turbidite sequences in the deep Mediterranean: a record of deposits from flood-generated turbidity currents? Geo-Mar. Lett. 21, 86–93. doi:10.1007/s003670100071

Piper, D.J.W., Normark, W.R., 2009. Processes That Initiate Turbidity Currents and Their Influence on Turbidites: A Marine Geology Perspective. J. Sediment. Res. 79, 347–362. doi:10.2110/jsr.2009.046

Ratzov, G., Cattaneo, A., Babonneau, N., Déverchère, J., Yelles, K., Bracene, R., Courboulex, F., 2015. Holocene turbidites record earthquake supercycles at a slow-rate plate boundary. Geology 43, 331–334. doi:10.1130/G36170.1

Sanchez-Vidal, A., Canals, M., Calafat, A.M., Lastras, G., Pedrosa-Pàmies, R., Menéndez, M., Medina, R., Company, J.B., Hereu, B., Romero, J., Alcoverro, T., 2012. Impacts on the Deep-Sea Ecosystem by a Severe Coastal Storm. PLoS ONE 7, e30395. doi:10.1371/journal.pone.0030395

Sparkes, R.B., Lin, I.-T., Hovius, N., Galy, A., Liu, J.T., Xu, X., Yang, R., 2015. Redistribution of multi-phase particulate organic carbon in a marine shelf and canyon system during an exceptional river flood: Effects of Typhoon Morakot on the Gaoping River–Canyon system. Mar. Geol. 363, 191–201. doi:10.1016/j.margeo.2015.02.013

Stow, D.A.V., Mayall, M., 2000. Deep-water sedimentary systems: New models for the 21st century. Mar. Pet. Geol. 17, 125–135. doi:10.1016/S0264-8172(99)00064-1

Talling, P.J., Masson, D.G., Sumner, E.J., Malgesini, G., 2012. Subaqueous sediment density flows: Depositional processes and deposit types. Sedimentology 59, 1937–2003. doi:10.1111/j.1365-3091.2012.01353.x

Talling, P.J., Paull, C.K., Piper, D.J.W., 2013. How are subaqueous sediment density flows triggered, what is their internal structure and how does it evolve? Direct observations from monitoring of active flows. Earth-Sci. Rev. 125, 244–287. doi:10.1016/j.earscirev.2013.07.005

Talling, P.J., 2014. On the triggers, resulting flow types and frequencies of subaqueous sediment density flows in different settings. Mar. Geol., 50th Anniversary Special Issue 352, 155–182. doi:10.1016/j.margeo.2014.02.006

Wynn, R.B., Masson, D.G., 2003. Canary Islands Landslides and Tsunami Generation: Can We Use Turbidite Deposits to Interpret Landslide Processes?, in: Locat, J., Mienert, J., Boisvert, L. (Eds.), Submarine Mass Movements and Their Consequences, Advances in Natural and Technological Hazards Research. Springer Netherlands, pp. 325–332.

Introduction (Français) :

INTRODUCTION GENERALE

1. Contexte général

Les écoulements gravitaires sont des processus de transport sédimentaire le long des pentes régis principalement par la gravité (Middleton and Hampton, 1973). Ils jouent un rôle important dans le transport sédimentaire dans l'océan profond, dans les lacs mais aussi dans la formation des réservoirs. Sur terre, les rivières sont responsables du transport de la majorité des sédiments depuis les chaînes de montagnes jusqu'à la côte. En milieu marin, les courants de turbidité, un type d'écoulement gravitaire caractérisé par une concentration de sédiments relativement faible, sont les premiers convoyeurs de sédiments depuis les zones peu profondes vers le domaine profond (Piper and Normark, 2009). Les canyons sous-marins ne sont que des incisions dans le talus continental et constituent des chemins préférentiels des courants de turbidité. L'activité des courants de turbidité, sur des échelles de temps géologiques, est à l'origine des accumulations de sédiments les plus importantes sur les marges continentales, et plus précisément sur les lobes distaux, partie distale des systèmes turbiditiques. Les nombreuses descriptions de ces dépôts dans différentes parties du monde suggèrent que ce type d'écoulements est bien compris. Cependant, malgré les nombreuses études menées à ce sujet, il est toujours difficile d'établir des relations entre les mécanismes de déclenchement, l'évolution du courant et le dépôt final (Piper and Normark, 2009 ; Talling et al., 2012). Les courants de turbidité se définissent comme généralement imprévisibles, fréquemment destructeurs, rares à des échelles du temps de l'observation et se produisent dans des environnements inaccessibles dans la plupart des cas. Les mesures de courants de turbidité marines sont éparses, très localisées et tendent à privilégier les domaines peu profonds et les flux les plus fréquents. En effet des écoulements pouvant contribuer à la construction des lobes distaux n'ont jamais été mesurés (Talling et al., 2013). C'est pourquoi il existe toujours une controverse sur la structure interne des courants de turbidité, leurs interactions avec les formes du fond marin ainsi que sur la relation entre les mécanismes de déclenchement du processus et le type d'écoulement qui produit différents types de dépôts.

2. Les courants de turbidité dans les canyons sous-marins de la Méditerranée.

La mer Méditerranée présente une densité élevée de canyons sous-marins, de par son passé géologique marqué par une tectonique active et grâce à l'apport sédimentaire provenant des rivières (Canals et al., 2013). Une caractéristique unique de la mer Méditerranée est sa dessiccation et la baisse du niveau de la mer au cours de la Crise de salinité Messinienne du Miocène supérieur (Hsü, 1972; Hsü et al., 1977). L'exposition et l'érosion subaériennes de la marge continentale pendant cette période ont pu favoriser l'incision des marges par des fleuves et le développement des canyons (Lofi et al. 2005). Le soulèvement tectonique et la progradation de la marge ont masqué et modifié certains des canyons formés pendant le Miocène supérieur (Bertoni and Cartwright, 2005; Ridente et al., 2007).

Les conditions océanographiques de la mer Méditerranée sont en partie expliquées du fait qu'il s'agisse d'un basin semi-fermé ; ainsi la marée est réduite à cause de l'étroite connexion avec l'océan Atlantique et la colonne d'eau est stratifiée en trois masses d'eau différentes dans sa partie occidentale. La masse d'eau « *Atlantic Water* » (AW) occupe les premiers 100-200 m de la colonne d'eau, il s'agit des eaux plus douces qui entrent en Méditerranée par le détroit de Gibraltar (Millot and Taupier-Letage, 2005). La masse « *Levantine Intermediate Water* » (LIW) est formée par une forte évaporation hivernale et occupe des profondeurs de 200 à 600-1000m. La masse d'eau

« *Western Mediterranean Deep Water* » (WMDW) est formée par des processus de refroidissement et d'évaporation en surface liés aux vents d'Ouest froids et secs sur le Golfe de Lion et occupe la partie plus profonde du bassin (MEDOC GROUP, 1970). La stratification de la colonne d'eau est plus importante pendant les périodes de haut niveau marin que pendant les périodes de bas niveau marin (Cacho et al., 2000). Ces deux caractéristiques, une marée limitée et une stratification de la colonne d'eau, facilitent la modélisation des courants de turbidité dans la mesure où des processus associés tels que les ondes internes y sont négligeables.

Dans cette thèse, nous nous sommes intéressés à deux canyons qui malgré leur proximité géographique, présentent des échelles temporelles de fonctionnement et des mécanismes de déclenchement différents. Les échelles spatiales très restreintes permettent la modélisation de l'ensemble du système dans chaque cas. Ainsi chacun des canyons peut être considéré comme un laboratoire naturel d'étude du fonctionnement associé à son mécanisme de déclenchement des courants de turbidité. Le canyon sous-marin La Fonera, dans la marge Catalane, à mi-chemin entre Barcelone et la frontière française, est un cas représentatif de l'activité turbiditique liée à la pêche au chalut. L'absence d'un plateau continental au niveau de Nice a permis une alimentation continue du système turbiditique du Var indépendamment des variations de la mer. Ainsi ce système s'avère être un laboratoire naturel pour l'étude du contrôle climatique sur l'activité turbiditique.

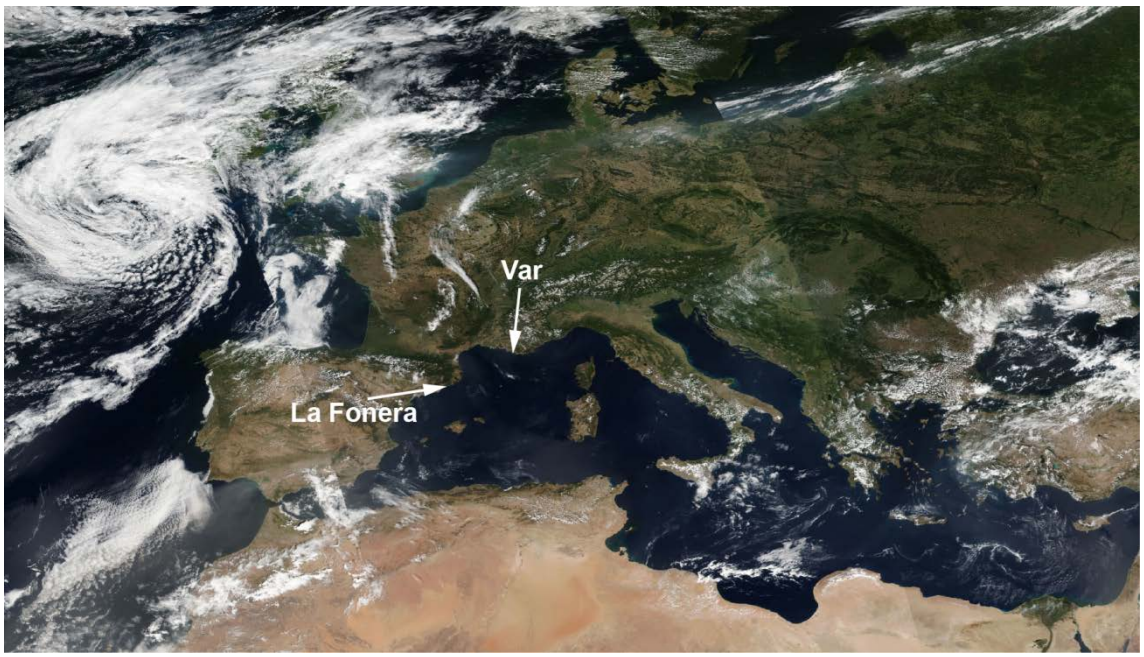

FIGURE 0. 2 IMAGE SATELLITE DE LA MEDITERRANEE (27 AOUT 2016, WGS84) SOURCE HTTPS://WORLDVIEW.EARTHDATA.NASA.GOV/). L'IMAGE MONTRE LA LOCALISATION DES DEUX CANYONS ETUDIES : LA FONERA ET LE VAR.

3. Implications et importance des courants de turbidité

Outre leur importance dans le transfert des sédiments et dans les études paléoclimatiques, les courants de turbidités présentent un intérêt sur le plan social et économique. Sur le continent, les courants de turbidité sont responsables de la sédimentation dans les réservoirs et les lacs et de la perte induite de capacité de stockage d'eau (e.g. Cesare et al., 2001). En eaux profondes, les dépôts turbiditiques anciens forment d'importants réservoirs d'hydrocarbures (e.g. Stow and Mayall, 2000). Les courants de turbidité représentent un danger potentiel pour les infrastructures posées sur le fond marin telles que les gazoducs et oléoducs ou les câbles sous-marins (e.g. Heezen and Ewing, 1952; Gennesseaux et al., 1980; Hsu et al., 2008; Cattaneo et al., 2012). Les 95% des liaisons

internationales du trafic téléphonique et des données sont garantis par des câbles sous-marins traversés par des courants de turbidité qui peuvent interrompre ces liaisons suite à leur passage (Carter et al., 2009). Une meilleure compréhension des courants de turbidité pourra aider à améliorer la caractérisation des risques auxquels les infrastructures sous-marines stratégiques peuvent être confrontées.

Afin de mieux comprendre l'impact de ces écoulements, il est aussi important de comprendre leur possibilité de se reproduire. Les turbidites enregistrent les périodes de récurrence de leur mécanisme déclencheur : courants hyperpycnaux (e.g. Mulder et al., 2001; Bonneau et al., 2014), tremblements de terre (e.g. Goldfinger, 2010; Cattaneo et al., 2012; Ratzov et al., 2015), glissements sous-marins et tsunamis (e.g. Wynn and Masson, 2003; Hunt et al., 2011). Une meilleure compréhension des courants de turbidité peut améliorer l'identification de ces dangers potentiels car aujourd'hui il n'existe aucune relation simple et généralisée qui relie le mécanisme déclencheur et le type de dépôt (Piper and Normark, 2009; Talling, 2014).

Les courants de turbidité acheminent d'importantes quantités de sédiments et de matière organique vers le milieu marin profond où le carbone organique est partiellement consommé et enfoui (e.g. Canals et al., 2006; Sanchez-Vidal et al., 2012; Sparkes et al., 2015). Ainsi les courants de turbidité jouent un rôle majeur dans le transfert de matière organique vers les écosystèmes du milieu marin profond et dans la modulation du taux d'enfouissement du carbone et par conséquent potentiellement dans les niveaux de CO_2 dans l'atmosphère (Galy et al., 2007). Dans le contexte actuel de l'augmentation des émissions atmosphériques de CO_2 et du changement climatique d'origine anthropique, l'amélioration des connaissances des processus des courants de turbidité peut contribuer à la quantification de son taux d'enfouissement et à la détermination de l'importance de cet enfouissement dans le cycle global du carbone.

C'est pourquoi la compréhension des courants de turbidité n'est pas seulement d'un intérêt scientifique mais elle est aussi d'un intérêt économique et sociétal.

4. Méthode de modélisation numérique

L'étude géologique des canyons sous-marins et des systèmes turbiditiques est fondamentalement limitée à des interprétations *a posteriori,* basées sur la répartition des dépôts (par carottages et sismiques) et à des mises en évidence morphologiques (accumulations et zones d'érosion) qui ont permis de déduire les mécanismes déclenchant ainsi que l'évolution et la décélération de l'écoulement. Les modèles analogiques et numériques ont largement contribué à approfondir les connaissances sur la structure interne des courants et les caractéristiques des dépôts associés à chaque type d'écoulement (e.g. Kuenen, 1937; Felix, 2002; Baas et al., 2011).

L'hydrodynamique des TC est difficile à étudier dans leur milieu naturel et les observations directes sont rares et très localisées géographiquement. Les modèles analogiques sont chronophages et les mesure des propriétés de l'écoulement et les relations entre le type d'écoulement et son dépôt sont difficiles à établir. Les modèles numériques permettent de s'affranchir de certaines limitations des données terrain et des modèles analogiques. Cependant, les trois approches utilisées pour étudier les courants de turbidité (i.e. données terrain, modèles analogiques et modélisation numérique) sont complémentaires et forment un système imbriqué et interconnecté. Les modèles basés sur des processus physiques sont plus précis puisqu'ils permettent de mieux comprendre les mécanismes physiques. Aujourd'hui des ordinateurs de grande puissance sont disponibles à des prix abordables et les progrès réalisés dans les méthodes numériques et les algorithmes mathématiques produisent des solutions précises pour des problèmes physiques. Ces améliorations ont permis le développement de modèles dynamiques de plus en plus complexes. Les courants de turbidité, en tant que processus de Sciences de la Terre, sont multi-échelles, à la fois dans le temps et dans l'espace. Les mécanismes des

plus petites échelles, qui ne sont pas encore bien compris (i.e. érosion et resuspension), déterminent largement les plus grandes échelles de l'écoulement. Les modèles numériques sont utilisés à des fins très diverses, en se focalisant sur des échelles différentes, de la prédiction de la géométrie des dépôts et la distribution granulométrique dans le cas des modèles 2DH, à la modélisation de la structure verticale de la turbulence dans le cas des modèles que résolvent la verticale. Le choix de l'outil de simulation numérique d'un certain écoulement doit être régi par l'échelle des processus à simuler.

Cette thèse vise à l'application du modèle numérique de processus Nixes-TC (Jacinto and Burel, 2003), afin de modéliser des courants de turbidité dans deux canyons sous-marins de la Méditerranée occidentale. Le modèle permet de simuler l'évolution spatiale et temporelle de l'écoulement ainsi que son dépôt final. Les équations à la base du modèle sont celles de conservation de la quantité de sédiments, de fluide et de mouvement. Les échelles verticales ne sont pas résolues mais les modèles 2DH fournissent des résultats réalistes en termes d'évolution de l'écoulement et des dépôts associés (Kneller and Buckee, 2000). Les modèles de processus sont d'une grande utilité dans la mesure dont ils permettent de confronter des hypothèses de fonctionnement tout en prenant en compte les processus physiques. Ce type de modèle peut combler le fossé entre les modèles stratigraphiques qui s'intéressent aux échelles de temps géologiques et les modèles hydrodynamiques qui s'intéressent aux courtes échelles de temps tout en mobilisant des moyens raisonnables en temps de calcul et en mémoire.

5. Objectifs principaux et organisation du manuscrit

La modélisation numérique permet de compléter et d'étendre les interprétations du fonctionnement sédimentaire des canyons étudiés basées sur des données éparses limitées à un cadre spatio-temporel précis. L'objectif principal de ce travail est d'appliquer un modèle 2DH basé sur des processus afin de simuler des courants de turbidité dans des systèmes actuels ou anciens et de combler le fossé entre les modèles hydrodynamiques (i.e. courtes échelles de temps) et les modèles stratigraphiques (i.e. longues échelles de temps). Afin d'évaluer la capacité du modèle à reproduire des écoulements réels, les résultats de modélisation sont comparés aux données de terrain disponibles. Si les résultats du modèle sont satisfaisants, ils peuvent contribuer à l'amélioration des connaissances du système. Pour répondre à l'objectif principal, des questions précises sont étudiées pour chacun des canyons :

1) **La Fonera et les questions associées** : a) Les courants de turbidité peuvent-il être modélisés sur la base des données du « Vessel Monitoring System » ? b) Quels sont les chemins préférentiels ainsi que les zones de dépôt des courants de turbidité liés au chalutage ? et c) Comment cette étude peut-elle aider à définir des zones de pêche au chalut avec un moindre impact ?

2) **Le Var et les questions associées :** a) Comment sont déclenchés les courants hyperpycnaux et ont-ils un contrôle climatique ? et b) Les forces de Coriolis jouent-elles un rôle important dans la construction de la Ride Sédimentaire du Var ?

Les deux canyons sont proches géographiquement mais ils présentent des forçages et des échelles temporelles différentes. Le type de données disponibles diffère aussi dans les deux cas. Pour La Fonera l'information disponible est celle relative à la source, tandis que l'impact des courants et leurs dépôts associés sont méconnus. Au contraire, pour le Var, la donnée disponible est l'enregistrement sédimentaire, tandis qu'il manque des informations concrètes relatives à la source.

Ce manuscrit est organisé en 4 chapitres principaux (Chapitres 1-4), qui sont cohérents et peuvent être lus de façon indépendante. Le **Chapitre 1** est une synthèse des connaissances préalables sur la genèse et l'évolution des canyons sous-marins ainsi que du rôle que les écoulements gravitaires y jouent. La deuxième partie du chapitre s'intéresse aux différents types de flux gravitaires, y compris

les controverses concernant les différentes classifications, et se focalise sur les processus physiques responsables de l'évolution et de la propagation des courants de turbidité ainsi que du dépôt final. La première partie du **Chapitre 2** présente et discute les différentes méthodes de recherche utilisées pour l'étude des courants de turbidité et le transport et dépôts associés. La deuxième partie s'intéresse aux aspects physiques et mathématiques du modèle numérique appliqué aux deux cas d'étude de cette thèse. La modélisation numérique vise à reproduire de la façon la plus précise possible les processus naturels; au cours de cette thèse le modèle a été appliqué à deux cas d'étude et les résultats de modélisation ont été comparés avec des données de terrain. Les deux canyons sont étudiés en détail dans leurs chapitres respectifs. Le **Chapitre 3** s'intéresse à la modélisation des courants de turbidité liés au chalutage de fond dans le canyon de La Fonera. Ce chapitre est en révision dans le journal Marine Geology et les travaux ont été présentés dans des congrès internationaux. Les courants hyperpycnaux à différentes périodes climatiques et le rôle des forces de Coriolis dans l'évolution spatiale de ces courants et leur dépôt sont présentés dans le **Chapitre 4**. Une synthèse générale des résultats issus de ce travail, ainsi que des perspectives et des possibles améliorations sont présentées dans le **Chapitre 5**. Les références bibliographiques utilisées dans ce manuscrit sont présentées à la fin de chaque chapitre.

Références

Baas, J.H., Best, J.L., Peakall, J., 2011. Depositional processes, bedform development and hybrid bed formation in rapidly decelerated cohesive (mud–sand) sediment flows. Sedimentology 58, 1953–1987. doi:10.1111/j.1365-3091.2011.01247.x

Bonneau, L., Jorry, S.J., Toucanne, S., Jacinto, R.S., Emmanuel, L., 2014. Millennial-Scale Response of a Western Mediterranean River to Late Quaternary Climate Changes: A View from the Deep Sea. J. Geol. 122, 687–703. doi:10.1086/677844

Bouma, A.H., 1962. Sedimentology of Some Flysch Deposits. A Graphic Approach to Facies Interpretation. Amsterdam, Elsevier.

Cacho, I., Grimalt, J.O., Sierro, F.J., Shackleton, N., Canals, M., 2000. Evidence for enhanced Mediterranean thermohaline circulation during rapid climatic coolings. Earth Planet. Sci. Lett. 183, 417–429. doi:10.1016/S0012-821X(00)00296-X

Canals, M., Puig, P., de Madron, X.D., Heussner, S., Palanques, A., Fabres, J., 2006. Flushing submarine canyons. Nature 444, 354–357. doi:10.1038/nature05271

Canals, M., Company, J.B., Martín, D., Sànchez-Vidal, A., Ramírez-Llodrà, E., 2013. Integrated study of Mediterranean deep canyons: Novel results and future challenges. Prog. Oceanogr., Integrated study of a deep submarine canyon and adjacent open slopes in the Western Mediterranean Sea: an essential habitat 118, 1–27. doi:10.1016/j.pocean.2013.09.004

Carter, L., Burnett, D., Drew, S., Hagadorn, L., Marle, G., Bartlett-McNeil, D., Irvine, N., 2009. Submarine Cables and the Oceans: Connecting the World. The United Nations Environment Programme World Conservation Monitoring Centre Biodiversity Series (No. 31). ICPC/UNEP/UNEP-WCMCWCMC.

Cattaneo, A., Babonneau, N., Ratzov, G., Dan-Unterseh, G., Yelles, K., Bracène, R., Mercier de Lépinay, B., Boudiaf, A., Déverchère, J., 2012. Searching for the seafloor signature of the 21 May 2003 Boumerdès earthquake offshore central Algeria. Nat Hazards Earth Syst Sci 12, 2159–2172. doi:10.5194/nhess-12-2159-2012

Cesare, G., Schleiss, A., Hermann, F., 2001. Impact of Turbidity Currents on Reservoir Sedimentation. J. Hydraul. Eng. 127, 6–16. doi:10.1061/(ASCE)0733-9429(2001)127:1(6)

Felix, M., 2002. Flow structure of turbidity currents. Sedimentology 49, 397–419. doi:10.1046/j.1365-3091.2002.00449.x

Galy, V., France-Lanord, C., Beyssac, O., Faure, P., Kudrass, H., Palhol, F., 2007. Efficient organic carbon burial in the Bengal fan sustained by the Himalayan erosional system. Nature 450, 407–410. doi:10.1038/nature06273

Gennesseaux, M., Mauffret, A., Pautot, G., 1980. Les glissements sous-marins de la pente continentale niçoise et la rupture des câbles en mer Ligure (Méditerranée occidentale). C R Acad Sci Paris Série D, 959–962.

Goldfinger, C., 2010. Submarine Paleoseismology Based on Turbidite Records. Annu. Rev. Mar. Sci. 3, 35–66. doi:10.1146/annurev-marine-120709-142852

Heezen, B.., Ewing, M., 1952. Turbidity currents and submarine slumps, and the 1929 Grand Banks earthquake. Am. J. Sci. 250, 849–873.

Hsu, S.-K., Kuo, J., Lo, C.-L., Tsai, C.-H., Doo, W.-B., Ku, C.-Y., Sibuet, J.-C., 2008. Turbidity Currents, Submarine Landslides and the 2006 Pingtung Earthquake off SW Taiwan. Terr. Atmospheric Ocean. Sci. 19, 767. doi:10.3319/TAO.2008.19.6.767(PT)

Hunt, J.E., Wynn, R.B., Masson, D.G., Talling, P.J., Teagle, D.A.H., 2011. Sedimentological and geochemical evidence for multistage failure of volcanic island landslides: A case study from Icod landslide on north Tenerife, Canary Islands. Geochem. Geophys. Geosystems 12, Q12007. doi:10.1029/2011GC003740

Jacinto, R.S., Burel, D., 2003. Modélisation du devenir à court terme des boues de dragage rejetées par clapage. Rev. Fr. Génie Civ. 7, 1151–1166. doi:10.1080/12795119.2003.9692539

Kuenen, P.H., 1937. Experiments in connection with Daly's hypothesis on the formation of submarine canyons. Leidse Geol Meded 8, 327–335.

MEDOC GROUP, 1970. Observation of Formation of Deep Water in the Mediterranean Sea, 1969. Nature 227, 1037–1040. doi:10.1038/2271037a0

Middleton, G.V., Hampton, M.A., 1973. Part I. Sediment Gravity Flows: Mechanics of Flow and Deposition 1–38.

Millot, C., Taupier-Letage, I., 2005. Circulation in the Mediterranean Sea, in: Saliot, A. (Ed.), The Mediterranean Sea, Handbook of Environmental Chemistry. Springer Berlin Heidelberg, pp. 29–66.

Mulder, T., Migeon, S., Savoye, B., Faugères, J.-C., 2001. Inversely graded turbidite sequences in the deep Mediterranean: a record of deposits from flood-generated turbidity currents? Geo-Mar. Lett. 21, 86–93. doi:10.1007/s003670100071

Piper, D.J.W., Normark, W.R., 2009. Processes That Initiate Turbidity Currents and Their Influence on Turbidites: A Marine Geology Perspective. J. Sediment. Res. 79, 347–362. doi:10.2110/jsr.2009.046

Ratzov, G., Cattaneo, A., Babonneau, N., Déverchère, J., Yelles, K., Bracene, R., Courboulex, F., 2015. Holocene turbidites record earthquake supercycles at a slow-rate plate boundary. Geology 43, 331–334. doi:10.1130/G36170.1

Sanchez-Vidal, A., Canals, M., Calafat, A.M., Lastras, G., Pedrosa-Pàmies, R., Menéndez, M., Medina, R., Company, J.B., Hereu, B., Romero, J., Alcoverro, T., 2012. Impacts on the Deep-Sea Ecosystem by a Severe Coastal Storm. PLoS ONE 7, e30395. doi:10.1371/journal.pone.0030395

Sparkes, R.B., Lin, I.-T., Hovius, N., Galy, A., Liu, J.T., Xu, X., Yang, R., 2015. Redistribution of multi-phase particulate organic carbon in a marine shelf and canyon system during an exceptional river flood: Effects of Typhoon Morakot on the Gaoping River–Canyon system. Mar. Geol. 363, 191–201. doi:10.1016/j.margeo.2015.02.013

Stow, D.A.V., Mayall, M., 2000. Deep-water sedimentary systems: New models for the 21st century. Mar. Pet. Geol. 17, 125–135. doi:10.1016/S0264-8172(99)00064-1

Talling, P.J., Masson, D.G., Sumner, E.J., Malgesini, G., 2012. Subaqueous sediment density flows: Depositional processes and deposit types. Sedimentology 59, 1937–2003. doi:10.1111/j.1365-3091.2012.01353.x

Talling, P.J., Paull, C.K., Piper, D.J.W., 2013. How are subaqueous sediment density flows triggered, what is their internal structure and how does it evolve? Direct observations from monitoring of active flows. Earth-Sci. Rev. 125, 244–287. doi:10.1016/j.earscirev.2013.07.005

Talling, P.J., 2014. On the triggers, resulting flow types and frequencies of subaqueous sediment density flows in different settings. Mar. Geol., 50th Anniversary Special Issue 352, 155–182. doi:10.1016/j.margeo.2014.02.006

Wynn, R.B., Masson, D.G., 2003. Canary Islands Landslides and Tsunami Generation: Can We Use Turbidite Deposits to Interpret Landslide Processes?, in: Locat, J., Mienert, J., Boisvert, L. (Eds.), Submarine Mass Movements and Their Consequences, Advances in Natural and Technological Hazards Research. Springer Netherlands, pp. 325–332.

Chapter 1:

TURBIDITY CURRENTS AND SUBMARINE CANYONS

ABSTRACT

Submarine canyons are preferential pathways for the transfer of sediment from shallow areas to the deep ocean. Turbidity currents, a particular type of the continuum of sediment gravity flows containing a relative low proportion of fine-grained sediment, are the most important process moving sediment from shallow areas to the deep ocean. This chapter aims to be a synthesis of background knowledge on the genesis and evolution of submarine canyons and the role that turbidity currents play in these environments. The second part of the chapter deals with the different types of sediment gravity flows, and the related controversies, and focuses on the physical processes that underlie the propagation of turbidity currents and the final result deposition. The chapter provides the definitions of the main concepts explored during this dissertation and summarizes the findings of some of the major studies related to turbidity currents in submarine canyons.

RESUME

Les canyons sous-marins sont des conduits préférentiels pour le transfert de sédiment depuis des zones peu profondes vers les abysses. Les courants de turbidité, ne sont qu'un cas particulier du continuum des flux gravitaires où l'excès de densité est dû à une charge, relativement faible, en sédiment fin. La première partie du chapitre peut être considérée comme une synthèse des connaissances préalables sur la genèse et l'évolution des canyons sous-marins ainsi que du rôle essentiel joué par les courants de turbidité dans l'origine et le fonctionnement de ces environnements. La deuxième partie du chapitre s'intéresse aux différents types de flux gravitaires, y compris les controverses concernant les différentes classifications, en focalisant sur les processus physiques responsables de l'évolution et de la propagation des courants de turbidité ainsi que du dépôt final. Les principaux concepts explorés dans cette thèse et les principaux travaux dans le milieu des courants de turbidité en relation avec les canyons sous-marins sont présentés dans ce premier chapitre.

1. Introduction

Submarine canyons are deep, long incisions into continental margins. They act as primary conduits for the transfer of sediment from coastal environments to deep basins. Jointly with turbidity currents, submarine canyons have been studied for over fifty years. However, we still know little of the mechanisms involved in the sediment transport and infill/erosion of submarine canyons. It is still difficult to link flow dynamics and deposit characteristics. Deep-water processes cover a wide range of temporal and spatial scales. Sedimentary processes due to flowing water and involving exchange with bed is a field of research in which Earth Science and Hydraulic Engineering converge. Generally, Earth Science is interested in long-term processes, whilst Hydraulic Engineering focuses on the shorter scales. The combination of both would lead to a higher level of detail and a better knowledge of these processes.

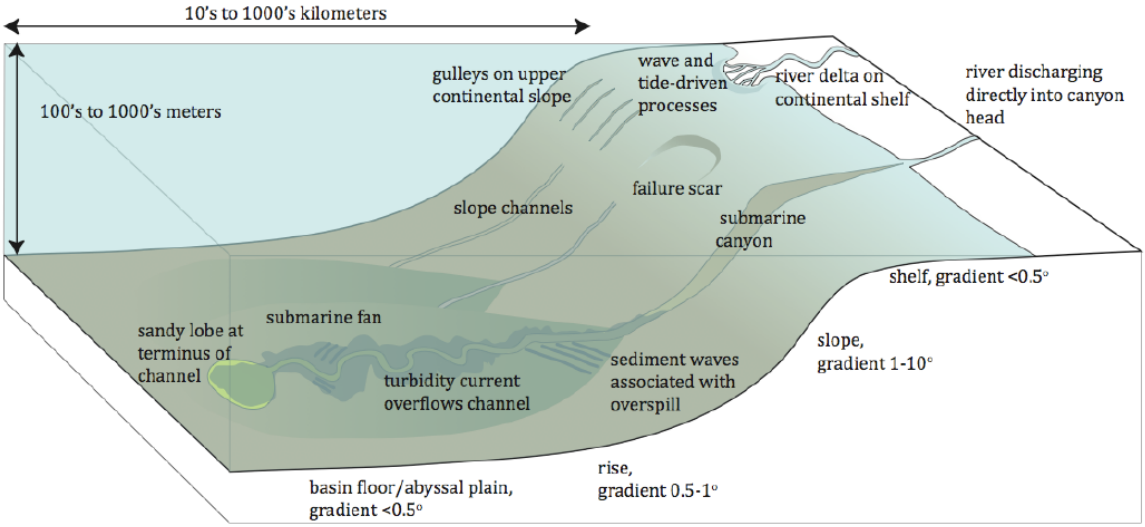

FIG.1.1 CONTEXT OF TURBIDITY CURRENTS ON CONTINENTAL MARGINS (MODIFIED FROM MEIBURG AND KNELLER, 2010)

2. Review on submarine canyons

By the second half of the 20th century, Shepard and collaborators identified seven types of seafloor valleys in his pioneering morphogenetic classification: delta-front troughs, fan valleys, slope gullies, fault valleys, shelf valleys, deep-sea channels and submarine canyons (Shepard, 1963, 1973; Shepard and Dill, 1966). Submarine canyons were defined as "steep-walled, sinuous valleys with V-shaped cross sections, axes sloping outward as continuously as river-cut land canyons and relief comparable to even the largest of land canyons".

Studies on canyons and related bottom structures were firstly driven by economic reasons, as they are a hotspot for exploration for fossil energy resources and exploitation of ancient deposits. Detailed studies on the morphology and dynamics of submarine canyons have been also performed in relation to cable and pipeline routing and in support of naval submarine operations. Moreover, canyons deeply indented in the continental shelf with their heads close to the shoreline are of high relevance for fisheries, as they intercept coastal fluxes of organic matter, interact with ocean circulation and ease the ascent of deep nutrient-rich waters and the formation of mesoscale oceanographic structures. Over the last years, their role as preferential conduits for exchanges

between coastal areas and the deep ocean, together with their value as high biodiversity ecosystems has increasingly attracted scientific attention.

2.1. Morphology

Submarine canyons are typical geomorphological features of continental slopes. Cronin et al. (2005) proposed the division of canyons in four domains: head, axis, walls and distal reaches. The canyon head is the upper end of the canyon and is the closer part to the coast. It is defined by a high gradient slope compared to the regional gradient slope and by a dense drainage network. The canyon head may display locally abrupt walls and amphitheatre-like shapes with abundant scars related to mass-wasting events (Green et al., 2007). The transition between the head of the canyon and the deeper course is usually defined by a decrease in slope gradient and a lowering of the complexity of the drainage network. The canyon main course is either V-shaped or U-shaped, with the thalweg depth increasing rapidly down canyon, also in comparison with the canyon rims. Often the canyon course is divided into upper, middle and lower canyon. Upper canyon courses tend to be more V-shaped whereas lower courses tend toward U shapes. The canyon floor usually presents a low profile and it might show axial incision, or inner channel, due to the erosive action of turbidity currents and other mass transport processes (Baztán et al., 2005; Canals et al., 2006; Lastras et al., 2007). Canyon walls are usually abrupt and may reach gradient slopes of 30-40° or nearly vertical at specific locations. Canyon walls are often affected by sediment failures and other erosion processes. However, depositional features such as terraces and confined levees can also be present (Babonneau et al., 2004). The sinuosity of canyon axes depends on structural control, local slope gradient and sediment supply. Underlying tectonic control on canyon and canyon axis paths have been documented in several cases (e.g. Laursen and Normark, 2002; Durán et al., 2014). The canyon mouth, also called canyon end, is located at the foot of the continental slope or over the continental rise. The seaward continuations of submarine canyons across deep-sea fans and channel-levee complexes are called turbidite channels. The limit between the canyon mouth and channel-levee complexes is usually defined by a strong decrease in slope gradient. Submarine canyons continued by turbidite channels are referred as “canyon-channel systems”, which may extend far over the continental rise and abyssal plain in the form of deep sea channels (Canals et al., 2004a, 2009).

A combination of factors such as sediment supply, slope angle, seafloor topography, basement topography, faulting and tectonic control, and geological history seem to determine the location, morphology and spacing of canyons along continental margins (Canals et al., 2004b). Tectonic and magmatic processes control active margins, whilst erosional and depositional processes prevail in passive margins. Harris and Whiteway (2011) analysed the geomorphic differences between submarine canyons in active and passive margins at a global scale. These authors found that canyons in active margins are steeper, shorter and more closely spaced than canyons in passivee margins. Sediment thickness is also larger in passive margin canyons with deposits up to twice as thick. They subdivided large submarine canyons into three main types according to the present position of the canyon head relative to the shelf edge: i) shelf incising and river associated (i.e. those which heads have a clear bathymetric connection to a major river system), ii) shelf incised (i.e. those with no clear bathymetric connection to a major river), and iii) blind or headless (those incised into the continental slope only). However, their classification is based on the present-day distribution and configuration of canyons and river mouths, without taking into account that river mouth-canyon head connections change through time, appearing, reappearing or disappearing. In the northwestern Mediterranean Sea, and elsewhere, most canyon heads were river-connected as recently as during Quaternary lowstands, while in Harris and Whiteway's (2011) classification, only La Fonera canyon appears as shelf-incising and river associated (Canals et al., 2013). Actually, at present La Fonera canyon head is some distance from the closest significant river mouth. A greater number of shelf incising canyons are found in margins with high rates of sediment export (Fig. 1.2). This implies that the shelf incision of submarine canyons would favour their ability to capture river, coast and inner shelf-sourced sediment. In that respect, Canals et al. (2013) considered shelf incision length from the shelf edge (IL)

and canyon head distance to shoreline (DS) as key variables in determining the dynamics of submarine canyons (see figures 2 and 3 in Canals et al., 2013). Other geomorphic elements such as coastline configuration may also play a relevant role in the ability of shelf incising canyons to intercept coastal and shelf sediments (Canals et al., 2006).

Jobe et al. (2011) also proposed a classification of submarine canyons based on sediment supply and shelf-indentation: **type I canyons** indent the shelf edge and are associated with high sediment supply because of their closeness to large fluvial systems or long-shore drift cells. They present V-shaped morphologies with terraces. Sand-rich turbidity currents and mass wasting events control their morphology, also favouring the development of submarine fan-channel systems. **Type II canyons** do not indent the shelf edge and occur in areas of low sediment supply. They exhibit smooth aggradational morphologies, U-shaped profiles with flat bottoms, and no or poor down-dip expression as this type of canyons dies out at the base the slope.

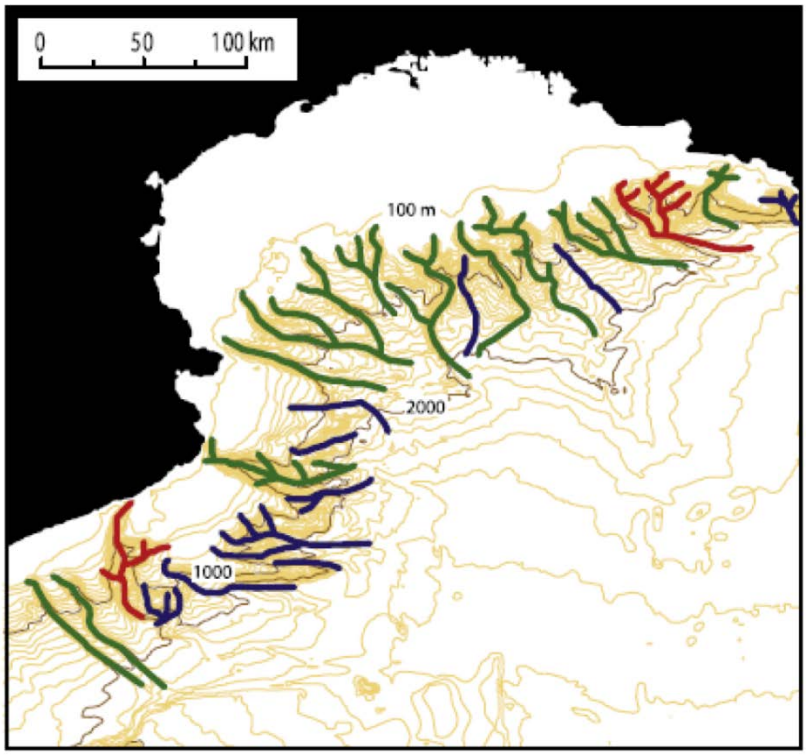

FIG.1.2. SUBMARINE CANYONS OF THE GULF OF LION AND THE NORTH CATALAN MARGINS, NORTHWESTERN MEDITERRANEAN SEA., WHICH INCLUDES ALL THREE CANYON TYPES DESCRIBED BY HARRIS AND WHITEWAY (2011) SPACED LESS THAN 10 KM APART: SHELF INCISING AND RIVER ASSOCIATED, IN RED ; SHELF INCISING, IN GREEN ; AND BLIND, IN BLUE . FROM HARRIS AND WHITEWAY (2011)

Mediterranean canyons show striking differences with canyons in other continental margins: they are more closely spaced (14.9 km), more dentritic (12.9 limbs per 100,000 km^2), shorter (mean length of 26.5 km) and among the steepest (mean slope of 6.5°) canyons in the world ocean (Harris and Whiteway, 2011). Canyons in the Mediterranean Sea also present a smaller depth range (1613 m) than canyons in other margins, for an average water depth of about 1500 m in the Mediterranean Sea (Amblàs et al., 2004). In the Mediterranean Basin, 518 submarine canyons spanning a minimum depth range of 1000 m have been identified (Harris and Whiteway, 2011). For all the above characteristics of its submarine canyons, and also because whilst representing a minimal part in terms of world's oceans surface (0.7%) or volume (0.3%) it contains up to 8.85% of the existing submarine canyons, the Mediterranean Sea stands out as a distinct region in a global perspective (Canals et al., 2013). Especially the Gulf of Lions (Fig 1.2) appears as one of the world's areas with higher density of shelf incising canyons, with 3 to 4 per 100 km along the shelf break) (Allen and Durrieu de Madron, 2009).

2.2. Origin and evolution

The origin of submarine canyons and the processes involved in sediment transport within them are still object of research due to their complexity and the diversity of settings where these geomorphic features occur. This adds to the difficulties in observing contemporary sediment transport and canyon formation processes directly on site. Furthermore, present day processes only allow a limited understanding of canyons evolution. Today, active submarine canyons coexist with essentially relict features. Also, there are submarine canyons that simply behave as bypass zones to deeper areas without net erosion or deposition along their course.

The origin of submarine canyons has intrigued marine geologists for a long time and still remains largely unsolved. The first hypothesis about the formation of submarine canyons dates from the second half of the 19th century (Dana, 1863). These early studies were based on sounding charts of canyons indented in the shelf break. The similarities between submarine canyons and river-cut land canyons led to the hypothesis that they represented the continuation of subaerial river beds that had been submerged by rising sea levels at the end of the Pleistocene, eventually eased by down-faulting (Shepard, 1934; Spencer, 1903). In the 1920s the development of echo-sounders revealed how common submarine canyons are and that they extend across continental slopes to depths of several thousand meters (Veatch and Smith, 1939).

The debate on canyon origin was reactivated in the 1930's. A paper by Daly (1936) summarized the knowledge on the origin of submarine canyons at the time, considering the newest data. In his paper, Daly challenged the well-established idea of relative sea level lowering as a result of tectonic uplift. Such an idea would imply a global uplift, followed by a stable period and finally a global subsidence of at least 3000 m needed for the subaerial excavation of canyons that extend down to 3000 m depth. Daly was the first to suggest that turbidity currents could carve submarine canyons on continental margins. Geologists were sceptical about the role of turbidity currents in the formation and evolution of submarine canyons until the tank experiments conducted by Kuenen (1938) and Kuenen and Migliorini (1950) to test the erosive power of turbidity currents. Furthermore, the investigations on submarine cable breaks following the 1929 Grand Banks earthquake demonstrated the canyon-forming potential and erosive power of turbidity currents (Heezen and Ewing, 1952; Heezen et al., 1954).

Following these early studies, two opposed models were proposed to explain the origin of submarine canyons: downslope erosion (Pratson et al., 1994) and upslope development (Twichell and Roberts, 1982; Farre, 1983). The first model involves the triggering of turbidity currents and/or mass failures at the mouth of fluvial systems close to the shelf edge. Hyperpycnal flows may initiate within the river and sediment overload due to rapid accumulation at the river mouth can trigger mass failures that can evolve into gravity flows (Normark and Piper, 1991; Mulder et al., 2003). The upslope development or "bottom-up" hypothesis (Twichell and Roberts, 1982) explains canyon development as a result of landslides initiated on the continental slope, which would progress upslope by retrogressive failures. These retrogressive failures may eventually capture fluvial systems. The upslope retrogressive model relies on the observation of two different types of canyons: "mature" canyons that incise the continental shelf, and "immature" canyons confined to the continental slope. The former would result from headward erosion of the latter. Farre (1983) further developed this idea of youthful and mature phases in canyon evolution and their relationship with sediment supply. During the youthful phase the canyon would be confined to the continental slope. Therefore, this early phase of development would be dominated by slope failure, with sedimentary transport being less important as the canyon does not reach the continental shelf edge. Once the canyon cuts the continental shelf, it becomes a "mature" canyon. The direct connection with fluvial and continental shelf sediment sources would favour the development of coarse-grained turbiditic flows during this mature phase of canyon evolution.

In the following years, several authors pointed out that both mechanisms (i.e. downwards and upwards erosion) were likely, eventually acting during different phases of canyon evolution (e.g. Canals, 1985). Numerical modelling further confirmed that both downslope erosion and headward erosion could be at play during canyon development (Pratson and Coakley, 1996). It was demonstrated that downslope currents initiated at the shelf edge could trigger failures along the slope. These failures may evolve upslope along rills and gullies thus leading to headward erosion.

Current consensus essentially follows the ideas of Shepard (1981): the history of each canyon is unique and several processes can be involved in its origin and evolution. Canyons are often superimposed on previous tectonic lineaments or faults and it is usually admitted that their evolution can result from various processes (Migeon et al., 2012). Five main processes have been proposed to be involved in submarine canyon formation: 1) subaerial or fluvial erosion of the upper canyon; 2) erosion by turbidity currents; 3) erosion by down-canyon mass movements including creeping, landsliding and grain flows, and sediment redistribution by bottom currents; 4) erosion by bottom currents other than turbidity currents; and 5) drowning by subsidence of subaerial valleys.

Many canyon heads present evidence of repeated cut and fill episodes that might be associated to sea level changes and related processes. In the Pleistocene, lowered sea levels favoured subaerial erosion. Also, local subsidence likely resulted in the submergence of many upper canyon reaches. Mass wasting processes contribute to the retrogressive erosion of canyon heads. Sediments remobilised in that way are transported downslope by gravity flows. Storms and earthquakes can destabilise unstable, recently deposited shelf edge and slope sediments. The resulting flows can subsequently evolve into turbidity currents, which are able to erode the seabed while transporting large quantities of sediment. Even though turbidity currents might not be at the origin of some submarine canyons, they contribute to its perpetuation as they prevent the canyon from being filled and may excavate it to greater depths. Other gravitational flows, such as those triggered by salinity or temperature gradients, up-and-down currents related to tides or internal waves and ordinary bottom currents can also contribute to the remobilisation of sediment and the excavation of submarine canyons. Upbuilding of canyon walls and axial downcutting over long periods of time allows the formation of huge canyons.

Examples of canyon-forming mechanisms acting with variable intensity and frequency are found in different continental margins. Headward erosion due to slope failures during an early phase of evolution followed by the development of turbiditic flows once the canyon reaches the shelf edge have been proposed to explain the origin of canyons unrelated to river mouths such as the Yoakum/Lavaca system in the Gulf of Mexico (Galloway et al., 1991), the Andoya canyon (Laberg et al., 2007), the Bari canyon (Ridente et al., 2007) and paleovalleys in the southern Tyrrhenian Sea (Lo Iacono et al., 2014). Headward erosion and contour current-controlled lateral migration explain the development of canyons in Argentina's continental margin (Lastras et al., 2011) and the origin of buried canyons in the South China Sea (He et al., 2013). The incisions of the Tugela canyon in the east coast of South Africa have been related to phases of hinterland infill and reworking of pelagic infill by oceanic currents (Wiles et al., 2013). The Aude canyon (also known as Bourcart canyon) in the Gulf of Lions also represents a good example of different processes acting at different scales: 1) turbidity currents are responsible for the carving of the axial incision observed in this canyon (Baztan et al., 2005); 2) hyperpycnal flows during low-stands in the case of fluvial connection; 3)lateral collapse of canyon flanks along the axial incision contribute to broaden it (Sultan et al., 2007); 4) oceanographic processes such as cascading explain sand transport within the canyon during highstands (Bassetti et al., 2006; Gaudin et al., 2006a; Jouet et al., 2006). Capbretron canyon in the Bay of Biscay also evidences how different mechanisms can be at play at different timescales. The axial incision of Capbreton canyon has been interpreted as an erosive-depositional imprint from a former period when the canyon and the Adour River where connected (Gaudin et al., 2006b). On the other hand, the recent morphosedimentary evolution of the Capbreton canyon is mainly dominated by the massive transfer of sand eroded from the coastline during major storms (Mazières et al., 2014).

Submarine canyons in Australia also evidence the key role of littoral drift and waves in sand transport to the deep during highstands (Boyd et al., 2008). Turbidity currents fed by littoral drift instead of direct river mouth discharge have been shown to be highly relevant for the evolution of Cap Lopez canyon in Gabon (Biscara et al., 2011) and La Jolla canyon in California (Covault et al., 2007). Also, Nakajima et al. (2014) relate sand and mud ejection from active pockmarks during sea-level falls to turbidity currents involved in canyon formation in the east Japanese margin (Normark and Piper, 1991).

Tectonics, riverine sediment input and the overall geological history of the basin are at play in the development and formation of **canyons in the Mediterranean** Basin (Canals et al., 2013). A unique feature of the Mediterranean Sea is its dessication during the Late Miocene "Messinian Salinity Crisis" (Hsü, 1972; Hsü et al., 1977). The subaerial exposition and erosion of entire Mediterranean continental margins during this period would have favoured widespread incision by rivers resulting in deep valleys that became submarine canyons following the post-Messinian or Zanclean flooding from the Atlantic (Lofi et al., 2005; García-Castellanos et al., 2009). Tectonic uplifting and margin progradation have reshaped some of the canyons formed during the Late Miocene (Bertoni and Cartwright, 2005; Ridente et al., 2007).

2.3.Novel insights on canyon functioning during sea leavel highstands

Sequence stratigraphy models (e.g. Posamentier and Vail, 1988; Wood et al., 1993) emphasize the role of sea level as a primary control of off-shelf transport and canyon incision. Increasing fluvial and continental shelf sediment supply to the continental slope occur during sea-level lowerings and lowstand conditions, whilst highstand periods are typically associated with canyon heads disconnection from fluvial systems and low sediment supply to the slope. Therefore, it has long been believed that submarine canyon formation and reshaping take place mainly during sea level lowstands. Erosion and canyon carving are eased when continental shelves are subaerially exposed during glacial and glacial transition periods. Numerous studies (Canals et al., 2009, 2006, Khripounoff et al., 2009, 2003; Lastras et al., 2007; Mulder et al., 1997; Palanques et al., 2005; Paull et al., 2003; Puig et al., 2012, 2008, 2004a; Sanchez-Vidal et al., 2012; Shepard et al., 1974; Stabholz et al., 2013; Xu et al., 2014) challenge the old idea of canyons being dormant features during sea level highstands, with only exceptional perturbations by high speed turbidity currents (Fig. 1.3).

Such novel vision on submarine canyon dynamics has been made possible thanks to a plethora of technological advances during the last decades, including multibeam mapping, deep-towed side scan sonars, 2D and 3D seismic reflection profiling systems, in situ monitoring with multi-instrumented moorings, remote underwater vehicles, and improved sediment and rock sampling techniques. While it is true that some of these efforts (i.e. in situ monitoring) are biased towards the more frequent types of events (sub-annual scales) in relatively shallow-water settings (Talling et al., 2013, 2015), it is also true that they are able to capture rare, decadal or longer-scale events and provide a unique understanding into contemporary oceanographic and sedimentary processes in submarine canyons. Such processes could be similar to those occurring during sea level lowstands (Puig et al., 2014). The results obtained so far also demonstrate that under highstand conditions, like the present ones, there are highly active submarine canyons.

In the Northwestern Mediterranean Sea three main high-energy oceanographic processes capable of eroding and carrying sediment to and from submarine canyons have been identified (Canals et al., 2013). These are dense shelf water cascading (Canals et al., 2006; Lastras et al., 2007; Puig et al., 2008; Ulses et al., 2008; Palanques et al., 2012; Durrieu de Madron et al., 2013), Eastern storms (Palanques et al., 2008; Sanchez-Vidal et al., 2012; Pedrosa-Pàmies et al., 2013) and offshore convection (Martín et al., 2010; Palanques et al., 2012; Durrieu de Madron et al., 2013; Lopez-Fernandez et al., 2013; Stabholz et al., 2013)

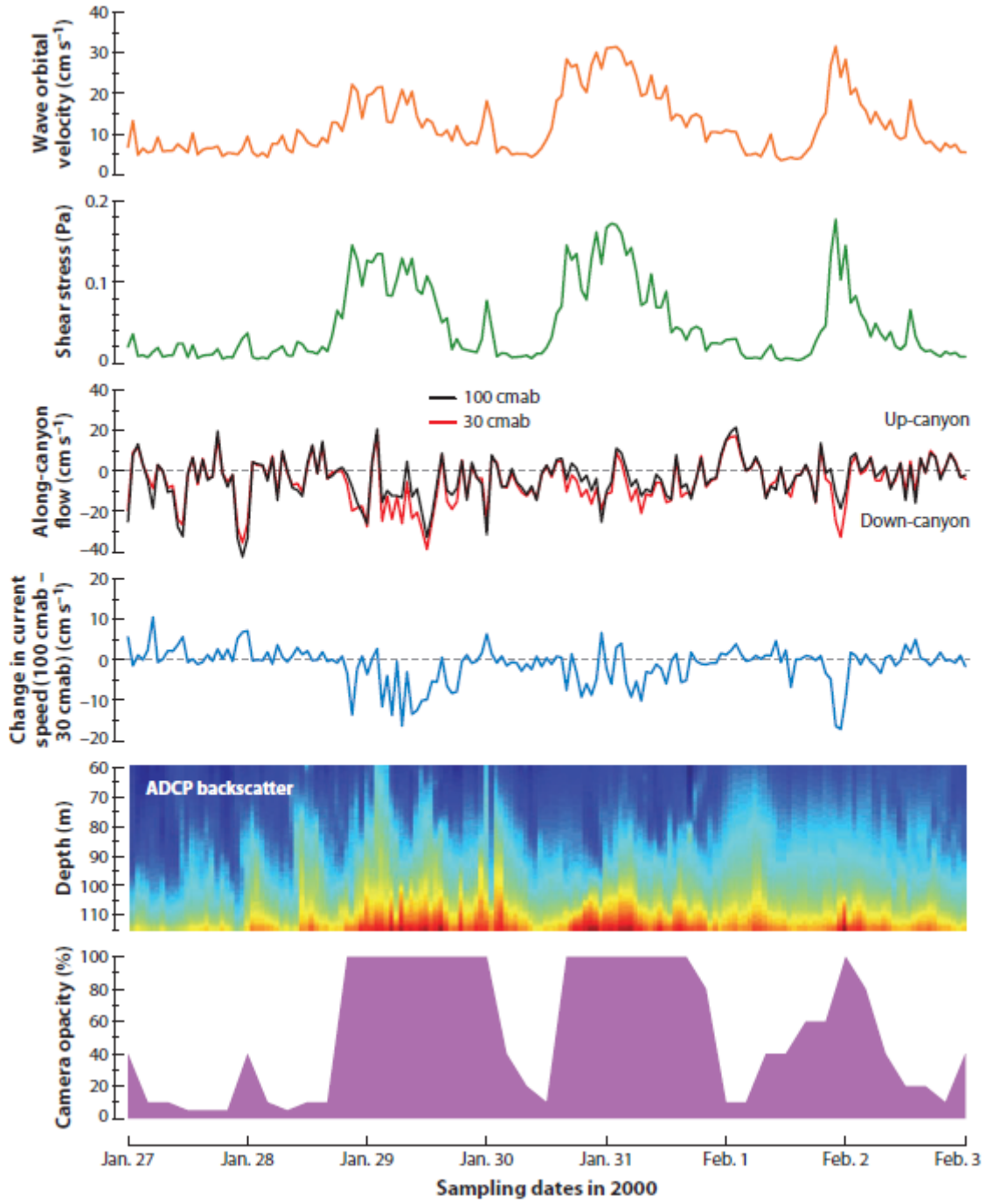

FIGURE. 1.3. MEASUREMENTS AT THE EEL CANYON HEAD DURING LATE JANUARY AND EARLY FEBRUARY STORMS, SHOWING THE CO-OCCURRENCE OF SEDIMENT GRAVITY FLOWS. INCREASES IN ORBITAL VELOCITY ARE CONCOMITANT WITH HIGHER ESTIMATES OF SUSPENDED SEDIMENT CONCENTRATIONS, AS ILLUSTRATED BY THE CAMERA OPACITY RECORD. CURRENTS AT 30 CM AB ARE GREATER THAN THOSE AT 100 CM AB DURING THE STORMS AND ARE DIRECTED DOWNCANYON (FROM PUIG ET AL., 2004B).

Several review papers summarize the current and novel knowledge derived from in situ monitoring and other data sources. Processes triggering turbidity currents have been addressed by Piper and Normark (2009). The role of canyons in shelf-exchange processes and on flow dynamics within submarine canyons has been discussed by Allen and Durrieu de Madron (2009). On its side, Xu (2011) has reviewed the key advances in submarine canyon hydrodynamics and sediment transport. Talling (2014a) has summarized the triggers, resulting flow types and frequencies of different types of

sediment density flows. Current knowledge on Mediterranean canyon functioning has been synthetized by Canals et al. (2013). More recently, Puig et al. (2014) have identified six major triggering mechanisms of contemporary sediment transport after high frequency, long-term in situ monitoring data. These processes are storm-induced turbidity currents and enhanced off-shelf advection, hyperpycnal flows and failures of recently deposited fluvial sediments, dense shelf water cascading (DSWC), canyon flank failures and large submarine slope failures, and trawling-induced resuspension. Additionally, internal waves can also contribute to the resuspension of ephemeral deposits within canyons.

The large amount of data made recently available to the scientific community has demonstrated the event-driven character of submarine canyon functioning, with short-lived periods of high activity followed by long periods of quiescence. In this setting, weather forcing and oceanographic conditions, and sediment supply play a pivotal role. The new data also show that various sediment transport mechanisms can occur simultaneously or almost, which results in a non-uniform along and across canyon pattern of transport. Ephemeral deposits in the various canyon sections are flushed down at sub-decadal and longer scales by, for instance, cascading flows. Centennial to millennial scale processes, such as large canyon and flank sediment failures, can transport large volumes of sediment onto canyon floors and ultimately to off-canyon channel-levee complexes and submarine fans.

2.4. Effects on circulation

Ocean basin physiography and seafloor relief interfere circulation patterns. Submarine canyons may deflect both the incoming and out-coming flows (Flexas et al., 2008). The greater or lesser effect of a given submarine canyon on ocean circulation depends on its distance to the coast; its size, orientation and overall morphology; the general circulation pattern and the local currents; the direction of the incoming flow, and other parameters such as river outputs close to the canyon or water stratification (Klinck, 1996). This results in a great variety of situations.

Geostrophic flows follow bathymetric contours, thus limiting the across-margin exchanges. In contrast, ageostrophic flow favours the across-margin exchanges with the deep ocean. Canyons can reduce the local length scale of the flow and increase its Rossby number, which is expressed by $Ro=U/fL$, where U is the horizontal velocity scale, f is the Coriolis parameter and L is a horizontal length scale. The Rossby number actually represents the ratio of magnitude of vorticity generated locally and the Coriolis vorticity. The spatial scale in canyons is usually one order of magnitude smaller than on the shelf or on the slope, thus increasing the local Rossby number. Large Rossby numbers imply that the flow is no longer purely geostrophic. The rotational effects of the current (i.e. the Coriolis forces) are reduced by the canyon topography and the flow is forced to cross the isobaths (Allen and Durrieu de Madron, 2009). Advective processes such as upwelling and downwelling due to wind-driven shelf currents, or dense shelf water cascades are cross-isobath flows (Ivanov et al., 2004). Submarine canyons can also cut across tidal currents that run parallel to the shelf topography subsequently generating strong baroclinic tides and internal waves that enhance mixing. Both, advection and mixing, favour the transport between the continental shelf and the deep ocean.

Whereas the regional circulation pattern tend to follow the bathymetry, two geomorphic parameters have been identified as proxies of the ability of a canyon to capture shelf dense waters and littoral drift: the incision length into the continental shelf and the shortest distance of the canyon tip to the shoreline (Canals et al., 2013) (cf. Section 2.1). Canyon width also is a relevant parameter, wide canyons cause flow deflection whilst narrow canyons strongly influence circulation and favour cross-shelf exchanges and vertical motions (Flexas et al., 2008; Klinck, 1996, 1989, 1988). Canyon effects on circulation and shelf-slope exchanges are largely dominated by the direction of the alongshore flow (Klinck, 1996). Left-bounded flows (i.e. flows with the coast on the left, looking downstream in the

Northern Hemisphere) lead to upwelling and strong ocean-shelf exchanges (Hickey, 1995; Klinck, 1996). On the other hand, right-bounded flows lead to shallow downwelling and weak exchange across the shelf. Canyons in the Mediterranean Sea are generally under the influence of right-bounded flows and thus favour net downwelling (i.e. downward flow and flow towards the ocean) (Allen and Durrieu de Madron, 2009). The interaction between currents and canyon causes asymmetry in the vertical velocity field of the canyon, with downwelling in the upstream wall and upwelling in the downstream wall in the case of right-bounded flows (Klinck, 1996; Jordi et al., 2005; Flexas et al., 2008; Ahumada-Sempoal et al., 2013). Vertical stratification appears to limit the vertical extent of the canyon's topographic influence. In case of strong stratification the alongshore flow above the canyon is weakly affected (Klinck, 1996; Ardhuin et al., 1999). Also, the response to topographic constraints seems to be different at surface and at deep: near surface flows are relatively unaffected by topography while in the deep closed circulation patterns develop (Hickey, 1997; She and Klinck, 2000; Allen, 2004; Palanques et al., 2005; Martín et al., 2007).

Deep water formation on the shelf due to cooling, evaporation, freezing or salinization also leads to strong cross-slope gradients (Allen and Durrieu de Madron, 2009). DSWC is a type of near-bottom current driven exclusively by sea-water density contrast (Canals et al., 2006). Over the last ten years several studies have revealed the major role of DSWC in the dynamics of submarine canyons (Puig et al., 2014 and references herein). In the Mediterranean Basin, the Gulf of Lions and the adjacent North Catalan shelves, the northern Adriatic shelf sea and the Aegean Sea act as cooling platforms where dense shelf water forms (Durrieu de Madron et al., 2005; Canals et al., 2006, 2009; Palanques et al., 2006; Ulses et al., 2008). The dense shelf water is forced over the shelf edge from where it cascades over the continental slope using submarine canyons as preferential conduits (Canals et al., 2006; Durrieu de Madron et al., 2013). The seascape-forming and deposit accumulation roles of DSWC have been evidenced in canyons of the Gulf of Lions and the Adriatic Sea (Canals et al., 2006; Gaudin et al., 2006a; Lastras et al., 2007; Trincardi et al., 2007a, 2007b; Puig et al., 2008). In situ monitoring has further confirmed the importance of DSWC in the deep sediment transport (Palanques et al., 2008, 2009, 2012; Sanchez-Vidal et al., 2008; Ulses et al., 2008; Ribó et al., 2011; Rumín-Caparrós et al., 2013). In the Northwestern Mediterranean Sea, Cap de Creus, La Fonera, Blanes and Lacaze-Duthiers canyons are the preferential paths for the export to the deep of dense shelf waters (Canals et al., 2013).

3. Sediment gravity flows

Sediment gravity flows are mixtures of sediment and fluid which flow down a slope due to gravity forces acting on sediment grains (Middleton and Hampton, 1973). Sediment gravity flows are one of the most important processes moving sediment from shallower areas to the deep ocean (Piper and Normark, 2009). Sustained sediment gravity flow activity over geologic time periods results in large accumulations of sediment that form the submarine fans. Sediment gravity flows have economic and societal importance in terms of natural hazards and protection of submarine facilities due to their potential to cause industrial, environmental and human disasters (Meiburg and Kneller, 2010). Despite their relevance, sediment gravity flows are not fully understood. Their generally unpredictable and infrequent occurrence, the hostile and remote environment where they take place and their destructive nature makes difficult their direct monitoring.

3.1. Historical review

The first description of density flows dates back to the late 19th century in the Swiss lakes (Forel, 1887). In the marine environment, Milne (1897) was the first to infer deep-water current action from submarine telegraph-cable breaks.

Prior to the seminal work of Kuenen and Migliorini (1950) on "Turbidity currents as a cause of graded bedding" geologists were sceptical on the role of sediment gravity flows in eroding submarine canyons and depositing graded beds (Shanmugam, 2000). Throughout the 1950s and 1960s scientists focused on the study of deep marine sediments and their origin, stimulated by Daly's hypothesis that density (turbidity) currents could carve submarine canyons (Heezen and Ewing, 1952). During this period studies were based on tank experiments (Kuenen, 1937; Kuenen and Migliorini, 1950; Bagnold, 1962; Middleton, 1966a, 1966b), observations of modern submarine canyons (Heezen and Ewing, 1952; Heezen et al., 1954) and analysis of inland outcrops and deep sea cores (Bouma, 1962).

During the 1960s, experimental work on gravity-driven sediment transport focused on the hydrodynamics of turbidity flows and sediment transport. Bagnold (1962) proposed the autosuspension concept, which implies that sediments within the flow add more energy than they utilize to remain suspended so long as the product of mean velocity of the flow and slope is greater than the particle settling velocity. Middleton (1966a, 1966b) studied in laboratory experiments the anatomy of turbidity currents and identified a head, a body and a tail.

The term *turbidity current* was introduced in the late 1930s by Johnson (1938). Twenty years later Kuenen (1957) proposed the term *turbidite* to refer to the deposit of a turbidity current. The vertical facies model of turbidites, known as the "Bouma sequence", was described by Bouma (1962) in the Annot sandstone outcrops of south-eastern France. However, the succession of structures had already been recognised by Sheldon (1928) and Signorini (1936). Sediment gravity flows other than turbidity currents were proposed during the 1950s and 1960s for sediment transport processes in the deep ocean, i.e. sliding and slumping (Doreen, 1951), debris flows (Crowell, 1957; Doreen, 1951) and high concentration granular flows (Bagnold, 1954; Hsu, 1959). The relevance of these processes in the formation of the Annot sandstone was first discussed by Stanley (1963). Then a new type of deposit derived from thermohaline-induced geostrophic bottom-currents that flow parallel to bathymetric contours, known as "contour currents", was described and defined by Heezen et al. (1966). The term "contourite" was introduced sometime after by Hollister and Heezen (1972) for the deposits associated to contour currents. Until the introduction of both the later concepts (bottom currents and contourite), it was thought that only sediment gravity-driven flows were capable of depositing and reworking sediment at depths greater than the continental slope (Hollister, 1993).

In the 1970s and 1980s, different classifications for sediment gravity flows appeared. Middleton and Hampton (1973) proposed a classification scheme based on sediment-support mechanism related to that of Dott (1963) based on fluid rheology. Later on, Lowe (1979) proposed a hybrid scheme considering both fluid rheology and sediment-support mechanism. Subsequently, the same author proposed a theorical model for the deposition of "high-density" currents (Lowe, 1982), concept that is still debated. The study of outcrops, cores and seismic reflection data brought the development of submarine fan models. Normark (1970) introduced the concept of supra-fan lobe for modern passive margin fans and Mutti and Lucchi (1972) developed the channel-lobe submarine fan model for ancient fan systems. A general submarine fan model based on both modern and ancient systems was then postulated by Walker (1978). Process-based research led Komar (1971) to first discuss the origin and significance of internal hydraulic jumps in turbidity currents and then to investigate turbidity-current behaviour through a one-dimensional hydrodynamic model (Komar, 1977). The first experiments on subaqueous debris flows and their relationship with turbidity currents were also conducted in the 1970s (i.e. Hampton, 1972).

Concerns about the incompatibility of the different approaches studying new and ancient systems arose soon (Normark et al., 1984). Newer schemes and classifications of sediment gravity flows are numerous (Morgenstern, 1967; Middleton and Hampton, 1973; Nardin et al., 1979; Lowe, 1982; Kneller, 1995; Mulder and Cochonat, 1996; Mulder and Alexander, 2001; Shanmugam, 2002; Talling et al., 2012). To some extent, the wealth of terminology and classification schemes has hampered scientific communication (Talling et al., 2012); with the same descriptive terms used both for

processes and products (Shanmugam, 1996). The same process can be named differently according to different authors (Mulder and Alexander, 2001; Talling et al., 2012) (Fig. 1.4).

Whereas progress in numerical and experimental modelling has been substantial, much of the understanding of sediment gravity flows is still based on observations of the resulting deposits due to the paucity of direct measurements. Classifications based on physical processes for which evidence is preserved in deposits might be preferable, as deposits are the only available record of the flows (Shanmugam, 2000; Talling et al., 2012). However, similar deposits can be due to different types of flows (Talling et al., 2012). For instance, sediments formerly recognised as turbidites probably are not, as processes like DSWC may lead to graded deposits (i.e. "cascadites") that may resemble turbidites (Gaudin et al., 2006a). Also, deposits deriving from a single event might be associated to a succession of different types of flows because of downflow transformation (Mulder and Alexander, 2001). Furthermore, sediment gravity flows form a continuum in which is difficult to establish strict boundaries. Talling et al. (2012) proposed a classification of sediment gravity flows based both on deposit type and flow state, rheology (that remains poorly known) and sediment support mechanisms. These authors distinguish four types of flows in their deposit-based classification, which to some extend reminds that of Middleton and Hampton (1976). The four types are: mud density flows, low-density turbidity currents, high-density turbidity currents and debris flows. The more diluted mudflows are fully turbulent whilst the denser are laminar and present non-Newtonian behaviour. Low-density turbidity currents are considered as fully turbulent and lacking of yield strength, with turbulence being the main support mechanism. In high-density turbidity currents the sediment is supported within the flow by a combination of fluid turbulence, grain-to-grain interactions and a limited density contrast between grains and surrounding fluid. Finally, debris flows are laminar or weakly turbulent, with moving sediment supported by processes other than turbulence such us the cohesive strength of the matrix, grain-to-grain interactions, excess pore pressure and the limited density contrast between the grains and the matrix.

Key information such as the time evolution of the flow or the driving force (density) is not preserved in the deposits. Others, such as fluid rheology or sediment support mechanism are processes for which evidence is preserved in the deposits. Classifications such as the ones by Mulder and Alexander (2001) or Talling et al. (2012) try to bridge the gap between product-based (deposits) and process-based classifications. Consideration of rheology (i.e. cohesive vs. frictional) and support mechanisms settles the basis to discuss the physics of sediment gravity flows. Parameters representing flow state, rheology and sediment support mechanisms are needed for numerical simulations and theoretical models. Taking into account the above, we decided to follow the principles of the classification Mulder and Alexander (2001). Whichever classification considered, one should keep in mind that flow transformations are common (Fisher, 1983) both with distance (down and cross flow) and with time at any point.

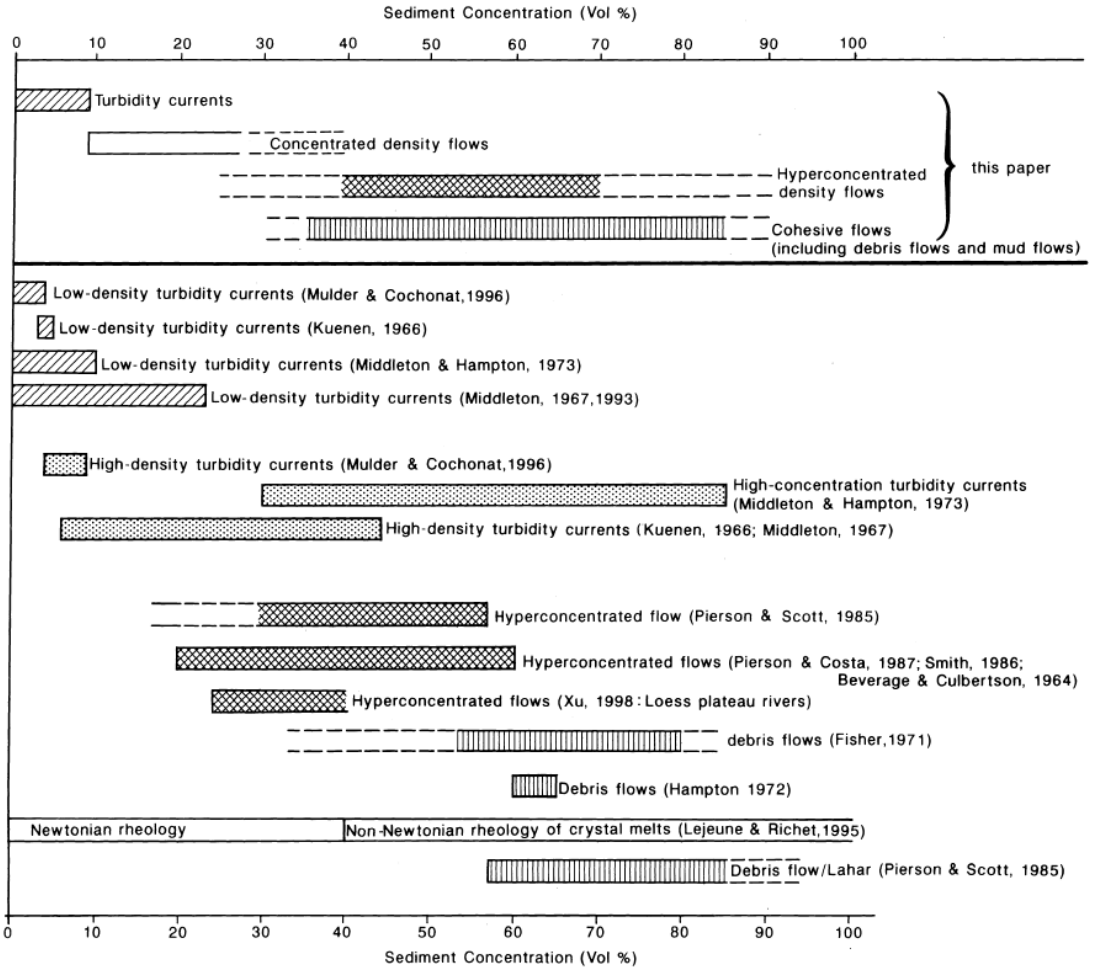

FIG.1. 4 TERMINOLOGY AND USAGE OF NOMENCLATURE FOR SEDIMENT GRAVITY FLOWS, WITH SEDIMENT CONCENTRATION EXPRESSED AS A PERCENTAGE BY VOLUME. IN MANY CASES, A GIVEN SEDIMENT CONCENTRATION CANNOT BE USED TO DEFINE BOUNDARIES, AS THE THRESHOLD PER CENT VOLUME DEPENDS ON OTHER FACTORS SUCH AS CLAY CONTENT. RANGES OF POSSIBLE CONDITIONS FOR BOUNDARIES ARE REPRESENTED BY DASHED LINES (FROM MULDER AND ALEXANDER, 2001).

3.2. Physical background and classifications

Gravity-driven density currents occur whenever fluid of one given density flows primarily horizontally underneath a fluid of different density (Huppert, 2006). The density contrast between the flowing fluid and the ambient fluid can be induced by differences of temperature, salinity or sediment concentration. Gravity currents occur in a variety of settings and scales throughout nature (e.g. snow avalanches, pyroclastic flows, lahars or turbidity currents).

Sediment gravity flows are mixtures of sediment and fluid, which flow downslope due to the force of gravity. Gravity moves the mixture down the slope and the mixture drags along the ambient fluid. Subaqueous sediment flows are one of the volumetrically more important processes moving sediment across the planet (Talling et al., 2013). Subaqueous sediment gravity flows can be classified according to the difference between the flow density (ρ_f) and the ambient fluid density (ρ_w) (Fig. 1.5). Mulder and Alexander (2001) distinguished four types of sediment gravity flows: hypopycnal flows or overflows ($\rho_f < \rho_w$); homopycnal flows ($\rho_f = \rho_w$); mesopycnal flows, or intraflows, or intrusive flows (ρ_f is between the densities of two layers in a stratified column); and hyperpycnal flows or underflows ($\rho_f > \rho_w$). Here we focus in the high-density end member of this classification, which are hyperpycnal flows. Modern language usage restricts the term hyperpycnal flow to underflows generated directly from river mouths due to river discharge, excluding failure induced density flows generated within ocean basins (Mulder and Alexander, 2001).

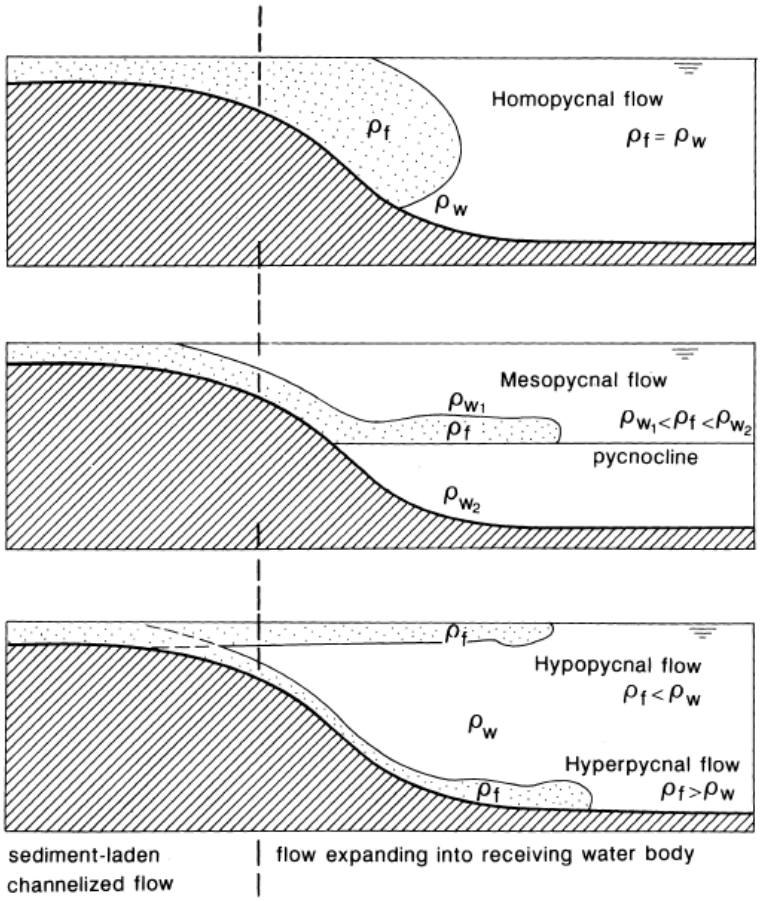

FIG1. 5 TYPES OF FLOWS ACCORDING TO THE RELATION BETWEEN THE DENSITY OF THE FLOW AND THAT OF THE AMBIENT FLUID. WHERE ρ_f IS THE FLOWING FLUID DENSITY AND ρ_w IS THE AMBIENT FLUID DENSITY . FROM MULDER AND ALEXANDER, 2001).

Four main parameters can be considered relevant in flow behaviour: rheology, sediment support mechanism, flow state (turbulent vs. pseudolaminar) and sediment concentration. The latter, sediment concentration influences directly the other three parameters. Clay content and grain size distribution, and the gradient and topographic confinement of the slope also influence flow behaviour.

Matrix strength, dispersive grain pressure arising from grain collisions, escaping pore fluid, hindered settling and fluid turbulence are the sediment support mechanisms in sediment gravity flows (cf. section 3.1). Several sediment support mechanisms may operate simultaneously in a specific sediment flow. Increasing concentration and clay content hamper turbulence and favour the gradual shift from turbulence-supported low-density flows to matrix-supported high-density cohesive flows. Modifications of the slope gradient may change flow state from turbulent to laminar and vice versa.

Classifications based on rheology distinguish sediment gravity flows depending on their behaviour under an applied stress (Fig. 1.6, e.g. Shanmugam (2000) and references therein). Newtonian fluids deform instantaneously when stress is applied, and the rate of strain is linearly related to the applied stress, water is a classic example of such flows. Non-Newtonian fluids deviate from the linear response when stress is applied, and can be divided into power-law fluids and plastic fluids. Power-law fluids are those whose viscosity changes with strain rate according to a power-law relationship. In dilatant fluids the viscosity increases with the rate of strain (i.e. strength increases with an increasing shear-strain rate), whilst in pseudoplastic (also known as contractional) fluids the viscosity decreases with the rate of strain (i.e. their strength decreases with increasing rate of deformation). Plastics differ from fluids in that they present yield strength that must be overcome for deformation to occur. If the strain rate is linearly related to the applied stress once the yield strength is overcome

the flow is considered a Bingham plastic fluid. Otherwise it is either yield-pseudo-plastic or yield-dilatant.

Grain flows, liquefied flows and debris flows in Middleton and Hampton's (1976) classification (cf. section 3.1) are non-Newtonian flows, whilst turbidity currents are Newtonian flows. Cohesive and non-cohesive (or frictional) flows are distinguished in Mulder and Alexander's (2001) classification based on physical flow properties and grain-support mechanisms. In their classification cohesive flows include debris flows and mud flows whilst grain flows and turbidity currents are frictional flows. Subdivisions within cohesive and frictional flows are also made after sediment characteristics and the dominant particle-support mechanism, respectively. Frictional flows can also be divided on the basis of flow duration.

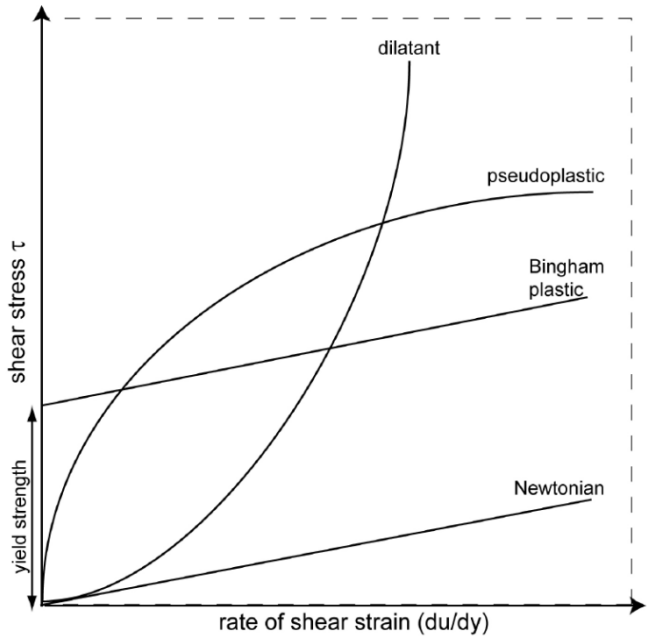

FIG1.6 RHEOLOGY OF NEWTONIAN AND NON-NEWTONIAN FLUIDS (MODIFIED FROM SHANMUGAM (2000)

3.3. Cohesive flows

Cohesive flows have sufficient cohesive material (clay) to develop a Bingham-plastic or pseudo-plastic rheology (Mulder and Alexander, 2001). Cohesion between fine-grained particles provides high-kinematic viscosity to the flow (Shanmugam, 2000), which makes cohesive flows to present low rates of dilution either by particle deposition or entrainment of ambient water.

As stated before, both mud flows and debris flows are cohesive flows. The division between both flow types is stabilised on the basis of grain size sorting. Mud flows contain mostly fine sediment and less than 5% gravel in volume. Debris flows display poor size sorting and can contain large proportions of sand and gravel. Debris flows have received considerable attention in the scientific literature. The little amount of mud (2-5%) contained in the flow is sufficient to render the flow cohesive. The force balance within a debris flow is established between interstitial flow pressure and grain-to-grain interactions. Therefore, the boundary conditions imposed by the ambient water are usually, although not always (e.g. when hydroplaning occurs), of little consequence (Parsons et al., 2007). Laboratory experiments have shown that hydroplaning can reduce bed drag and thus increases head flow velocity (e.g. Mohrig et al., 1998, 1999). Hydroplaning seems to be at the heart of the seemingly contradictory characteristics of debris flows, which are dense, high-speed flows with little erosive capacity able to travel several hundreds of kilometres (Pickering et al., 1989; Gee et al., 1999; Talling et al., 2007). Dynamic pressure develops at the front of debris flows as they move downslope. When such pressures are similar to the submerged weight per unit bed area of the flow, it can no longer maintain contact with the bed (Hampton, 1972; Mohrig et al., 1998). The coherent

nature of the flow makes difficult the entrainment into the flow of the water placed between the bed and the flow base. The thin layer of water that develops under the flow reduces friction and limits erosion. According to the experiments of Mohrig et al. (1998, 1999), the thickness of the lubricating layer decreases with distance from the flow front. This spatial change in the thickness of the basal water layer triggers differences in propagation velocity between the debris part riding on the layer of water and the trailing portion of the flow that is more attached to the bed (Parsons et al., 2007). These differences in velocity lead to stretching and attenuation of the flow behind the head and in some cases to the detachment of the head from the body and the formation of a new head.

The main process for debris flow deposition is freezing or en masse deposition (Lowe, 1982; Postma, 1986). The flow stops by cohesive freezing when its force-related shear resistance, which is controlled by viscosity and friction, equals and overcomes the driving force of gravity. The majority of larger and smaller grains do not segregate by differential settling during deposition. Due to the low water content of debris flows, the thickness of the deposit is similar to that of the flow while in motion (Mulder and Alexander, 2001), and may reach tens of meters (Lastras et al., 2005; Piper and Normark, 2009; Tripsanas et al., 2008). Low strength cohesive flows are more prone to mixing and diluting processes than high strength cohesive flows (Talling et al., 2012). The inclusion of water in a debris flow can lower its cohesive strength to a level where frictional forces overcome cohesive forces, and thus the flow becomes frictional. The threshold between cohesive and frictional behaviour is defined by the proportion of cohesive (clay) and non-cohesive (sand) particles. However, the limit boundary is not well constrained and varies according to concentration and flow conditions (Fisher, 1983; Iverson, 1997). Fine grained sediment flows can move cohesively with as little as a 2% clay volume, whilst in coarse-grained sediment the clay threshold to move as a cohesive flow reaches 19% (Hampton, 1975).

Debris flows may undergo transformation during flow by mixing and dilution of the head (Hampton, 1972), through water entrainment at the upper boundary of the flow body or after experiencing a hydraulic jump (Fisher, 1983). These processes favour the increase of turbulence and the generation of turbidity currents and grain flows. Laboratory experiments have shown how small amounts of clay can hamper turbulence in an initially highly turbulent flow and transform it into an almost laminar plug flow (Baas et al., 2009, 2011; Sumner et al., 2009).

3.4. Frictional flows

In addition to the ones mentioned above, in their classification of subaqueous sediment gravity flows Mulder and Alexander (2001), based primarily on sediment concentration, also considered aspects such as Reynold stresses and dominant depositional characteristics that are closely related. As a result they defined three main classes of frictional flows with no discrete boundaries amongst them: hyperconcentrated density flows, concentrated density flows and turbidity currents. Such subdivision takes into account flow transformation with space and time and its progressive dilution. Flow behaviour, particle support mechanisms and deposit characteristics appear to depend on concentration following a continuous pattern (Fig. 1.7).

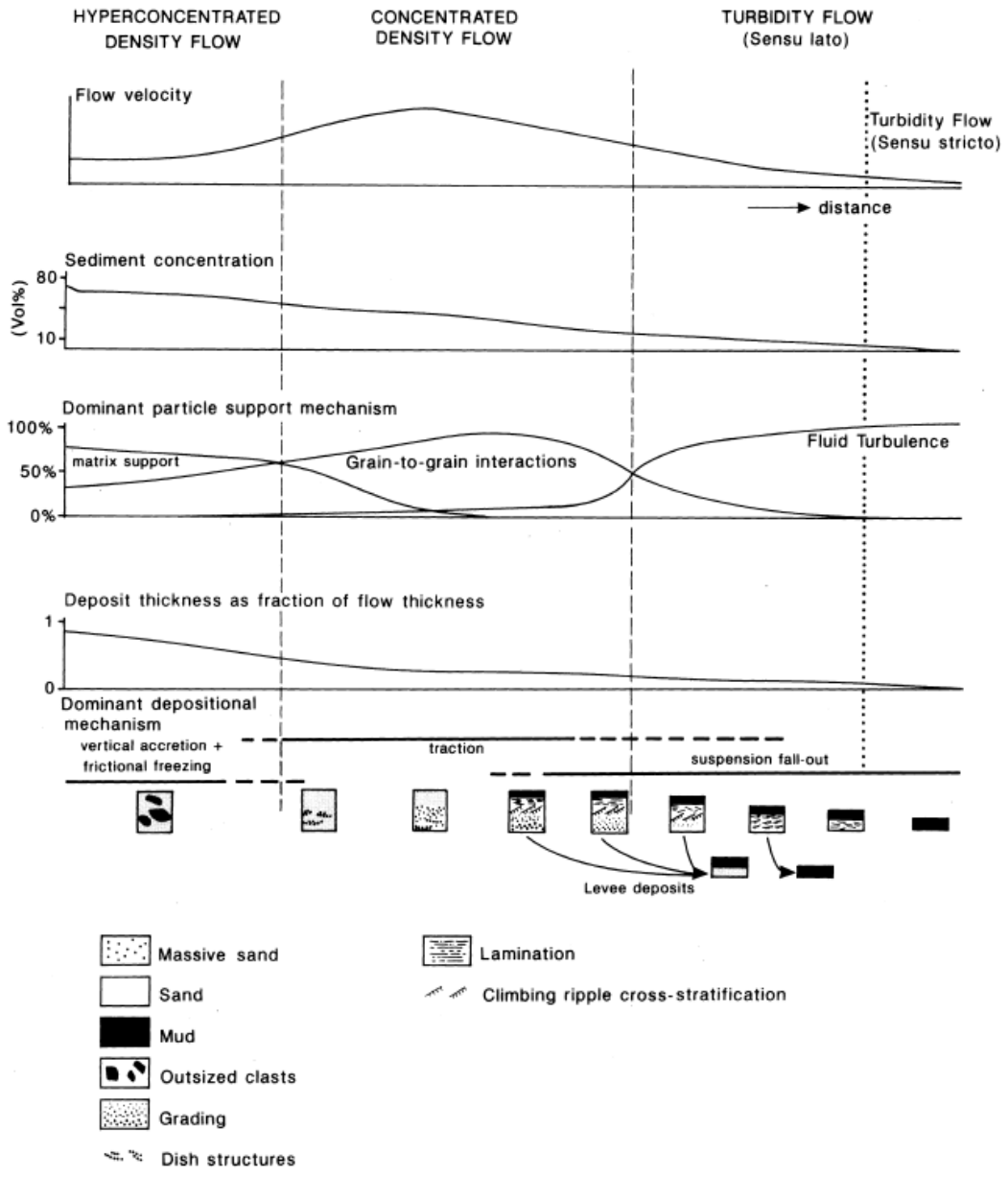

FIG.1.7 COMPOSITE DIAGRAM ILLUSTRATING THE RELATIONSHIPS BETWEEN FLOW VARIABLES, FLOW BEHAVIOUR AND DEPOSIT CHARACTERISTICS FOR FRICTIONAL FLOWS (FROM MULDER AND ALEXANDER, 2001).

Hyperconcentrated density flows have similar proportions of solid and liquid components than cohesive flows. They are presented as non-Newtonian fluids lacking of yield strength.Since contents of cohesive material are low (<2%) cohesive forces can be easily overcome by grain-to-grain collisions and turbulence. Clean-sand debris (Talling et al., 2012), sandy debris flows (Shanmugam, 1996) or fluidized density flows (Mutti et al., 2003) fit into the hyperconcentrated density flows category proposed by Mulder and Alexander (2001). Under low levels of cohesive particles turbulence can be easily generated by changes in topography, which can lead to density flows with lower concentration (i.e. concentrated density flows) (Kneller and Buckee, 2000a).

According to this classification concentrated flows typically present sediment concentrations in excess of 25% volume, with segregation of larger grains (i.e. differential settling), and are partially turbulent. However, turbulence is not the only important support mechanism. Several particle support mechanisms are at play in concentrated density flows, with grain-to-grain interaction playing a major role. Grain-to-grain interactions act in two ways: causing dispersive pressures and non-

elastic collisions between grains. Dispersive pressures contribute to keep the grain in motion, while non-elastic collisions result in energy dissipation and flow deceleration. As the flow moves along a slope it can suffer transformations too. Flows over low gradient slopes show low rates of water entrainment. Hence grain-to-grain interactions may lead to more concentrated flows and frictional freezing and deposition. On the contrary, concentrated flows can reach high velocities over steep slopes due to the large density contrast with the ambient water. The erosion and entrainment of bed sediment contribute to the acceleration and growth of the flow. The upper part of concentrated flows can be fully turbulent whilst in the lower part of the flow near-bed transport of coarse particles due to particle fall-out within the flow may take place. These flows are similar to the stratified high-density currents of Lowe (1982), Postma (1986), Kneller and Branney (1995), and Talling et al. (2012).

Mulder and Alexander (2001) proposed the 9% volume concentration limit for turbulent suspensions given by Bagnold (1962) as the threshold value to define turbidity currents *sensu stricto*. Additionally, they gave a second criteria following Middleton and Hampton (1973): turbidity currents *sensu lato* are those flows in which turbulence is the main particle support mechanism. Whereas Bagnold's limit considers exclusively concentration of non-cohesive sediment in a flow, devoted experiments have shown that turbulence damping can occur at clay concentrations as low as <1% (Baas et al., 2011).

Mulder and Alexander's (2001) classification is instructive and widely used, however it presents several weaknesses. The given discrete boundaries in sediment concentration ranges (Fig. 1.7) can be misleading. In reality sediment concentration determines flow behaviour and deposit in a continuous manner. The classification mostly focuses on frictional non-cohesive flows, in reality mud-free flows are a minority in nature. Sandy debris flows and grain flows imply plastic behaviour whilst in the classification they are considered as non Newtonian fluids. The notion of flow density is also misleading because it refers to both flow's absolute density (i.e. sediment concentration) when talking of flow behaviour and to relative density of different flows (i.e. more or less concentrated) in a comparative way. As such a flow can be "low density" compared to a hyperconcentrated flow, be "high density" when turbulence is suppressed due to sediment concentration and again "high density" when it spreads as an underflow along the sea floor (in contraposition to hypopycnal flows). The term turbidity is limited in their classification to flows with Newtonian behaviour (i.e. highly diluted, extremely low density turbidity currents only). The misconception of turbidity currents being exclusively Newtonian fluids might have its origins in hydrodynamic calculations since a constant viscosity is often assumed for simplicity. Nemec (1995) pointed out the influence of the volumetric concentration of sediment on the apparent viscosity, since the volumetric concentration of a turbidity current varies both in time and space, so should do the viscosity.

3.5. Depositional features

Changes in grain support mechanisms are expected to be reflected in the deposits. Higher concentration values lead to hindered sediment settling. Hence, hyperconcentrated flows present little or no normal grading whilst well-developed normal vertical grading (fining upward) is associated with turbidity currents. Size segregation and incremental deposition produce graded deposits, unless only a single grain size is available in the flow or concentration and velocity are steady (Kneller and Branney, 1995). Concentrated flows are situated in the continuum between the two end members of frictional flows (i.e. hyperconcentrated flows and turbidity currents). Their deposits are probably influenced by the sediment-support mechanisms acting simultaneously. At high concentrations, sediment sorting is hindered, and thus normal grading as proposed by the classic Bouma sequence does not develop. Normal grading can develop from deposition of the upper fully turbulent layer in stratified concentrated flows. Deposits of concentrated flows can show an irregular basal surface indicative of erosion. Massive sands or gravel overlay this erosional surface. Inversely graded deposits may develop under highly concentrated basal layers. Several causes have been pointed out

to explain the origin of inverse grading, such as traction carpets, sediment supply variation or pulsing flow of turbulent sweeps. The waning phase of quasi-steady hyperpycnal turbidity currents can also deposit inversely graded sequences (Kneller, 1995).

Bedform development under conditions of quasi-steady flow has received significant attention. If the lower basal layer presents low concentration, bedforms can develop as long as flow conditions are maintained long enough to achieve hydrodynamic equilibrium. Bedforms are thought to occur in deposits of concentrated density flows and turbidity currents (Mulder and Alexander, 2001). Ripple-cross laminations record deposition from a relatively dilute and fully turbulent suspension with relative low rates of sediment fallout (Walker, 1965; Baas et al., 2011). Ripples do not develop in laminar flows or flows in which turbulence is dumped by cohesive mud. Dunes form beneath dilute flows with very low sediment fallout rates (Southard, 1991). Dunes are commonly absent when turbulence is damped by high near-bed sediment concentrations (Baas et al., 2011), although dune-like features can form in high concentration flows (Lowe, 1982). Sumner et al. (2012) suggested that dunes would form under faster flow conditions than ripples. Concentrated flows are partly turbulent and more prolonged, and may maintain high velocities depending on the slope angle. The longer duration and turbulence favour erosion. Therefore, erosional features are likely to develop more extensively in deposits from concentrated flows than in those from turbidity currents or hyperconcentrated flows. Turbidites are formed incrementally in a layer-by-layer fashion in contrast to debrites formed by *en masse* deposition. Consquently, the vertical structure of a turbidite at a given location records the changing conditions experienced by the flow at that location. Changes through time at a specific location result from phases of waxing and waning (Kneller, 1995; Kneller and Branney, 1995). Changes in deposits are also due to spatial transformations of the flow (i.e. dissipation and accumulation). This means that turbidite thickness is unrelated to flow thickness. On the other hand, in *en masse* settling, deposit thickness is more closely related to flow thickness (Iverson, 1997). After freezing, the flow can continue consolidating in situ. Water entrainment can transform a dense flow into a more dilute one. Flow can also pass from a more dilute (turbulent) state towards a more concentrated (laminar) state (Talling et al., 2007). Studies by Baas et al. (2009, 2011), Sumner et al. (2009) and Cantero et al. (2012)) have shown how small amounts of cohesive mud strongly influence the character of the deposits and flow behaviour, with transformation of initially highly turbulent flows into almost laminar plug flows as they induce changes in fluid viscosity and yield strength. These results based on experimental modelling and direct observations show deviations from the classical sequences of Bouma (1962) and Lowe (1982).

4. Turbidity currents

The term “turbidity current” illustrates a lack of consensus within the scientific community. When Johnson (1938) introduced the term “turbidity current” he was referring to a current made of turbid or muddy sediment (cf. section 3.1). Kuenen and Migliorini (1950) defined “turbidity currents” as sediment-laden (turbid) flows that move downslope due to excess density. However, depending on the author, the term “turbidity current” denotes a flow state (turbulent), a dominant support mechanism (turbulence), or a given rheological behaviour (non-Newtonian) within a process by which sediment is accumulated layer-by-layer rather than en-masse. Here we consider turbidity currents as relatively diluted, fully turbulent flows in which sediment is primarily supported by turbulence. Turbidity currents would correspond to the diluted low-density member of the continuum of sediment gravity flows, but would also constitute the high-density member of a classification based on the density difference between the flow and the ambient water.

Present knowledge on turbidity currents is heavily based on studies on turbidites and to a lesser extent on the results of numerical and experimental modelling based on physical theory. However, it is true that often it is very difficult to infer the character of the flow from the deposits alone, as the links between deposits or erosion and flow conditions still are poorly constrained (Piper and Normark, 2009; Talling et al., 2012). Direct observations of turbidity currents are scarce and localized

due to their unpredictable and sometimes destructive character (i.e. also for scientific equipment) and to the remoteness of the environments where they most commonly occur. The first ever in-situ measurements of velocity structure within turbidity currents were reported by Xu et al. (2004). Many numerical and experimental models have been proposed within the past years with the aim of understanding the dynamics of turbidity currents. Laboratory flows differ from full-scale turbidity currents due to scaling issues and input conditions. Box models and depth-averaged models provide insight on key physical processes but fail in yielding information about the vertical structure of the flow. 3D models are useful but computationally too expensive. These aspects will be further explored in Chapter 2.

4.1. Initiation mechanisms

Turbidity currents require an initiation process so that sediment is brought into suspension in water and a sufficient gradient slope for flow to be maintained develops (Normark and Piper, 1991). Three main triggering mechanisms have been proposed for the initiation of turbidity currents: oceanographic processes, transformation of slope slides and debris flows, and discharges of sediment-laden river flows or subglacial meltwater (Piper and Normark, 2009; Talling et al., 2013).

Already in the 1950's Heezen and Ewing (1952) recognised the role of sediment failures as an initiation mechanism of turbidity currents. The resulting submarine slides or debris flows evolve due to progressive dilution into turbidity currents (Hampton, 1972; Normark and Piper, 1991; Parsons et al., 2007). Many slope failures are associated to earthquakes (Heezen et al., 1954; Cattaneo et al., 2012), but they can also occur as a result of rapid deposition and oversteepening (Khripounoff et al., 2012). Turbidity currents associated with hyperpycnal river discharge have been monitored in the Var canyon in France (Khripounoff et al., 2009) and the Gaoping canyon offshore Taiwan (Liu et al., 2012). Hyperpycnal activity has also been inferred from sediment cores in the Var canyon (Mulder et al., 2001) and the Sepik canyon off New Guinea (Walsh and Nittrouer, 2003). Sediment resuspended by wave action can later be transported to canyons during storms triggering turbidity currents (Puig et al., 2004a; Palanques et al., 2009; Mulder et al., 2012).

Other initiating mechanisms for turbidity currents include volcanic eruptions (Hunt et al., 2011) and anthropogenic structures and activities, such as dam bursts (Mulder et al., 2009), destabilisation of mine tailings deposits (Normark, 1989), dumping of dredge material at a canyon head (Xu et al., 2004) and bottom trawling (A. Palanques et al., 2006; Puig et al., 2012). Turbidity currents can initiate in a wide framework of settings: freshwater lakes and reservoirs, delta fronts, river-fed canyons, canyon-fan and channel-levee systems and open continental slopes (Talling et al., 2013; Talling, 2014a). The duration of the triggering processes determines to some extent whether a surge (short events) or a more steady flow (larger duration events) is produced and the quantity of sediment remobilized (Piper and Normark, 2009)

4.2. Anatomy

Three sections can be differentiated along a turbidity current: head, body and tail, although the latter may lack (Fig. 1.8) (Middleton, 1966a, 1966b).

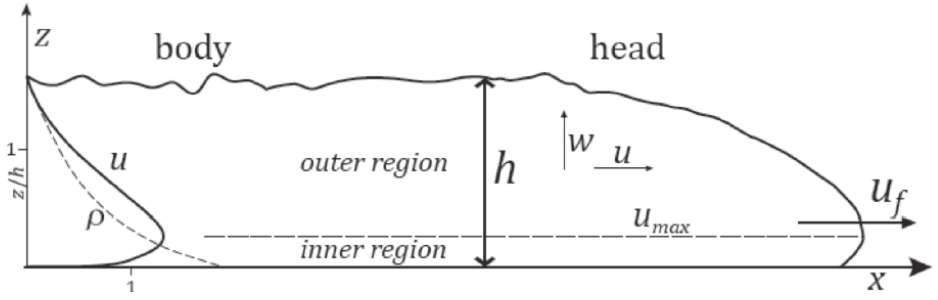

FIG1.8 SCHEMA OF TURBIDITY CURRENT SHOWING GENERALIZED VELOCITY AND DENSITY PROFILES BASED ON AN INTEGRAL LENGTH SCALE FOR CURRENT THICKNESS (FROM MEIBURG AND KNELLER, 2010).

The dynamics of the head play a key role in the transport within any turbidity current. Moreover, they appear to set a variable boundary condition to the flow (Simpson and Britter, 1979). The head is mainly erosional leaving behind structures such as grooves and flute marks, and, therefore, of high sedimentological relevance (Allen, 1971; Middleton, 1993). The no-slip condition at the lower boundary (i.e. velocity must decrease to zero at the contact) and the frictional resistance at the upper boundary of the current cause the overhanging nose at the front of the head. An increase in the density difference between the current and the ambient water can reduce the height of the nose and enhance the extent of the overall turbulent mixing pattern of the flow (Simpson, 1997). Friction-induced entrainment at the upper boundary result in Kelvin-Helmholtz (K-H) billows (Britter and Simpson, 1978). The lobe and cleft structures at the base of the head are due to buoyancy instabilities when the head overrides and incorporates the ambient water (Simpson, 1969; Allen, 1971) (Fig. 1.9). These structures are also related to K-H instabilities. Middleton (1966a) showed that increasing the slope gradient has a limited contribution to the velocity of the head for lower slopes (<2°-3°). Some experiments showed that for steeper slope gradient (5-90°) the velocity of the head is only weakly dependent (Britter and Linden, 1980). Head velocity depends on the current thickness and its reduced gravity (e.g. Graf and Altinakar, 1998). The downstream velocity of the body does depend on the slope gradient, and also on its thickness and its reduced gravity,and often exceeds that of the head (Middleton, 1966a; Britter and Linden, 1980; Kneller et al., 1997). The body increases its velocity with the slope gradient, overtaking the current head and reinforcing it, as a result the head thickens (Britter and Linden, 1980; Simpson, 1997).

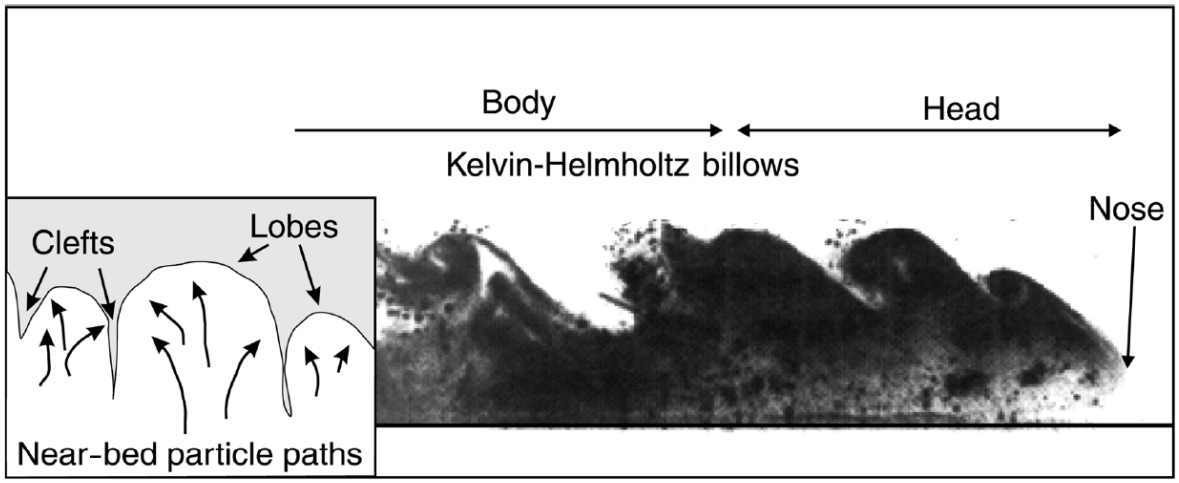

FIG1.9 PROFILE VIEW OF THE HEAD AND BODY OF A SALINE GRAVITY CURRENT ILLUSTRATING WELL DEVELOPED K-H BILLOWS. INSET SHOWS AN SCHEMATIC VIEW OF LOBES AND CLEFTS SEEN FROM BELOW (FROM KNELLER AND BUCKEE, 2000, AND SIMPSON, 1969).

During the initiation and development of a turbidity current, the head is subjected to forces such as pressure (due to the density difference), downslope component of the gravity force, bottom drag, interfacial frictions and buoyancy. The balance between driving forces (e.g. gravity) and resistant forces (e.g. frictional forces) controls the hydrodynamics, shape, duration and sedimentation of the flow. The higher density of the turbidity current leads to higher pressure force in the head, the pressure balance at the front of the head and in the head itself yields a net driving force. Turbidity currents over inclined planes are also driven by the along-slope component of the gravity force. The gravity force tends to dominate the motion of the current, although on steep slopes the gravity force component is reduced due to entrainment processes in the head. Buoyancy counteracts friction to produce steady flows (i.e. with constant head velocity) for slopes >0.34° (Britter and Linden, 1980). For slopes >5° bottom drag plays a less important role, and friction at the upper boundary becomes the force compensating buoyancy due to increased entrainment

Interfacial friction and bottom drag increase the level of turbulence in the head. Two types of instabilities appear in fully turbulent flows and are responsible for the entrainment of ambient water and the associated kinetic energy loss. Interfacial friction causes K-H instabilities and entrainment of ambient water. Buoyancy-induced instabilities are associated to bottom drag, causing the flow to override the ambient fluid which is subsequently entrained into the current forming lobes and clefts. Despite the increasing interfacial mixing due to K-H instabilities in increasing slopes, the front speed remains constant because the larger gravitational force in steeper slopes is counterbalanced by the increased entrainment in the head and the flow behind (Siegenthaler and Buhler, 1985). The turbulence structure of turbidity currents is dominated by shearing at the upper boundary. Kneller et al. (1997, 1999) and Parsons and García (1998) investigated experimentally the turbulence structure: time series of instantaneous downstream velocity record a quasi-steady flow with superimposed low frequency K-H billows. García and Parsons (1996) demonstrated experimentally that mixing in the head of gravity currents is dependent on the Reynolds number, with dimensionless mixing rates decreasing with diminishing Reynolds numbers. In currents with high Reynolds number, entrainment is due mainly to secondary instabilities (i.e. K-H vortex breakdown), whilst in currents with low Reynolds number entrainment due to secondary instabilities is less important as viscous effects appear to be enhanced. Ellison and Turner (1959) showed that entrainment into the current head is function of the densiometric Froude number thus depending on the initial reduced gravity of the current. Further experimental studies have shown that entrainment due to overriding is rather irrelevant (Simpson and Britter, 1979; Parsons and García, 1995).

The body of the current is the region behind the head. According to Ellison and Turner (1959), the body constitutes a region of steady downstream velocity. Two different regions can be identified along the current body, which keeps its thickness essentially constant: a lower denser part and an upper less dense region due to mixing with the ambient fluid (Ellison and Turner, 1959; Britter and Simpson, 1978). The latter has also been described as a succession of large eddies (Ellison and Turner, 1959). K-H billows would be the responsible for the transfer of sediment from the current head back into the body. Laboratory measurements have revealed the presence of large advective coherent structures within quasi-steady currents (Kneller et al., 1997). Instantaneous downstream velocities have shown values up to 40% higher than the maximum mean downstream velocities (Buckee et al., 2001). High turbulent velocities would imply high Reynolds stresses (Kneller et al., 1997) and, thus, high potential erosion rates. Therefore, the body of the current may play a significant role in the sediment entrainment. Velocities in the body are higher than those in the head (Kneller and Buckee, 2000) as such the body might overtake the head increasing its thickness for a given slope.

Surge type currents seem to be dominated by the properties of the head whilst sustained or quasi-steady flows appear to be dominated by those of the body (Meiburg and Kneller, 2010). In quasi-steady state or equilibrium conditions, minor changes occurring in the downstream direction are limited to the effects of the gradual entrainment of ambient water and entrainment or deposition of suspended sediment. The velocity remains approximately constant even in net depositional currents due to the balance between the decreasing density and increasing current thickness due to ambient fluid entrainment (Turner, 1973).

The tail is the thin and diluted part of the flow behind the body (Mulder, 2011). Sediment transported by the tail gradually settles due to energy loss during downslope flow of turbidity currents. As such, it is responsible for most of the deposition of the turbidity current.

Turbidity currents are described as vertically stratified both in velocity and density. Stratification is an important characteristic of turbidity currents as it has effects on depositional processes (e.g. flow spilling and stripping on obstacles). The vertical structure of turbidity currents allows the distinction of 2 different zones: an inner wall bounded region and an upper region bounded at the upper end by the interface between the current and the ambient flow. The lower region shows a positive velocity gradient similar to a conventional turbulent boundary layer (Altinakar et al., 1996; Simpson, 1997).

The upper outer region presents a negative velocity gradient. The limit between both regions is determined by the height of the velocity maximum. The ratio of the drag forces at the upper and lower boundaries appears to control the height of the velocity maximum (Middleton, 1966b; Kneller et al., 1997). Results from experimental studies place the velocity maximum at about 0.2-0.3 times the total height of the current (Altinakar et al., 1996; Kneller et al., 1997, 1999). Different values for the location of the velocity maximum were proposed by Sloff (1997) depending on the state of the flow. For internally supercritical currents (i.e. with Froude number >1) the velocity maximum would be located at about 15% of the total height of the turbidity current. For internally subcritical currents (i.e. with Froude number <1) the velocity maximum would be located at about 40% of the total height of the turbidity current. Turbulent kinetic energy is close to zero at the height of the velocity maximum (Kneller et al., 1999; Kneller and Buckee, 2000b).

Gravity currents also are density stratified (Stacey and Bowen, 1988) following the vertical distribution of suspended sediment. They present a poorly mixed lower dense layer and a homogeneous mixed upper layer. Currents with different dynamics display different concentration profiles. Low concentration, weakly depositional currents show smoother profiles (Garcia, 1994; Altinakar et al., 1996) than erosional currents (Garcia, 1993) or currents with high entrainment rates at the upper boundary (Peakall et al., 2000). Fine-grained sediment is uniformly distributed in the vertical direction whilst coarser sediment appears to concentrate in the lower part of the current (Garcia, 1994). The vertical sediment concentration seems to follow a power law distribution with an exponent proportional to the ratio of the shear velocity to the sediment settling velocity (Middleton and Southard, 1984). Therefore, currents with a broad range of grain sizes appear to be stratified both in concentration and grain size, and grain size ranges appear to be broader near the base than in the upper part of the current.

4.3. Magnitude and duration

In most settings there is a complex feedback between triggering mechanisms, flow transformations and the associated slope morphology (Piper and Normark, 2009). The scale of the triggering mechanism determines the duration of the flow (i.e. whether a surge or a more steady flow is developed) and, to some extent, the total flux of sediment.

Steady turbulent flow occurs when the mean velocity at a point remains unchanged over a specific period of time. Flows presenting increasing velocity at a given point are called **waxing flows** whilst those having decreasing velocity are called **waning flows**. A flow is considered **uniform** when there are no spatial changes in velocity. Changes in velocity can also occur along a streamline at a given time in non-uniform flows. Flow non-uniformity is mainly related to changes of the slope gradient (McCaffrey et al., 2003). Flows moving above a convex-up slope profile or confined by a channel accelerate and become **accumulative**. Flows moving above a concave-up slope or spreading at a canyon mouth decelerate and become **depletive**. Kneller (1995) and Kneller and Branney (1995) established a relationship between velocity changes, both in time and space, and vertical grain size trends of the deposit (Fig. 1.10).

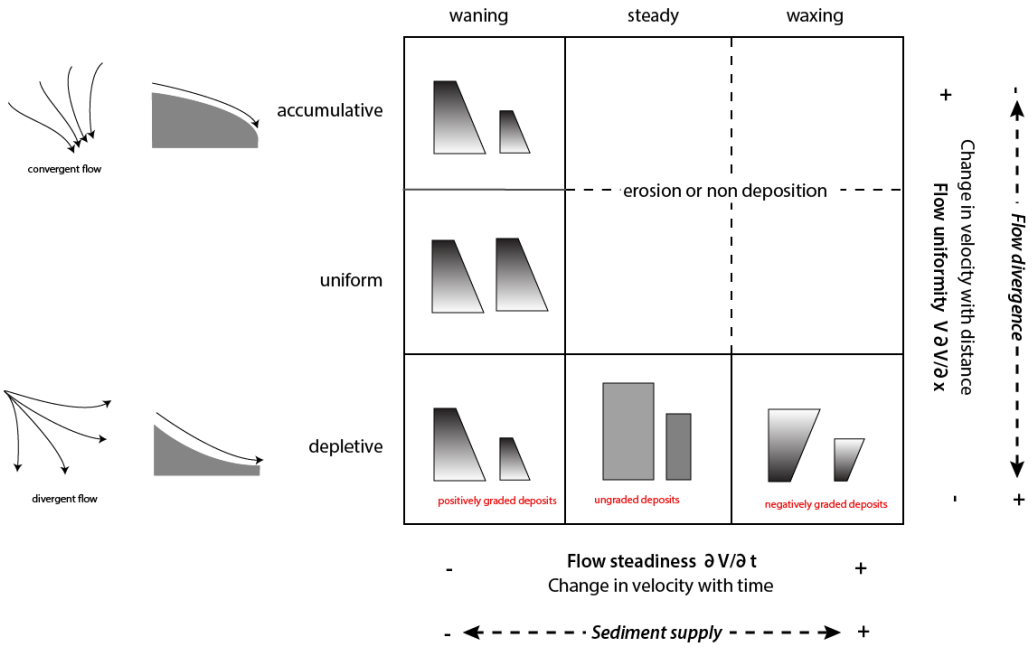

FIG1.10 ACCELERATION MATRIX MODIFIED FROM KNELLER, 1995, AND KNELLER AND BRANNEY, 1995)

All natural flows are unsteady, but in certain situations they can be quasi-steady for hours to days (Shepard et al., 1979). Taking into account the steadiness of the flow, Mulder and Alexander (2001) differentiated surge-like flows (i.e. associated with short-lived events) and quasi-steady flows (i.e. associated with quasi-continuous events).

Surge-like turbidity currents are often related to short-lived events with no permanent supply, such as some oceanographic processes and slope failures. Surge-like flows are strongly non-uniform and often show a negligible body and no tail (Middleton, 1966a). Their evolution is dominated by the dynamics of the head. The body, if developed, is highly unsteady and non-uniform. These flows display non-uniform velocity profiles along their length (Middleton, 1966a), and a strong vertical concentration gradient with turbulent flow at the top and concentrated flow at the base (Stacey and Bowen, 1988; Kneller and Buckee, 2000b). Surge- type turbidity currents are mostly depletive waning-flows producing normally graded sequences. Surges are mainly depositional and transport particles with grain sizes smaller than sand (Mulder and Alexander, 2001). There is no long distance bed load transport and turbulence is the main particle support mechanism. Their duration, capacity and net depositional result depend on the scale of the event. Small events are likely to have thickness of centimetres to metres and may last for seconds to minutes. At the other end, large events (i.e. those triggered by earthquakes) may last for hours and have thicknesses of tens to hundreds of meters. Large scale events may involve the development of a long body. The head and part of the body are usually waxing and erosive while the rest of the body and the tail are waning. Some surge like turbidity currents can be generated by retroregressive slumps and slides so that the sediment supply is maintained for weeks to moths. In this case, the dynamics of the turbidity current would be similar to those of quasi-steady turbidity currents.

Quasi-steady hyperpycnal turbidity currents are fed by prolonged sediment supply at river mouths, which usually lasts from hours to months (Mulder and Syvitski, 1995). The dynamics of these turbidity currents is governed by those of their long steady body, as they present insignificant head or tail. They have more gradual vertical gradients than surge-like turbidity currents (Mulder and Alexander, 2001; Alexander and Mulder, 2002). The flow may be uniform or non-uniform, depending on slope gradient and initial momentum. Generally, for an equal slope angle, the average velocity of hyperpycnal flows is smaller than that of surge-like turbidity currents (Alexander and Mulder, 2002).

Hyperpycnal currents have received considerable attention, as they may be responsible for deposits previously attributed to slope failures. Hyperpycnal fluxes tend to mimic those of the river system they are associated to (Talling, 2014a). Subsequently, the sedimentary features they produce are more complex than those of other gravity flows. Velocity changes at the river mouth depend on the origin of the flood, rain distribution and intensity, and catchment behaviour, which control discharge volume and overall pattern. The flow is accumulative at the nearshore if it presents a steep slope or the flow is channelled, which eases sediment reworking. Insignificant deposition is expected for waxing flows. Beyond the break-of-slope the flow spreads and becomes depletive. Sediment can then accumulate following a coarsening-up trend during the waxing phase. Erosional areas move seaward as the flow continues to wax and thus areas that were initially depositional can become erosional. The maximum deposition area moves landward once the flow starts to wane. Variations in flood development and sediment flux patterns, together with shifts of environmental conditions with distance from the river mouth, usually results in a large diversity of sedimentary sequences (Mulder and Alexander, 2001). Three main criteria have been used to identify the deposits of hyperpycnal currents deposits (hyperpycnites): inverse to normal grading sequences in which the inversely-graded unit has been partly or totally eroded before deposition of the normally graded unit; presence of climbing ripples due to the steady migration of sedimentary bedforms as long as sediment supply is maintained; and abundant allochtonous freshwater fossils (Mulder and Alexander, 2001; Mulder et al., 2001). Recent studies have shown that a single flood peak can generate a flow with multiple pulses thus, deposit grading can be substantially more complex than inverse-to-normal grading (Khripounoff et al., 2012; Liu et al., 2012). Abundant freshwater organic matter doesn't seem to be a strong proxy for hyperpycnal flows as failure of recently deposited flood sediment may also generate flows with abundant organic matter (Talling, 2014b).

4.4. Depositional features

Three parameters of the flow are closely related to the ability of turbidity currents to transport sediment in suspension to a certain distance: flow competence, flow capacity, and flow efficiency. **Flow competence** is the ability of the flow to transport large grain sizes; **flow capacity** is the total amount of sediment a flow can carry; and **flow efficiency** is the ability of a flow to carry sediment according to its clay content (Pickering et al., 1989). High energy turbidity currents show high values for these three parameters, which means that they are able to transport large volumes of sediment with high proportions of coarse material over long distances to finally form well-sorted deposits.

Erosive flows become denser and faster as they entrain sediment, thereby causing further erosion and acceleration in a process called **ignition** (Parker, 1982; Parker et al., 1986; Sequeiros et al., 2009). **Autosuspending flows** are sufficiently powerful to suspend all the sedimentary particles they carry but do not erode the seafloor. Deposits form as the flow decelerates. Deceleration can be due to exhaustion of sediment supply or to slopes gradient lowering subsequently leading to gradual lessening of the driving force of gravity. Flows that deposit sediment become more diluted and move slower, causing further sediment deposition and deceleration in a process called **dissipation**. Grains settle out of the suspension, mainly from the body and the tail, as the flow loses capacity. Coarser grains would settle first and finer ones in a later stage, finally resulting in a normally graded sequence.

A turbidite is a sedimentary bed deposited layer-by-layer by a (low concentration) turbidity current. It is composed of layered particles that grade upward from coarser to finer sizes. Turbidites ideally display complete or incomplete Bouma sequences (Bouma, 1962). The Annot sandstone, where the Bouma sequence was defined (cf. section 3.1), contains five intervals above a sharp boundary or erosion contact, which from base to top are: Ta (massive to graded sand), Tb (parallel laminated sand), Tc (cross laminated sand and silt), Td (parallel laminated sand to silt) and Te (laminated to homogeneous mud). The ideal complete Bouma sequence is not always observed in the turbidites. It

is usually truncated either in its upper or basal part. Bouma linked the vertical evolution of the sequence to the evolution in time of transport capacity and current speed of the turbidity current. The proposed sequence was quickly criticized. In 1964, Sanders, associated that sequence to two different processes: a “lit coulant" of grains for the Ta interval and a turbulent current for intervals Tb to Te. Also, turbidity flows can develop from stratified flows with strong vertical velocity gradient (Fisher, 1983). Stratified flows show a basal laminar flow and an upper turbulent flow. The basal part displays hindered suspension settling due to high sediment concentration (Mulder, 2011). The lower, poorly graded Ta interval was then associated to deposition from such concentrated basal laminar flow. Intervals Tb to Te would record the passage of the fully turbulent upper part of the flow and would reflect the deceleration it experiences (Walker, 1965). The parallel laminated sand interval Tb responds to the plane-bed transport of sand in the upper turbulent flow regime. The cross-laminated sand and silt Tc interval results from the settling of sand and silt from suspension in the upper flow while the lower-flow regime current ripples migrate on the seabed. Climbing ripple cross-lamination (i.e. Tc) derives from rapid fallout, whereas convolute lamination indicates short-lived liquefaction. The ripple cross-lamination in Tc is the most common structure in turbidites (Mulder, 2011). The two uppermost intervals, Td and Te, are direct products of suspension settling. The Te division results from the interaction of pelagic and fine particle settling from the tail of the turbulent flow.

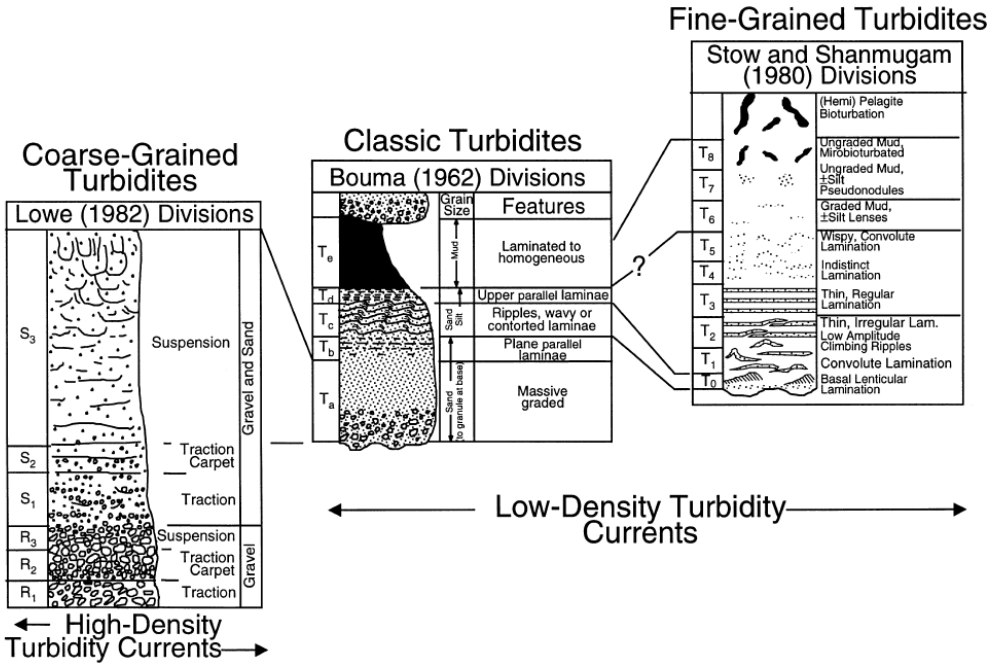

FIG1. 11 VERTICAL FACIES MODELS OF COARSE-GRAINED TURBIDITES (LOWE, 1982), CLASSIC TURBIDITES ALSO KNOWN AS THE BOUMA SEQUENCE (BOUMA, 1962), AND FINE-GRAINED TURBIDITES (STOW AND SHANMUGAM, 1980) IN SHANMUGAM, (2000).

It has to be noted that many deep-water deposits do not fit Bouma’s description as “a graded deposit originating through suspension fall-out from a turbid underflow” (Bouma, 1962). Nevertheless, the Bouma sequence is useful for describing deposits from waning turbidity currents with fine grain sizes. Lowe (1982) proposed a theoretical model for deposits from high-density turbidity currents with the aim of complementing (i.e not replacing) the better known Bouma sequence. Talling et al. (2012) provided an exhaustive review on the different criteria and classifications proposed to date. Assuming their limitations, idealized vertical sequences with characteristic sedimentary structures, such as the models proposed by Bouma (1962) and Lowe (1982), are useful proxies for approaching natural flow conditions and for experimental and numerical modelling of turbidity currents (Baas et al., 2000). However, we must recognise that field observations show significant deviations from the previously cited models and that the precise link of turbidity current dynamics with resulting deposits still remains an unsolved question.

4.5. Classic models of turbidite systems: a quick overview

Single turbidity currents produce individual turbidity packages with thicknesses ranging from millimetres to meters. At geological scales, the succession of turbidity events over long periods of time can lead to the outbuilding of channel-levee complexes and submarine fans tens to hundreds of meters thick. Gravity currents including turbidity currents move down submarine canyons and channels to finally spread over the wider base of slope and basin where they form deep-sea turbidite systems. Several models of turbidite systems have been proposed since the 1970s. The first models focused on morphological aspects of deep-sea fan channels (Normark, 1970; Mutti and Lucchi, 1972). Later on deposits and related flows in passive margins were taken into account to develop the so-called Walker model (Walker, 1978; Shanmugam and Moiola, 1991). This model considers the progradational architecture of deep-sea fans and distinguishes three provinces in the fan: upper fan, middle fan, and lower fan. Slides and debris flows generate at the proximal feeder channel in the upper slope. The flows progress downslope and coarse-grained hyperconcentrated flow deposits develop in the main feeder channels of the upper fan whilst overspilling and flow stripping lead to thin-bedded levee deposits. Distributary channels and lobes characterise the middle fan and the lower fan displays Bouma type turbidites. This model, however, is not suitable for giant muddy fans on passive continental margins and its definition of upper fan is rather inconsistent with most modern data (Mulder, 2011).

Sequence stratigraphy places submarine fans and related turbidite systems in the temporal and spatial context of sedimentary basin development (Posamentier and Vail, 1988). Therefore, sequence stratigraphic models consider basin scale factors, such as sediment supply, tectonic context and changes in eustacy. Shanmugam and Moiola (1988, 1991) and Reading and Richards (1994) provide good examples of sequence stratigraphy models. The Shanmugam model distinguishes four different types of turbidite systems: small sandy systems with well-developed lobes from immature passive margins (e.g. North Sea); large muddy systems with small lobes from mature passive margins (e.g. Atlantic); small sandy systems with large lobes from active margins (e.g. Pacific); and mixed systems that display characteristics either of Atlantic type (e.g. Bengal Fan) or Pacific type (e.g. Orinoco Fan) (Shanmugam and Moiola, 1988, 1991).

Reading and Richards (1994) proposed a twelve member classification based on the character of the sediment source (i.e. point, linear or multiple source) and on grain size (i.e. mud-rich, mud-sand rich, sand rich and gravel-rich). Bouma (2000, 2004) suggested two end members: coarse-grained, sand-rich turbidite systems, and fine-grained, mud-rich turbidity systems. Coarse-grained systems are typical from active margins and show low confinement, whereas fine-grained turbidite systems typically occur in passive margins confined settings. However, this vision is challenged by the most recent findings on modern hydrosedimentary processes that are able to carry large amounts of coarse sediment to deep-sea depositional systems in passive margins (e.g. Canals et al., 2006; Lastras et al., 2008).

References

Ahumada-Sempoal, M.-A., Flexas, M.M., Bernardello, R., Bahamon, N., Cruzado, A., 2013. Northern Current variability and its impact on the Blanes Canyon circulation: A numerical study. Prog. Oceanogr. 118, 61–70. doi: 10.1016/j.pocean.2013.07.030.

Alexander, J., Mulder, T., 2002. Experimental quasi-steady density currents. Mar. Geol. 186, 195–210. doi: 10.1016/S0025-3227(02)00313-4.

Allen, J.R.L., 1971. Mixing at turbidity current heads, and its geological implications. J. Sediment. Res. 41, 1, 97-113.

Allen, S.E., 2004. Restrictions on deep flow across the shelf-break and the role of submarine canyons in facilitating such flow. Surv. Geophys. 25, 221–247. doi: 10.1007/s10712-004-1275-0.

Allen, S.E., Durrieu de Madron, X., 2009. A review of the role of submarine canyons in deep-ocean exchange with the shelf. Ocean Sci. Discuss. 6, 1369–1406. doi:10.5194/osd-6-1369-2009.

Altinakar, M.S., Graf, W.H., Hopfinger, E.J., 1996. Flow structure in turbidity currents. J. Hydraul. Res. 34, 713–718. doi: 10.1080/00221689609498467.

Amblàs, D., Canals, M., Lastras, G., Berné, S., Loubrieu, B., 2004. Imaging the seascapes of the Mediterranean. Oceanography 17, 144–155. Doi: 10.5670/oceanog.2004.11.

Ardhuin, F., Pinot, J.-M., Tintoré, J., 1999. Numerical study of the circulation in a steep canyon off the Catalan coast (western Mediterranean). J. Geophys. Res. Oceans 104, 11115–11135. doi:10.1029/1999JC900029

Baas, J.H., van Dam, R.L., Storms, J.E.A., 2000. Duration of deposition from decelerating high-density turbidity currents. Sediment. Geol. 136, 71–88. doi:10.1016/S0037-0738(00)00088-9

Baas, J.H., Best, J.L., Peakall, J., Wang, M., 2009. A phase diagram for turbulent, transitional, and laminar clay suspension flows. J. Sediment. Res. 79, 162–183. doi:10.2110/jsr.2009.025

Baas, J.H., Best, J.L., Peakall, J., 2011. Depositional processes, bedform development and hybrid bed formation in rapidly decelerated cohesive (mud–sand) sediment flows. Sedimentology 58, 1953–1987. doi:10.1111/j.1365-3091.2011.01247.x

Babonneau, N., Savoye, B., Cremer, M., Bez, M., 2004. Multiple terraces within the deep incised Zaire Valley (ZaïAngo Project): are they confined levees? Geol. Soc. Lond. Spec. Publ. 222, 91–114. doi:10.1144/GSL.SP.2004.222.01.06

Bagnold, R.A., 1954. Experiments on a gravity-free dispersion of large solid spheres in a Newtonian fluid under shear. Proc. R. Soc. Lond. Math. Phys. Eng. Sci. 225, 49–63. doi:10.1098/rspa.1954.0186

Bagnold, R.A., 1962. Auto-suspension of transported sediment; turbidity currents. Proc. R. Soc. Lond. Ser. Math. Phys. Sci. 265, 315–319. doi:10.1098/rspa.1962.0012

Bassetti, M.A., Jouet, G., Dufois, F., Berné, S., Rabineau, M., Taviani, M., 2006. Sand bodies at the shelf edge in the Gulf of Lions (Western Mediterranean): Deglacial history and modern processes. Mar. Geol. 234, 93–109. doi:10.1016/j.margeo.2006.09.010

Baztan, J., Berné, S., Olivet, J.-L., Rabineau, M., Aslanian, D., Gaudin, M., Réhault, J.-P., Canals, M., 2005. Axial incision: The key to understand submarine canyon evolution (in the western Gulf of Lion). Mar. Pet. Geol. 22, 805–826. doi:10.1016/j.marpetgeo.2005.03.011

Bertoni, C., Cartwright, J., 2005. 3D seismic analysis of slope-confined canyons from the Plio–Pleistocene of the Ebro Continental Margin (Western Mediterranean). Basin Res. 17, 43–62. doi:10.1111/j.1365-2117.2005.00254.x

Biscara, L., Mulder, T., Martinez, P., Baudin, F., Etcheber, H., Jouanneau, J.-M., Garlan, T., 2011. Transport of terrestrial organic matter in the Ogooué deep sea turbidite system (Gabon). Mar. Pet. Geol. 28, 1061–1072. doi:10.1016/j.marpetgeo.2010.12.002

Bouma, A.H., 1962. Sedimentology of some flysch deposits. A graphic approach to facies interpretation. Amsterdam, Elsevier.

Bouma, A.H., 2000. Coarse-grained and fine-grained turbidite systems as end member models: applicability and dangers. Mar. Pet. Geol. 17, 137–143. doi:10.1016/S0264-8172(99)00020-3

Bouma, A.H., 2004. Key controls on the characteristics of turbidite systems. Geol. Soc. Lond. Spec. Publ. 222, 9–22. doi:10.1144/GSL.SP.2004.222.01.02

Boyd, R., Ruming, K., Goodwin, I., Sandstrom, M., Schröder-Adams, C., 2008. Highstand transport of coastal sand to the deep ocean: A case study from Fraser Island, southeast Australia. Geology 36, 15–18. doi:10.1130/G24211A.1

Britter, R.E., Simpson, J.E., 1978. Experiments on the dynamics of a gravity current head. J. Fluid Mech. 88, 223–240. doi:10.1017/S0022112078002074

Britter, R.E., Linden, P.F., 1980. The motion of the front of a gravity current travelling down an incline. J. Fluid Mech. 99, 531–543. doi:10.1017/S0022112080000754

Buckee, C., Kneller, B., Peakall, J., 2001. Turbulence structure in steady, solute-driven gravity currents, in: McCaffrey, W., Kneller, B., Peakall, J. (Eds.), Particulate Gravity Currents. Blackwell Publishing Ltd., pp. 173–187. doi: 10.1002/9781444304275.ch13

Canals, M., 1985. Estructura sedimentaria y evolución morfológica del talud y glacis continentales del Golfo de León: fenómenos de desestabilización de la cobertura sedimentaria Plio-Cuaternaria. PhD Thesis, Univ. Barcelona, Spain, 618 p.

Canals, M., Casamor, J.L., Lastras, G., Monaco, A., Acosta, J., Berné, S., Loubrieu, B., Weaver, P., Grehan, A., Dennielou, B., 2004. The role of canyons on strata formation. Oceanography 17, 80–91. doi:10.5670/oceanog.2004.06

Canals, M., Puig, P., de Madron, X.D., Heussner, S., Palanques, A., Fabres, J., 2006. Flushing submarine canyons. Nature 444, 354–357. doi:10.1038/nature05271

Canals, M., Danovaro, R., Heussner, S., Lykousis, V., Puig, P., Trincardi, F., Calafat, A., Durrieu de Madron, X., Palanques, A., 2009. Cascades in Mediterranean submarine grand canyons. Oceanography 22, 26–43. doi:10.5670/oceanog.2009.03

Canals, M., Company, J.B., Martín, D., Sànchez-Vidal, A., Ramírez-Llodrà, E., 2013. Integrated study of Mediterranean deep canyons: Novel results and future challenges. Prog. Oceanogr., Integrated study of a deep submarine canyon and adjacent open slopes in the Western Mediterranean Sea: an essential habitat 118, 1–27. doi:10.1016/j.pocean.2013.09.004

Cantero, M.I., Cantelli, A., Pirmez, C., Balachandar, S., Mohrig, D., Hickson, T.A., Yeh, T., Naruse, H., Parker, G., 2012. Emplacement of massive turbidites linked to extinction of turbulence in turbidity currents. Nat. Geosci. 5, 42–45. doi:10.1038/ngeo1320

Cattaneo, A., Babonneau, N., Ratzov, G., Dan-Unterseh, G., Yelles, K., Bracène, R., Mercier de Lépinay, B., Boudiaf, A., Déverchère, J., 2012. Searching for the seafloor signature of the 21 May 2003 Boumerdès earthquake offshore central Algeria. Nat Hazards Earth Syst Sci 12, 2159–2172. doi:10.5194/nhess-12-2159-2012

Covault, J.A., Normark, W.R., Romans, B.W., Graham, S.A., 2007. Highstand fans in the California borderland: The overlooked deep-water depositional systems. Geology 35, 783–786. doi:10.1130/G23800A.1

Cronin, B.T., Akhmetzhanov, A.M., Mazzini, A., Akhmanov, G., Ivanov, M., Kenyon, N.H., 2005. Morphology, evolution and fill: Implications for sand and mud distribution in filling deep-water canyons and slope channel complexes. Sediment. Geol., Sedimentary Gravity Flows: Recent Advances in Process and Field Analysis 179, 71–97. doi:10.1016/j.sedgeo.2005.04.013

Crowell, J.C., 1957. Origin of pebbly mudstones. Geol. Soc. Am. Bull. 68, 993–1009.

Daly, R.A., 1936. Origin of submarine canyons. Am. J. Sci. s5-31, 401–420. doi:10.2475/ajs.s5-31.186.401

Dana, J.D., 1863. A manual of Geology. American Book Company.Doreen Jr, J.M., 1951. Rubble bedding and graded bedding in Talara Formation of northwestern Peru. Am. Assoc. Pet. Geol. Bull. 35, 1829–1849.

Durán, R., Canals, M., Sanz, J.L., Lastras, G., Amblas, D., Micallef, A., 2014. Morphology and sediment dynamics of the northern Catalan continental shelf, northwestern Mediterranean Sea. Geomorphology 204, 1–20. doi:10.1016/j.geomorph.2012.10.004

Durrieu de Madron, X., Zervakis, V., Theocharis, A., Georgopoulos, D., 2005. Comments on “Cascades of dense water around the world ocean.” Prog. Oceanogr. 64, 83–90. doi:10.1016/j.pocean.2004.08.004

Durrieu de Madron, X., Houpert, L., Puig, P., Sanchez-Vidal, A., Testor, P., Bosse, A., Estournel, C., Somot, S., Bourrin, F., Bouin, M.N., Beauverger, M., Beguery, L., Calafat, A., Canals, M., Cassou, C., Coppola, L., Dausse, D., D’Ortenzio, F., Font, J., Heussner, S., Kunesch, S., Lefevre, D., Le Goff, H., Martín, J., Mortier, L., Palanques, A., Raimbault, P., 2013. Interaction of dense shelf water cascading and open-sea convection in the northwestern Mediterranean during winter 2012: Shelf cascading and open-sea convection. Geophys. Res. Lett. 40, 1379–1385. doi:10.1002/grl.50331

Ellison, T.H., Turner, J.S., 1959. Turbulent entrainment in stratified flows. J. Fluid Mech. 6, 423–448.

Farre, J.A., 1983. Breaching the shelfbreak: passage from youthful to mature phase in submarine canyon evolution. SEPM Special Publication, 33, 25-39

Fisher, R.V., 1983. Flow transformations in sediment gravity flows. Geology 11, 273–274. doi:10.1130/0091-7613(1983)11<273:FTISGF>2.0.CO;2

Flexas, M.M., Boyer, D.L., Espino, M., Puigdefàbregas, J., Rubio, A., Company, J.B., 2008. Circulation over a submarine canyon in the NW Mediterranean. J. Geophys. Res. Oceans 113, C12002. doi:10.1029/2006JC003998

Forel, R.A., 1887. Le ravin sous-lacustre de Rhone dans le lac Leman. Bull. Société Vaudoise Sci. Na 23, 85–107.

Galloway, W.E., Dingus, W.F., Paige, R.E., 1991. Seismic and depositional facies of Paleocene-Eocene Wilcox group submarine canyon fills, northwest Gulf Coast, U.S.A., in: Weimer, P., Link, M.H. (Eds.), Seismic Facies and Sedimentary Processes of Submarine Fans and Turbidite Systems, Frontiers in Sedimentary Geology. Springer New York, pp. 247–271.

Garcia, M., 1993. Hydraulic jumps in sediment - driven bottom currents. J. Hydraul. Eng. 119, 1094–1117. doi:10.1061/(ASCE)0733-9429(1993)119:10(1094)

Garcia, M.H., 1994. Depositional turbidity currents laden with poorly sorted sediment. J. Hydraul. Eng. 120, 1240–1263. doi:10.1061/(ASCE)0733-9429(1994)120:11(1240)

Garcia, M.H., Parsons, J.D., 1996. Mixing at the front of gravity currents. Dyn. Atmospheres Oceans, Stratified flows 24, 197–205. doi:10.1016/0377-0265(95)00442-4

Garcia-Castellanos, D., Estrada, F. Jiménez-Munt, I. Gorini, C. Fernàndez, M. Vergés, J. De Vicente, R.,2009. Catastrophic flood of the Mediterranean after the Messinian salinity crisis. Nature 462, 778-782. doi:10.1038/nature08555

Gaudin, M., Berne, S., Jouanneau, J.-M., Palanques, A., Puig, P., Mulder, T., Cirac, P., Rabineau, M., Imbert, P., 2006a. Massive sand beds attributed to deposition by dense water cascades in the Bourcart canyon head, Gulf of Lions (northwestern Mediterranean Sea). Mar. Geol. 234, 111–128. doi:10.1016/j.margeo.2006.09.020

Gaudin, M., Mulder, T., Cirac, P., Berné, S., Imbert, P., 2006b. Past and present sedimentary activity in the Capbreton Canyon, southern Bay of Biscay. Geo-Mar. Lett. 26, 331–345. doi:10.1007/s00367-006-0043-1

Gee, Masson, Watts, Allen, 1999. The Saharan debris flow: an insight into the mechanics of long runout submarine debris flows. Sedimentology 46, 317–335. doi:10.1046/j.1365-3091.1999.00215.x

Green, A.N., Goff, J.A., Uken, R., 2007. Geomorphological evidence for upslope canyon-forming processes on the northern KwaZulu-Natal shelf, SW Indian Ocean, South Africa. Geo-Mar. Lett. 27, 399–409. doi:10.1007/s00367-007-0082-2

Hampton, M.A., 1972. The role of subaqueous debris flow in generating turbidity currents. J. Sediment. Res. 42, 775–793. doi:10.1306/74D7262B-2B21-11D7-8648000102C1865D

Hampton, M.A., 1975. Competence of Fine-grained Debris Flows. J. Sediment. Res. 45. 4, 834-844.

Harris, P.T., Whiteway, T., 2011a. Global distribution of large submarine canyons: Geomorphic differences between active and passive continental margins. Mar. Geol. 285, 69–86. doi:10.1016/j.margeo.2011.05.008

Heezen, B.., Ewing, M., 1952. Turbidity currents and submarine slumps, and the 1929 Grand Banks earthquake. Am. J. Sci. 250, 849–873.

Heezen, B.C., Ericson, D.B., Ewing, M., 1954. Further evidence for a turbidity current following the 1929 Grand banks earthquake. Deep Sea Res. 1953 1, 193–202. doi:10.1016/0146-6313(54)90001-5

Heezen, B.C., Hollister, C.D., Ruddiman, W.F., 1966. Shaping of the continental rise by deep geostrophic contour currents. Science 152, 502–508. doi:10.1126/science.152.3721.502

He, Y., Xie, X., Kneller, B.C., Wang, Z., Li, X., 2013. Architecture and controlling factors of canyon fills on the shelf margin in the Qiongdongnan Basin, northern South China Sea. Mar. Pet. Geol., Special Issue: Internal architecture, bedforms and geometry of turbidite channels 41, 264–276. doi:10.1016/j.marpetgeo.2012.03.002

Hickey, B.M., 1995. Coastal submarine canyons, in: Topographic effects in the ocean. Presented at the Aha Hulico: Hawaiian Winter Workshop, University of Hawaii, Honololu.

Hickey, B.M., 1997. The response of a steep-sided, narrow canyon to time-variable wind forcing. J. Phys. Oceanogr. 27, 697–726. doi:10.1175/1520-0485(1997)027<0697:TROASS>2.0.CO;2

Hollister, C.D., Heezen, B.., 1972. Geologic effects of ocean botttom currents: western North Atlantic, in: Studies in Physical Oceanography, A.L. Gordon. Gordon and Breach Science Publishers, New York, pp. 37–66.

Hollister, C.D., 1993. The concept of deep-sea contourites. Sediment. Geol. 82, 5–11. doi:10.1016/0037-0738(93)90109-I

Hsu, K.J., 1959. Flute- and groove-casts in the Prealpine Flysch, Switzerland. Am. J. Sci. 257, 529–536. doi:10.2475/ajs.257.7.529

Hsü, K.J., 1972. When the Mediterranean dried up. Sci. Am. 227, 26–36. doi:10.1038/scientificamerican1272-26

Hsü, K.J., Montadert, L., Bernoulli, D., Cita, M.B., Erickson, A., Garrison, R.E., Kidd, R.B., Mèlierés, F., Müller, C., Wright, R., 1977. History of the Mediterranean salinity crisis. Nature 267, 399–403. doi:10.1038/267399a0

Hunt, J.E., Wynn, R.B., Masson, D.G., Talling, P.J., Teagle, D.A.H., 2011. Sedimentological and geochemical evidence for multistage failure of volcanic island landslides: A case study from Icod landslide on north Tenerife, Canary Islands. Geochem. Geophys. Geosystems 12, Q12007. doi:10.1029/2011GC003740

Huppert, H.E., 2006. Gravity currents: a personal perspective. J. Fluid Mech. 554, 299–322. doi:10.1017/S002211200600930X

Ivanov, V.V., Shapiro, G.I., Huthnance, J.M., Aleynik, D.L., Golovin, P.N., 2004. Cascades of dense water around the world ocean. Prog. Oceanogr. 60, 47–98. doi:10.1016/j.pocean.2003.12.002

Iverson, R.M., 1997. The physics of debris flows. Rev. Geophys. 35, 245–296. doi:10.1029/97RG00426

Jobe, Z.R., Lowe, D.R., Uchytil, S.J., 2011. Two fundamentally different types of submarine canyons along the continental margin of Equatorial Guinea. Mar. Pet. Geol., Thematic Set on Stratigraphic evolution of deep-water architecture 28, 843–860. doi:10.1016/j.marpetgeo.2010.07.012

Johnson, D., 1938. The origin of submarine canyons. J. Geomorphol. 1, 11–340.

Jordi, A., Orfila, A., Basterretxea, G., Tintoré, J., 2005. Shelf-slope exchanges by frontal variability in a steep submarine canyon. Prog. Oceanogr. 66, 120–141. doi:10.1016/j.pocean.2004.07.009

Jouet, G., Berné, S., Rabineau, M., Bassetti, M.A., Bernier, P., Dennielou, B., Sierro, F.J., Flores, J.A., Taviani, M., 2006. Shoreface migrations at the shelf edge and sea-level changes around the Last Glacial Maximum (Gulf of Lions, NW Mediterranean). Mar. Geol., EUROSTRATAFORM VOL. 1: Source to Sink Sedimentation on the European Margin 234, 21–42. doi:10.1016/j.margeo.2006.09.012

Khripounoff, A., Vangriesheim, A., Babonneau, N., Crassous, P., Dennielou, B., Savoye, B., 2003. Direct observation of intense turbidity current activity in the Zaire submarine valley at 4000 m water depth. Mar. Geol. 194, 151–158. doi:10.1016/S0025-3227(02)00677-1

Khripounoff, A., Vangriesheim, A., Crassous, P., Etoubleau, J., 2009. High frequency of sediment gravity flow events in the Var submarine canyon (Mediterranean Sea). Mar. Geol. 263, 1–6. doi:10.1016/j.margeo.2009.03.014

Khripounoff, A., Crassous, P., Lo Bue, N., Dennielou, B., Jacinto, R.S., 2012. Different types of sediment gravity flows detected in the Var submarine canyon (northwestern Mediterranean Sea). Prog. Oceanogr. 106, 138–153. doi:10.1016/j.pocean.2012.09.001

Klinck, J.M., 1988. The influence of a narrow transverse canyon on initially geostrophic flow. J. Geophys. Res. Oceans 93, 509–515. doi:10.1029/JC093iC01p00509

Klinck, J.M., 1989. Geostrophic adjustment over submarine canyons. J. Geophys. Res. Oceans 94, 6133–6144. doi:10.1029/JC094iC05p06133

Klinck, J.M., 1996. Circulation near submarine canyons: A modeling study. J. Geophys. Res. Oceans 101, 1211–1223. doi:10.1029/95JC02901

Kneller, B.C., 1995. Beyond the turbidite paradigm: physical models for deposition of turbidites and their implications for reservoir prediction. A.J. Hartley and D.J. Prosser. Geological Society of London, special Publication.

Kneller, B.C., Branney, M.J., 1995. Sustained high-density turbidity currents and the deposition of thick massive sands. Sedimentology 42, 607–616. doi:10.1111/j.1365-3091.1995.tb00395.x

Kneller, B.C., Bennett, S.J., McCaffrey, W.D., 1997. Velocity and turbulence structure of density currents and internal solitary waves: potential sediment transport and the formation of wave ripples in deep water. Sediment. Geol. 112, 235–250. doi:10.1016/S0037-0738(97)00031-6

Kneller, B.C., Bennett, S.J., McCaffrey, W.D., 1999. Velocity structure, turbulence and fluid stresses in experimental gravity currents. J. Geophys. Res. Oceans 104, 5381–5391. doi:10.1029/1998JC900077

Kneller, B., Buckee, C., 2000. The structure and fluid mechanics of turbidity currents: a review of some recent studies and their geological implications. Sedimentology 47, 62–94. doi:10.1046/j.1365-3091.2000.047s1062.x

Komar, P.D., 1971. Hydraulic jumps in turbidity currents. Geol. Soc. Am. Bull. 82, 1477–1488. doi:10.1130/0016-7606(1971)82[1477:HJITC]2.0.CO;2

Komar, P.D., 1977. Computer simulation of turbidity current flow and the study of deep-sea channels and fan sedimentation. Sea Ideas Obs. Prog. Study Seas Vol6 Mar. Model.

Kuenen, P.H., 1937. Experiments in connection with Daly's hypothesis on the formation of submarine canyons. Leidse Geol Meded 8, 327–335Kuenen, P.H., 1938. Density currents in connection with the problem of submarine anyons. Geol. Mag. LXXV, 241–249.

Kuenen, P.H., Migliorini, C.I., 1950. Turbidity currents as a cause of graded bedding. J. Geol. 58, 91–127Kuenen, P.H., 1957. Sole markings of graded graywacke beds. J. Geol. 65, 231–258.

Laberg, J.S., Guidard, S., Mienert, J., Vorren, T.O., Haflidason, H., Nygård, A., 2007. Morphology and morphogenesis of a high-latitude canyon; the Andøya Canyon, Norwegian Sea. Mar. Geol., EUROSTRATAFORM: Role and functioning of Canyons 246, 68–85. doi:10.1016/j.margeo.2007.01.009

Lastras, G., Blasio, F.V.D., Canals, M., Elverhøi, A., 2005. Conceptual and numerical modeling of the BIG'95 Debris flow, western Mediterranean Sea. J. Sediment. Res. 75, 784–797. doi:10.2110/jsr.2005.063

Lastras, G., Canals, M., Urgeles, R., Amblas, D., Ivanov, M., Droz, L., Dennielou, B., Fabrés, J., Schoolmeester, T., Akhmetzhanov, A., Orange, D., García-García, A., 2007. A walk down the Cap de Creus canyon, northwestern Mediterranean Sea: Recent processes inferred from morphology and sediment bedforms. Mar. Geol. 246, 176–192. doi:10.1016/j.margeo.2007.09.002

Lastras, G., Acosta, J., Muñoz, A., Canals, M., 2011. Submarine canyon formation and evolution in the Argentine continental margin between 44°30'S and 48°S. Geomorphology 128, 116–136. doi:10.1016/j.geomorph.2010.12.027

Laursen, J., Normark, W.R., 2002. Late Quaternary evolution of the San Antonio Submarine Canyon in the central Chile forearc (~33°S). Mar. Geol. 188, 365–390. doi:10.1016/S0025-3227(02)00421-8

Liu, J.T., Wang, Y.-H., Yang, R.J., Hsu, R.T., Kao, S.-J., Lin, H.-L., Kuo, F.H., 2012. Cyclone-induced hyperpycnal turbidity currents in a submarine canyon. J. Geophys. Res. Oceans 117, C04033. doi:10.1029/2011JC007630

Lofi, J., Gorini, C., Berné, S., Clauzon, G., Tadeu Dos Reis, A., Ryan, W.B.F., Steckler, M.S., 2005. Erosional processes and paleo-environmental changes in the Western Gulf of Lions (SW France) during the Messinian Salinity Crisis. Mar. Geol. 217, 1–30. doi:10.1016/j.margeo.2005.02.014

Lo Iacono, C., Sulli, A., Agate, M., 2014. Submarine canyons of north-western Sicily (Southern Tyrrhenian Sea): Variability in morphology, sedimentary processes and evolution on a tectonically active margin. Deep Sea Res. Part II Top. Stud. Oceanogr., Submarine Canyons:

Complex Deep-Sea Environments Unravelled by Multidisciplinary Research 104, 93–105. doi:10.1016/j.dsr2.2013.06.018

Lopez-Fernandez, P., Calafat, A., Sanchez-Vidal, A., Canals, M., Mar Flexas, M., Cateura, J., Company, J.B., 2013. Multiple drivers of particle fluxes in the Blanes submarine canyon and southern open slope: Results of a year round experiment. Prog. Oceanogr. 118, 95–107. doi:10.1016/j.pocean.2013.07.029

Lowe, D.R., 1979. Sediment gravity flows: their classification and some problems of application to natural flows and deposits.

Lowe, D.R., 1982. Sediment gravity flows: II. Depositional models with special reference to the deposits of high-density turbidity currents. J. Sediment. Res. 52.

Martín, J., Miquel, J.-C., Khripounoff, A., 2010. Impact of open sea deep convection on sediment remobilization in the western Mediterranean. Geophys. Res. Lett. 37, L13604. doi:10.1029/2010GL043704

Martín, J., Palanques, A., Puig, P., 2007. Near-bottom horizontal transfer of particulate matter in the Palamós Submarine Canyon (NW Mediterranean). J. Mar. Res. 65, 193–218.

Mazières, A., Gillet, H., Castelle, B., Mulder, T., Guyot, C., Garlan, T., Mallet, C., 2014. High-Resolution morphobathymetric analysis and evolution of Capbreton submarine canyon head (southeast Bay of Biscay—French Atlantic Coast) over the last decade using descriptive and numerical modeling. Mar. Geol. doi:10.1016/j.margeo.2014.03.001

McCaffrey, W.D., Choux, C.M., Baas, J.H., Haughton, P.D.W., 2003. Spatio-temporal evolution of velocity structure, concentration and grain-size stratification within experimental particulate gravity currents. Mar. Pet. Geol., Turbidites: Models and Problems 20, 851–860. doi:10.1016/j.marpetgeo.2003.02.002

Meiburg, E., Kneller, B., 2010. Turbidity currents and their deposits, in: Annual Review of Fluid Mechanics. Annual Reviews, Palo Alto, pp. 135–156.

Middleton, G.V., 1966a. Experiments on density and turbidity currents: I. motion of the head. Can. J. Earth Sci. 3, 523–546. doi:10.1139/e66-038

Middleton, G.V., 1966b. Experiments on density and turbidity currents: Ii. uniform flow of density currents. Can. J. Earth Sci. 3, 627–637. doi:10.1139/e66-044

Middleton, G.V., Hampton, M.A., 1973. Part I. Sediment gravity flows: Mechanics of Flow and Deposition 1–38.

Middleton, G.V., Hampton, M.A., 1976. Subaqueous sediment transport and deposition by sediment gravity flows, in: Marine Sediment Transport and Environmental Management, Willey. Stanley D.J. & Swift D.J.P., New York, pp. 197–218.

Middleton, G.V., Southard, J.B., 1984. Mechanics of sediment movementSEPM

Middleton, G.V., 1993. Sediment deposition from turbidity currents. Annu. Rev. Earth Planet. Sci. 21, 89–114. doi:10.1146/annurev.ea.21.050193.000513

Migeon, S., Mascle, J., Coste, M., Rouillard, P., 2012. Mediterranean submarine canyons and channels: Morphological and geological backgrounds. Int. Union Conserv. Nat. Nat. Resour. IUCN Gland. SwitzerlandSpainWürtz M Ed Mediterr. Submar. Canyons Ecol. Gov. 27–41.

Milne, J., 1897. Sub-Oceanic Changes. Geogr. J. 10, 129–146, 259–289. doi:10.2307/1774597

Mohrig, D., Ellis, C., Parker, G., Whipple, K.X., Hondzo, M., 1998. Hydroplaning of subaqueous debris flows. Geol. Soc. Am. Bull. 110, 387–394.

Mohrig, D., Elverhøi, A., Parker, G., 1999. Experiments on the relative mobility of muddy subaqueous and subaerial debris flows, and their capacity to remobilize antecedent deposits. Mar. Geol. 154, 117–129. doi:10.1016/S0025-3227(98)00107-8

Morgenstern, N.R., 1967. Submarine slumping and the initiation of turbidity currents. In A.F. Richards (Ed.): Marine geotechnique. Univ of Illinois Press, Urbana, United States, p. 189-220.

Mulder, T., Syvitski, J.P.M., 1995. Turbidity Currents Generated at River Mouths during Exceptional Discharges to the World Oceans. J. Geol. 103, 285–299.

Mulder, T., Savoye, B., Syvitski, J.P.M., 1997. Numerical modelling of a mid-sized gravity flow: the 1979 Nice turbidity current (dynamics, processes, sediment budget and seafloor impact). Sedimentology 44, 305–326. doi:10.1111/j.1365-3091.1997.tb01526.x

Mulder, T., and Cochonat, P., 1996. Classification of offshore mass movements. Journal of Sedimentary Research 66, 43–47.

Mulder, T., Alexander, J., 2001. The physical character of subaqueous sedimentary density flows and their deposits. Sedimentology 48, 269–299. doi:10.1046/j.1365-3091.2001.00360.x

Mulder, T., Migeon, S., Savoye, B., Faugères, J.-C., 2001. Inversely graded turbidite sequences in the deep Mediterranean: a record of deposits from flood-generated turbidity currents? Geo-Mar. Lett. 21, 86–93. doi:10.1007/s003670100071

Mulder, T., Syvitski, J.P.M., Migeon, S., Faugères, J.-C., Savoye, B., 2003. Marine hyperpycnal flows: initiation, behavior and related deposits. A review. Mar. Pet. Geol. 20, 861–882. doi:10.1016/j.marpetgeo.2003.01.003

Mulder, T., Zaragosi, S., Jouanneau, J.-M., Bellaiche, G., Guérinaud, S., Querneau, J., 2009. Deposits related to the failure of the Malpasset Dam in 1959: An analogue for hyperpycnal deposits from jökulhlaups. Mar. Geol. 260, 81–89. doi:10.1016/j.margeo.2009.02.002

Mulder, T., 2011. Chapter 2 - Gravity processes and deposits on continental slope, rise and abyssal plains, in: Mulder, H.H. and T. (Ed.), Developments in sedimentology, deep-sea sediments. Elsevier, pp. 25–148.

Mulder, T., Zaragosi, S., Garlan, T., Mavel, J., Cremer, M., Sottolichio, A., Sénéchal, N., Schmidt, S., 2012. Present deep-submarine canyons activity in the Bay of Biscay (NE Atlantic). Mar. Geol. 295–298, 113–127. doi:10.1016/j.margeo.2011.12.005

Mutti, E., Lucchi, F.R., 1972. Turbidites of the northern Apennines: introduction to facies analysis. Int. Geol. Rev. 20, 125–166. doi:10.1080/00206817809471524

Mutti, E., Tinterri, R., Benevelli, G., Biase, D. di, Cavanna, G., 2003. Deltaic, mixed and turbidite sedimentation of ancient foreland basins. Mar. Pet. Geol., Turbidites: Models and Problems 20, 733–755. doi:10.1016/j.marpetgeo.2003.09.001

Nakajima, T., Kakuwa, Y., Yasudomi, Y., Itaki, T., Motoyama, I., Tomiyama, T., Machiyama, H., Katayama, H., Okitsu, O., Morita, S., Tanahashi, M., Matsumoto, R., 2014. Formation of pockmarks and submarine canyons associated with dissociation of gas hydrates on the Joetsu Knoll, eastern margin of the Sea of Japan. J. Asian Earth Sci. 90, 228–242. doi:10.1016/j.jseaes.2013.10.011

Nardin et al., 1979. SEPM Sp. Publ. 27, 61-73

Nemec, W. (1995) The dynamics of deltaic suspension plumes. In: Oti, M.N., Postma, G. (Eds.), *The Geology of Deltas*. A.A. Balkema, Rotterdam, p. 31-93

Nemec, W. (1995) The dynamics of deltaic suspension plumes. In: Oti, M.N., Postma, G. (Eds.), *The Geology of Deltas*. A.A. Balkema, Rotterdam, p. 31-93

Normark, W.R., 1970. Growth Patterns of Deep-Sea Fans. AAPG Bull. 54, 2170–2195.

Normark, W.R., Mutti, E., Bouma, A.H., 1984. Problems in turbidite research: A need for COMFAN. Geo-Mar. Lett. 3, 5356. doi:10.1007/BF02462447

Normark, W.R., 1989. Observed parameters for turbidity-current flow in channels, Reserve Fan, Lake Superior. J. Sediment. Res. 59., 423-431

Normark, W. R., Piper, D. J. W, 1991. Initiation processes and flow evolution of turbidity currents: Implications for the depositional record. Shorel. Abyss Contrib. Mar. Geol. Honor Francis Park. Shepard Spec. Publ. Soc. Sediment. Geol. 46 207–230.

Palanques, A., García-Ladona, E., Gomis, D., Martín, J., Marcos, M., Pascual, A., Puig, P., Gili, J.-M., Emelianov, M., Monserrat, S., Guillén, J., Tintoré, J., Segura, M., Jordi, A., Ruiz, S., Basterretxea, G., Font, J., Blasco, D., Pagès, F., 2005. General patterns of circulation, sediment fluxes and ecology of the Palamós (La Fonera) submarine canyon, northwestern Mediterranean. Prog. Oceanogr. 66, 89–119. doi:10.1016/j.pocean.2004.07.016

Palanques, A., de Madron, X.D., Puig, P., Fabres, J., Guillen, J., Calafat, A., Canals, M., Heussner, S., Bonnin, J., 2006. Suspended sediment fluxes and transport processes in the Gulf of Lions

submarine canyons. The role of storms and dense water cascading. Mar. Geol. 234, 43–61. doi:10.1016/j.margeo.2006.09.002

Palanques, A., Guillén, J., Puig, P., Durrieu de Madron, X., 2008. Storm-driven shelf-to-canyon suspended sediment transport at the southwestern Gulf of Lions. Cont. Shelf Res., Sediment Dynamics in the Gulf of Lions; the Impact of Extreme Events 28, 1947–1956. doi:10.1016/j.csr.2008.03.020

Palanques, A., Puig, P., Latasa, M., Scharek, R., 2009. Deep sediment transport induced by storms and dense shelf-water cascading in the northwestern Mediterranean basin. Deep Sea Res. Part Oceanogr. Res. Pap. 56, 425–434. doi:10.1016/j.dsr.2008.11.002

Palanques, A., Puig, P., Durrieu de Madron, X., Sanchez-Vidal, A., Pasqual, C., Martín, J., Calafat, A., Heussner, S., Canals, M., 2012. Sediment transport to the deep canyons and open-slope of the western Gulf of Lions during the 2006 intense cascading and open-sea convection period. Prog. Oceanogr. 106, 1–15. doi:10.1016/j.pocean.2012.05.002

Parker, G., 1982. Conditions for the ignition of catastrophically erosive turbidity currents. Mar. Geol. 46, 307–327. doi:10.1016/0025-3227(82)90086-X

Parker, G., Fukushima, Y., Pantin, H.M., 1986. Self-accelerating turbidity currents. J. Fluid Mech. 171, 145–181. doi:10.1017/S0022112086001404

Parsons, J.D., Garcia, M.H., 1995. Flow structure and mixing characteristics in saline gravity current fronts. University of Illinois at Urbana-Champaign, Department of Civil Engineering.

Parsons, J.D., Friedrichs, C.T., Traykovski, P.A., Mohrig, D., Imran, J., Syvitski, J.P.M., Parker, G., Puig, P., Buttles, J.L., García, M.H., 2007. The Mechanics of Marine Sediment Gravity Flows, in: Nittrouer, C.A., Austin, J.A., Field, M.E., Kravitz, J.H., Syvitski, J.P.M., Wiberg, P.L. (Eds.), Continental margin sedimentation. Blackwell Publishing Ltd., pp. 275–337.

Parsons, J.D., Garcia, M.H., 1998. Similarity of gravity current fronts. Phys. Fluids 1994-Present 10, 3209–3213. doi:10.1063/1.869848

Paull, C.K., Ussler, W., Greene, H.G., Keaten, R., Mitts, P., Barry, J., 2003. Caught in the act: the 20 December 2001 gravity flow event in Monterey Canyon. Geo-Mar. Lett. 22, 227–232. doi:10.1007/s00367-003-0117-2

Peakall, J., McCaffrey, B., Kneller, B., 2000. A process model for the evolution, morphology, and architecture of sinuous submarine channels. J. Sediment. Res. 70, 434–448. doi:10.1306/2DC4091C-0E47-11D7-8643000102C1865D

Pedrosa-Pàmies, R., Sanchez-Vidal, A., Calafat, A., Canals, M., Durán, R., 2013. Impact of storm-induced remobilization on grain size distribution and organic carbon content in sediments from the Blanes canyon area, NW Mediterranean Sea. Prog. Oceanogr. 118, 122–136. doi:10.1016/j.pocean.2013.07.023

Pickering, K.T., Hiscott, R.N., Hein, R.J., 1989. Deep marine environments: clastic sedimentation and tectonics. Unwin Hyman, London.

Piper, D.J.W., Normark, W.R., 2009. Processes that initiate turbidity currents and their influence on turbidites: a marine geology perspective. J. Sediment. Res. 79, 347–362. doi:10.2110/jsr.2009.046

Posamentier, H., Vail, P., 1988. Sequences, systems tracts, and eustatic cycles. Aapg Bull.-Am. Assoc. Pet. Geol. 72, 237–237.

Postma, G., 1986. Classification for sediment gravity-flow deposits based on flow conditions during sedimentation. Geology 14, 291–294. doi:10.1130/0091-7613(1986)14<291:CFSGDB>2.0.CO;2

Pratson, L.F., Ryan, W.B.F., Mountain, G.S., Twichell, D.C., 1994. Submarine canyon initiation by downslope-eroding sediment flows: evidence in late Cenozoic strata on the New Jersey continental slope. Geol. Soc. Am. Bull. 106, 395–412. doi:10.1130/0016-7606(1994)106<0395:SCIBDE>2.3.CO;2

Pratson, L.F., Coakley, B.J., 1996. A model for the headward erosion of submarine canyons induced by downslope-eroding sediment flows. Geol. Soc. Am. Bull. 108, 225–234. doi:10.1130/0016-7606(1996)108<0225:AMFTHE>2.3.CO;2

Puig, P., Ogston, A.S., Mullenbach, B.L., Nittrouer, C.A., Parsons, J.D., Sternberg, R.W., 2004. Storm-induced sediment gravity flows at the head of the Eel submarine canyon, northern California margin. J. Geophys. Res. Oceans 109, C03019. doi:10.1029/2003JC001918

Puig, P., Palanques, A., Orange, D.L., Lastras, G., Canals, M., 2008. Dense shelf water cascades and sedimentary furrow formation in the Cap de Creus canyon, northwestern Mediterranean Sea. Cont. Shelf Res. 28, 2017–2030. doi:10.1016/j.csr.2008.05.002

Puig, P., Canals, M., Company, J.B., Martín, J., Amblas, D., Lastras, G., Palanques, A., Calafat, A.M., 2012. Ploughing the deep sea floor. Nature 489, 286–289. doi:10.1038/nature11410

Puig, P., Palanques, A., Martín, J., 2014. Contemporary sediment-transport processes in submarine canyons. Annu. Rev. Mar. Sci. 6, 53–77. doi:10.1146/annurev-marine-010213-135037

Reading, H.G., Richards, M., 1994. Turbidite systems in deep-water basin margins classified by grain size and feeder system. AAPG Bull. 78, 792–822.

R. H. Dott, J., 1963. Dynamics of Subaqueous Gravity Depositional Processes. AAPG Bull. 47, 104–128.

Ribó, M., Puig, P., Palanques, A., Lo Iacono, C., 2011. Dense shelf water cascades in the Cap de Creus and Palamós submarine canyons during winters 2007 and 2008. Mar. Geol. 284, 175–188. doi:10.1016/j.margeo.2011.04.001

Ridente, D., Foglini, F., Minisini, D., Trincardi, F., Verdicchio, G., 2007. Shelf-edge erosion, sediment failure and inception of Bari Canyon on the Southwestern Adriatic Margin (Central Mediterranean). Mar. Geol., EUROSTRATAFORM: Role and functioning of Canyons 246, 193–207. doi:10.1016/j.margeo.2007.01.014

Rumín-Caparrós, A., Sanchez-Vidal, A., Calafat, A., Canals, M., Martín, J., Puig, P., Pedrosa-Pàmies, R., 2013. External forcings, oceanographic processes and particle flux dynamics in Cap de Creus submarine canyon, NW Mediterranean Sea. Biogeosciences 10, 3493–3505. doi:10.5194/bg-10-3493-2013

Sanchez-Vidal, A., Pasqual, C., Kerhervé, P., Calafat, A., Heussner, S., Palanques, A., Durrieu de Madron, X., Canals, M., Puig, P., 2008. Impact of dense shelf water cascading on the transfer of organic matter to the deep western Mediterranean basin. Geophys. Res. Lett. 35, n/a–n/a. doi:10.1029/2007GL032825

Sanchez-Vidal, A., Canals, M., Calafat, A.M., Lastras, G., Pedrosa-Pàmies, R., Menéndez, M., Medina, R., Company, J.B., Hereu, B., Romero, J., Alcoverro, T., 2012. Impacts on the deep-sea ecosystem by a severe coastal storm. PLoS ONE 7, e30395. doi:10.1371/journal.pone.0030395

Sanders, J.E., 1964. Primary Sedimentary Structures Produced By Turbidity Currents: ABSTRACT. AAPG Bull. 48, 545–545.

Sequeiros, O.E., Naruse, H., Endo, N., Garcia, M.H., Parker, G., 2009. Experimental study on self-accelerating turbidity currents. J. Geophys. Res. Oceans 114, C05025. doi:10.1029/2008JC005149

Shanmugam, G., Moiola, R.J., 1988. Submarine fans: characteristics, models, classification, and reservoir potential. Earth-Sci. Rev. 24, 383–428. doi:10.1016/0012-8252(88)90064-5

Shanmugam, G., Moiola, R.J., 1991. Types of submarine fan lobes: models and implications (1). AAPG Bull. 75, 156–179.

Shanmugam, G., 1996. High-density turbidity currents; are they sandy debris flows? J. Sediment. Res. 66, 2–10.

Shanmugam, G., 2000. 50 years of the turbidite paradigm (1950s—1990s): deep-water processes and facies models—a critical perspective. Mar. Pet. Geol. 17, 285–342. doi:10.1016/S0264-8172(99)00011-2

Shanmugam, G., 2002. Ten turbidite myths. Earth-Sci. Rev. 58, 311–341. doi:10.1016/S0012-8252(02)00065-X

She, J., Klinck, J.M., 2000. Flow near submarine canyons driven by constant winds. J. Geophys. Res. Oceans 105, 28671–28694. doi:10.1029/2000JC900126

Sheldon, P.G., 1928. Some sedimentation conditions in middle Portage rocks. Am. J. Sci. s5-15, 243–252. doi:10.2475/ajs.s5-15.87.243

Shepard, F.P., 1934. Canyons off the New England Coast. Am. J. Sci. 27, 24–36.
Shepard, F.P., 1963. Submarine geology. Harper & Row Publ., New York, 557p
Shepard, F.P., 1973. Submarine geology. Harper & Row Publ., New York, 517 p.
Shepard, F.P., Dill, R.F., 1966. Submarine canyons and other sea valleys. Rand McNally, Chicago, 381 pp.
Shepard, F.P., Marshall, N.F., McLoughlin, P.A., 1974. Currents in submarine canyons. Deep Sea Res. Oceanogr. Abstr. 21, 691–706. doi:10.1016/0011-7471(74)90077-1
Shepard, F.P., Marshall, N.F., McLoughlin, P.A., Sullivan, G.G., 1979. Currents in submarine canyons and other seavalleys 147, 1–2.
Shepard, F., 1981. Submarine canyons - multiple causes and long-time persistence. AAPG Bull., -Am. Assoc. Pet. Geol. 65, 1062–1077.
Siegenthaler, C., Buhler, J., 1985. The kinematics of turbulent suspension currents (turbidity currents) on inclined boundaries. Mar. Geol. 64, 19–40. doi:10.1016/0025-3227(85)90158-6
Signorini, R., 1936. Determinazione del senso di sedimentazione degli strati nelle formazione arenacea dell' Appennino settentrionale. Boll Soc Geol Ital 55, 259–267.
Simpson, J.E., 1969. A comparison between laboratory and atmospheric density currents. Q. J. R. Meteorol. Soc. 95, 758–765. doi:10.1002/qj.49709540609
Simpson, J.E., 1997. Gravity Currents: In the Environment and the Laboratory. Cambridge University Press.
Simpson, J.E., Britter, R.E., 1979. The dynamics of the head of a gravity current advancing over a horizontal surface. J. Fluid Mech. 94, 477–495. doi:10.1017/S0022112079001142
Sloff, C.J., 1997. Sedimentation in reservoirs. PhD Thesis TU Delft, Delft University of Technology. p 284.
Southard, J.B., 1991. Experimental determination of bed-form stability. Annu. Rev. Earth Planet. Sci. 19, 423–455. doi:10.1146/annurev.ea.19.050191.002231
Spencer, J.W., 1903. Submarine valleys off the American coast and in the north Atlantic. Geol. Soc. Am. Bull. 14, 207–226. doi:10.1130/GSAB-14-207
Stabholz, M., Durrieu de Madron, X., Canals, M., Khripounoff, A., Taupier-Letage, I., Testor, P., Heussner, S., Kerhervé, P., Delsaut, N., Houpert, L., Lastras, G., Dennielou, B., 2013. Impact of open-ocean convection on particle fluxes and sediment dynamics in the deep margin of the Gulf of Lions. Biogeosciences 10, 1097–1116. doi:10.5194/bg-10-1097-2013
Stacey, M.W., Bowen, A.J., 1988. The vertical structure of density and turbidity currents: Theory and observations. J. Geophys. Res. 93, 3528. doi:10.1029/JC093iC04p03528
Stanley, D.G., 1963. Vertical petrographic variability in Annot Sandstone Turbidites: ABSTRACT. AAPG Bull. 47, 371–371.
Stow, D.A.V., Shanmugam, G., 1980. Sequence of structures in fine-grained turbidites: Comparison of recent deep-sea and ancient flysch sediments. Sediment. Geol. 25, 23–42. doi:10.1016/0037-0738(80)90052-4
Sultan, N., Gaudin, M., Berne, S., Canals, M., Urgeles, R., Lafuerza, S., 2007. Analysis of slope failures in submarine canyon heads: An example from the Gulf of Lions. J. Geophys. Res. Earth Surf. 112, n/a–n/a. doi:10.1029/2005JF000408
Sumner, E.J., Talling, P.J., Amy, L.A., 2009. Deposits of flows transitional between turbidity current and debris flow. Geology 37, 991–994. doi:10.1130/G30059A.1
Sumner, E.J., Talling, P.J., Amy, L.A., Wynn, R.B., Stevenson, C.J., Frenz, M., 2012. Facies architecture of individual basin-plain turbidites: Comparison with existing models and implications for flow processes. Sedimentology 59, 1850–1887. doi:10.1111/j.1365-3091.2012.01329.x
Talling, P.J., Wynn, R.B., Masson, D.G., Frenz, M., Cronin, B.T., Schiebel, R., Akhmetzhanov, A.M., Dallmeier-Tiessen, S., Benetti, S., Weaver, P.P.E., Georgiopoulou, A., Zühlsdorff, C., Amy, L.A., 2007. Onset of submarine debris flow deposition far from original giant landslide. Nature 450, 541–544. doi:10.1038/nature06313.

Talling, P.J., Masson, D.G., Sumner, E.J., Malgesini, G., 2012. Subaqueous sediment density flows: Depositional processes and deposit types. Sedimentology 59, 1937–2003. doi:10.1111/j.1365-3091.2012.01353.x

Talling, P.J., Paull, C.K., Piper, D.J.W., 2013. How are subaqueous sediment density flows triggered, what is their internal structure and how does it evolve? Direct observations from monitoring of active flows. Earth-Sci. Rev. 125, 244–287. doi:10.1016/j.earscirev.2013.07.005

Talling, P.J., 2014. On the triggers, resulting flow types and frequencies of subaqueous sediment density flows in different settings. Mar. Geol. 352, 155–182. doi:10.1016/j.margeo.2014.02.006

Talling, P.J., Allin, J., Armitage, D.A., Arnott, R.W.C., Cartigny, M.J.B., Clare, M.A., Felletti, F., Covault, J.A., Girardclos, S., Hansen, E., Hill, P.R., Hiscott, R.N., Hogg, A.J., Clarke, J.H., Jobe, Z.R., Malgesini, G., Mozzato, A., Naruse, H., Parkinson, S., Peel, F.J., Piper, D.J.W., Pope, E., Postma, G., Rowley, P., Sguazzini, A., Stevenson, C.J., Sumner, E.J., Sylvester, Z., Watts, C., Xu, J., 2015. Key Future Directions For Research On Turbidity Currents and Their Deposits. J. Sediment. Res. 85, 153–169. doi:10.2110/jsr.2015.03

Trincardi, F., Foglini, F., Verdicchio, G., Asioli, A., Correggiari, A., Minisini, S.,Piva, A. ,Remia, A.,Ridente, D., Taviani, M., 2007a. The impact of cascading currents on the Bari Canyon System, SW-Adriatic Margin (Central Mediterranean). Marine Geology 246, 208–230. doi: 10.1016/j.margeo.2007.01.013

Trincardi, F., Verdicchio, G., Miserocchi, S. ,2007b. Sea-floor evidence for the interaction between cascading and along-slope bottom-water masses. Journal of Geophysical Research (Earth Surface) 112, F03011. Doi:10.1029/2006JF000620.

Tripsanas, E.K., Piper, D.J.W., Campbell, D.C., 2008. Evolution and depositional structure of earthquake-induced mass movements and gravity flows: Southwest Orphan Basin, Labrador Sea. Mar. Pet. Geol. 25, 645–662. doi:10.1016/j.marpetgeo.2007.08.002

Turner, J.S., 1973. Buoyancy Effects in Fluids. Cambridge University Press, Cambridge.

Twichell, D., Roberts, D., 1982. Morphology, distribution, and Development of Submarine Canyons on the United-States Atlantic Continental-Slope Between Hudson and Baltimore Canyons. Geology 10, 408–412. doi:10.1130/0091-7613(1982)10<408:MDADOS>2.0.CO;2

Ulses, C., Estournel, C., Puig, P., Durrieu de Madron, X., Marsaleix, P., 2008. Dense shelf water cascading in the northwestern Mediterranean during the cold winter 2005: Quantification of the export through the Gulf of Lion and the Catalan margin. Geophys. Res. Lett. 35, n/a–n/a. doi:10.1029/2008GL033257

Veatch, A.C., Smith, P.A., 1939. Atlantic submarine valleys of the United States and the Congo Submarine Valley., Special Papers 7. Geological Society of America. Washington DC.

Walker, R.G., 1965. The Origin and Significance of the Internal Sedimentary Structures of Turbidites. Proc. Yorks. Geol. Polytech. Soc. 35, 1–32. doi:10.1144/pygs.35.1.1

Walker, R.G., 1978. Deep-Water Sandstone Facies and Ancient Submarine Fans: Models for Exploration for Stratigraphic Traps. AAPG Bull. 62, 932–966.

Walsh, J.P., Nittrouer, C.A., 2003. Contrasting styles of off-shelf sediment accumulation in New Guinea. Mar. Geol. 196, 105–125. doi:10.1016/S0025-3227(03)00069-0

Wiles, E., Green, A., Watkeys, M., Jokat, W., Krocker, R., 2013. The evolution of the Tugela canyon and submarine fan: A complex interaction between margin erosion and bottom current sweeping, southwest Indian Ocean, South Africa. Mar. Pet. Geol. 44, 60–70. doi:10.1016/j.marpetgeo.2013.03.012

Wood, L.J., Ethridge, F.G., Schumm, S.A., 1993. The effects of rate of base-level fluctuation on coastal-plain, shelf and slope depositional systems: an experimental approach, in: Posamentier, H.W., Summerhayes, C.P., Haq, B.U., Allen, G.P. (Eds.), Sequence stratigraphy and facies associations. Blackwell Publishing Ltd., pp. 43–53.

Würtz (Ed.), M., 2012. Mediterranean submarine canyons: ecology and governance. IUCN, Gland, Switzerland and Malaga, Spain MAGRAMA.

Xu, J.P., Noble, M.A., Rosenfeld, L.K., 2004. In-situ measurements of velocity structure within turbidity currents. Geophys. Res. Lett. 31, L09311. doi:10.1029/2004GL019718

Xu, J.P., 2011. Measuring currents in submarine canyons: technological and scientific progress in the past 30 years. Geosphere 7, 868–876. doi:10.1130/GES00640.1

Xu, J.P., Sequeiros, O.E., Noble, M.A., 2014. Sediment concentrations, flow conditions, and downstream evolution of two turbidity currents, Monterey Canyon, USA. Deep Sea Res. Part Oceanogr. Res. Pap. 89, 11–34. doi:10.1016/j.dsr.2014.04.001

Chapter 2:

MODELLING TURBIDITY CURRENTS

ABSTRACT

Turbidity currents are generally unpredictable, often catastrophic, rare at observational scales and happen in relatively inaccessible environments. As such, measurements of marine turbidity currents are scarce, highly localised and usually biased towards shallow environments and frequent flows. Much of the present knowledge on turbidity currents comes from their preserved deposits. Triggering mechanisms, flow evolution and deceleration were primarily inferred from observations on the resulting deposits because in most cases the only information available from a submarine flow is its deposit. Laboratory-scale experiments and numerical modelling have provided insight into both the internal structure of turbidity currents and the characteristics of the deposits associated to a given type of flow. The three approaches (i.e. field observations, experimental modelling and numerical modelling) are complementary and form an interlinked feedback system. Prior to the discussion of the numerical model used in the present thesis from a physical and mathematical point of view, commonly used research methods and approaches to modelling turbidity currents and sediment transport are presented.

2DH process-based models are preferred since they can produce accurate predictions of current evolution and deposit characteristics of large scale flows with affordable computing resources. Among the 2DH models available, the use of Nixes-TC is justified given the key improvements of this model: the inclusion of a non-linear sedimentation model (settling velocity) in the equation of flux conservation, the development of a non-linear flow-dependent shear stress coefficient valid for all Reynolds numbers from laminar to fully turbulent flows, the inclusion of Coriolis effects, the treatment of the head and the existence of equilibrium solutions.

RESUME

Les observations directes et la quantification des évènements turbiditiques sont rares et très localisées géographiquement. Ainsi, l'étude géologique des canyons sous-marins et des systèmes turbiditiques est fondamentalement limitée à des interprétations *a posteriori,* basées sur la répartition des dépôts (par carottages et sismiques) et à des mises en évidence morphologiques (accumulations et zones d'érosion) qui ont permis de déduire les mécanismes déclenchants ainsi que l'évolution et décélération de l'écoulement. Les modèles analogiques et numériques ont largement contribué à approfondir les connaissances sur la structure interne des courants et les caractéristiques des dépôts associés à chaque type d'écoulement. Les trois approches utilisées pour étudier les courants de turbidité (i.e. données terrain, modèles analogiques et modélisation numérique) sont complémentaires et souvent déterminants. La première partie de ce chapitre présente et discute ces trois différentes méthodes de recherche utilisées pour l'étude des courants de turbidité et le transport et dépôt associés. La deuxième partie s'intéresse aux aspects physiques et mathématiques du modèle numérique appliqué aux deux cas d'étude de cette thèse.

Les modèles 2DH basés sur des processus physiques sont plus précis puisqu'ils fournissent des résultats en termes d'évolution de l'écoulement et des dépôts associés réalistes tout en mobilisant des moyens raisonnables en temps de calcul et en mémoire. Nixes-TC apporte des améliorations clés par rapport à d'autres modèles 2DH existants, ce qui justifie son utilisation comme outil de simulation dans le cadre de cette thèse. Parmi ces améliorations, on peut citer l'inclusion d'un modèle de sédimentation (vitesse de chute) dans l'équation de conservation du flux sédimentaire, le développement d'un coefficient de frottement non-linéaire valide pour des écoulements laminaires et turbulents, l'incorporation des forces de Coriolis, le traitement de la tête de l'écoulement et l'existence de solutions à l'équilibre.

1. Introduction: research methods on turbidity currents

Since the seminal works of (Kuenen, 1937; Kuenen and Migliorini, 1950), the research on turbidity currents (hereafter TC) follows three complementary approaches: field observations, experimental modelling and numerical modelling based on physical processes. The former provides data needed for validation of the two latter whilst the latter provide insight and understanding into field data forming an interlinked feedback system. In the following the three different methods are reviewed, especial emphasis is given to the numerical modelling of TC.

2. Field observations

Field observations comprise outcrops, seismic data, cores and direct monitoring of active flows. Current knowledge on turbidity currents is mainly based on observations (i.e. outcrops, sedimentary cores and seismic profiles) of the sedimentary deposits they leave behind on the modern seafloor and on outcrops of ancient turbidites (e.g. Bouma, 1962; Piper et al., 1985, 1999; Hughes Clarke et al., 1990; Piper and Savoye, 1993; Savoye et al., 1993; Kneller and Branney, 1995; Sumner et al., 2008; Migeon et al., 2012). These deposits are at the basis of a posteriori interpretations on flow character and evolution. However the link between flow conditions and sediment deposition or erosion is not always clear, the hypothesis these relationships are based on are often not well tested, and it is very difficult to infer unambiguously the character of the flow from the deposit alone (Talling et al., 2012). In addition to this, main limitations of cores, seismic data and outcrop studies arise from the fact that they provide limited one dimensional or two dimensional sections through three dimensional geological features. Cores are generally used to validate information from other sources as their one dimensional nature makes difficult to infer three dimensional information. In the case of seismic data and outcrops, the features can be interpreted with certainty if their scale is smaller than the dimensions of the section and the three dimensional vision can only be achieved when the spacing between sections is inferior to the dimensions of the architectural elements of the depositional system. If these limitations are considered, the interpretations might be often hypothetical, speculative and unverifiable. In order to produce reliable interpretations, solid theoretical and experimental basis are needed.

Direct monitoring observations must be combined with seismic data and cores in order to link deposits and flow character (Talling et al., 2012). However whilst deposits of turbidity currents (TC) have been described in numerous locations, direct observations of submarine flows are scarce and highly localised due to their relative inaccessible location, and hence high cost of these observations, their unpredictable occurrence and their destructiveness. Indirect evidence about the speeds of turbidity currents has been obtained from the breaks of submarine cables crossed by the currents triggered for example for the 1929 earthquake of Grand Banks in Newfoundland (Heezen and Ewing, 1952) or for the landslide of Nice airport 1979 (Gennesseaux et al., 1980). Direct measurements of flows in action including the key parameter of sediment concentration are available in only a few locations: Var Canyon (Khripounoff et al., 2012), Zaire Canyon (Khripounoff et al., 2003; Cooper et al., 2012; Andrieux et al., 2013), Squamish Delta (Hughes Clarke et al., 2012), Lake Geneva (Lambert and Giovanoli, 1988), Monterey Canyon (Paull et al., 2003; Xu et al., 2004, 2014; Xu, 2010;), Gaoping Canyon in Taiwan (Liu et al., 2012, 2013), Eel canyon (Puig et al., 2003, 2004), Cap de Creus (Canals et al., 2006; Palanques et al., 2008), La Fonera (Puig et al., 2012), Nazaré (Martín et al., 2011) or Bute Inlet in British Columbia (Hughes Clarke, 2016) among others. Measurements of sediment concentration are fundamental for a better understanding of TC dynamics. Sediment concentration

provides the potential energy of TC and it influences the flow state, the rheology, the sediment support mechanism and the processes of deposition and re-entrainment of sediment. Most of the data available is biased towards shallow environments and frequent (sub-annual) flows (Talling et al., 2013) with measurements retrieved from ADCP close to bed whilst measurements at different depths at the same location and for deeper water and long run-out flows are scarce. Direct monitoring of active flows at several locations along their pathway is the most obvious way of achieving insightful understanding of the dynamics of TC and would provide field data necessary for (physical and mathematical) model validation.

3. Experimental modelling

Physical modelling is an alternative method to the study of the mechanics of turbidity currents (TC). Scale models attempt to reproduce some or all of the key parameters of the system. First experimental works (Kuenen, 1937; Middleton, 1966a; Simpson, 1997) provided broad descriptions of TC dynamics. Advances in experimental technology have increased our knowledge of TC dynamics providing insight on the vertical structure of turbulence (Kneller et al., 1997, 1999; Best et al., 2001; Buckee et al., 2001; Baas et al., 2005, 2009) and on supercritical flows (Kostic and Parker, 2006; Cartigny et al., 2014). Experimental modelling presents two main advantages: 1) processes present a reduced time frame and take place within the friendly controlled (and reproducible) environment of the laboratory and 2) they allow the monitoring of variables that are not known a priori and that might have non-linear effects on the dynamics and morphodynamics (e.g. settling velocity). These advantages are offset by prototype to model scaling issues (Middleton and Southard, 1984; Peakall et al., 1996).

There are four different approaches to the scaling of physical models: 1) one-to-one replicas of the field prototype; 2) distorted-scale modelling; 3) non-scaled experimental analogues; and 4) Froude scaled modelling. The large scale of turbidity currents in the ocean renders them impossible to reproduce at 1:1 scales. Distorted scaled experiments with supplementary slope have being used to reproduce appropriate bed shear stress (Postma et al., 1988), however in this cases additional verification is used and systematic changes in other variables are imposed until the model reproduces the changes observed in the prototype (Peakall et al., 1996). Analogue unscaled experiments as those performed by Alexander and Morris (1994) provide qualitative information on processes. Physical scaled models are based on similarity theory and dimensional analysis. A series of controlling variables is identified and grouped into a smaller number of dimensionless parameters. These dimensionless parameters fully characterise the flow. Ideally every variable should be perfectly scaled; however in the majority of the experiments using sediments it is not possible to fulfil this requirement. As long as the dimensionless parameters in the model are comparable to those of the prototype, the experiment is adequately scaled with respect to the variables included in those parameters (Middleton, 1966a).

Two parameters are usually considered in order to characterise the flow: Reynolds number and Froude number. The Reynolds number Re is the ratio of inertial to viscous forces:

$$Re = \frac{\rho_f u h}{\mu} \tag{2.1}$$

Where u is the flow velocity, h is the flow thickness, ρ_f is the TC density and μ the dynamic viscosity of the TC. The Froude number Fr is the ratio of the inertial forces to the gravity forces acting on a TC:

$$Fr = \frac{u}{\sqrt{gh}} \tag{2.2}$$

Currents that share the same values of Re and Fr are said to be dynamically similar. In Froude scale modelling, Fr is scaled correctly and Re is relaxed. Kinematically water is the least viscous fluid available, which means that experimental models nearly always have significantly lower Re than their prototypes. As long as Re is high enough in both systems (i.e. prototype and experimental model), its exact value does not strongly influence the overall dynamics. The relaxation on the value of Re is based on two assumptions: 1) viscous effects are negligible if the current is turbulent (Re>2000) and 2) turbulence is self-similar across the range of scales of the model and prototype (Kneller and Buckee, 2000). In the case of TC, the gravity action depends on the fractional density difference between the TC (ρ_f) and the ambient fluid (ρ_w) thus it is used the densiometric Froude number Fr_d:

$$Fr_d = \frac{u}{\sqrt{g'h}} \qquad g' = g\frac{\rho_f - \rho_w}{\rho_w} \tag{2.3}$$

Additionally sediment dynamics must also be scaled. Under the assumption that the settling velocity describes the particle hydrodynamics, a dimensionless settling velocity is generally used (i.e. ratio of the terminal settling velocity to some velocity scale considered as characteristic of the current) (Middleton, 1966a; Laval et al., 1988). Intermolecular forces (i.e. van der Waals forces and ionic bonds) are a major constrain on scale modelling, as they might modify the correctly scaled settling velocity of fine sediment in experiments (Peakall et al., 1996). The problem can be overcome by using inert silica flour or glass beads (Parker et al., 1987; Garcia, 1993). Another additional problem when scaling fine sediment are the capillary forces that arise once the sediment is settled and that can only be reduced using larger sediment. Middleton (1966b, 1967) proposed the use of reduced density grains in order to appropriately scale settling velocity, however this demands an increase in sediment concentration. Any change in sediment concentration and particle size affects the whole current behaviour and it may no longer scale the prototype (Middleton, 1966a; Peakall et al., 1996).

Other dense solutions have also been used in experiments for TC (e.g. Middleton, 1993; Keevil et al., 2006) since saline and fine grained TC are assumed to be dynamically similar (Stacey and Bowen, 1988). Comparisons of saline and TC are scarce in the bibliography: Garcia (1994) showed that for coarse grained TC the vertical structure might be considerably different to that of saline currents and Gray et al. (2006) showed that the mixing appears to be more vigorous in TC than in saline currents. The use of saline currents simplifies the current dynamics since erosion and deposition are neglected and have largely contributed to the current knowledge of large scale flow mechanics (Simpson and Britter, 1979; Middleton, 1993; Kneller and Buckee, 2000). Sediment-fluid interactions influence the turbulence structure and the sediment exchange with the bed (Parker et al., 1986; Pratson et al., 2000; McCaffrey et al., 2003; Baas et al., 2005). Hence the use of saline currents as a proxy for TC seems reasonable in the case of fine-grained low concentration weakly depositional TC that have concentration and velocity profiles very similar to the ones of saline currents (Kneller and Buckee, 2000; Sequeiros et al., 2009).

Two different methodologies are applied to physically model TC: 1) lock exchange (Middleton, 1966a, 1966b; Simpson and Britter, 1979) and 2) external input (Best et al., 2001; Buckee et al., 2001; De Rooij and Dalziel, 2001). In the former (i.e. lock exchange) a fixed volume of fluid is released by lifting a gate between two areas of the same tank. In the latter, the fixed volume is placed in an external tank separated from the main flume; this allows the production of more sustained currents. It is suggested that using an external input tank would be more appropriate for modelling both natural surge type and continuous currents. In lock-exchange experiments the importance of the head is over-emphasised due to two phenomena affecting the dynamics of the head: the counter-current filling the lock-box and the intense turbulence caused by the sudden release of the static mass of fully suspended sediment (Peakall et al., 2001). The use of external tanks improves the realism of experimental modelling and extends the range of flows that can be studied.

Deep turbidity systems are the result of multiple deposits issued of successive TC. Modelling the effects of successive flows is extremely difficult. Another issue arising from the scale of flume experiments is that the sediment deposit produced is often not thick enough to document its internal structure and its grading pattern. Not being able to reproduce sedimentary structures makes difficult to test the hypothesis linking deposit type and depositional process. The first attempts focussed on solving the deposits of a single flow (Lüthi, 1981a) and later extended to series of TC (Parsons et al., 2002; Groenenberg, 2007).

Experimental models provide information in the three spatial dimensions and at different evolution stages whilst field studies such as outcrops, seismic data and cores display a static frame of a dynamic process. Models are simplified representations of nature or hypothetical limit cases where key processes are taken into account. The differences between models and nature need to be kept in mind when upscaling models to natural situations. TC (as any Earth Science process) are multiscale both in time and space, small scale mechanisms, not yet well understood (i.e. erosion and resuspension), determine the large scale evolution of the flow. Small scale processes on the boundary layer are not well understood and experimental models can provide insight into them (Sumner et al., 2008; Cantero et al., 2012).

Despite the problems related to scaling or the difficulty in the reproduction of sedimentary structures, laboratory experiments provide insight in individual physical processes. Experimental models can closely approximate the assumptions that underpin numerical models (Peakall et al., 1996) and provide cost-effective datasets for testing them (Boyer et al., 2004).

4. Mathematical and numerical modelling

Turbidity currents (TC) are a highly complex phenomenon: they are non-uniform, unsteady, non-linear, free boundary flows driven by the combination of gravitational, body and pressure forces (Allen, 1985). Mathematical models can provide considerable insights into TC dynamics, their complex system of controlling variables and the feedback mechanisms operating. In order to understand TC several approaches have been proposed spanning the entire range between the more simple models based on dimensional analysis to the more complex approaches of high resolution of Direct Numerical Simulation DNS. The range of applications of numerical models have accordingly evolved from providing estimates of current velocity and thickness to predicting deposit geometries and grain size distribution or modelling the vertical structure of turbulence.

Paola (2000) classified mathematical model into two types: process based models (i.e. deterministic), rule-based models (i.e. empirical). Process-based models consist on a set of ordinary or partial differential equations that provide a detailed physical description of the processes involved. On the other hand, in ruled based models, the behaviour of the system is translated into rules that merely capture the essence of the processes. The rules are the synthesis of the dynamics of the system obtained from a combination of field and laboratory observations and a detailed knowledge of the physics of the processes involved. Ruled based models are effective and widely used in fields such as ecology or biochemistry of living organisms where processes can be represented by a reduce number of patterns (Paola, 2000). In ruled-based models the smaller scales processes are usually considered negligible making difficult a quantitative validation of these models, thus in the field of sediment-transport and sedimentation processes their application is limited to large temporal and spatial scales as stratigraphy models (e.g. cellular automata model).

Process-based models of TC start with a common system of equations (i.e. conservation of fluid mass, conservation of sediment mass and conservation of momentum). Some processes such as those involving sediment transport lack of fundamental equation and are substituted by semi-empirical relationships based on experimental data (e.g. drag coefficients or empirical sediment flux

laws). In most of the cases there are more variables involved than equations. In order to reduce the complexity of the system (and hence, the computer power involved), models rely on simplifications such as steady-state or inviscid flow or reduction of the number of dimensions. The validity of each one of the approaches depends on the choice and validity of the assumptions made in order to simulate a particular process. Numerical models were first developed on the basis of small-scale tanks experiments of particle-driven density currents. Today, experimental models provide a valuable way of testing the assumptions of numerical models as they allow constraining some of the variables involved under controlled conditions.

In the following, we will review the different modelling approaches, with an emphasis on the assumptions and simplifications of each model and on the different parameterizations of relevant mechanisms (i.e. sediment entrainment, turbulent mixing along and within the current, front condition, friction).

4.1.Dimensional analysis & conceptual models

Conceptual models and dimensional analysis models provide fundamental insight into the dynamics of turbidity currents (TC). One of the first attempts to determine the front velocity u_f of a gravity current of excess density $\Delta\rho$ in an ambient fluid of density ρ_o is that of (von Kármán, 1940), whose dimensional analysis of the balance between the inertial and buoyancy forces found that the velocity of the front u_f is proportional to the square root of the reduced gravity $g' = \frac{\Delta\rho}{\rho} g$ and the front height h.

$$u_f \propto \sqrt{g'h} \tag{2.4}$$

Benjamin (1968) considered a gravity current in a channel of depth H and hydrostatic pressure distribution and found that the proportionality factor (i.e. Froude number of the current) has a value of $\sqrt{2}$ for inviscid flows in deep ambient (i.e. H>>h). If the depth of the ambient, H, is comparable to the thickness of the current h, the experiments by Huppert and Simpson (1980) predict that the Froude number becomes a function of the ratio h/H.

Ellison and Turner (1959) proposed one of the first quantitative works on mixing of TC with ambient fluid. The model applies for conservative continuous flows and uses the layer-integrated conservation equations for flow momentum, flow volume and solute mass. It proposes that the motion of the turbulent layer is function of the rate of fluid entrainment which is related empirically with the Richardson number (Ri). The model was developed for flows driven by differences in salinity and temperature however can be used as an approximation for clay or silt-laden flows.

Bagnold (1962) developed a conceptual model for TC based on the autosuspension concept proposed by Knapp (1938) for streams. The autosuspension criterion is based on energy balance of steady currents: potential energy is lost as work is done to counteract friction and to keep sediment in suspension. The energy expended in unit time by the fluid in keeping in suspension sediment must be compensated by the power input of the tangential pull of gravity acting on the excess mass of the solids in the direction of transport:

$$g' m U S > g' m w_s \quad \frac{US}{w_s} > 1 \tag{2.5}$$

Where U is the mean flow velocity, S is the bed slope and w_s is the settling velocity of the sediment. If the criterion is satisfied, the concentration and then the velocity of the TC might increase indefinitely, limited only by the availability of solid material, since the sediment entrained from bed would excess the sediment settled. The concept of autosuspension on TC was further developed by Pantin (1979) and Parker et al. (1986)

First quantitative models of TC were based on modified forms of the Chèzy equation for steady uniform flow (Kuenen, 1952; Komar, 1977; Stacey and Bowen, 1988). The balance of forces acting was established between the gravity force and the force due to the fluid resistance on the lower and

upper boundaries. This type of models has been frequently used to model the motion of ignitive TC (Bowen et al., 1984; Piper and Savoye, 1993; Mulder et al., 1998) and to study erosion and deposition (Mulder et al., 1998).

4.2. 2D models and 2DH

The next level of complexity in the numerical and analytical modelling of TC is that of the 2D models that solve the dynamics of the current in the plane of the flow. Two different types of models can be distinguished: box models and 2DH/shallow water models.

Box models are not directly based on Navier Sokes equations and can be appropriate for finite volume releases. In box models it is assumed that the current evolves as a series of rectangles of constant area and any horizontal and vertical or streamwise variation of properties inside the current is neglected (Huppert, 1998). The current evolves in the form of a constant area or volume of well-mixed sediment (Huppert, 1998; Harris et al., 2002;). Box models have been applied to lock exchange flows to estimate the velocity of the current (Dade and Huppert, 1995; Gladstone and Woods, 2000; Salles et al., 2008, 2007) however the flow front velocity is given by a Froude number condition that depends on whether the interstitial fluid (i.e. water) is fresh or saline. This type of models usually does not consider water entrainment and the sedimentation rate is given by the product of mean sediment concentration and the rate settling particles. Since particles settle continuously and no entrainment of sediment is considered, the concentration invariable decreases with time. This decreasing concentration leads to smaller driving force, lower velocities and hence deposition. Due to the previous assumptions this type of models might only be appropriate for collapsing depletive flows and lock exchange problems.

Depth integrated models/shallow water models are applied to currents whose length is substantially larger than their depth and are derived from equations of flow mass conservation, flow momentum, sediment mass conservation. Sometimes an additional equation is included accounting for the balance between the production and dissipation of turbulent kinetic energy (Parker, 1982; Parker et al., 1986; Zeng and Lowe, 1997; Salaheldin et al., 2000). Depth integrated models temporally assume steady flow and, contrary to box models, 2DH models allow for streamwise variations of current height and velocity. Viscous stresses are assumed to be negligible in comparison to turbulent stresses. Vertical accelerations are assumed to be small, so that the pressure field is purely hydrostatic. In depth integrated models, velocity (and also concentration) is assumed to maintain an approximately similar profile in the vertical as it changes in time or in space. The vertical scale of the current results from the integration of the hypothetical vertical velocity profile over the thickness:

$$Uh = \int_0^\infty u(z)dz \tag{2.6}$$

where U is the depth integrated velocity, h the current thickness, $u(z)$ the a priori supposed vertical velocity profile. Given the definition of the vertical scale of the current, the suspended phase is implicitly considered well mixed across the height of the current so no vertical variations of volume concentration are taken into account. This assumption holds for fine sediment although it can be questionable in the case of coarser particles or during the late stages of the flow when turbulence decays and may no longer be able to distribute sediment across the whole height of the current (Meiburg and Kneller, 2010).

Model variables are the current thickness h, the average streamwise u and transverse v velocities and the average volume concentration for each specie c_i with $i = 1, \dots, n_s$. To close the model, all the remaining terms appearing in the equations (i.e. fluid entrainment, erosion and deposition, bed shear stress, shape factors related to the assumption of similarity of vertical profiles of flow velocity and sediment concentration and front velocity) must be expressed as function of model variables and derived values. These closure relationship are semi-empirical and derived using data from

observations of TC under controlled laboratory conditions (Parker et al., 1987; Altinakar et al., 1990, 1996; Garcia and Parker, 1991, 1993; Garcia, 1993, 1994).

Most of 2DH models follow a single-layer approach, which holds for deep environments where the motion of the overlying fluid can be neglected. In the case of shallow environments it is necessary to take into account the dynamics of the overlying fluid layer (Baines, 1995). Fluid entrainment at the upper boundary is a continuous process for most turbidity currents (Lüthi, 1981b; Laval et al., 1988; Stacey and Bowen, 1988) and is a standard component of depth averaged TC models (Parker et al., 1986) in the form of explicit functions. Models that use higher order turbulence closure (Stacey and Bowen, 1988; Felix, 2001) do not need to explicitly incorporate fluid entrainment effects. Detrainment, on the other hand, is not usually modelled although detrainment mechanisms have been identified through experimental modelling (Baines, 2001; De Rooij and Dalziel, 2001; Hogg and Huppert, 2001)

Depth integrated models, this is also valid for depth solving models, assume that sediment suspension is maintained through turbulent diffusive mixing of particles away from near bed areas with higher concentration. The diffusive transport is counteracted by sediment settling. Then the mass to and from the bed is the difference between the downward settling flux and the re-entrainment flux (Garcia and Parker, 1993; Skene et al., 1997). In depth integrated models the total mass of sediment suspended is determined as a function of the near bed sediment concentration, the sediment entrainment and the settling velocity. The sediment diffusion rate is related to the bed shear stress and the sediment characteristics (i.e. settling velocity) (Parker et al., 1986; Garcia, 1990). If the rate of re-entrainment of sediment exceeds the rate of near-bed sediment settling, the current increases its load, and therefore its density, accelerating with time; these type of flows are called ignitive currents (Parker, 1982). These flows are erosive and leave no deposit. On the other hand, in the case of depletive collapsing flows, the rate of downward sediment settling exceeds the rate of re-entrainment, and then the concentration decreases and the current decelerates. Most of the numerical models to date are limited to non-erodible seafloor (Meiburg et al., 2015) or the sediment available to be re-entrained is limited to the sediment deposited just before (models at bypass condition with sediment entrainment rate equalling the sediment deposition rate). A complete understanding of erosion deposition and re-entrainment processes has not been achieved but these processes are critical in the long term behaviour of TC and turbidity systems evolution. As such, they must be taken into account despite the limitations inherent in empirical formulations derived from experimental measurements.

Since turbulence processes are not completely understood and the small scales cannot be solved in 2DH models, closure relationships are needed in order to account for it. Two different possibilities exist: 1) by using an empirically derived function for fluid entrainment at the upper boundary or 2) by adding a 4^{th} equation that assumes proportionality between the turbulent kinetic energy and the bed shear stress (e.g. Parker et al., 1986; Salaheldin et al., 2000). The assumptions made in depth integrated models have been shown to be valid and comparable to higher-order turbulence closure schemes (Choi and Garcia, 2002).

The dynamics of the head play a key role in the overall hydrodynamic evolution of a TC (Simpson and Britter, 1979). The most popular way to treat the front is to identify the front grid cell and to impose a “front condition” based on experimental data from TC that have reached a steady-state (e.g. Benjamin (1968) or Huppert and Simpson, (1980)). However, since these relations are empirical they require calibration and verification. Another alternative is to treat the front as a discontinuous solution. The head of the TC resembles a dam-break (shock-)wave, hence numerical shock capturing techniques that are well established in the field of dam-break modelling can be applied (Bradford and Katopodes, 1999; Groenenberg, 2007).

Depth integrated models do not actually model the fluid dynamic processes within TC; the vertical scales are not solved. However, 2DH models can produce relatively accurate predictions of current evolution and deposit characteristics (Kneller and Buckee, 2000).

4.3.Depth solving models

Depth solving models can compute the velocity field and distribution of suspended sediment in the streamwise and upward-normal direction (Felix, 2001, 2002; Blanchette et al., 2005). The problem with depth solving models is the scarce number of field measures covering the vertical structure of turbidity currents. The overall shape of the current and the propagation speed are easy to monitor in laboratory but the velocity and concentration fields are difficult to measure accurately (Necker et al., 2005). The development of new technologies such as Ultrasonic Doppler Velocimetry Profiling (UDVP, i.e. measurement of current velocities over a depth range) (Best et al., 2001; Baas et al., 2005) or Acoustic Doppler Velocimetry (ADV, i.e. record instantaneous velocity components, including the effect of turbulent velocities fluctuations, at a single-point with a relatively high frequency) (Hogg et al., 2000) provide accurate measurements of flow structure but their application is still complicated. In addition the difficulty in the measurement, small scale processes are not that well known.

Depth solving models have appeared with the development of Computational Fluids Dynamics (CFD). Accurate numerical algorithms allow solving the governing equations describing the fluid flow. Three different methods can be discerned in CFD: Reynolds Averaged Navier Stokes (RANS), Large Eddy Simulation (LES) and Direct Numerical Simulation (DNS).

Reynolds Averaged Navier Stokes (RANS) is the older approach to turbulence modelling. An instantaneous quantity is decomposed into its time-averaged and fluctuating quantities. Equations are solved introducing new apparent stresses (i.e. Reynolds stresses). The Reynolds stresses are obtained through empirical closure models for which initial and boundary conditions are also needed. Two different approaches can be followed: the Reynolds stress model that attempts to actually solve the transport equations for the Reynolds stresses, and the Boussinesq hypothesis that uses an algebraic equation for the Reynolds stresses and determines the turbulent viscosity and the turbulent kinetic energy and dissipation (e.g. k-ε, mixing length model of Prandlt). Since RANS are averaged over time, the turbulence closure models are valid only as long as the time over which the changes in the mean occur is large compared to the time scales of the turbulent motion containing most of the energy.

In **Large Eddy Simulation (LES)** smallest scales of turbulence are removed through filtering and their effect is modelled using subgrid scale models (e.g. eddy viscosity models). In LES the largest and more important scales of the turbulence are resolved and the computational cost is reduced.

Direct numerical simulation (DNS) resolves numerically Navier-Stokes equations without any turbulence model. The entire range of turbulent length scales from the smallest dissipative scales (i.e. Kolmogorov microscales) up to the integral scale associated with the motions containing most of the kinetic energy. The computational cost is proportional to Re^3 (Pope, 2000) what makes impossible its application to flows with complex geometries or flow configurations.

With the exception of Direct numerical simulation, all other depth solving models use Reynolds averaged or empirical formulations for the vertical mixing (Felix, 2001; Choi and Garcia, 2002; Imran et al., 2004; Kassem and Imran, 2004). In addition to these, they generally assume that the turbulence is a result only of the water motion phase whilst given the size of the sediment transported, it can interfere with the smallest scales of Kolmogorov that are responsible for the dissipation of the kinetic turbulent energy. In the case of stratified flows, the stratification of the flow can damp the turbulence (i.e. the vertical turbulent momentum and heat exchanges are reduced) in a process that is not fully understood and only partially incorporated in high order turbulence closure models (Mellor and Yamada, 1982) as such this type of turbulence closure works adequately for low stratification flows (Yeh et al., 2013). When mixing becomes important (most often at the front of the

TC), even the higher order turbulence closure models cannot accurately describe the velocity field due to the importance of variability at small length scales and to the importance of the strong influence of the fluid-mechanics instabilities (Parsons et al., 2007).

Today large scale computational power is available at low cost and advances in numerical methods and mathematical algorithms produce accurate solutions for physical problems. These improvements have led to the development of more complex dynamic models. Numerical models are used with a wide range of purposes focused on different scales, from prediction of turbidite geometries and grain-size distribution (2DH models) to modelling of the vertical structure of turbulence (depth solving model). The choice of model to simulate a certain flow should be based in the scales of the processes to be simulated. The behaviour and limitations of simplified models are well known and interactions between sediment, ambient fluid and bed at the small scales are not fully understood. Adding process/parameters to a model to the limit of computational power is easy to justify. However the computational limit might be beyond the limit of our comprehension, and we might lose control on the processes and results since not all the processes (nor their interactions) involved are fully understood. Leaving things out and focusing in the essential processes for the phenomena simulated demands deep and real understanding of the physics driving the phenomena.

5. Governing equations and processes

The governing equations of an instantaneous Newtonian flow are the Navier-Stokes equation of conservation of momentum, the conservation of fluid mass and the conservation of sediment mass. The Navier-Stokes equation is a non-linear partial differential equation. The fluid is assumed to be a continuum and the stress in the fluid is the sum of a diffusing viscous term (term proportional to the gradient of velocity) and a pressure term. To date, it has not yet been proved that in three dimensions smooth solutions always exist and analytical solutions for the full equations are not available. In order to be analytically solved, simplifying assumptions are needed. The extent to which the simplifications are appropriate depends on the scale of interest. In the case of 2DH models of TC several simplifying assumptions are applied to the system of equations that drive the flow: incompressibility, Reynolds averaging, inviscid (or negligible viscous terms when the flow is fully turbulent) flow, boundary-layer (i.e. slender-flow approximation), layer-averaging, Boussinesq approximation. Additional closure relationships are needed for turbulence and sediment transport. In the following the derivation of the shallow water equations (i.e. conservation of mass and momentum of an arbitrary fluid of density ρ over an arbitrary volume control) and parameterization of sediment transport are presented.

In some early parts of the derivation index notation is used to reduce the clutter in the analysis. Position and instantaneous velocity vector are given by:

$$x_i = (x_1,\ x_2,\ x_3) = (x, y, z) \qquad u_i = (u_1,\ u_2, u_3) = \left(u_x, u_y, u_z\right) \tag{2.7}$$

Incompressibility simplifies the conservation of fluid mass and momentum equation (i.e. the divergence of the flow velocity is zero and $\frac{\partial \rho}{\partial p} = 0$). Incompressible flow refers to a flow with negligible pressure-induced density variations.

$$\frac{\partial u_x}{\partial t} + u_x \frac{\partial u_x}{\partial x} + u_y \frac{\partial u_x}{\partial y} + u_z \frac{\partial u_x}{\partial z} = -\frac{1}{\rho}\frac{\partial p}{\partial x} + \nu \frac{\partial^2 u_x}{\partial x^2} + \nu \frac{\partial^2 u_x}{\partial y^2} + \nu \frac{\partial^2 u_x}{\partial z^2} + g_x \tag{2.8a}$$

$$\frac{\partial u_y}{\partial t} + u_x \frac{\partial u_y}{\partial x} + u_y \frac{\partial u_y}{\partial y} + u_z \frac{\partial u_y}{\partial z} = -\frac{1}{\rho}\frac{\partial p}{\partial y} + \nu \frac{\partial^2 u_y}{\partial x^2} + \nu \frac{\partial^2 u_y}{\partial y^2} + \nu \frac{\partial^2 u_y}{\partial z^2} + g_y \tag{2.8b}$$

$$\frac{\partial u_z}{\partial t} + u_x \frac{\partial u_z}{\partial x} + u_y \frac{\partial u_z}{\partial y} + u_z \frac{\partial u_z}{\partial z} = -\frac{1}{\rho}\frac{\partial p}{\partial z} + \nu \frac{\partial^2 u_z}{\partial x^2} + \nu \frac{\partial^2 u_z}{\partial y^2} + \nu \frac{\partial^2 u_z}{\partial z^2} + g_z \tag{2.8c}$$

$$\frac{\partial u_x}{\partial x} + \frac{\partial u_y}{\partial y} + \frac{\partial u_z}{\partial z} = 0 \tag{2.8d}$$

Equations (2.8a) to (2.8c) are the momentum conservation equation in x, y and z direction and equation (2.8d) is the fluid mass conservation equation. The vectors $(u_x,\ u_y,\ u_z)$ and $(g_x,\ g_y,\ g_z)$ are respectively the vector of fluid velocity and the vector of gravitational acceleration, p is the pressure and ν the kinematic viscosity of the fluid. Spatial and temporal changes in the velocity field of an incompressible fluid are due to spatial changes of pressure, viscous forces and gravity.

Reynolds-averaging In the case of turbulent flows, instantaneous values u_i and p (same is valid for concentration c in the equation for sediment mass conservation) fluctuate about mean values. Here the mean values are denoted with an overbar, and the fluctuating values are denoted with a prime superscript, values of i correspond to x, y, and z:

$$u_i = \overline{u_i} + u_i' \qquad\qquad p = \bar{p} + p' \tag{2.9}$$

Averaging the equations (2.8a) to (2.8d) over turbulence results in the so called Reynolds-averaged form of the Navier Stokes equations (here after RANS):

$$\frac{\partial \overline{u_x}}{\partial t} + \overline{u_x}\frac{\partial \overline{u_x}}{\partial x} + \overline{u_y}\frac{\partial \overline{u_x}}{\partial y} + \overline{u_z}\frac{\partial \overline{u_x}}{\partial z} = -\frac{1}{\rho}\frac{\partial \bar{p}}{\partial x} + \frac{1}{\rho}\left(\frac{\partial\, \tau_{v,xx}}{\partial x} + \frac{\partial\, \tau_{v,xy}}{\partial y} + \partial\frac{\tau_{v,xz}}{\partial z}\right) + \frac{1}{\rho}\left(\frac{\partial\, \tau_{R,xx}}{\partial x} + \frac{\partial\, \tau_{R,xy}}{\partial y} + \partial\frac{\tau_{R,xz}}{\partial z}\right) + g_x$$

$$\frac{\partial \overline{u_y}}{\partial t} + \overline{u_x}\frac{\partial \overline{u_y}}{\partial x} + \overline{u_y}\frac{\partial \overline{u_y}}{\partial y} + \overline{u_z}\frac{\partial \overline{u_y}}{\partial z} = -\frac{1}{\rho}\frac{\partial \bar{p}}{\partial y} + \frac{1}{\rho}\left(\frac{\partial\, \tau_{v,yx}}{\partial x} + \frac{\partial\, \tau_{v,yy}}{\partial y} + \partial\frac{\tau_{v,yz}}{\partial z}\right) + \frac{1}{\rho}\left(\frac{\partial\, \tau_{R,yx}}{\partial x} + \frac{\partial\, \tau_{R,yy}}{\partial y} + \partial\frac{\tau_{R,yz}}{\partial z}\right) + g_y$$

$$\frac{\partial \overline{u_z}}{\partial t} + \overline{u_x}\frac{\partial \overline{u_z}}{\partial x} + \overline{u_y}\frac{\partial \overline{u_z}}{\partial y} + \overline{u_z}\frac{\partial \overline{u_z}}{\partial z} = -\frac{1}{\rho}\frac{\partial \bar{p}}{\partial z} + \frac{1}{\rho}\left(\frac{\partial\, \tau_{v,zx}}{\partial x} + \frac{\partial\, \tau_{v,zy}}{\partial y} + \partial\frac{\tau_{v,zz}}{\partial z}\right) + \frac{1}{\rho}\left(\frac{\partial\, \tau_{R,zx}}{\partial x} + \frac{\partial\, \tau_{R,zy}}{\partial y} + \partial\frac{\tau_{R,zz}}{\partial z}\right) + g_z$$

$$\frac{\partial \overline{u_x}}{\partial x} + \frac{\partial \overline{u_y}}{\partial y} + \frac{\partial \overline{u_z}}{\partial z} = 0 \tag{2.10}$$

Where $\tau_{v,ij}$ is the average viscous stress tensor and $\tau_{Ri,ij}$ represents the Reynolds stress tensor:

$$\tau_{v,ij} = \rho\nu\left(\frac{\partial \overline{u_i}}{\partial x_j} + \frac{\partial \overline{u_j}}{\partial x_i}\right) \qquad\qquad \tau_{R,ij} = \frac{\partial\left(-\rho\overline{u_i' u_j'}\right)}{\partial x_j} \tag{2.11}$$

Reynolds stresses account for turbulent fluctuations in fluid momentum (i.e. they quantify the tendency of turbulence to mix momentum at rates that exceed molecular processes).

When the viscous forces are small in comparison to the inertial forces, the assumption of **inviscid flow** may hold. These flows are generally identified by high Reynolds number. Viscous stress terms are omitted of the RANS and the equations (2.10) are reduced to:

$$\frac{\partial \overline{u_x}}{\partial t} + \overline{u_x}\frac{\partial \overline{u_x}}{\partial x} + \overline{u_y}\frac{\partial \overline{u_x}}{\partial y} + \overline{u_z}\frac{\partial \overline{u_x}}{\partial z} = -\frac{1}{\rho}\frac{\partial \bar{p}}{\partial x} + \frac{1}{\rho}\left(\frac{\partial\, \tau_{R,xx}}{\partial x} + \frac{\partial\, \tau_{R,xy}}{\partial y} + \frac{\partial \tau_{R,xz}}{\partial z}\right) + g_x$$

$$\frac{\partial \overline{u_y}}{\partial t} + \overline{u_x}\frac{\partial \overline{u_y}}{\partial x} + \overline{u_y}\frac{\partial \overline{u_y}}{\partial y} + \overline{u_z}\frac{\partial \overline{u_y}}{\partial z} = -\frac{1}{\rho}\frac{\partial \bar{p}}{\partial y} + \frac{1}{\rho}\left(\frac{\partial\, \tau_{R,yx}}{\partial x} + \frac{\partial\, \tau_{R,yy}}{\partial y} + \frac{\partial \tau_{R,yz}}{\partial z}\right) + g_y$$

$$\frac{\partial \overline{u_z}}{\partial t} + \overline{u_x}\frac{\partial \overline{u_z}}{\partial x} + \overline{u_y}\frac{\partial \overline{u_z}}{\partial y} + \overline{u_z}\frac{\partial \overline{u_z}}{\partial z} = -\frac{1}{\rho}\frac{\partial \bar{p}}{\partial z} + \frac{1}{\rho}\left(\frac{\partial\, \tau_{R,zx}}{\partial x} + \frac{\partial\, \tau_{R,zy}}{\partial y} + \frac{\partial \tau_{R,zz}}{\partial z}\right) + g_z$$

$$\frac{\partial \overline{u_x}}{\partial x} + \frac{\partial \overline{u_y}}{\partial y} + \frac{\partial \overline{u_z}}{\partial z} = 0 \qquad (2.12)$$

Slender-flow approximation (i.e. boundary layer approximation) this approximation states that for sufficiently high Reynolds number the flow over a surface can be divided into an outer region of inviscid flow (i.e. the majority of the flow) unaffected by viscosity and a region close to the surface where the viscosity is important (i.e. the boundary layer). The boundary layer approximation assumes that the streamwise and transverse length scales L_x and L_y are significantly larger than the length scale normal to the bed L_z over which the flow changes in the upward normal (z) direction ($L_x, L_y \gg L_z$). In addition to this, the approximation assumes that changes in flow lateral direction occur much more slowly than in the upward direction normal to the bed ($\frac{\partial^n}{\partial x^n}, \frac{\partial^n}{\partial y^n} \ll \frac{\partial^n}{\partial z^n}$). The mean pressure term can be decomposed into a hydrostatic pressure p_h and a dynamic pressure p_d related to the flow. The changes in the dynamic pressure p_d are considered very small due to the scaling considerations for slender flows; vertical component of velocity is much smaller than horizontal components ($u_z << u_x, u_y$). Reynolds stresses $\tau_{R,xx}$, $\tau_{R,yx}, \tau_{R,yx}$ and $\tau_{R,yy}$ associated to turbulence in the horizontal directions are neglected compared to those in the vertical directions $\tau_{R,xz}$ and $\tau_{R,zx}$ (no horizontal diffusion). Hence for fully turbulent flows small magnitude terms are considered negligible. Here after the gravity field vector g_i is replaced by its components according to the bed slope: $g_i = g(S_x, S_y, -1)$

The application of the boundary layer approximation to the momentum balance in the upward-normal direction reduces into the equation for hydrostatic pressure:

$$-\frac{1}{\rho}\frac{\partial \overline{p_h}}{\partial z} + g_z = 0 \qquad (2.13)$$

After integration and considering $\overline{p_h}|_{z=\infty} = 0$ it yields:

$$\overline{p_h} = \rho g(H - z) \qquad (2.14)$$

In the previous integration the upper limit of integration $y = H$ substitutes $y = \infty$, this approximation is valid as long as $\frac{H}{h} \ll 1$, where H is the current thickness and h is the total water depth.

The expression (2.14) can be differentiated in x and y and substituted in (2.12a) and (2.12b). Hence the system of equations, after application of the boundary layer approximation, is reduced to:

$$\frac{\partial \overline{u_x}}{\partial t} + \overline{u_x}\frac{\partial \overline{u_x}}{\partial x} + \overline{u_y}\frac{\partial \overline{u_x}}{\partial y} + \overline{u_z}\frac{\partial \overline{u_x}}{\partial z} = -g\,\frac{\partial H}{\partial x} + \frac{1}{\rho}\,\frac{\partial \tau_{R,xz}}{\partial z} + gS_x \qquad (2.15a)$$

$$\frac{\partial \overline{u_y}}{\partial t} + \overline{u_x}\frac{\partial \overline{u_y}}{\partial x} + \overline{u_y}\frac{\partial \overline{u_y}}{\partial y} + \overline{u_z}\frac{\partial \overline{u_y}}{\partial z} = -g\,\frac{\partial H}{\partial y} + \frac{1}{\rho}\frac{\partial \tau_{R,yz}}{\partial z} + gS_y \qquad (2.15b)$$

$$\frac{\partial \overline{u_x}}{\partial x} + \frac{\partial \overline{u_y}}{\partial y} = 0 \qquad (2.15c)$$

Further simplification can be achieved by applying the **depth-averaging** technique. The technique is valid as long as the horizontal length scale is much greater than the vertical length scale. The conservation of mass implies that the vertical velocity of the fluid is small. This technique assumes that the velocity u maintains an approximately similar profile in the vertical direction as it changes in time or in the flow. The integration of the vertical velocity profile of the flow over the thickness H of the underflow yields:

$$UH = \int_0^H \bar{u} dz \tag{2.16}$$

The equations are integrated from $z = 0$ to $z = \infty$ (i.e. far above the current, where the ambient water is in hydrostatic balance) under the boundary conditions $\overline{u_{x,y}}\big|_{z=\infty} = \overline{u_z}|_{z=0} = \overline{\tau_i}|_{z=\infty} = 0$ and $\overline{\tau_i}|_{z=0} = \tau_{b,i}$ (shear stresses evaluated at the bed). Vertically integrating allows the vertical velocity to be removed from the equations. The velocity term is not present in these equations, although it is not necessarily zero. As stated before, the vertical velocity field is assumed to be small and thus, negligible. Hence, after integration the equations can be rewritten in the form of the **shallow water equations** (also called Saint Venant equations in their unidimensional form):

$$\frac{\partial U_x H}{\partial t} + \frac{\partial U_x^2 H}{\partial x} + \frac{\partial U_x U_y}{\partial y} = -g\, H \frac{\partial H}{\partial x} + gHS_x - \frac{\tau_{b,x}}{\rho} \tag{2.17a}$$

$$\frac{\partial U_y H}{\partial t} + \frac{\partial U_x\, U_y H}{\partial x} + \frac{\partial U_y^2}{\partial y} = -g\, H \frac{\partial H}{\partial y} + gHS_y - \frac{\tau_{b,y}}{\rho} \tag{2.17b}$$

$$\frac{\partial H}{\partial t} + \frac{\partial U_x\, H}{\partial x} + \frac{\partial U_y\, H}{\partial y} = 0 \tag{2.17c}$$

Shallow water equations are widely used in fluid dynamics as situations where the horizontal length scale is much greater than the vertical scale are common. Shallow water equations describe the movement of a shallow flow driven by the force of gravity. In the case of turbidity currents the flow (i.e. turbidity current) is driven by the difference of density provided by the sediment in suspension with the ambient flow. Moreover due to the sediment entrainment and deposition the assumption of incompressibility does not hold. Instead, the **Boussinesq approximation** is commonly invoked for buoyancy-driven flows. Boussinesq approximation states that as long as the difference in density of the buoyancy driven flow and the ambient fluid are small, it can be neglected except where they appear in terms multiplied by g (i.e. the acceleration of gravity). The approximation assumes that the difference in inertia is negligible but the gravity is strong enough to make the specific weight appreciably different between the two fluids. Hence a reduced gravity $g' = g\frac{\rho_{sed} - \rho_w}{\rho_w}$ enters the equation of momentum conservation. Hence, the shallow water equations after application of the Boussinesq approximation are:

$$\underbrace{\frac{\partial U_x H}{\partial t}}_{a} + \underbrace{\frac{\partial U_x^2 H}{\partial x} + \frac{\partial U_x U_y}{\partial y}}_{b} = \underbrace{-g'\, H \frac{\partial H}{\partial x} + g' H S_x}_{c} - \underbrace{\frac{\tau_{b,x}}{\rho}}_{d} \tag{2.18a}$$

$$\frac{\partial U_y H}{\partial t} + \frac{\partial U_x\, U_y H}{\partial x} + \frac{\partial U_y^2 H}{\partial y} = -g'\, H \frac{\partial H}{\partial y} + g' H S_y - \frac{\tau_{b,y}}{\rho} \tag{2.18b}$$

$$\underbrace{\frac{\partial H}{\partial t}}_{e} + \underbrace{\frac{\partial U_x\, H}{\partial x} + \frac{\partial U_y\, H}{\partial y}}_{f} = 0 \tag{2.18c}$$

The equations (2.18a) to (2.18c) are the most common governing equations used in numerical model of turbidity currents (Parsons et al., 2007). The term a describes the steadiness of the flow. The term

b describes the change in the velocity caused by advection of a fluid parcel from one location to another. The term c is the driving force: the excess density and resulting pressure gradient supplied by the sediment in suspension. Term d is the turbulent dissipation term. The term e is the unsteadiness in mass of the flow at a particular location. The terms f are the fluxes of mass in and out of that same location.

Only DNS solve equations (2.8a) to (2.8d) directly. Equations (2.10a) to (2.10d) are the starting point for RANS models where conservation of mass and flow momentum are spatially averaged over water depth and time-averaged over all the turbulent fluctuations. In the case of LES the equations are time averaged over only the smaller turbulent fluctuations. For all the remaining cases, turbulence closure relationships are needed for the turbulence dissipation.

Reducing the number of dimensions is a common technique in order to reduce computational time. Depth averaging reduces the number of dimensions by one. Flow velocity and suspended sediment concentration are averaged over the thickness of the current, hence this type of models are called 2DH (where H stands for horizontal plane). 2DV models provide insight into the vertical structure of the current as equations are solved in the stream-wise and vertical plane. 1D models only consider variations in the streamwise direction of the flow and neglect lateral mass fluxes which are considered small when compared to fluxes in the streamwise direction. This type of models constituted the first approach to mathematical modelling of TC and was later extrapolated to 2DH models. Today the path followed should be the inverse one, provided that a fully dynamic process is available, the reduction of dimensions decreases the computational time and allows insight into the underlying physics. It should be noted the difference in stratigraphy and hydrodynamics in "naming" models. 2D models compute erosion and deposition providing a 3D evolution of turbidity systems. Hence 2D models are often called 3D models in the field of stratigraphy, a term reserved in hydrodynamics for a model that computes the flow variables in the three directions. Along the present thesis, the hydrodynamic convention is preferred as equations are solved in the two horizontal dimensions.

Suspended sediment transport in turbidity currents can be describe with a convection-diffusion equation (Sloff, 1993). The equation is obtained through conservation of mass for a unit volume and yields:

$$\frac{\partial ch}{\partial t} + \underbrace{\frac{\partial u_x ch}{\partial x} + \frac{\partial u_y ch}{\partial y} + \frac{\partial u_z ch}{\partial z}}_{a} - \underbrace{\frac{\partial}{\partial x}\left(\varepsilon_x \frac{\partial ch}{\partial x}\right) - \frac{\partial}{\partial y}\left(\varepsilon_y \frac{\partial ch}{\partial y}\right)}_{b} - \underbrace{\frac{\partial}{\partial z}\left(\varepsilon_z \frac{\partial ch}{\partial z}\right)}_{c} = \underbrace{w_s \frac{\partial ch}{\partial z}}_{d} \qquad (2.19a)$$

where ε_x, ε_y, ε_z are the diffusion coefficients and w_s is the settling velocity. The terms a are the advective transport. The terms b and c are the horizontal and vertical diffusion respectively. Finally the term d represents the settling of sediment out of the current. Since in TC the horizontal diffusion (i.e. terms b) is much smaller than the advection (i.e. terms a), they can be neglected in the sediment transport equation. Hence, the equation (2.19a) can be rewritten so that the changes in sediment concentration due to the exchanges with bed are contained on the right side of the equation:

$$\frac{\partial ch}{\partial t} + \frac{\partial u_x ch}{\partial x} + \frac{\partial u_y ch}{\partial y} + \frac{\partial u_z ch}{\partial z} = \frac{\partial}{\partial z}\left(\varepsilon_z \frac{\partial ch}{\partial z}\right) + w_s \frac{\partial ch}{\partial z} \qquad (2.19b)$$

Complex processes at the interface between bed and turbidity current and not completely known. In addition to this, when using a depth integrated model boundary terms gather various physical processes. These boundary terms should comprise friction, sediment entrainment, sediment concentration and interfacial mixing. Hence a parameterization of the right hand of the equation is needed. This parameterization can be based on two different concepts of sediment transport: flow capacity and flow competence. The former (i.e. flow capacity) is the total amount of sediment (of all different sizes) that the flow can transport and is related to the level of turbulent kinetic energy in

the flow. The latter (i.e. flow competence) is the ability of the flow to carry sediment of a given size and is usually parameterized by the ratio of the shear velocity to grain settling velocity. Since the shear velocity is function of the mean velocity and the bed drag coefficient, it is assumed to represent the vertical upward component of turbulence near the bed. The commonly used entrainment coefficient developed by Garcia and Parker (1991, 1993) is a representative case of competence-driven transport. The formulation was developed from experimental data of steady flow, sandy well-sorted sediment and moderately erosive turbidity current and has been successfully extended to unsteady flows (Admiraal et al., 2000) and flows where the sediment distribution is not uniform (Garcia, 1994).

Coriolis forces. Owing the spatial and temporal scales that turbidity currents can reach, the flow properties and sediment deposition patterns are likely to be influenced by the Coriolis forces due to the Earth's rotation. The Coriolis force is an inertial force that allows explaining the curved trajectory that follows a given object that perceives an observer in a rotating frame (see Fig.2.1). This deflection in the motion is known as Coriolis effect. The horizontal and unforced motion of a particle free of any external force in a rotating frame as the one in Fig.2.1 can be described as:

$$\frac{DU_x}{Dt} = +2\Omega U_y \qquad (2.20a)$$

$$\frac{DU_y}{Dt} = -2\Omega U_x \qquad (2.20b)$$

Where U_x and U_y are the velocities in x and y directions, respectively and Ω is the rate of rotation perpendicular to the xy plane (angular velocity).

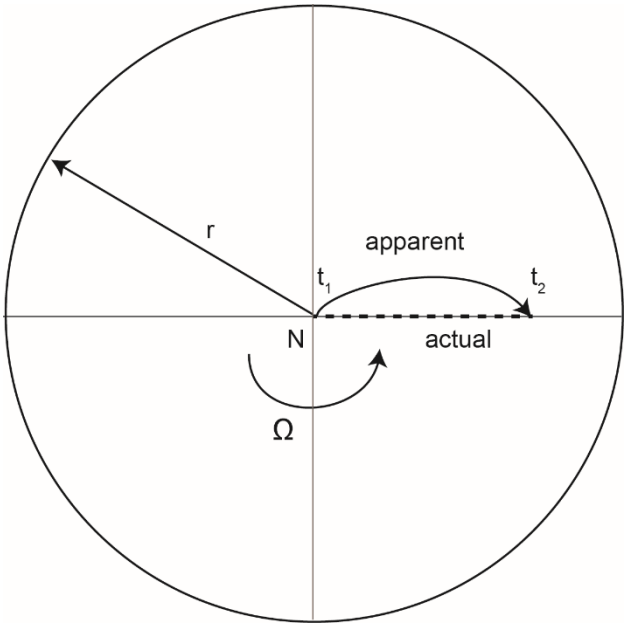

FIG.2. 1 PARTICLE MOVING IN A ROTATING PLATFORM. THE PLATFORM HAS AN ANGULAR VELOCITY Ω. THE PARTICLE MOVES FROM t_1 TO t_2. AN OBSERVER SITUATED ON THE PLATFORM WOULD SEE THE PARTICLE TRAJECTORY BETWEEN t_1 AND t_2 DEFLECTED. AN OBSERVER NOT ROTATING WITH THE PLATFORM WOULD SEE THE TRAJECTORY PERFECTLY STRAIGHT (DASHED LINE).

Since the Earth is a rotating system, the equations describing TC need an additional term to correctly describe fluid or particle motion. Large scale geophysical problems should be solved using a spherical polar coordinate system. At small scale problems, the curvature of the Earth can be ignored and a local Cartesian system on a tangent plane, as the one shown in Fig. 2.2a, can be adopted (e.g. Kundu et al., 1990). In this thesis, the horizontal length scales of the systems analysed are smaller than the radius of the Earth (r= 6371km) and a local Cartesian coordinate system is adopted. Coriolis forces change with latitude φ as shown in Fig.2.2b. The Coriolis parameter is defined as $f = 2\Omega sin\varphi$ where

$\Omega = 2\pi\ rad/s$. The effect of the Coriolis force (and hence f) increases with increasing distances to the Equator. By definition, f is positive in the Northern Hemisphere (counterclockwise sense of rotation) and negative in the Southern Hemisphere (clockwise sense of rotation). The Coriolis force tends to deflect the trajectory of a particle to the right of its direction of travel and to the left in the Southern Hemisphere. The unforced motion of a particle on a local Cartesian framework in the Earth can be written:

$$\frac{DU_x}{Dt} = +fU_y \qquad (2.21a)$$

$$\frac{DU_y}{Dt} = -fU_x \qquad (2.21b)$$

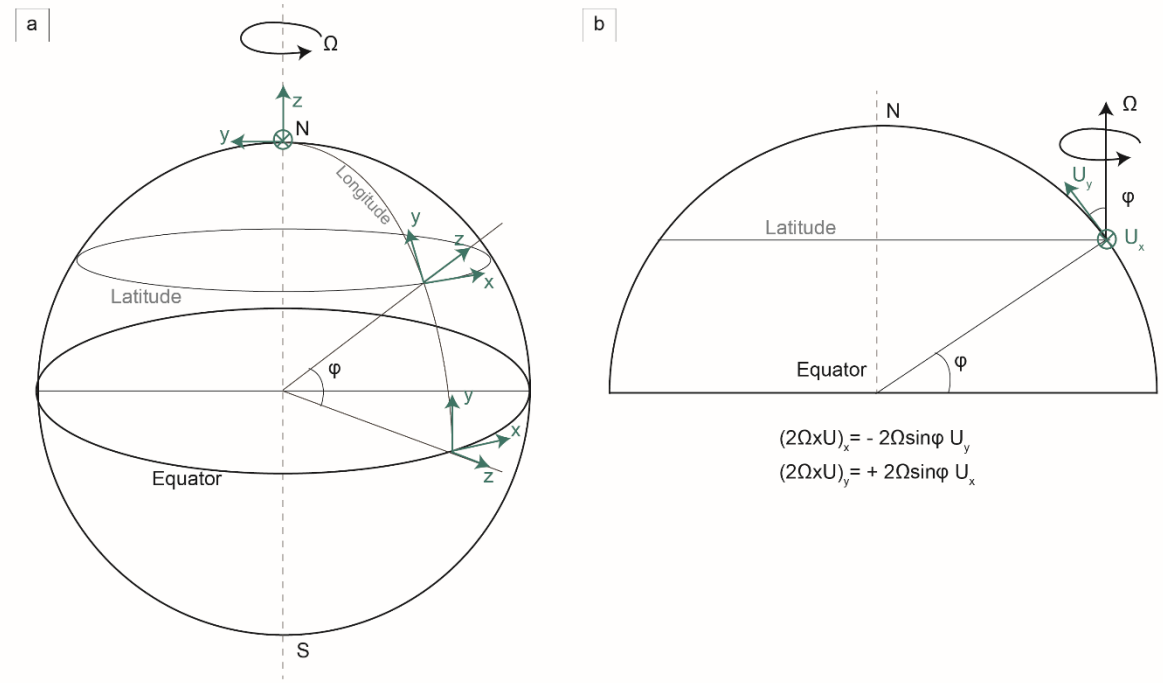

FIG.2. 2 DEFINITION OF A LOCAL CARTESIAN FRAMEWORK ON A ROTATING SPHERICAL EARTH. A) THE EARTH ROTATES COUNTER CLOCKWISE LOOKING FROM ABOVE THE NORTH POLE WITH A ROTATION RATE Ω.THE COORDINATE x IS DIRECTED EASTWARD, y NORTHWARD AND z UPWARD. THE CORRESPONDING VELOCITIES ARE U_x (EASTWARD), U_y (NORTHWARD) AND U_z (UPWARD). B) THE CORIOLIS FORCE ($-2\Omega \times U$) DEPENDS ON THE LATITUDE Φ.

The importance of the Coriolis force is determined by the time, space and velocity scales. The Rossby number Ro is the ratio of the inertial forces to the Coriolis forces and it determines whether rotation can be important in a system. It is defined as

$$Ro = \frac{U}{fL} \qquad (2.22)$$

where U is the horizontal velocity, f the Coriolis parameter and L the length scale of the system (i.e. total length, radios of curvature and channel width). Large Ro numbers indicate that the inertial forces dominate the system, whilst for small Ro Coriolis forces become important. As such, when the $Ro \sim 1$ the travel time is comparable to a rotation period of the Earth and the trajectory will be influenced by the Earth's rotation.

Coriolis forces play an important role in large scale geophysical flows such us low pressure systems, jet streams, surface ocean currents or western boundary currents, bottom geostrophic flows,

deflecting the flows to the right in the Northern Hemisphere. Given the large spatial and temporal scales of turbidity currents, it seems likely that Coriolis forces might play a role in their dynamics and final deposition patterns. Earth's rotation influence on the trajectories of turbidity currents and in the asymmetric construction of channel levees has previously been acknowledged (Komar, 1969; Middleton, 1993; Piper and Savoye, 1993; Nof, 1996; Kneller and Buckee, 2000) however the effect of Coriolis forces have often been neglected when studying or modelling turbidity systems. This fact seems surprising considering the architectural similarities (i.e. aggradational nature and levee formation, asymmetry in sedimentation and lateral migration) between some turbidity systems and contourite channels which are known to be driven by Coriolis forces and between TC and the bottom thermohaline circulation (Mulder et al., 2008; Cossu et al., 2015).

Recent experimental models and field observations have documented the role of Coriolis forces in large scale turbidity current dynamics for mid- and high latitudes. Coriolis forces can limit the spatial extent of sediment deposition (Wells, 2007, 2009), they play an important role in the latitudinal variation observed in submarine channel sinuosity (Peakall et al., 2012; Cossu and Wells, 2013; Cossu et al., 2015) and they also can result in a significant tilt of the interface and alter the 3D flow field (Cossu and Wells, 2010; Cossu et al., 2010; Wei et al., 2013). To my best knowledge, the effects of Earth's rotation which are taken into account in Nixes-TC (e.g. the application to the Alger canyon by Jamet (2010)) have not been considered in other numerical modelling of turbidity currents, maybe because "real" large scale applications of numerical models are scarce and better known systems are close to Equator.

6. Nixes-TC

Nixes-TC (Jacinto and Burel, 2003) is a numerical process-based model developed to reproduce underwater sediment-laden flows. The model follows the principles of those developed by Parker et al. (1986) and Bradford and Katopodes (1999). The spatial development of an unsteady turbidity current flowing in deep ambient fluid (Fig 2.3) can be described by the following set of vertically integrated partial differential equations derived by Parker et. (1986): the vertically integrated fluid, momentum and sediment conservation equation. Key improvements of Nixes-TC are the inclusion of a non-linear sedimentation model (settling velocity) in the equation of flux conservation, the development of a non-linear flow-dependent shear stress coefficient valid for all Re from laminar to fully turbulent flows, the inclusion of Coriolis effects, the treatment of the head and the existence of equilibrium solutions.

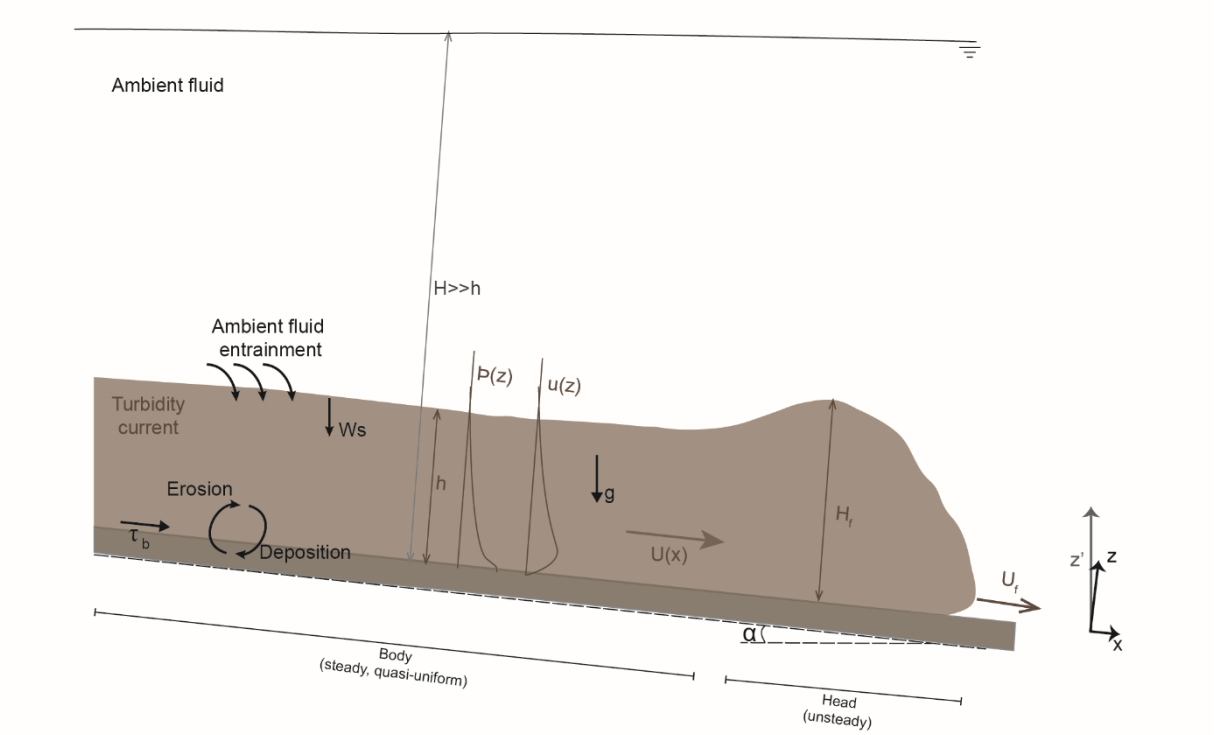

FIG.2. 3 DEFINITION SKETCH OF A TURBIDITY CURRENT FLOWING FROM LEFT TO RIGHT IN DEEP AMBIENT FLUID. MAJOR PROCESSES TAKEN INTO ACCOUNT ARE INCLUDED AS WELL AS VERTICAL PROFILES OF CONCENTRATION AND VELOCITY. THE TWO MAIN PARTS IN TC ARE SHOWN: THE UNSTEADY HEAD AND THE STEADY, QUASI-UNIFORM BODY.

6.1.Equations and processes included

The continuity and momentum equations at the basis of the model are virtually identical to the shallow water equations (equations 2.7 a, b & c) with the exception of the hydrostatic thrust. The inertial pressure is given by Bernoulli's principle (i.e. the pressure is proportional to the loss of kinetic energy along a streamline) and it is the reduced specific gravity of the particles that gives the deviation from hydrostatic pressure. Since the density difference between the TC and the ambient fluid is small, the Boussinesq approximation can be applied. The effect of the density difference is neglected in the acceleration terms but kept in the gravity terms, where it drives the flow. To solve the governing equations given above, closure relationships for the ambient fluid and sediment entrainment coefficients, shear velocity and near-bed sediment concentration are needed. In addition to the previous equations, Nixes-TC includes an equation of bed continuity, similar to Exner equation, due to sediment entrainment and deposition.

The system of equations can be expressed in the integral form as proposed by (Parker et al. (1986):

$$\frac{\partial \boldsymbol{U}}{\partial t}+\frac{\partial \boldsymbol{F}}{\partial x}+\frac{\partial \boldsymbol{G}}{\partial y}=\boldsymbol{Q} \qquad (2.23)$$

Where $\boldsymbol{U}=\left(h, hU_x, hU_y, h\emptyset_1, \ldots, h\emptyset_{n_s}\right)^T$ is the vector of conservative variables. The parameter h represents the flow thickness, hU and hU_y are the momentum flux in x and y respectively and $h\emptyset_i$ is the sediment flux for the ith sediment class. U_x and U_y , the vertically integrated velocities in x and y directions over the current thickness h, respectively; and $\emptyset_i$ the vertically integrated volume concentration of the i[th] sediment and n_s the total number of sediment classes contained in the current. Along this thesis, a single class of sediment is considered to better cope with data

limitations; sensitivity grain analyses are performed in order to assess grain size influence in TC dynamics. $\boldsymbol{F}$ and $\boldsymbol{G}$ are the flux vectors in x and y directions respectively containing the advection transport terms, and $\boldsymbol{Q}$ is the vector containing the sources and sinks (i.e. water entrainment, settling velocity, slope, shear stress, erosion and deposition).

6.1.1. Definition of the depth integrated variables

The TC model proposed by Parker et al. (1986) and other 2DH numerical and analytical models (e.g. Choi, 1998; Bradford and Katopodes, 1999; Felix, 2004, Princevac et al., 2005) are based on the depth integrated quantities proposed by Ellison and Turner (1959):

$$Uh = \int u dz \tag{2.24a}$$

$$U^2 h = \int u^2 dz \tag{2.24b}$$

$$U\emptyset_i h = \int u\emptyset_i dz \tag{2.24c}$$

The vertical scale of the flow (i.e. its thickness h) is based on the *a priori* supposed vertical velocity profile for TC. The thickness h is related to the mean position of the overall momentum in the flow, this is to say, a slab of thickness h and uniform velocity U having the same momentum as the TC. The definition of h is completely disconnected from sediment concentration $\emptyset$. This is problematic because it is $\emptyset$ that provides the potential energy to the TC to flow; without the sediment, the TC cannot exist. According to this definition (2.23), a TC can exist no matter whether there is or not sediment. Theoretically, following this definition of h, a TC would continue to grow indefinitely since, as $\emptyset$ and h are not coupled, the variations in h are only controlled by the water entrainment. There is no possibility of attaining equilibrium solution.

In Nixes-TC, the definition of h is different and allows the existence of equilibrium solutions. The parameter h provides the vertical scale of the TC and is defined as the thickness over which sediment is present according to:

$$\overline{z} = \frac{h}{2} = \frac{\int \emptyset z dz}{\int \emptyset dz} \tag{2.25a}$$

where $\overline{z}$ is the average position of the sediment, hence the current thickness can be defined as twice this value:

$$h = 2\frac{\int \emptyset z dz}{\int \emptyset dz} \tag{2.25a}$$

This definition of h implies that the current exists as long as there is sediment in it. The depth integrated volumetric concentration $\emptyset$ and the depth integrated current speed are based on this definition of h and write:

$$\emptyset_i = \frac{\int \emptyset dz}{h} \tag{2.25b}$$

$$U = \frac{\int U dz}{h} \tag{2.25c}$$

Since h is defined on the basis of the average position of the sediment ($\overline{z}$), the potential energy of the particles is available to balance the loss of kinetic energy due to the shear stress as it advances downslope. The work done by the gravity on the sediment is the source of power for the TC; it counteracts the loss of kinetic energy due to the turbulence and enables the energetic balance of the TC.

6.1.2. Equation of continuity

In the **fluid continuity equation** (Eq. 2.26), the evolution of the current thickness is governed by the variations at the interface with the ambient fluid. The current thickness varies according to convergence or divergence of the current due to water entrainment ($e_w U$) and the settling velocity (w_s). Water entrainment takes into account the turbulence effect at the interface between the ambient fluid and the turbidity current. The term $e_w U$ represents the rate of increase of current thickness due to entrainment of ambient fluid. The settling velocity w_s counteracts the ambient fluid entrainment since it favours the decrease of current thickness due to decantation.

$$\frac{\partial h}{\partial t} + \frac{\partial U_x h}{\partial x} + \frac{\partial U_y h}{\partial y} = e_w U - w_s \tag{2.26}$$

The fluid entrainment coefficient used in the model is the one derived by Parker et al. (1987) from experimental data of turbidity currents and conservative saline currents:

$$e_w = \frac{0.0075}{\sqrt{1+718 {Ri_b}^{2.4}}} \tag{2.27}$$

where Ri_b is the bulk Richardson number, which measures the stratification of the flow and is related to the densiometric Froude number Fr_d as it represents the ratio between the gravitational potential energy and the turbulent kinetic energy:

$$Ri_b = \frac{Rg\emptyset h}{U^2} = \frac{g\prime \emptyset h}{U^2} = \frac{1}{{Fr_d}^2} \tag{2.28}$$

The settling velocity w_s in the suspension is function of the settling velocity in clear water $w_{s,w}$. The settling velocity of sediment with grain size D is computed by the Zanke's formula (Zanke, 1977) that extends the Stokes' law for larger particles:

$$w_{s,w} = 10\frac{\nu}{D}\sqrt{1 + \frac{0.01\left(\frac{\rho_s}{\rho}-1\right)gD^3}{\nu^2}} \tag{2.29}$$

The viscosity is also calculated for every time step at every point and allows taking into account the effects of gel at high concentrations (Migniot, 1989a, 1989b):

$$\mu = \mu_w \left[1 + \left(\frac{\emptyset}{\emptyset_g}\right)^6\right] \tag{2.30}$$

where $\emptyset_g$is the gel concentration ($\emptyset_g \sim 3.5\%$) and the dynamic viscosity of water $\mu_w = 10^{-3} Pa.s$. However, due to the range of concentrations of turbidity currents the effects of gelification on the dynamic viscosity will be negligible for the calculus of the settling velocity.

The neighbouring particles can potentially undermine the settling velocity of a sediment particle for high concentrations. This process is called hindered settling and its effect can be modulated by taking into account the concentration of the suspension and the type of sediment (Richardson and Zaki, 1954; van Rijn, 1984):

$$\frac{w_s}{w_{s,w}} = \frac{1-\emptyset}{1+\left(\frac{\emptyset}{\emptyset_g}\right)^6} \qquad \text{for cohesive sediments} \tag{2.31a}$$

$$\frac{w_s}{w_{s,w}} = (1-\emptyset)^n, \quad n = 4 \qquad \text{for non-cohesive sediments} \tag{2.31b}$$

where $\emptyset_g$ is the gel concentration ($\emptyset_g = 3.5\%$). Taking into account the concentration values (<10^{-2}) considered for the turbidity currents in the present thesis, the hindered effects become negligible.

The settling velocity also appears in the equations of balance of sediment mass in the expression for erosion and deposition.

The inclusion of a sedimentation model (w_s) in the equation of continuity is one of the novelties of Nixes-TC and enables the existence of equilibrium solutions. It arises from the definition of the current thickness h (Eq. 2.25a). If no entrainment is considered, the variation of the current thickness can be derived from the definition of h. Since h is defined as twice the average position of the particles $\overline{z}$, the variation of the average position of the particles will give the variation of h:

$$\frac{dh}{dt} = \frac{d\overline{z}}{dt} = \frac{d}{dt}\left(\frac{\int \emptyset z\prime dz}{\int \emptyset dz}\right) \tag{2.32a}$$

The previous expression can be expressed in its discrete form as follows:

$$\frac{dh}{dt} = \frac{d}{dt}\left(\frac{\sum m_i z_i}{\sum m_i}\right) \tag{2.32b}$$

Where m_i is the mass of the ith particle and z_i the position of the ith particle. Since the mass m_i of the particles is constant, when deriving the right hand of the previous expression, it writes:

$$\frac{dh}{dt} = \frac{d}{dt}\left(\frac{\sum m_i z_i}{\sum m_i}\right) = \frac{\sum m_i}{\sum m_i}\frac{dz_i}{dt} = \frac{dz_i}{dt} = w_s \tag{2.32c}$$

Where the evolution of the mean position of the particles will be given by the settling velocity:

$$\frac{dh}{dt} = w_s \tag{2.32d}$$

Hence given that the nature of the TC is defined by the existence of sediment in suspension, evolution of the current thickness h is given by the balance between fluid entrainment and settling velocity.

6.1.3. Momentum equations

The **momentum equations** provide the energy equilibrium between the different forces acting in the current. Variations in momentum are due to the relative importance of the forces acting (i.e. inertial and hydrostatique pressure, gravity along slope, shear stress and Coriolis forces) and cause accelerations and decelerations of the TC. The equations in x and y write:

$$\frac{\partial U_x h}{\partial t} + \frac{\partial\left(U_x{}^2\, h\right)}{\partial x} + \frac{\partial\left(U_x U_y\, h\right)}{\partial y} = -\frac{1}{2}Rg\frac{\partial \emptyset h^2}{\partial x} + R\emptyset ghS_x - (u_{*x})^2 + fhU_y \tag{2.33a}$$

$$\frac{\partial U_y h}{\partial t} + \frac{\partial\left(U_x U_y\, h\right)}{\partial x} + \frac{\partial\left(U_x{}^2\, h\right)}{\partial y} = -\frac{1}{2}Rg\frac{\partial \emptyset h^2}{\partial y} + R\emptyset ghS_y - \left(u_{*y}\right)^2 - fhU_x \tag{2.33b}$$

where $R = (\rho_s - \rho)/\rho$ is the submerged specific gravity, where ρ_s is the grain solid density and ρ is the ambient fluid density. $S_x = \tan\alpha_x$ and $S_y = \tan\alpha_y$ are the bottom slope in the x and y

directions. The gravity acceleration writes g. The terms u_{*x} and u_{*y} are the x and y components of the shear velocity; fhU_y and fhU_x are the contribution of the Coriolis forces, where f is the Coriolis parameter function of the latitude.

The driving force is given by the projection of the reduced mass over the slope corresponding to the terms $ghR\emptyset_T S_x$ and $ghR\emptyset_T S_y$ along the x and y directions. The hydrostatic pressure balance is established between the deviatory pressure and the excess of gravitational force provided by the sediment in the flow. The contribution of the bed shear stress to motion is expressed by the quadratic formulation $\tau_b = \rho C_d U^2$ for fully developed turbulence, hence, the shear velocities in x and y write: $u_{*x}^2 = C_d U_x U$ and $u_{*y}^2 = C_d U_y U$ where U is the magnitude of the current speed and C_d is the coefficient of bed friction. Viscous stresses are given by the equation of Poiseuille. At equilibrium conditions, the driving force of the slope must be compensated by the bed shear. Hence, C_d is not constant and it may change as much as the forcing slope, with values ranging between 10^{-3} and 10^{-2} for turbulent flows as shown in the Moody diagram in Fig 2.4. The bed drag depends on the local properties of the flow: Reynolds number Re and relative roughness k_s/h, where $k_s = D$. Provided that the local flow properties may change at every time step and from one grid point to another, C_d is calculated at every time step for every grid point. It modulates the nature of the shear stress (viscous, smooth turbulence and rough turbulence), thus it is valid for all Re from laminar to fully turbulent.

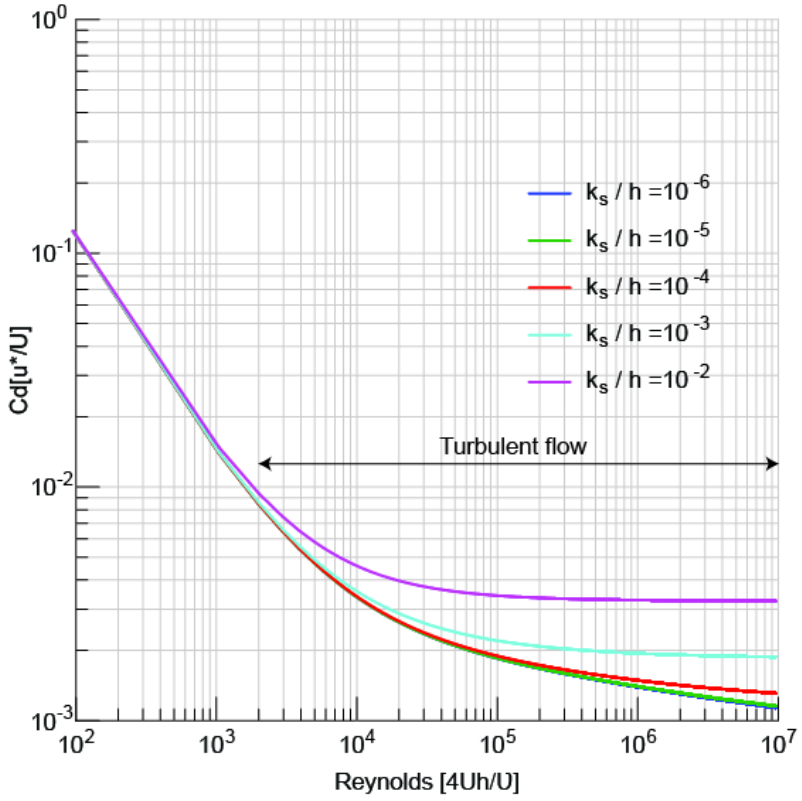

FIG.2. 4 BED FRICTION COEFFICIENT (CD) AS A FUNCTION OF THE REYNOLDS NUMBER FOR DIFFERENT RELATIVE ROUGHNESS (KS/H, WHERE KS IS THE BED ROUGHNESS AND H THE CURRENT THICKNESS). THE RANGE OF VALUES CORRESPONDING TO TURBULENT FLOWS IS ALSO INDICATED.

The momentum equations also include the contribution of the Coriolis forces: fhU_y and $-fhU_x$, where f is the Coriolis parameter. The Coriolis parameter expresses the influence of the rotation of the Earth and it writes $= 2\Omega sin\varphi$, where Ω is the angular speed of the Earth and φ is the latitude of

the system studied. Hence Coriolis forces might be important for mid and high latitudes depending on the temporal and spatial scales of the flow.

6.1.4. Sediment mass conservation

The sediment mass conservation equation expresses the balance between the divergence of the horizontal flux of particles, the erosion and the deposition:

$$\frac{\partial \emptyset h}{\partial t} + \frac{\partial \emptyset U h}{\partial x} = w_s(pE_s - \emptyset_b) \quad (2.34)$$

The term $w_s(pE_s - \emptyset_b)$ represents the net flux of sediment into the current due to erosion and deposition. Both erosion and deposition are expressed as empirical relationships depending on the settling velocity w_s of the sediment. E_s is the sediment entrainment coefficient, which is generally related to local bed shear stress and the settling velocity of particles. The sediment entrainment coefficient is formulated with the empirical relationship developed by Garcia and Parker (1991, 1993) from experimental data:

$$E_s = \frac{AZ_u^5}{1+\frac{A}{0.3}Z_u^5} \quad (2.35)$$

where $Z_u = \frac{u_*}{w_s} Re_p^{0.6}$, $u_* = \sqrt{\frac{\tau_b}{\rho}}$, $A = 1.3 \cdot 10^{-7}$ and $Re_p = \frac{\sqrt{RgD}D}{\nu}$ is the particle Reynolds number, where D is the particle diameter and ν is the kinematic viscosity.

The inclusion of the porosity $(1 - p)$ in the equation allows us to consider a possible consolidation of the sediment and thus a mobilization threshold. Likewise, $\emptyset_b$ represents the near-bed sediment concentration. In the simulations run in the present thesis, it is considered $\emptyset_b = \emptyset$. If pE_s exceeds $\emptyset_b$, the current entrains more sediment than it loses through deposition. Hence, the current may become heavier, increasing the terms $ghR\emptyset_T S_x$ and $ghR\emptyset_T S_y$ which is the term quantifying the driving force of the turbidity current. As a result of this, the current may accelerate increasing U and thus, increasing also the sediment entrainment $w_s pE_s$ entering the current in a self-reinforcing cycle.

6.1.5. Bed evolution

Turbidity currents can gain sediment through entrainment and can lose it through deposition altering the bed over which they flow. Modifications in bed can affect the hydrodynamics of the TC in turn. Nixes-TC includes a bed continuity equation similar to the Exner equation, although here the sediment flux is vertical.

$$\frac{\partial z}{dt} = \frac{D-E}{1-\gamma} \quad (2.36)$$

where and $\partial z/\partial t$ is the temporal evolution of the bed, $D - E$ is the net vertical flux of sediment onto the bed ($w_s\emptyset_b - w_s E_s$) and γ is the porosity of the bed.

The bed continuity equation is computed at each time step and hence enables tracking bed evolution. The equation is coupled to the hydrodynamics and allows one to keep track of the loose sediment and the development of an erodible bed (for deposition larger than erosion) that can be removed in later stages of the flow. Additionally, it allows the calculation of the slopes needed for momentum equation.

The inclusion of the bed continuity equation is the starting point for morphodynamics and stratigraphic models. To my knowledge one of the few process-based models specially developed for long-term stratigraphic evolution of TC is FanBuilder (Groenenberg, 2007; Groenenberg et al., 2009).

The stratigraphic evolution is achieved by modelling multiple successive turbidity current events; tectonic activity and background sedimentation alter the basin floor during the quiet intervals between TC events.

Whilst in short-event scales subsidence and tectonic uplifting can be negligible and it is relatively feasible to calculate the flow in detail and hence the bed evolution, at large time scales sediment and bedrock surfaces evolve together. Stratigraphic modelling might be achieved through upscaling of morphodynamics and the use of Morphological Acceleration Factor (MORFAC). The concept of MORFAC was introduced by Lesser et al. (2004) and Roelvink (2006) in coastal environments. The use of MORFAC would enable to bridge the gap between short-term hydrodynamics varying from hours to days and morphological changes taking place over much longer periods.

6.2.Numerical scheme, inputs and outputs

The model is coded in Fortran. The **Volume Finite Method** permits evaluating the coupled system of nonlinear hyperbolic partial differential equations (Bradford and Katopodes, 1999). The source terms (i.e. $\boldsymbol{Q}$) are calculated following a local implicit scheme first implemented in Nixes-TC. The Riemann problem at each interface (numerical fluxes F_h and F_v) is solved approximately following Roe (1981). The dam-break shock wave front is accurately captured by the order numerical method implemented (Roe, 1981; Hirsch, 1990). Non-reflective open outflow boundaries are implemented by using ghost cells (outside the domain of interest). The reflection of $\emptyset_i$, h, U_x and U_y are placed in the ghost cell (i.e. values of $\emptyset_i$,, h, U_x and U_y remain unchanged). This type of boundary ensures that the information can freely exit the computational domain without causing disturbances to the solution. Additionally, two different types of inflow boundary conditions can be provided depending on the whether the inflow is subcritical or supercritical. In the former case (e.g. resuspension from deposited sediment) only two independent quantities must be specified generally h and $\emptyset_i$. In the case of supercritical flow (e.g. hyperpycnal flow) the current speed at the inflow boundary must also be specified. The semi- implicit numerical scheme ensures numerical stability as this type of algorithms can cope with sharp changes in solution by using reduced time steps. The condition of stability applied is the Courant-Friedrichs-Levy (CFL) condition.

Inputs of the model are the regular orthogonal grid of the bathymetry, sediment properties (i.e. grain size, fraction of a given sediment grain size and density) and initial deposit (i.e. volume concentration and porosity). The kinematic viscosity and density of water as well as the von Karman coefficient for the turbulence closure are also included in the parameters file. Initial and boundary conditions are provided to the model in terms of position, mass and volume of sediment remobilized in the case of sediment remobilized due to trawling (i.e. La Fonera). In the case of hyperpycnal flow (i.e. Var and Boucart) values of $\emptyset_i$, h, U_x and U_y are placed at position of the river mouth.

Outputs of the model are the values of current thickness, current velocity (streamwise and transverse direction) and sediment concentration at each grid point and each time step. These variables allow the calculation of mass flux and instantaneous sediment transport and bed shear stress. Variations of the floor in terms or sediment balance and horizontal distribution of the sediment are also computed by the model.

The **model work flow** is structured as follows (see Fig. 2.5): at $t = t_0$ initial slope, boundary conditions and initial inflow variables are assigned from the input files and the flow loop starts. For each time step two different parts can be discerned: the flow time step computation as such and the update of the different variables involved in the calculation. The calculation of the numerical fluxes at the interfaces (F_h and F_v) and the source terms (Q, including erosion and deposition) allows solving the hydrodynamics (h, U_x and U_y), and once the hydrodynamic variables are known, the sediment transport $\emptyset_i$ can be calculated. Once the flow time step computation is over, the values of time step slope, deposition and porosity as well as the boundary conditions are updated. The new time step inflow conditions ("event" in Fig 2.5 varies with time) are read and assigned before starting the calculation of the new flow time step. The flow loop finishes once the final time step, provided in

the parameters file, is reached. Different output files are produced throughout the calculation: control point output files providing the temporal evolution of current variables for a single point; time step control files providing at a given time step the values of the current values and sediment distribution for the whole grid and the final deposition output file.

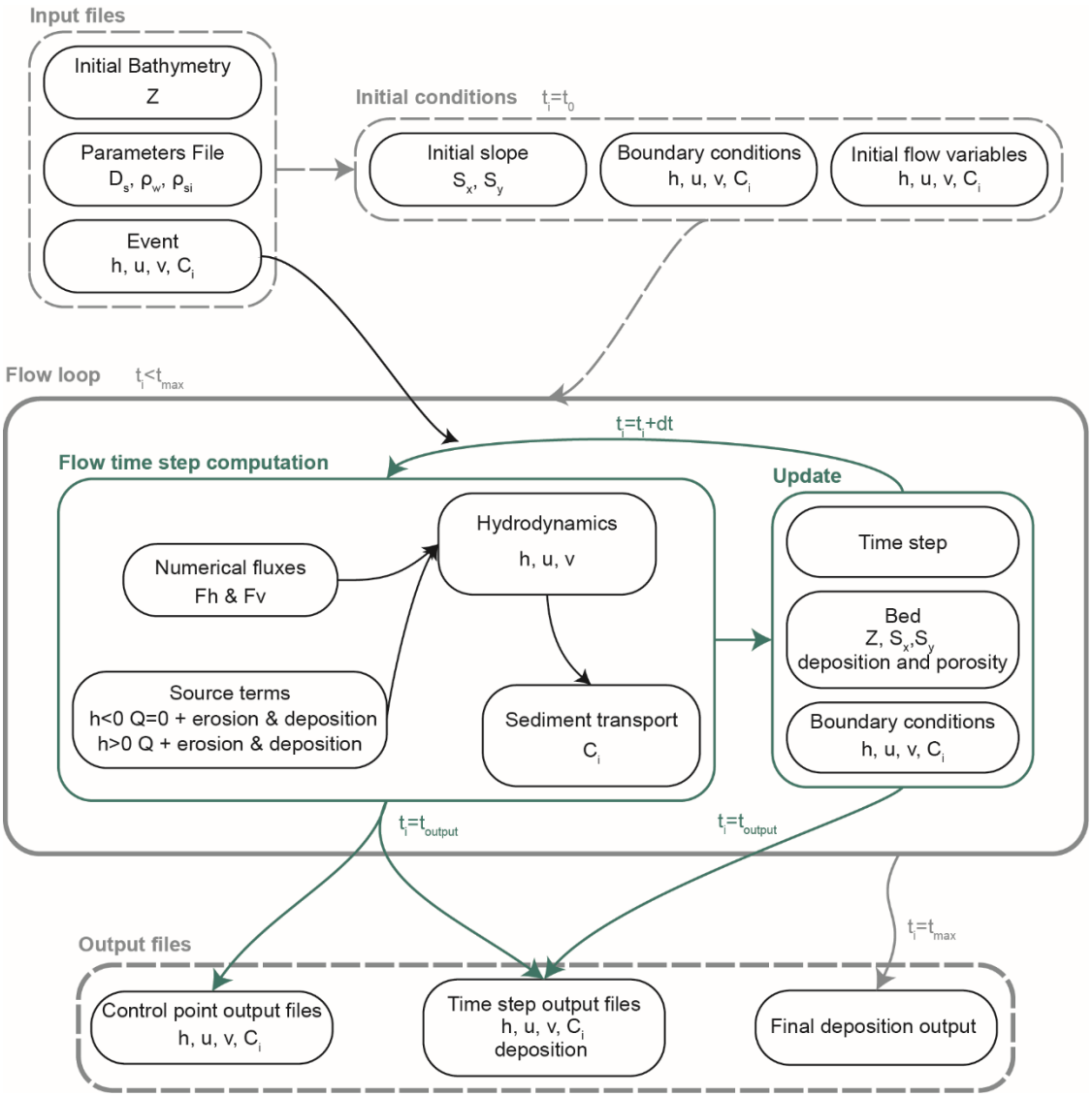

FIG.2. 5 WORK FLOW OF THE MODEL: ONCE THE INITIAL CONDITIONS ARE DEFINED FROM THE INPUT FILES, THE FLOW LOOP STARTS. AT EVERY FLOW TIME STEP COMPUTATION THE NUMERICAL FLUXES AND THE SOURCE TERMS THAT ALLOW THE COMPUTATION OF THE HYDRODYNAMICS ARE COMPUTED. ONCE THE HYDRODYNAMIC VARIABLES ARE SOLVED, THE SEDIMENT CONCENTRATION IS DETERMINED. ONCE THE FLOW TIME STEP COMPUTATION IS FINISHED, THE BOUNDARY CONDITIONS, BED PARAMETERS AND TIME STEP ARE UPDATED. THE NEW TIME STEP INFLOW CONDITIONS ARE ASSIGNED BEFORE ENTERING THE CALCULATION OF THE NEXT FLOW TIME STEP. OUTPUT FILES CONTAIN INFORMATION ON THE CURRENT VELOCITY, THICKNESS AND CONCENTRATION AS WELL AS OF THE HORIZONTAL DISTRIBUTION OF SEDIMENT.

6.3.Equilibrium solutions

Since natural systems have a tendency to come to balance it seems important to have a model that is able to simulate and reproduce this equilibrium in earth systems and to provide realistic solutions for the equilibrium. Two different forms of equilibrium can be considered: stasis (or static equilibrium) and dynamic equilibrium. The former is a theoretical ideal since it is characteristic of isolated systems

where there is no interaction across the boundaries and the conditions in the system remain constant. The latter means that the different forces or processes acting in the system are balanced for a given spatial and temporal scale.

A TC is in equilibrium when a uniform steady state is reached. This equilibrium state implies that temporal and spatial variations of the current variables are negligible ($\frac{\partial}{\partial t}\sim 0$ and $\frac{\partial}{\partial x}\sim 0$). For simplicity the equations are presented in the direction of the flow and Coriolis effects are considered negligible in order to evaluate the equilibrium solutions:

$$\frac{\partial h}{\partial t}+\frac{\partial Uh}{\partial x}=e_w U-w_s \tag{2.37a}$$

$$\frac{\partial Uh}{\partial t}+\frac{\partial(U^2\,h)}{\partial x}=-\frac{1}{2}Rg\frac{\partial \emptyset h^2}{\partial x}+R\emptyset ghS-C_d U^2 \tag{2.37b}$$

$$\frac{\partial \emptyset h}{\partial t}+\frac{\partial \emptyset Uh}{\partial x}=w_s(pE_s-\emptyset_b) \tag{2.37c}$$

The previous equations provide a potential equilibrium since for each one of the equations sources and sinks can be potentially balanced contrary to other TC models (e.g. Parker et al., (1986)). The equilibrium arises from the vertical scale of the flow considered. 2DH models (e.g. Parker et al., 1986) define h on the basis of a mean position of the overall momentum in the flow whilst in Nixes-TC the current thickness h is given by the averaged position of the sediment grains, which results in the inclusion of a sedimentation model (w_s) in the continuity equation (Eq. 2.37). In fact (with the exception of Nixes-TC) h is generally decoupled from the sediment concentration ($\emptyset$) that gives its nature to the TC and its evolution is exclusively controlled by the water entrainment ($e_w U$). These models have no equilibrium solution, the h can theoretically increase to the point that there is virtually no sediment included. This means that the TC is self-accelerated and can grow its thickness continuously resulting in flows that grow physically to unrealistic proportions.

The presence of sediment enables the energetic equilibrium in the TC since it provides the potential energy that balances the dissipation due to shear stress as the TC flows downslope. The work done by the gravity on the sediment is the source of power for the TC. The potential energy of the particles counteracts the loss of kinetic energy due to shear stress and increasing turbulence and enables the energetic balance of the TC. By considering a constant value of shear stress, as is the case in most models, the type of flow is preconditioned. Since C_d is related to Ri_b and hence to Fr, by imposing a constant C_d one would also impose the Fr. The approach followed by the model takes into account the non-linearities inherent to TC and allows the current to propagate over long distances once the low gradient slopes of the deep basin slope and floor are reached, before finally waning and depositing.

The equations (2.37a) to (2.37c) can be rewritten for the equilibrium as follows:

$$e_w U=w_s \tag{2.38a}$$

$$R\emptyset ghS=C_d U^2 \tag{2.38b}$$

$$pE_s=\emptyset_b \tag{2.38c}$$

This equilibrium implies that the current thickness is constant and uniform and is determined by the balance between ambient fluid entrainment ($e_w U$) and sediment decantation (w_s) at the interface between the ambient fluid and the flow. In addition head and body of the current have the same current speed and it doesn't evolve in time due to the driving force of the current ($R\emptyset ghS$) being

counteracted by the shear stress $(C_d U^2)$, hence head and body share the same Fr_d. This equilibrium condition is achieved when the current reaches bypass conditions, this is to say, the sediment deposited is immediately entrained.

The existence of equilibrium solution means that TC variables can be predicted provided the slope (S) and grain size (i.e. settling velocity, w_s) are known and a value of Re is assumed (see Fig 2.6). At equilibrium conditions, the C_d can be expressed in terms of Ri_b. Since C_d varies with Re and the slope S is known, the Ri_b of the flow can be determined. Since water entrainment e_w is function of Ri and the settling velocity w_s is known, the current speed U is determined from the continuity equation. Once U is known, h can be inferred from the Re and the missing $\emptyset$ of the flow can be easily retrieved from the Fr_d.

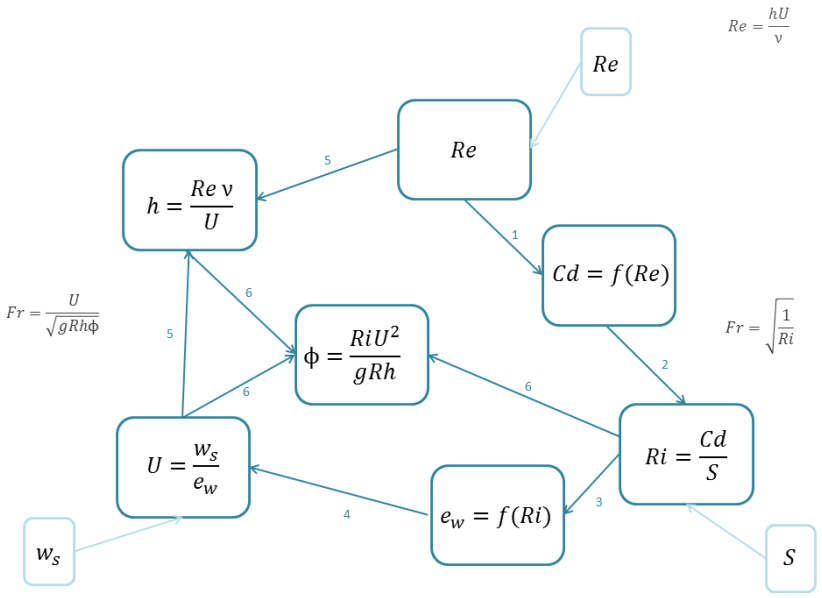

FIG.2. 6 PROVIDED A GIVEN TYPE OF SEDIMENT (w_s) AND A SLOPE (S), DIFFERENT EQUILIBRIUM CONDITIONS CAN BE ACHIEVED FOR DIFFERENT VALUES OF Re. Cd IS EASILY DETERMINED SINCE IT IS FUNCTION OF Re (1). AT EQUILIBRIUM, Ri_bCAN BE RETRIEVED FROM THE MOMENTUM EQUATION (2). ONCE THE Ri_b IS DEFINED, e_w IS KNOWN (3). THE U IS DETERMINED FROM THE CONTINUITY EQUATION FOR A GIVEN SEDIMENT TYPE (w_s) AND e_w (4). THE CURRENT THICKNESS h CAN BE DETERMINED FROM THE Re ONCE U IS KNOWN (5). FINALLY, $\emptyset$ IS OBTAINED FROM Ri SINCE U AND h ARE ALREADY KNOWN (6).

This equilibrium doesn't mean that the TC flows from the source point to the deposition point with the same current speed, sediment concentration and thickness. It means that for a set of given conditions (i.e. constant slope) it will show a tendency towards the equilibrium and that if the acting forces are balanced, it will continue flowing "indefinitely" with constant values of h, Fr and U. If the TC encounters new conditions (i.e. slope), it will move towards a new state of equilibrium. Let consider a TC flowing from shallower areas to deeper regions. Presumably it will move through decreasing slopes along its pathway and it might reach equilibrium conditions on each slope. Fig 2.7 shows the results obtained for different combinations of w_s and S with varying Re. The analysis of equilibrium solutions provides insight into features observed in the field such as long run out flows or sand deposits on terraces.

The equilibrium solutions analysis is performed for grain sizes of 10µm ($w_s = 7.8477 \cdot 10^{-5}$m/s), 20µm ($w_s = 3.1382 \cdot 10^{-4}$m/s), 40µm ($w_s = 1.2525 \cdot 10^{-3}$m/s), 63 µm ($w_s = 3.0849 \cdot 10^{-3}$) and 100µ ($w_s = 7.5621 \cdot 10^{-3}$m/s), and slopes of S =0.001 (0.1%), S =0.005 (0.5%), S =0.010 (1%), S =0.025(2.5%), S =0.050(5%) and S =0.100 (10%). For simplicity and in order to account for realistic solutions, only the results for the range of concentrations 0.0001g/l and 100g/l are presented.

The analysis of the response of Fr and Re to different conditions of slope S and grain size show the classic result of Fr decreasing with the slope S and for a fixed S higher Re and Fr are needed to keep in equilibrium a flow containing bigger size particles (Fig. 2.7).

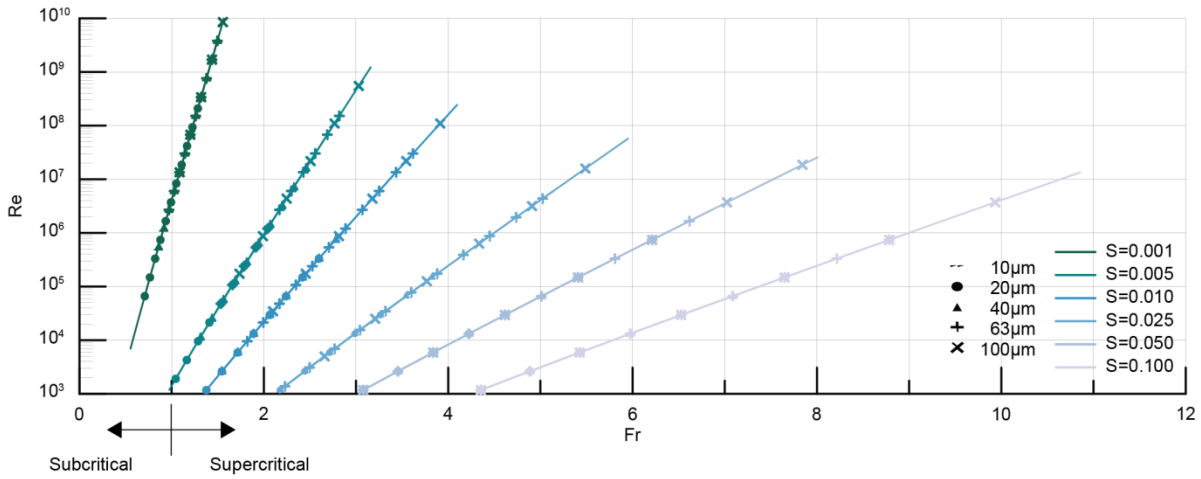

FIG.2. 7 EQUILIBRIUM SOLUTIONS OBTAINED FOR DIFFERENT COMBINATIONS OF w_s AND S WITH VARYING Re.

For slope values as those present offshore of the continental rise and on submarine channels (i.e. $S = (0.001, 0.005)$), equilibrium values are around Fr=1 (Fig 2.7). The head and the body of the TC travel at different speeds, at least in the early stages of the flow, with the speed of the front being smaller than that of the body. At the TC head, the pressure gradient is balance by the inertia term; as such head speed is determined by its thickness and its reduced gravity (see Eq. 2.4). The speed of the body depends on its thickness, on the reduced gravity and on the slope (see Eq. 2.38b). Since by definition the canyon head has a $Fr = 1$, in a situation of equilibrium at low slopes, body and head would share the same Fr , would have similar thickness and would be able to travel as a single entity along long distances. Body and head of the current travelling as a single entity could explain the long run outs observed in TC in some deep fan areas. For higher values of slope, two different possibilities arise, as the velocity of the head tends to remain constant (Britter and Linden, 1980; Altinakar et al., 1990). The first possibility is that the body gets into the head and with distance the head may expand increasing its thickness due to the material feeding from the body and to increased entrainment of the dilute water (Middleton, 1966a; Britter and Linden, 1980; Simpson, 1997) in a mechanism similar to a surge (surge-type currents). The second possibility is that they advance down the slope together (i.e. when the velocity of the body is similar to that of the head) in a more continuous body way depending on the values of h, U, and $\emptyset$ (the different possibilities will be explored in the following).

For a given slope, higher Re are needed for larger particle size, Larger slopes present smaller spanning ranges of Re. It is remarkable that for high slopes such as S=0.1, there are equilibrium solution for grain sizes corresponding to sand. This means that in turbidity systems, sand is not only transported by bed load transport but that it can also be transported in suspension in the flow. This would explain the sandy deposits found in terraces and levees (e.g the terraces in the Var canyon (Mas et al., 2010)).

The influence of the slope and the grain size in the current variables concentration of sediments C, current thickness H and current speed U at the equilibrium and the non-linear interactions between variables are explored in Fig. 2.8. C and h seem to depend more on the slope that on the grain size since they are directly related by the conservation of momentum (Eq. 2.38b) and U suffers a bigger influence of the grain size as it is linearly dependent on the grain size in the continuity equation (Eq. 2.38a). The values obtained for the equilibrium solution for the range of concentrations evaluated are realistic and correspond to those measured of inferred from field studies (e.g. Xu et al., 2004;

Khripounoff et al., 2012; Hughes Clarke, 2016) with values of current speed up to 25m/s for the larger grain sizes (see Fig. 2.8b) and current thickness up to 100-200m for the larger grain sizes and larger slopes (see Fig 2.8c), indeed there seems to exist a threshold for current thickness.

At the equilibrium TC flowing over higher slopes, present higher Fr values. Lower Fr are equivalent to higher Ri and hence lower water entrainment (e_w), for a given slope S. For a given grain size (i.e. given w_s), this implies a higher current speed U for lower slopes according to the equation (2.38a). Conversely, lower Fr imply higher e_w and hence lower U for a given grain size (i.e. w_s). Since at the equilibrium the momentum equation (2.38b) should also hold, and should the quantity of sediment in suspension (hC) be constant, lower slopes would imply higher Ri, lower e_w and higher U , and hence higher shear stress values (C_d). Since the e_w is smaller, the current thickness h grows less, and in order to maintain the conservation of sediment mass, C needs to increase more as can be seen in Fig 2.8a and Fig 2.8b.

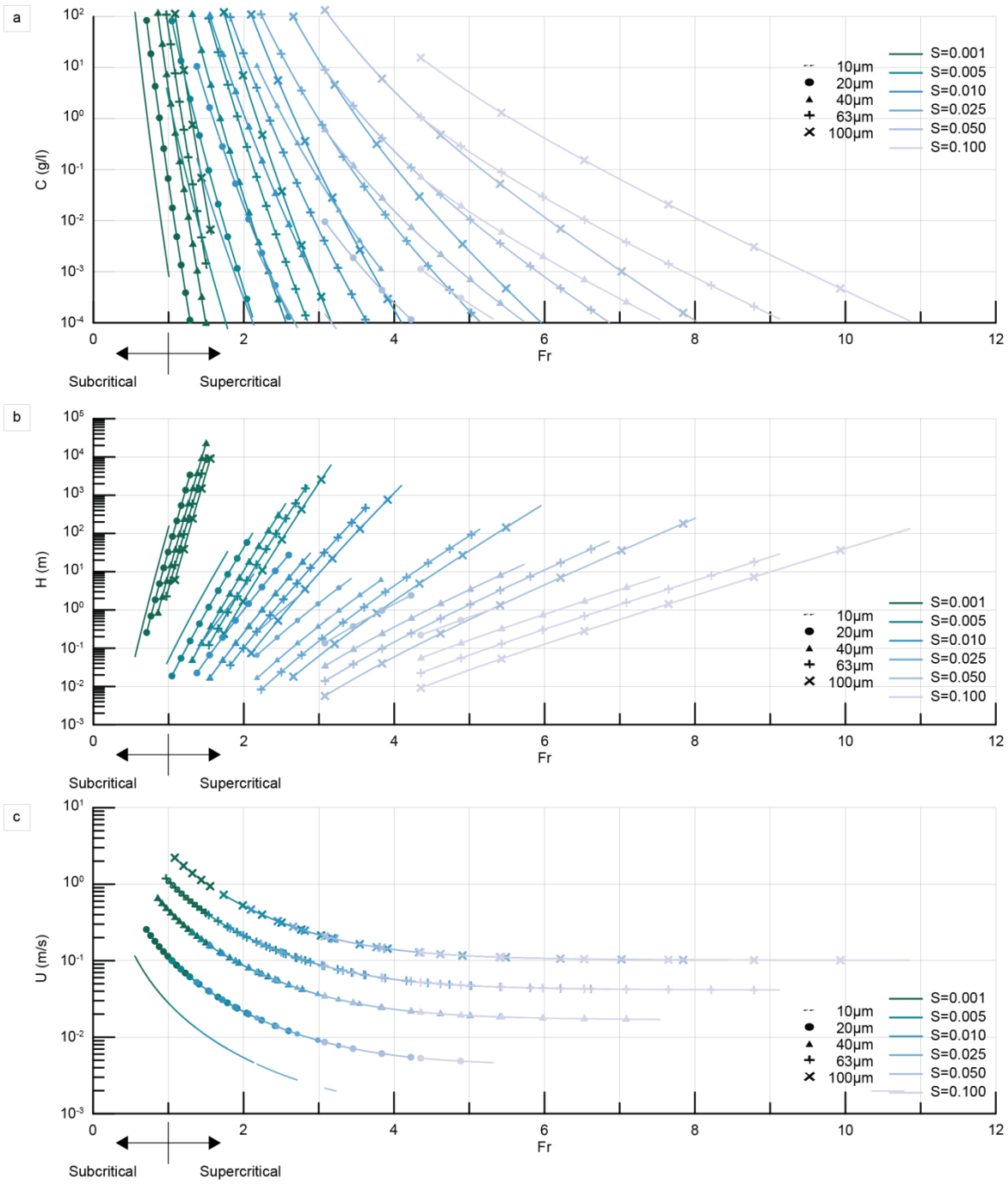

FIG. 2. 8 EQUILIBRIUM SOLUTIONS OBTAINED FOR DIFFERENT COMBINATIONS OF w_s AND S. THE RESULTS ARE SHOWED IN TERMS OF A) CONCENTRATION (G/L); B) CURRENT THICKNESS H (M) AND C) CURRENT SPEED U (M/S).

The equilibrium solutions in terms of instantaneous sediment transport hC $(kg\ m^{-2})$ and sediment flux hCU $(kg\ m^{-1}s^{-1})$ are shown in Fig. 2. 9 and confirm the ideas proposed for h, C and U: higher values of slope show lower Ri and hence lower hC and hCU values. The possible range of solutions is smaller for higher slopes, as such in the majority of the cases the body of the TC would catch the head of the current that would see its thickness increased and the current would evolve in a surge-type way. The solutions for which at the equilibrium the head and the body can evolve together in a "continuous" flow-type for high slopes are limited to the cases where $U_f \sim U_b$ and hence hC are also similar. This case of "continuous" flow type is easily achieved on the other hand for low slopes, once this equilibrium is achieved the current can propagate over long distances. The existence of an

potential equilibrium would explain the long run-out of TC over low slopes as in the case of the Madeira Channel (Stevenson et al., 2013, 2014, 2015) or the Bute Inlet in British Columbia (Prior et al., 1987) and the construction of deep sea fans reaching scales up to several thousands of kilometres such us the Zaire Fan System in West Africa (e.g. Khripounoff et al., 2003 and references therein). The equilibrium existence arises from the inclusion of the sediment settling in the bulk fluid continuity equation and from the definition of current thickness.

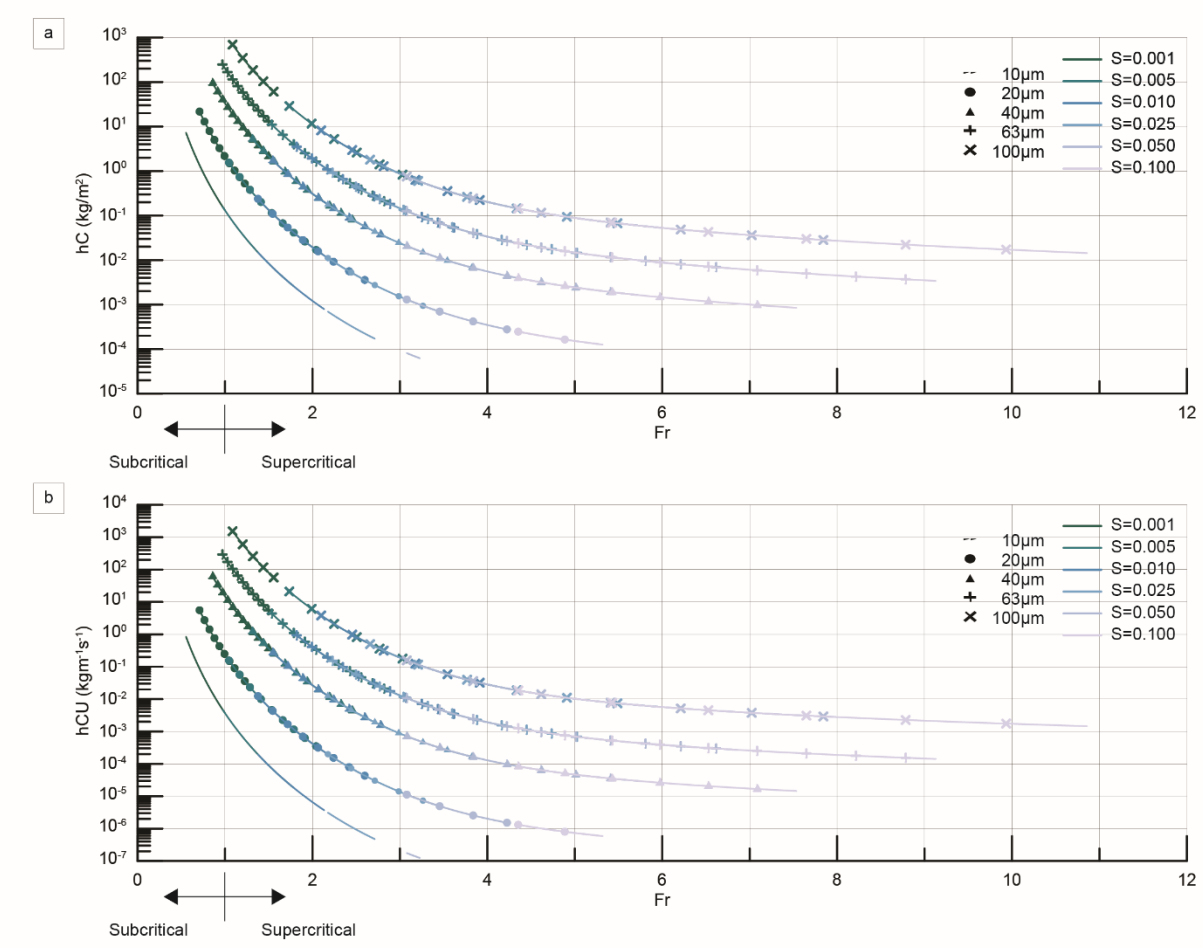

FIG. 2. 9 RESULTS IN TERMS OF INSTANTANEOUS SEDIMENT TRANSPORT $hC\ (kg\ m^{-2})$ AND SEDIMENT FLUX $hCU(kgm^{-1}\ s^{-1})$

The equilibrium solutions also allow the exploration of the evolution of a current for a given grain size along different slopes (Fig. 2.10). A TC flowing from shallower environments in the canyon head to deeper environments at the most distal part of the system will travel along different slopes for which different equilibrium solutions are possible.

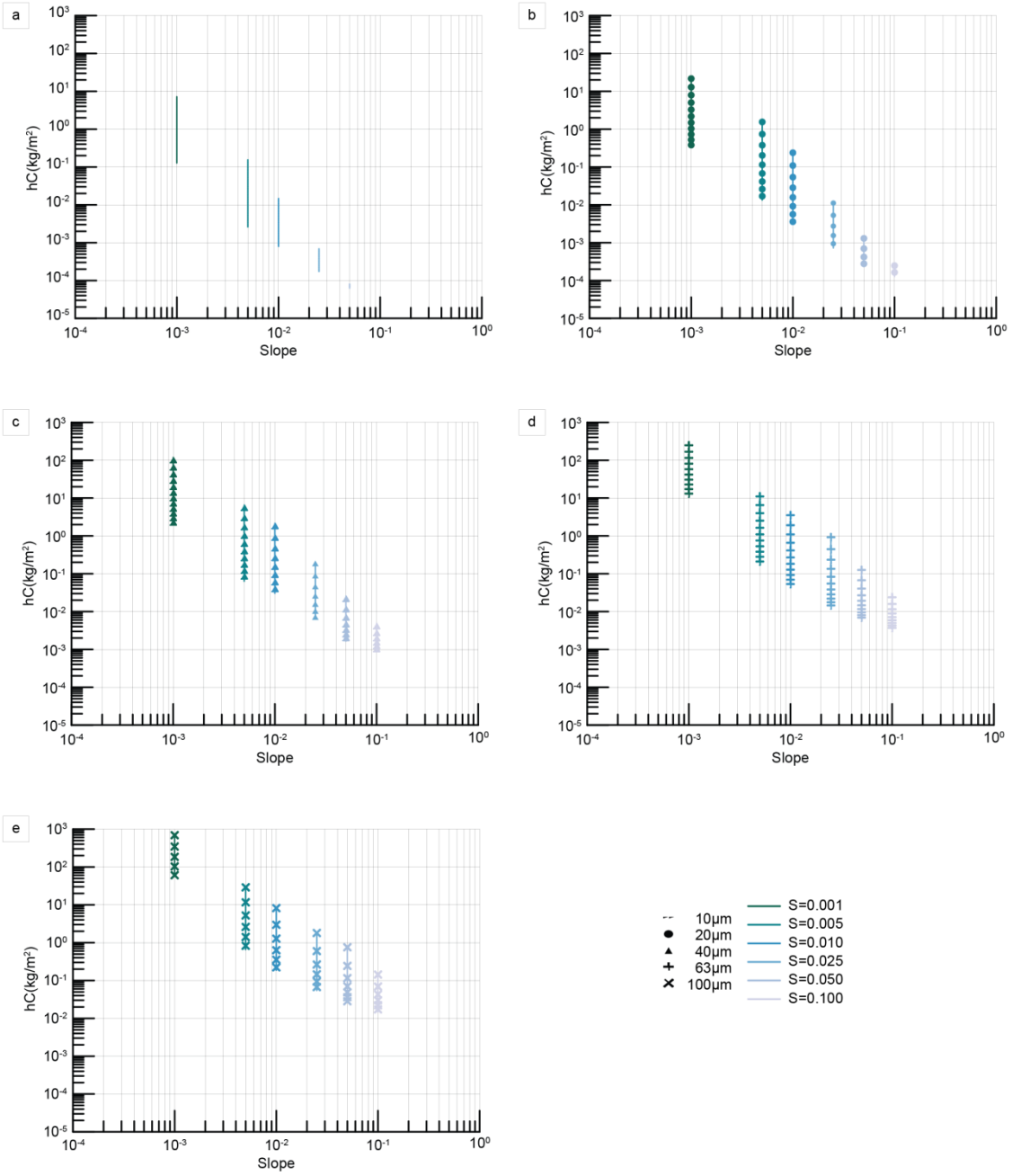

FIG. 2. 10 EQUILIBRIUM SOLUTIONS IN TERMS OF INSTANTANEOUS SEDIMENT TRANSPORT FOR DIFFERENT GRAIN SIZES AND SLOPES. EACH GRAPHIC SHOWS THE SOLUTIONS CORRESPONDING TO A GIVEN GRAIN SIZE FOR DIFFERENT SLOPES. A) 10μM ($w_s = 7.8477 \cdot 10^{-5}$m/s); B) 20μM ($w_s = 3.1382 \cdot 10^{-4}$M/S), C) 40μM ($w_s = 1.2525 \cdot 10^{-3}$M/S); D) 63 μM ($w_s = 3.0849 \cdot 10^{-3}$) AND E) 100μ ($w_s = 7.5621 \cdot 10^{-3}$M/S).

A TC in equilibrium conditions would transport a constant sediment mass, as seen in Fig.2.10, hC values overlap for different slopes. This implies that a current can pass from a higher slope to a lower slope in a "quasi-equilibrium" state. When passing to a lower slope S, the Ri will potentially increase, and hence the entrainment e_w decrease. In order to compensate this decrease, assuming that there is no gain or loss of sediment, for a given grain size the current might increase its current speed in order to achieve a new equilibrium state. However, the TC can recover its equilibrium by depositing part of its charge, in this case hC would decrease and so would U, and a new equilibrium state could be reached.

The existence of realistic solutions is of major importance since it provides insight in physical processes governing TC and enables to justify and explain field observations such as the observed threshold in the current thickness, the long run out of TC over low slopes and the deposition of sand over terraces and levees.

7. Conclusions

The hydrodynamics of TC are difficult to study in natural environments. Laboratory experiments are time consuming and measurement of flow properties and relationships between flow structure and transport and deposition remain difficult to be established. Numerical modelling can cope with some of the limitations of field data and experimental modelling, nonetheless the three different approaches are complementary and form and an interlinked feedback system.

2DH models are preferred since they can produce accurate predictions of current evolution and deposit characteristics of large scale flows with affordable computing resources. Among the 2DH models available, the use of Nixes-TC is justified given the key improvements of this model: the inclusion of a non-linear sedimentation model (settling velocity) in the equation of flux conservation, the development of a non-linear flow-dependent shear stress coefficient valid for all Re from laminar to fully turbulent flows, the inclusion of Coriolis effects, the treatment of the head and the existence of equilibrium solutions.

References

Admiraal, D.M., García, M.H., Rodríguez, J.F., 2000. Entrainment response of bed sediment to time-varying flows. Water Resour. Res. 36, 335–348. doi:10.1029/1999WR900227

Alexander, J., Morris, S., 1994. Observations on experimental, nonchannelized, high-concentration turbidity currents and variations in deposits around obstacles. J. Sediment. Res. 64.

Allen, J., 1985. Principles of Physical Sedimentology. Allen and Unwin, Boston.

Altinakar, M.S., Graf, W.H., Hopfinger, E.J., 1990. Weakly depositing turbidity current on a small slope. J. Hydraul. Res. 28, 55–80. doi:10.1080/00221689009499147

Altinakar, M.S., Graf, W.H., Hopfinger, E.J., 1996. Flow structure in turbidity currents. J. Hydraul. Res. 34, 713–718. doi:10.1080/00221689609498467

Andrieux, O., Cooper, C.K., Wood, J., 2013. Turbidity current measurements in the Congo Canyon. Offshore Technology Conference. doi:10.4043/23992-MS

Baas, J.H., McCaffrey, W.D., Haughton, P.D.W., Choux, C., 2005. Coupling between suspended sediment distribution and turbulence structure in a laboratory turbidity current. J. Geophys. Res. Oceans 110, C11015. doi:10.1029/2004JC002668

Baas, J.H., Best, J.L., Peakall, J., Wang, M., 2009. A phase diagram for turbulent, transitional, and laminar clay suspension flows. J. Sediment. Res. 79, 162–183. doi:10.2110/jsr.2009.025

Bagnold, R.A., 1962. Auto-suspension of transported sediment; turbidity currents. Proc. R. Soc. Lond. Ser. Math. Phys. Sci. 265, 315–319. doi:10.1098/rspa.1962.0012

Baines, P.G., 1995. Topographic effects in stratified flows [WWW Document]. Camb. Univ. Press. URL http://www.cambridge.org/us/academic/subjects/mathematics/fluid-dynamics-and-solid-mechanics/topographic-effects-stratified-flows (accessed 8.31.15).

Baines, P.G., 2001. Downslope flows into rotating and stratified environments. Part. Gravity Curr. Publ. 31 IAS 55, 113.

Benjamin, T.B., 1968. Gravity currents and related phenomena. J. Fluid Mech. 31, 209–248. doi:10.1017/S0022112068000133

Best, J.L., Kirkbride, A.D., Peakall, J., 2001. Mean flow and turbulence structure of sediment-laden gravity currents: new insights using ultrasonic Doppler velocity profiling, in: McCaffrey, W., Kneller, B., Peakall, J. (Eds.), Particulate Gravity Currents. Blackwell Science Publ, Oxford, pp. 159–172.

Blanchette, F., Strauss, M., Meiburg, E., Kneller, B., Glinsky, M.E., 2005. High-resolution numerical simulations of resuspending gravity currents: Conditions for self-sustainment. J. Geophys. Res. Oceans 110, C12022. doi:10.1029/2005JC002927

Bouma, A.H., 1962. Sedimentology of some flysch deposits. A graphic approach to facies interpretation. Amsterdam, Elsevier.

Bowen, A.J., Normark, W.R., Piper, D.J.W., 1984. Modelling of turbidity currents on Navy Submarine Fan, California Continental Borderland. Sedimentology 31, 169–185. doi:10.1111/j.1365-3091.1984.tb01957.x

Boyer, D.L., Haidvogel, D.B., Pérenne, N., 2004. Laboratory–numerical model comparisons of canyon flows: A parameter study. J. Phys. Oceanogr. 34, 1588–1609. doi:10.1175/1520-0485(2004)034<1588:LMCOCF>2.0.CO;2

Bradford, S.F., Katopodes, N.D., 1999. Hydrodynamics of turbid underflows. I: Formulation and numerical analysis. J. Hydraul. Eng.-Asce 125, 1006–1015. doi:10.1061/(ASCE)0733-9429(1999)125:10(1006)

Britter, R.E., Linden, P.F., 1980. The motion of the front of a gravity current travelling down an incline. J. Fluid Mech. 99, 531–543. doi:10.1017/S0022112080000754

Buckee, C., Kneller, B., Peakall, J., 2001. Turbulence structure in steady, solute-driven gravity currents, in: McCaffrey, W., Kneller, B., Peakall, J. (Eds.), Particulate Gravity Currents. Blackwell Publishing Ltd., pp. 173–187.

Canals, M., Puig, P., de Madron, X.D., Heussner, S., Palanques, A., Fabres, J., 2006. Flushing submarine canyons. Nature 444, 354–357. doi:10.1038/nature05271

Cantero, M.I., Cantelli, A., Pirmez, C., Balachandar, S., Mohrig, D., Hickson, T.A., Yeh, T., Naruse, H., Parker, G., 2012. Emplacement of massive turbidites linked to extinction of turbulence in turbidity currents. Nat. Geosci. 5, 42–45. doi:10.1038/ngeo1320

Cartigny, M.J.B., Ventra, D., Postma, G., van Den Berg, J.H., 2014. Morphodynamics and sedimentary structures of bedforms under supercritical-flow conditions: New insights from flume experiments. Sedimentology 61, 712–748. doi:10.1111/sed.12076

Choi, S.-U., 1998. Layer-averaged modeling of two-dimensional turbidity currents with a dissipative-Galerkin finite element method Part I: Formulation and application example. J. Hydraul. Res. 36, 339–362. doi:10.1080/00221689809498623

Choi, S.-U., Garcia, M.H., 2002. k-ε Turbulence modeling of density currents developing two dimensionally on a slope. J. Hydraul. Eng. 128, 55–63. doi:10.1061/(ASCE)0733-9429(2002)128:1(55)

Cooper, C., Wood, J., Andrieux, A., 2012. Turbidity current measurements in the Congo Canyon, in: OTC Abstract 23992. Presented at the Offshore Technology Conference, Houston, Texas, USA, p. 12.

Cossu, R., Wells, M.G., 2010. Coriolis forces influence the secondary circulation of gravity currents flowing in large-scale sinuous submarine channel systems. Geophys. Res. Lett. 37, L17603. doi:10.1029/2010GL044296

Cossu, R., Wells, M.G., Wåhlin, A.K., 2010. Influence of the Coriolis force on the velocity structure of gravity currents in straight submarine channel systems. J. Geophys. Res. Oceans 115, C11016. doi:10.1029/2010JC006208

Cossu, R., Wells, M.G., 2013. The evolution of submarine channels under the influence of Coriolis forces: experimental observations of flow structures. Terra Nova 25, 65–71. doi:10.1111/ter.12006

Cossu, R., Wells, M.G., Peakall, J., 2015. Latitudinal variations in submarine channel sedimentation patterns: the role of Coriolis forces. J. Geol. Soc. 172, 161–174. doi:10.1144/jgs2014-043

Dade, W.B., Huppert, H.E., 1995. A box model for non-entraining, suspension-driven gravity surges on horizontal surfaces. Sedimentology 42, 453–470. doi:10.1111/j.1365-3091.1995.tb00384.x

De Rooij, F., Dalziel, S.B., 2001. Time- and space-resolved measurements of deposition under turbidity currents, in: McCaffrey, W., Kneller, B., Peakall, J. (Eds.), Particulate Gravity Currents. Blackwell Publishing Ltd., pp. 207–215.

Ellison, T.H., Turner, J.S., 1959. Turbulent entrainment in stratified flows. J. Fluid Mech. 6, 423–448.

Felix, M., 2001. A two-dimensional numerical model for a turbidity current, in: McCaffrey, W., Kneller, B., Peakall, J. (Eds.), Particulate Gravity Currents. Blackwell Publishing Ltd., pp. 71–81.

Felix, M., 2002. Flow structure of turbidity currents. Sedimentology 49, 397–419. doi:10.1046/j.1365-3091.2002.00449.x

Felix, M., 2004. The significance of single value variables in turbidity currents. J. Hydraul. Res. 42, 323–330. doi:10.1080/00221686.2004.9728398

Garcia, M.H., 1990. Depositing and eroding sediment-driven flows: Turbidity currents (Report). St. Anthony Falls Hydraulic Laboratory.

Garcia, M.H, Parker, G., 1991. Entrainment of bed sediment into suspension. J. Hydraul. Eng. 117, 414–435. doi:10.1061/(ASCE)0733-9429(1991)117:4(414)

Garcia, M.H, 1993. Hydraulic jumps in sediment-driven bottom currents. J. Hydraul. Eng. 119, 1094–1117. doi:10.1061/(ASCE)0733-9429(1993)119:10(1094)

Garcia, M.H, Parker, G., 1993. Experiments on the entrainment of sediment into suspension by a dense bottom current. J. Geophys. Res.-Oceans 98, 4793–4807. doi:10.1029/92JC02404

Garcia, M.H., 1994. Depositional turbidity currents laden with poorly sorted sediment. J. Hydraul. Eng. 120, 1240–1263. doi:10.1061/(ASCE)0733-9429(1994)120:11(1240)

Gennesseaux, M., Mauffret, A., Pautot, G., 1980. Les glissements sous-marins de la pente continentale niçoise et la rupture des câbles en mer Ligure (Méditerranée occidentale). C R Acad Sci Paris Série D, 959–962.

Gladstone, C., Woods, A.W., 2000. On the application of box models to particle-driven gravity currents. J. Fluid Mech. 416, 187–195. doi:10.1017/S0022112000008879

Gray, T.E., Alexander, J., Leeder, M.R., 2006. Longitudinal flow evolution and turbulence structure of dynamically similar, sustained, saline density and turbidity currents. J. Geophys. Res. Oceans 111, C08015. doi:10.1029/2005JC003089

Groenenberg, R.M., 2007. Process-based modelling of turbidity-current hydrodynamics and sedimentation (TU Delft: Civil Engineering and Geosciences). TU Delft, Delft University of Technology, Delft, Netherlands.

Groenenberg, R.M., Sloff, K., Weltje, G.J., 2009. A high-resolution 2-DH numerical scheme for process-based modeling of 3-D turbidite fan stratigraphy. Comput. Geosci. 35, 1686–1700. doi:10.1016/j.cageo.2009.01.004

Harris, T.C., Hogg, A.J., Huppert, H.E., 2002. Polydisperse particle-driven gravity currents. J. Fluid Mech. 472, 333–371. doi:10.1017/S0022112002002379

Heezen, B.., Ewing, M., 1952. Turbidity currents and submarine slumps, and the 1929 Grand Banks earthquake. Am. J. Sci. 250, 849–873.

Hirsch, C., 1990. Numerical Computation Of Internal And External Flows, Volume 1, Fundamentals Of Numerical Discretization. Wiley, New York.

Hogg, A.J., Ungarish, M., Huppert, H.E., 2000. Particle-driven gravity currents: Asymptotic and box model solutions. Eur. J. Mech. - BFluids 19, 139–165. doi:10.1016/S0997-7546(00)00102-3

Hogg, A.J., Huppert, H.E., 2001. Two-dimensional and axisymmetric models for compositional and particle-driven gravity currents in uniform ambient flows, in: McCaffrey, W., Kneller, B., Peakall, J. (Eds.), Particulate Gravity Currents. Blackwell Publishing Ltd., pp. 121–134.

Hughes Clarke, J.E., Shor, A.N., Piper, D.J.W., Mayer, L.A., 1990. Large-scale current-induced erosion and deposition in the path of the 1929 Grand Banks turbidity current. Sedimentology 37, 613–629. doi:10.1111/j.1365-3091.1990.tb00625.x

Hughes Clarke, J.E., Brucker, S., Muggah, J., Church, I., Cartwright, D., Kuus, P., Hamilton, T., Pratomo, D., Eisan, B., 2012. The Squamish ProDelta: Monitoring active landslides and turbidity currents, in: Canadian Hydrographic Conference 2012 Proceedings. Presented at the Canadian Hydrographic Conference 2012, Niagara Falls, Canada.

Hughes Clarke, J.E., 2016. First wide-angle view of channelized turbidity currents links migrating cyclic steps to flow characteristics. Nat. Commun. 7, 11896. doi:10.1038/ncomms11896

Huppert, H.E., Simpson, J.E., 1980. The slumping of gravity currents. J. Fluid Mech. 99, 785–799. doi:10.1017/S0022112080000894

Huppert, H.E., 1998. Quantitative modelling of granular suspension flows. Philos. Trans. R. Soc. Lond. Ser. Math. Phys. Eng. Sci. 356, 2471–2496. doi:10.1098/rsta.1998.0282

Imran, J., Kassem, A., Khan, S.M., 2004. Three-dimensional modeling of density current. I. Flow in straight confined and unconfined channels. J. Hydraul. Res. 42, 578–590. doi:10.1080/00221686.2004.9628312

Jacinto, R.S., Burel, D., 2003. Modélisation du devenir à court terme des boues de dragage rejetées par clapage. Rev. Fr. Génie Civ. 7, 1151–1166. doi:10.1080/12795119.2003.9692539

Jamet, G., 2010. Modélisation de courants de turbidité: Application à l'étude de la marge algérienne et du séisme de Bourmerdès en 2003 (MSc Thesis). UBO, Brest.

Kassem, A., Imran, J., 2004. Three-dimensional modeling of density current. II. Flow in sinuous confined and uncontined channels. J. Hydraul. Res. 42, 591–602. doi:10.1080/00221686.2004.9628313

Keevil, G.M., Peakall, J., Best, J.L., Amos, K.J., 2006. Flow structure in sinuous submarine channels: Velocity and turbulence structure of an experimental submarine channel. Mar. Geol. 229, 241–257. doi:10.1016/j.margeo.2006.03.010

Khripounoff, A., Vangriesheim, A., Babonneau, N., Crassous, P., Dennielou, B., Savoye, B., 2003. Direct observation of intense turbidity current activity in the Zaire submarine valley at 4000 m water depth. Mar. Geol. 194, 151–158. doi:10.1016/S0025-3227(02)00677-1

Khripounoff, A., Crassous, P., Lo Bue, N., Dennielou, B., Jacinto, R.S., 2012. Different types of sediment gravity flows detected in the Var submarine canyon (northwestern Mediterranean Sea). Prog. Oceanogr. 106, 138–153. doi:10.1016/j.pocean.2012.09.001

Knapp, R.T., 1938. Energy-balance in stream-flows carrying suspended load. Eos Trans. Am. Geophys. Union 19, 501–505.

Kneller, B.C., Branney, M.J., 1995. Sustained high-density turbidity currents and the deposition of thick massive sands. Sedimentology 42, 607–616. doi:10.1111/j.1365-3091.1995.tb00395.x

Kneller, B.C., Bennett, S.J., McCaffrey, W.D., 1997. Velocity and turbulence structure of density currents and internal solitary waves: Potential sediment transport and the formation of wave ripples in deep water. Sediment. Geol. 112, 235–250. doi:10.1016/S0037-0738(97)00031-6

Kneller, B.C., Bennett, S.J., McCaffrey, W.D., 1999. Velocity structure, turbulence and fluid stresses in experimental gravity currents. J. Geophys. Res. Oceans 104, 5381–5391. doi:10.1029/1998JC900077

Kneller, B.C, Buckee, C., 2000. The structure and fluid mechanics of turbidity currents: A review of some recent studies and their geological implications. Sedimentology 47, 62–94. doi:10.1046/j.1365-3091.2000.047s1062.x

Komar, P.D., 1969. The channelized flow of turbidity currents with application to Monterey Deep-Sea Fan Channel. J. Geophys. Res. 74, 4544–4558. doi:10.1029/JC074i018p04544

Komar, P.D., 1977. Computer simulation of turbidity current flow and the study of deep-sea channels and fan sedimentation. Sea Ideas Obs. Prog. Study Seas Vol6 Mar. Model.

Kostic, S., Parker, G., 2006. The response of turbidity currents to a canyon–fan transition: Internal hydraulic jumps and depositional signatures. J. Hydraul. Res. 44, 631–653. doi:10.1080/00221686.2006.9521713

Kuenen, P.H., 1937. Experiments in connection with Daly's hypothesis on the formation of submarine canyons. Leidse Geol Meded 8, 327–335.

Kuenen, P.H., Migliorini, C.I., 1950. Turbidity currents as a cause of graded bedding. J. Geol. 58, 91–127.

Kuenen, P.H., 1952. Estimated size of the grand banks [Newfoundland] turbidity current. Am. J. Sci. 250, 874–884. doi:10.2475/ajs.250.12.874

Kundu, P.K., Cohen, I.M., Dowling, D.R., 1990. Fluid Mechanics. Academic Press, San Diego.

Lambert, A., Giovanoli, F., 1988. Records of riverbome turbidity currents and indications of slope failures in the Rhone delta of Lake Geneva. Limnol. Oceanogr. 33, 458–468. doi:10.4319/lo.1988.33.3.0458

Laval, A., Cremer, M., Beghin, P., Ravenne, C., 1988. Density surges: Two-dimensional experiments. Sedimentology 35, 73–84. doi:10.1111/j.1365-3091.1988.tb00905.x

Lesser, G.R., Roelvink, J.A., van Kester, J.A.T.M., Stelling, G.S., 2004. Development and validation of a three-dimensional morphological model. Coast. Eng., Coastal Morphodynamic Modeling 51, 883–915. doi:10.1016/j.coastaleng.2004.07.014

Liu, J.T., Wang, Y.-H., Yang, R.J., Hsu, R.T., Kao, S.-J., Lin, H.-L., Kuo, F.H., 2012. Cyclone-induced hyperpycnal turbidity currents in a submarine canyon. J. Geophys. Res. Oceans 117, C04033. doi:10.1029/2011JC007630

Liu, J.T., Kao, S.-J., Huh, C.-A., Hung, C.-C., 2013. Gravity flows associated with flood events and carbon burial: Taiwan as instructional source area. Annu. Rev. Mar. Sci. 5, 47–68. doi:10.1146/annurev-marine-121211-172307

Lüthi, S., 1981a. Experiments on non-channelized turbidity currents and their deposits. Mar. Geol. 40, M59–M68. doi:10.1016/0025-3227(81)90139-0

Lüthi, S., 1981b. Some new aspects of two-dimensional turbidity currents. Sedimentology 28, 97–105. doi:10.1111/j.1365-3091.1981.tb01666.x

Martín, J., Palanques, A., Vitorino, J., Oliveira, A., de Stigter, H.C., 2011. Near-bottom particulate matter dynamics in the Nazaré submarine canyon under calm and stormy conditions. Deep Sea Res. Part II Top. Stud. Oceanogr. 58, 2388–2400. doi:10.1016/j.dsr2.2011.04.004

Mas, V., Mulder, T., Dennielou, B., Schmidt, S., Khripounoff, A., Savoye, B., 2010. Multiscale spatio-temporal variability of sedimentary deposits in the Var turbidite system (North-Western Mediterranean Sea). Mar. Geol. 275, 37–52. doi:10.1016/j.margeo.2010.04.006

McCaffrey, W.D., Choux, C.M., Baas, J.H., Haughton, P.D.W., 2003. Spatio-temporal evolution of velocity structure, concentration and grain-size stratification within experimental particulate gravity currents. Mar. Pet. Geol. 20, 851–860. doi:10.1016/j.marpetgeo.2003.02.002

Meiburg, E., Kneller, B., 2010. Turbidity currents and their deposits. Annu. Rev. Fluid Mech. 42 135-156. doi: 10.1146/annurev-fluid-121108-145618

Meiburg, E., Radhakrishnan, S., Nasr-Azadani, M., 2015. Modeling gravity and turbidity currents: computational approaches and challenges. Appl. Mech. Rev. 67, 040802–040802. doi:10.1115/1.4031040

Mellor, G.L., Yamada, T., 1982. Development of a turbulence closure model for geophysical fluid problems. Rev. Geophys. 20, 851–875. doi:10.1029/RG020i004p00851

Middleton, G.V., 1966a. Experiments on density and turbidity currents: I. Motion of the head. Can. J. Earth Sci. 3, 523–546. doi:10.1139/e66-038

Middleton, G.V., 1966b. Experiments on density and turbidity currents: II. Uniform flow of density currents. Can. J. Earth Sci. 3, 627–637. doi:10.1139/e66-044

Middleton, G.V., 1967. Experiments on density and turbidity currents: III. Deposition of sediment. Can. J. Earth Sci. 4, 475–505. doi:10.1139/e67-025

Middleton, G.V., Southard, J.B., 1984. Mechanics of sediment movement. Lecture notes for Short Course no. 3. Soc. of Econ. Paleontol. and Mineral., Providence.

Middleton, G.V., 1993. Sediment deposition from turbidity currents. Annu. Rev. Earth Planet. Sci. 21, 89–114. doi:10.1146/annurev.ea.21.050193.000513

Migeon, S., Mulder, T., Savoye, B., Sage, F., 2012. Hydrodynamic processes, velocity structure and stratification in natural turbidity currents: Results inferred from field data in the Var Turbidite System. Sediment. Geol. 245–246, 48–62. doi:10.1016/j.sedgeo.2011.12.007

Migniot, C., 1989a. Tassement et rhéologie des vases. Première partie. Houille Blanche 11–29. doi:10.1051/lhb/1989001

Migniot, C., 1989b. Tassement et rhéologie des vases. Deuxième partie. Houille Blanche 95–112. doi:10.1051/lhb/1989006

Mulder, T., Syvitski, J.P.M., Skene, K.I., 1998. Modeling of erosion and deposition by turbidity currents generated by river mouths. J. Sediment. Res. 68, 124–137.

Mulder, T., Faugères, J.-C., Gonthier, E., 2008. Mixed turbidite–contourite systems, in: Camerlenghi, M.R. and A. (Ed.), Developments in Sedimentology, Contourites. Elsevier, pp. 435–456.

Necker, F., Härtel, C., Kleiser, L., Meiburg, E., 2005. Mixing and dissipation in particle-driven gravity currents. J. Fluid Mech. 545, 339–372. doi:10.1017/S0022112005006932

Nof, D., 1996. Rotational turbidity flows and the 1929 Grand Banks earthquake. Deep-Sea Res. Part 1 Oceanogr. Res. Pap. 43, 1143–1163.

Palanques, A., Guillen, J., Puig, P., de Madron, X.D., 2008. Storm-driven shelf-to-canyon suspended sediment transport at the southwestern Gulf of Lions. Cont. Shelf Res. 28, 1947–1956. doi:10.1016/j.csr.2008.03.020

Pantin, H.M., 1979. Interaction between velocity and effective density in turbidity flow: Phase-plane analysis, with criteria for autosuspension. Mar. Geol. 31, 59–99. doi:10.1016/0025-3227(79)90057-4

Paola, C., 2000. Quantitative models of sedimentary basin filling. Sedimentology 47, 121–178.

Parker, G., 1982. Conditions for the ignition of catastrophically erosive turbidity currents. Mar. Geol. 46, 307–327. doi:10.1016/0025-3227(82)90086-X

Parker, G., Fukushima, Y., Pantin, H.M., 1986. Self-accelerating turbidity currents. J. Fluid Mech. 171, 145–181. doi:10.1017/S0022112086001404

Parker, G., Garcia, M., Fukushima, Y., Yu, W., 1987. Experiments on turbidity currents over an erodible bed. J. Hydraul. Res. 25, 123–147. doi:10.1080/00221688709499292

Parsons, J.D., Schweller, W.J., Stelting, C.W., Southard, J.B., Lyons, W.J., Grotzinger, J.P., 2002. A preliminary experimental study of turbidite fan deposits. J. Sediment. Res. 72, 619–628. doi:10.1306/032102720619

Parsons, J.D., Friedrich, C.T., Traykovski, P.A., Mohrig, D., Imran, J., Syvitski, J.P.M., Parker, G., Puig, P., Buttles, J., Garcia, M., 2007. The mechanics of submarine sediment gravity flows, in: Continental Margin Sedimentation: From Sediment Transport to Sequence Stratigraphy. Blackwell Publishing Ltd., Oxford, UK., pp. 275–337.

Paull, C.K., Ussler, W., Greene, H.G., Keaten, R., Mitts, P., Barry, J., 2003. Caught in the act: The 20 December 2001 gravity flow event in Monterey Canyon. Geo-Mar. Lett. 22, 227–232. doi:10.1007/s00367-003-0117-2

Peakall, J., Ashworth, P., Best, J.L., 1996. Physical modelling in fluvial geomorphology: Principles, applications and unresolved issues, in: The Scientific Nature of Geomorphology: Proceedings of the 27th Binghamton Symposium in Geomorphology, John Wiley and Sons, Chichester, UK, pp. 221–253.

Peakall, J., Felix, M., McCaffrey, B., Kneller, B., 2001. Particulate gravity currents: Perspectives, in: McCaffrey, W., Kneller, B., Peakall, J. (Eds.), Particulate Gravity Currents. Blackwell Science Publ, Oxford, pp. 1–8.

Peakall, J., Kane, I.A., Masson, D.G., Keevil, G., McCaffrey, W., Corney, R., 2012. Global (latitudinal) variation in submarine channel sinuosity. Geology 40, 11–14. doi:10.1130/G32295.1

Piper, D.J.W., Shor, A.N., Farre, J.A., O'Connell, S., Jacobi, R., 1985. Sediment slides and turbidity currents on the Laurentian Fan: Sidescan sonar investigations near the epicenter of the 1929 Grand Banks earthquake. Geology 13, 538–541. doi:10.1130/0091-7613(1985)13<538:SSATCO>2.0.CO;2

Piper, D.J.W., Savoye, B., 1993. Processes of late Quaternary turbidity current flow and deposition on the Var deep-sea fan, north-west Mediterranean Sea. Sedimentology 40, 557–582. doi:10.1111/j.1365-3091.1993.tb01350.x

Piper, D.J.W., Cochonat, P., Morrison, M.L., 1999. The sequence of events around the epicentre of the 1929 Grand Banks earthquake: Initiation of debris flows and turbidity current inferred from sidescan sonar. Sedimentology 46, 79–97. doi:10.1046/j.1365-3091.1999.00204.x

Pope, S.B., 2000. Turbulent Flows, 1st edition. Cambridge University Press, Cambridge.

Postma, G., Nemec, W., Kleinspehn, K.L., 1988. Large floating clasts in turbidites: A mechanism for their emplacement. Sediment. Geol. 58, 47–61. doi:10.1016/0037-0738(88)90005-X

Pratson, L.F., Imran, J., Parker, G., Syvitski, J., Hutton, E.W.H., 2000. Debris flows vs. turbidity currents: A modeling comparison of their dynamics and deposits, in: Fine-Grained Turbidite Systems, AAPG Memoir 72 / SEPM Special Publication 68. A.H. Bouma and C.G. Stone, pp. 57–72.

Princevac, M., Fernando, H.J.S., Whiteman, C.D., 2005. Turbulent entrainment into natural gravity-driven flows. J. Fluid Mech. 533, 259–268. doi:10.1017/S0022112005004441

Prior, D.B., Bornhold, B.D., Wiseman, W.J., Lowe, D.R., 1987. Turbidity current activity in a British Columbia fjord. Science 237, 1330–1333. doi:10.1126/science.237.4820.1330

Puig, P., Ogston, A.S., Mullenbach, B.L., Nittrouer, C.A., Sternberg, R.W., 2003. Shelf-to-canyon sediment-transport processes on the Eel continental margin (northern California). Mar. Geol. 193, 129–149. doi:10.1016/S0025-3227(02)00641-2

Puig, P., Ogston, A.S., Mullenbach, B.L., Nittrouer, C.A., Parsons, J.D., Sternberg, R.W., 2004. Storm-induced sediment gravity flows at the head of the Eel submarine canyon, northern California margin. J. Geophys. Res. Oceans 109, n/a–n/a. doi:10.1029/2003JC001918

Puig, P., Canals, M., Company, J.B., Martín, J., Amblas, D., Lastras, G., Palanques, A., Calafat, A.M., 2012. Ploughing the deep sea floor. Nature 489, 286–289. doi:10.1038/nature11410

Richardson, J.F., Zaki, W.N., 1954. The sedimentation of a suspension of uniform spheres under conditions of viscous flow. Chem. Eng. Sci. 3, 65–73. doi:10.1016/0009-2509(54)85015-9

Rijn, L.C. van, 1984. Sediment transport, part II: Suspended load transport. J. Hydraul. Eng. 110, 1613–1641.

Roe, P.L., 1981. Approximate Riemann solvers, parameter vectors, and difference schemes. J. Comput. Phys. 43, 357–372. doi:10.1016/0021-9991(81)90128-5

Roelvink, J.A., 2006. Coastal morphodynamic evolution techniques. Coast. Eng. 53, 277–287. doi:10.1016/j.coastaleng.2005.10.015

Salaheldin, T.M., Imran, J., Chaudhry, M.H., Reed, C., 2000. Role of fine-grained sediment in turbidity current flow dynamics and resulting deposits. Mar. Geol. 171, 21–38. doi:10.1016/S0025-3227(00)00114-6

Salles, T., Lopez, S., Cacas, M.C., Mulder, T., 2007. Cellular automata model of density currents. Geomorphology 88, 1–20. doi:10.1016/j.geomorph.2006.10.016

Salles, T., Mulder, T., Gaudin, M., Cacas, M.C., Lopez, S., Cirac, P., 2008. Simulating the 1999 Capbreton canyon turbidity current with a Cellular Automata model. Geomorphology 97, 516–537. doi:10.1016/j.geomorph.2007.09.005

Savoye, B., Piper, D.J.W., Droz, L., 1993. Plio-Pleistocene evolution of the Var deep-sea fan off the French Riviera. Mar. Pet. Geol. 10, 550–571. doi:10.1016/0264-8172(93)90059-2

Sequeiros, O.E., Naruse, H., Endo, N., Garcia, M.H., Parker, G., 2009. Experimental study on self-accelerating turbidity currents. J. Geophys. Res. Oceans 114, C05025. doi:10.1029/2008JC005149

Simpson, J.E., Britter, R.E., 1979. The dynamics of the head of a gravity current advancing over a horizontal surface. J. Fluid Mech. 94, 477–495. doi:10.1017/S0022112079001142

Simpson, J.E., 1997. Gravity Currents: In the Environment and the Laboratory. Cambridge University Press, Cambridge.

Skene, K.I., Mulder, T., Syvitski, J.P.M., 1997. INFLO1: A model predicting the behaviour of turbidity currents generated at river mouths. Comput. Geosci. 23, 975–991. doi:10.1016/S0098-3004(97)00064-2

Sloff, C.J., 1993. Analysis of basic equations for sediment-laden flows. (Report) TU Delft.

Stacey, M.W., Bowen, A.J., 1988. The vertical structure of density and turbidity currents: Theory and observations. J. Geophys. Res. 93, 3528. doi:10.1029/JC093iC04p03528

Stevenson, C.J., Talling, P.J., Wynn, R.B., Masson, D.G., Hunt, J.E., Frenz, M., Akhmetzhanhov, A., Cronin, B.T., 2013. The flows that left no trace: Very large-volume turbidity currents that bypassed sediment through submarine channels without eroding the sea floor. Mar. Pet. Geol. 41, 186–205. doi:10.1016/j.marpetgeo.2012.02.008

Stevenson, C. J., Talling, P. J., Sumner, E. J., Masson, D. G., Frenz, M., Wynn, R. B., 2014. On how thin submarine flows transported large volumes of sand for hundreds of kilometres across a flat basin plain without eroding the seafloor. Sedimentology 61 1982-2019. doi:10.1111/sed.12125

Stevenson, C.J., Jackson, C.A.-L., Hodgson, D.M., Hubbard, S.M., Eggenhuisen, J.T., 2015. Deep-water sediment bypass. J. Sediment. Res. 85, 1058–1081. doi:10.2110/jsr.2015.63

Sumner, E.J., Amy, L.A., Talling, P.J., 2008. Deposit structure and processes of sand deposition from decelerating sediment suspensions. J. Sediment. Res. 78, 529–547. doi:10.2110/jsr.2008.062

Talling, P.J., Masson, D.G., Sumner, E.J., Malgesini, G., 2012. Subaqueous sediment density flows: Depositional processes and deposit types. Sedimentology 59, 1937–2003. doi:10.1111/j.1365-3091.2012.01353.x

Talling, P.J., Paull, C.K., Piper, D.J.W., 2013. How are subaqueous sediment density flows triggered, what is their internal structure and how does it evolve? Direct observations from monitoring of active flows. Earth-Sci. Rev. 125, 244–287. doi:10.1016/j.earscirev.2013.07.005

von Kármán, T., 1940. The engineer grapples with nonlinear problems. Bull. Am. Math. Soc. 46, 615–683. doi:10.1090/S0002-9904-1940-07266-0

Wei, T., Peakall, J., Parsons, D.R., Chen, Z., Zhao, B., Best, J., 2013. Three-dimensional gravity-current flow within a subaqueous bend: Spatial evolution and force balance variations. Sedimentology 60, 1668–1680. doi:10.1111/sed.12052

Wells, M.G., 2007. Influence of Coriolis forces on turbidity currents and sediment deposition, in: Geurts, B.J., Clercx, H., Uijttewaal, W. (Eds.), Particle-Laden Flow, ERCOFTAC Series. Springer Netherlands, pp. 331–343.

Wells, M.G., 2009. How Coriolis forces can limit the spatial extent of sediment deposition of a large-scale turbidity current. Sediment. Geol. 218, 1–5. doi:10.1016/j.sedgeo.2009.04.011

Xu, J.P., Noble, M.A., Rosenfeld, L.K., 2004. In-situ measurements of velocity structure within turbidity currents. Geophys. Res. Lett. 31, L09311. doi:10.1029/2004GL019718

Xu, J.P., 2010. Normalized velocity profiles of field-measured turbidity currents. Geology 38. doi:10.1130/g30582.1

Xu, J.P., Sequeiros, O.E., Noble, M.A., 2014. Sediment concentrations, flow conditions, and downstream evolution of two turbidity currents, Monterey Canyon, USA. Deep Sea Res. Part Oceanogr. Res. Pap. 89, 11–34. doi:10.1016/j.dsr.2014.04.001

Yeh, T., Cantero, M., Cantelli, A., Pirmez, C., Parker, G., 2013. Turbidity current with a roof: Success and failure of RANS modeling for turbidity currents under strongly stratified conditions. J. Geophys. Res. Earth Surf. 118, 1975–1998. doi:10.1002/jgrf.20126

Zanke, U., 1977. Berechnung der sinkgeschindigkeiten von sedimenten (No. 46). Mitt. des Franzius-Instituts für Wasserbau, Heft46, Seite 243, Technical University, Hannover, West Deutschland.

Zeng, J., Lowe, D.R., 1997. Numerical simulation of turbidity current flow and sedimentation: I. Theory. Sedimentology 44, 67–84. doi:10.1111/j.1365-3091.1997.tb00424.x

Chapter 3:

NUMERICAL MODELLING OF BOTTOM TRAWLING INDUCED SEDIMENT TRANSPORT AND ACCUMULATION IN LA FONERA SUBMARINE CANYON (NW MEDITERRANEAN SEA).

ABSTRACT

Bottom trawling leads to recurrent sediment resuspension events over fishing grounds. Recent studies have shown how bottom trawling can drive seascape reshaping at large spatial scales and enhance sediment transport in submarine canyons, which subsequently impacts deep-sea ecosystems. Present knowledge on the transfer and accumulation of sediment flows triggered by bottom trawling is based on localized and seldom measurements whilst a more complete picture of the process is needed. The present work focuses on the modelling of sediment transport and accumulation resulting from trawling activities in La Fonera submarine canyon, north-western Mediterranean Sea, thus contributing to an improved assessment of trawling impacts. Based on mooring data, an inverse model is used to reproduce sediment resuspension time series over an area defined on the basis of Vessel Monitoring System data. Our numerical process-based model simulates trawling-induced flows through the canyon and provides a 3D visualization of potential trawling impacts on sediment dynamics, including the identification of the propagation patterns of sediments resuspended by trawling. Flows coming from shallower fishing grounds are funnelled through canyon flank gullies towards the canyon axis, with part of the resuspended sediment reaching the continental rise out of the canyon across the open continental slope. Trawling-induced sediment flows promote sediment accumulation beyond the canyon mouth. Given the wide geographical distribution of bottom trawling, our results have far-reaching implications that go much beyond La Fonera submarine canyon. Our study represents a starting point for the assessment of the sedimentary impact of bottom trawling in deep continental margins.

RESUME

Le chalutage entraine la mise en suspension de sédiments sur les zones de pêche. Des études récentes ont montré que le chalutage peut modifier la nature et la morphologie du fond marin sur des larges échelles spatiales et favoriser le transport sédimentaire dans les canyons sous-marins, impactant ainsi les écosystèmes du milieu profond. L'état actuel des connaissances sur le transfert et l'accumulation des flux sédimentaires liés au chalutage est basé sur des mesures éparses et très localisées, c'est pourquoi une vision globale basée sur des processus physiques s'avère aujourd'hui nécessaire. Les travaux présentés dans ce chapitre sont axés sur la modélisation du transport et l'accumulation des sédiments issus du chalutage sur les flancs du canyon sous-marin de La Fonera, situé en Méditerranée occidentale. L'objectif principal est de contribuer à une amélioration de la quantification des impacts environnementaux du chalutage. Le sédiment remobilisé dans la zone de chalutage, définie en se basant sur les données du « Vessel Monitoring System », a été quantifié par analyse inverse afin d'obtenir des évènements turbiditiques comparables à ceux enregistrés au point de mouillage et de mesure. L'application du modèle numérique basé sur des processus physiques a permis de prédire la réponse du système en termes de courants de turbidité et a fourni une vision spatiale et globale des impacts potentiels du chalutage sur la dynamique sédimentaire du canyon. Les écoulements se propagent à partir des zones de chalutage vers l'axe du canyon en prenant les ravines comme chemins préférentiels, cependant une partie de l'écoulement atteint le glacis continental par la pente continentale orientale. Les écoulements gravitaires liés au chalutage favorisent l'accumulation sédimentaire au-delà de l'embouchure du canyon, ainsi l'action du chalutage n'est pas restreinte aux zones mitoyennes de cette activité. Compte-tenue de la large répartition géographique du chalutage, les résultats ici montrés ont des importantes implications qui vont au-delà du cas d'étude particulier du canyon de La Fonera. Cette étude représente un point de départ pour la quantification des impacts sédimentaires liés au chalutage sur les marges continentales.

1. Introduction

Bottom trawling is a non-selective fishing technique involving the towing of heavy collecting devices to harvest living resources. Bottom trawling is a widespread activity with a global trawled surface of up to $22\ x\ 10^6 km^2$ (WRI, 2001) with 40% of this activity extending beyond the continental shelf-break; this is a surface equivalent to twice the surface of Europe. At present, bottom trawling may be considered one of the anthropogenic activities with a stronger and more widespread impact on the seafloor due to its recurrence, intensity, mobility and wide geographical extent (Eastwood et al., 2007; Benn et al., 2010; Puig et al. 2012; Martín et al., 2014a) Demersal fisheries, and bottom trawling among them, have extended their activity from traditional shallow fishing grounds towards the continental slope and further offshore (Haedrich et al., 2001; Morato et al., 2006). This forced expansion is due to the depletion of shallow coastal resources as well as to the development of new and more powerful engines and heavier and larger gears allowing the exploitation of previously inaccessible resources. Also, the adoption of Exclusive Economic Zones (EEZ) since the seventies has pushed fisheries offshore beyond the 200 nautical miles from coastal baselines. Government subsidies have also favoured the offshore expansion of deep fisheries (Sumaila et al., 2008, 2010; Martín et al., 2014a). Artificial disturbances of the seafloor tend to be more severe and long-lasting in deep sea environments than in shallow environments due to their lower resilience and higher vulnerability to external disturbances (e.g. Pusceddu et al., 2014). Natural processes such as waves and storms able to overcome human imprints are weaker in the former (Dyerkjaer et al., 1995). Thus, the heavier and bigger gears and the more powerful engines employed at greater depth have an enhanced impact on the deep seafloor (Martín et al., 2014a and references therein).

Trawling-induced sediment resuspension and transport, or the initiation of trawling-induced sediment gravity flows, are not fully understood. Present knowledge is based on seldom and geographically localized direct observations from shallow environments and continental shelves (Churchill, 1989; Palanques et al., 2001; Durrieu de Madron et al., 2005; Dellapenna et al., 2006; Ferré et al., 2008), monitoring surveys in the wake of trawl gears (O'Neill and Summerbell, 2011; O'Neill et al., 2013), numerical modelling of the physical impact of the gear on the seabed (Prat et al., 2008; Ivanović et al., 2011; Esmaeli et Ivanović, 2014) and time series analysis from moored instruments (Palanques et al., 2005; Puig et al., 2012; Martín et al., 2014b). A better understanding and prediction of trawling impact would allow the development of methodologies to assess the biological and environmental effects of fishing and the design of low impact gears (Diesing et al., 2013; Depestele et al., 2015). Process-based models can complete insight into physical processes in deep environments but are rarely applied in such systems on a wide scale.

In the present paper, a numerical process-based model developed to reproduce underwater sediment-laden flows is implemented in La Fonera canyon (hereafter LFC, also known as Palamós), in the north-western Mediterranean Sea, an area where extensive bottom trawling takes place. The consequences in terms of sediment fluxes (i.e. suspended sediment concentration and current speed) have been monitored at several depths within the water column by means of an instrumented mooring (Puig et al., 2012; Martín et al., 2014b). We use an inverse model based on mooring data to reproduce the resuspension of sediment over the fishing ground triggering turbidity events of the same order of magnitude as those observed in the mooring site. The obtained resuspension is used as forcing to model sediment fluxes triggered by trawling and their interaction with the seafloor with the aim of an improved understanding of trawling-induced processes.

2. Regional setting

2.1.Physiography, hydrodynamics and sediment transport

LFC runs about 110 km from 80 m down to 2550 m depth (Fig. 3.1) (Amblas et al., 2006). Its head is deeply incised in the 30 km wide North Catalan continental shelf, with its axis located deeper than 1200 m at the equivalent position of the shelf break. The western canyon rim is only about 2-3 km from the coastline, with the tip of its western branch at barely 800 m (Palanques et al., 2005; Lastras et al., 2011). The canyon head presents a N-S orientation whilst the main canyon axis is orientated WNW-ESE. The canyon walls are steep (over 25°) and indented by numerous gullies (Lastras et al., 2011).

Two hydrosedimentary domains have been identified within the canyon (Palanques et al., 2005; Martín et al., 2006): an "inner" domain, up to 1200 m depth, and an "outer" domain. In the first one the closed circulation is dominated by the influence of the topography and the sediment inputs from the adjacent shelf whilst in the second one the slope dynamics and the seasonal trends play a major role on particle fluxes (Palanques et al., 2005; Martín et al., 2006). The main feature of the regional circulation is a slope current referred to as the Northern Current (Millot, 1999), which flows from the Ligurian Sea to the Gulf of Lions (GoL) and then southwards over the continental slope off Catalonia. This baroclinic current separates lighter, continental-influenced waters from denser open sea saline waters and plays a decisive role in the exchange processes between shelf and oceanic waters. The microtidal environment of the area facilitates studying the dynamics of the currents within the canyon and its interactions with topography. The closeness of the canyon head to the shore and its incision on the continental shelf allows the canyon to capture the sediments from littoral drift, major storms and dense shelf water cascading (DSWC) via both its head and northern flank (Lastras et al., 2011; Ribó et al, 2011; Canals et al., 2013). LFC has been identified through numerical modelling as the second most important canyon (after Cap de Creus canyon, CCC) in terms of export of dense shelf waters in the western Mediterranean (Ulses et al., 2008). LFC collects cold waters formed over the wide Gulf of Lions continental shelf that do not enter CCC but also those formed over the Gulf of Roses shelf (GoR) between CCC and LFC (Ulses et al., 2008; Ribó et al., 2011). Enhanced downcanyon sediment transport due to coastal downwelling caused by eastern storms has also been reported in LFC and in adjacent canyons (Martín et al., 2006, Sanchez Vidal et al., 2012).

2.2.Anthropogenic forcing

Deep-sea trawling has been conducted along the flanks of LFC since the early 20th century (Alegret and Garrido, 2008). The local fleet targets the deep sea shrimp *Aristeus antennatus* (Riso 1816). Trawling activities are conducted on the canyon flanks mainly from 200 to 800 m depth along three main fishing grounds: Sant Sebastià and Llevant on the northern flank and Rostoll on the southern flank. Fishing is more intense between 400 m and 750 m (Company et al., 2008; Puig et al., 2012; Martín et al., 2014c). The otter trawl gears employed by the local vessels present heavy doors (400-1300 kg) that spread apart approximately 100 m while fishing (Palanques et al., 2006a). Previous studies have revealed the importance of trawling-induced sediment resuspension and associated flows on the near-bottom turbidity and on the sediment dynamics in this canyon (Palanques et al., 2006; Martín et al., 2014b). It has been shown that chronic trawling along the rims of this canyon has resulted in significant modification of the seascape (Puig et al., 2012).

Mooring observations revealed the occurrence of frequent peaks in suspended sediment concentration (SSC) and sharp increases in near-bottom velocity. Since these bursts always occurred on working days and hours, and not under rough sea conditions, they were related to turbidity currents associated to bottom trawling activities along the northern canyon flank. Such trawling-induced turbidity currents were initially recorded in 2001 with a mooring located 12 m above the bottom in the canyon axis at 1200 m depth, (P2 in Fig. 3.1c) reaching velocities of ~25 cm/s and SSCs of ~35 mg/l, but were not recorded at a mooring located at 1700 m depth in the canyon axis at a

deeper position (P4 in Fig. 3.1c) (Palanques et al., 2005, 2006; Martín et al., 2007). Mooring data showed that currents only affected a limited part of the canyon and sediment did not travel too far along the canyon axis. Isolated turbidity currents observed in the records at 1700 m depth in the canyon axis were associated with slope failures from the untrawled southern canyon flank (Martín et al., 2007).

In 2011 an instrumented mooring (hereafter MGM, from Montgrí gully mooring, Fig. 3.1c) was placed inside the tributary gully of Montgrí at 980 m depth. The position of deployment, 200 m below the limit of the Sant Sebastià fishing ground on the northern flank, was limited by the operational working depth of the instrumented mooring. A tight coupling was observed between the temporal distribution of high turbidity events and the working schedule of the local fleet with turbidity currents observed repeatedly on weekdays at working hours. Maximum velocities of up to 38 cm/s at 12 m above seafloor and SSCs of 236 mg/l at 5 m above seafloor were recorded (Puig et al., 2012; Martín et al., 2014b)

The effects of trawling were found to extend beyond the fishing grounds, modifying sediment accumulation rates in the lower canyon (Martín et al., 2008). A sediment core (P4 in Fig. 3.1c) retrieved in 2002 from the canyon axis at 1700 m depth allowed the identification of two sedimentary regimes. The upper part of the core showed a fine layering corresponding to enhanced sediment accumulation that allowed the preservation of physical structures. The lower part records a relatively slow accumulation and significant bioturbation. The transition from non-laminated to laminated sediments in the cores coincides with a two-fold increase in the sediment accumulation rate linked to the rapid technical development and increase in the engine power undergone by the local trawling fleet in the seventies. A recent study that analysed a sediment core at the same site 9 years later, suggests that the accumulation rate during the last decade has dramatically increased and could approach 2.4 cm/yr (Puig et al., 2015).

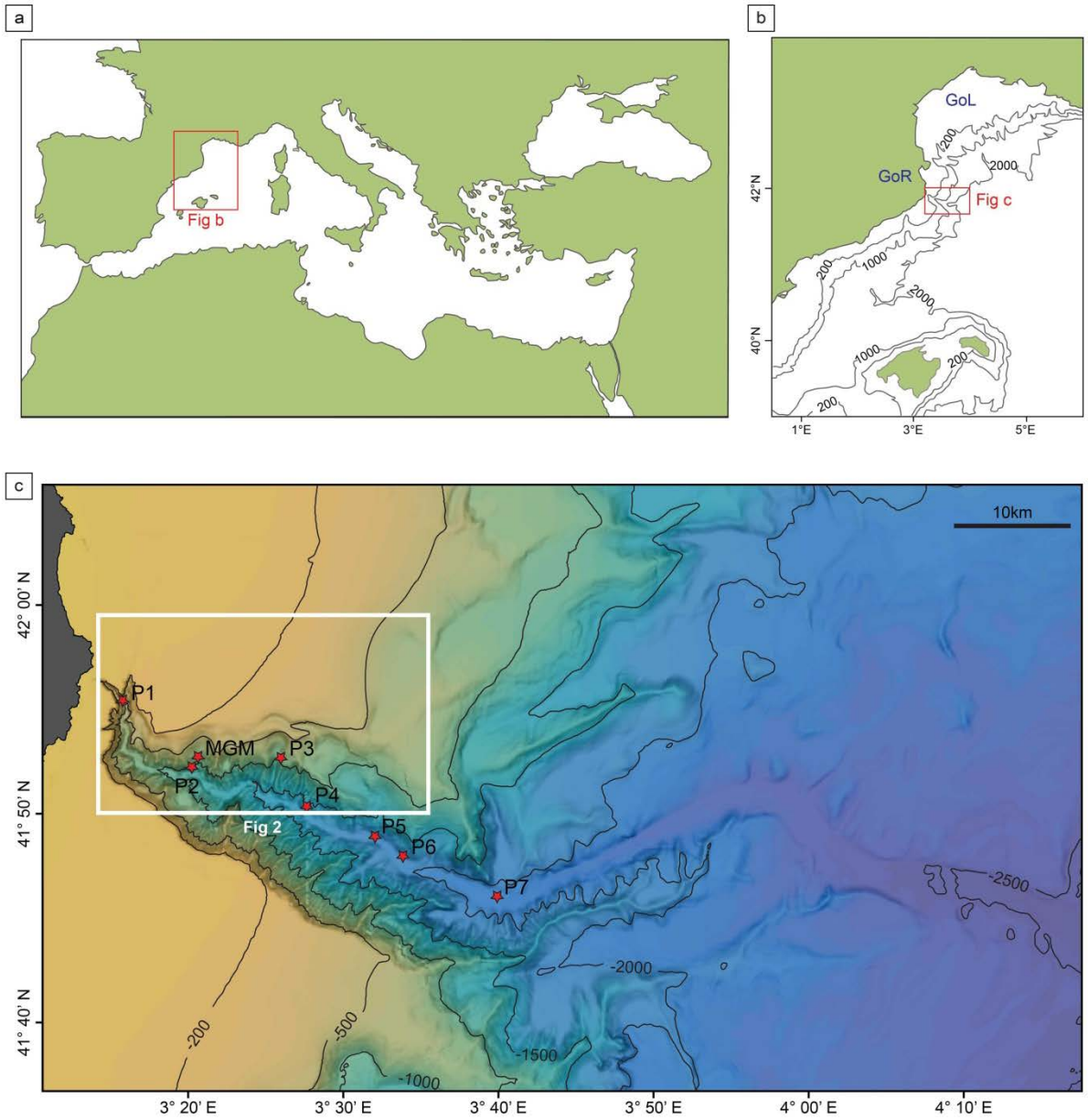

FIG. 3. 1. LOCATION OF LA FONERA SUBMARINE CANYON. (A) THE STUDY AREA IS LOCATED IN THE MEDITERRANEAN SEA. (B) BATHYMETRIC MAP OF THE NORTH-WESTERN MEDITERRANEAN SEA. GOL: GULF OF LION, GOR: GULF OF ROSES. THE RED RECTANGLE REPRESENTS THE EXTENSION OF THE MODELLING DOMAIN IN THIS STUDY. (C) BATHYMETRIC DATA USED FOR NUMERICAL MODELLING. RED STARS INDICATE THE POSITION OF THE MOORING SITE (MGM) AND OUTPUT POINTS (P1-P7) ANALYSED. THE WHITE RECTANGLE REPRESENTS THE ZOOM OVER THE FISHING GROUNDS PROVIDED IN FIG. 2.

3. Materials and methods

3.1. Data

Bathymetric data is derived from a compilation of several datasets including multibeam bathymetry data from multiple cruises from French and Spanish research institutions, including the University of Western Brittany, University of Barcelona and Ifremer. A 100 m resolution bathymetric grid was generated from this compilation and has been included in the model (Fig. 3.1c).

In situ monitoring data is used both to calibrate sediment fluxes and to reliably reproduce sediment resuspension due to trawling. Current velocity and suspended sediment concentration data (Puig et

al., 2012) from MGM (41°52.49'N; 3°20.66'E, Fig. 3.1c) has been used to construct a synthetic time series of instantaneous sediment transport through integration over the vertical of the available dataset.

The area coverd by the fishing fleet over the canyon flanks is defined on the basis of navigation tracks recorded by the Vessel Monitoring System (VMS) between the years 2007 and 2010 provided by the Fishing Monitoring Centre of the Spanish Secretariat of Marine Fishing (SEGEMAR). EU fishing vessels in excess of 15 m length must transmit every two hours their identification, position, speed and heading. The data depicts two active fishing grounds in the zone: Sant Sebastià and Llevant on the northern flank and Rostoll on the southern flank (Fig. 3.2a). A straight line delimits the NE border of the fishing grounds as resuspension here was deemed not to influence MGM dynamics where data is available.

Surface sediment near MGM corresponds to silty mud with sand content less than 3%. However, in the trawled areas, previous studies have described an upward coarsening trend and a sorting of grains (Martín et al., 2014a, 2014c). A grain solid density (ρ_s) of 2600 kg/m^3 is considered for the sediment in the area.

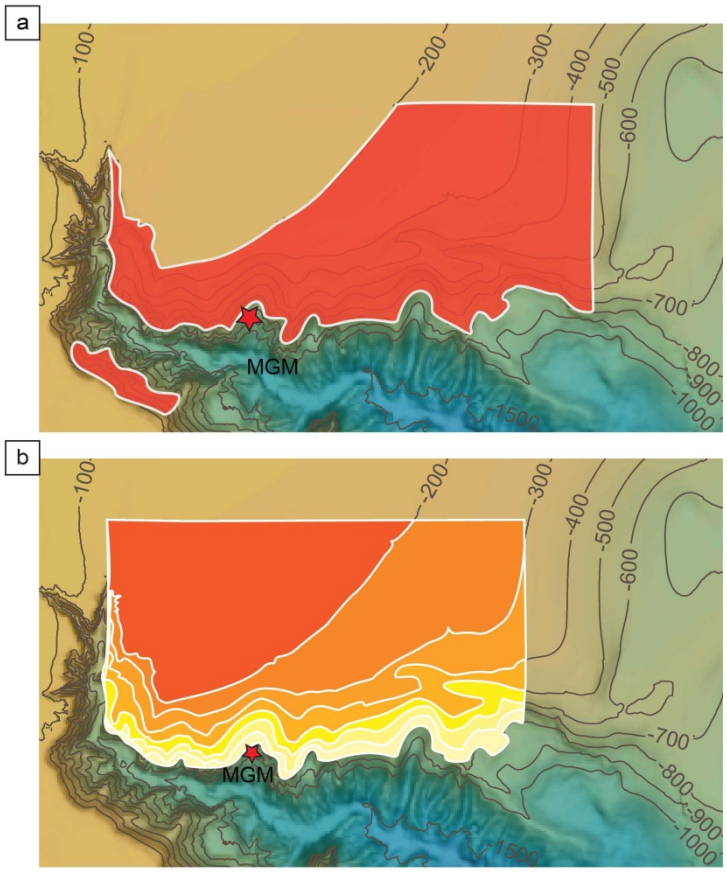

FIG. 3.2. FISHING GROUNDS CONSIDERED IN THE PRESENT STUDY. (A) FISHING GROUNDS OF ROSTOLL (SOUTHERN FLANK) AND SANT SEBASTIÀ AND LLEVANT (NORTHERN FLANK) DEFINED ON THE BASIS OF VMS DATA. (B) THE ANALYSED FISHING GROUNDS EXTEND OVER THE CONTINENTAL SHELF AND TOWARDS LA FONERA CANYON AXIS REACHING DIFFERENT DEPTHS FROM THE CANYON RIMS (200 M) TO THE ISOBATHS OF 800 M THAT DEFINES THE LIMIT OF REAL TRAWLING ACTIVITY OVER THE NORTHERN CANYON FLANK.

3.2.Numerical model

We implement Nixes-TC (Jacinto and Burel, 2003), a numerical process-based model developed to reproduce underwater sediment-laden flows, to LFC. The model follows the principles of those developed by Parker et al. (1986) and Bradford and Katopodes (1999). The spatial development of an unsteady turbidity current flowing in deep ambient fluid (Fig. 3.3) can be described by the following

set of vertically integrated partial differential equations derived by (Parker et al., 1986): the vertically integrated fluid, momentum and sediment conservation equations. Key improvements of Nixes-TC are the inclusion of the sedimentation model (settling velocity) in the equation of flux conservation, together with the development of a non-linear flow-dependent shear stress coefficient valid for all Reynolds numbers from laminar to fully turbulent flows.

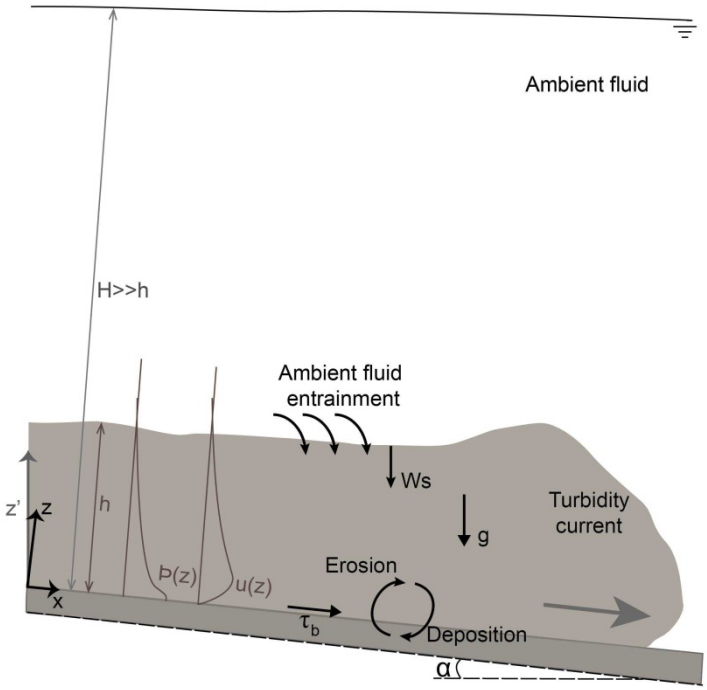

FIG. 3.3. DEFINITION SKETCH OF A TURBIDITY CURRENT FLOWING FROM LEFT TO RIGHT IN DEEP AMBIENT FLUID. MAJOR PROCESSES TAKEN INTO ACCOUNT ARE INCLUDED AS WELL AS VERTICAL PROFILES OF CONCENTRATION AND VELOCITY.

3.2.1. Equations and processes included

The continuity and momentum equations at the basis of the model are virtually identical to the shallow water equations with the exception of the hydrostatic thrust. In our case, the inertial pressure is still given by Bernoulli's principle (i.e. pressure is proportional to the loss of kinetic energy along a streamline); however, the deviation from hydrostatic pressure is given by the reduced specific gravity of the particles. We use the Boussinesq approximation, which implies that the effect of density difference between the turbidity current and the ambient fluid is neglected in the acceleration terms but kept in the gravity terms, where it drives the flow.

Equations forming the basis of the model are presented for a two-dimensional current for simplicity. The streamwise coordinate x and the upward normal coordinate z are assumed to be boundary-attached coordinates along the ocean bed. The main equations are:

$$\frac{\partial h}{\partial t} + \frac{\partial Uh}{\partial x} = E_w U - w_s \quad (1)$$

$$\frac{\partial Uh}{\partial t} + \frac{\partial (U^2 h)}{\partial x} = -\frac{1}{2} Rg \frac{\partial \emptyset h^2}{\partial x} + R\emptyset ghS - u_*^2 \quad (2)$$

$$\frac{\partial \emptyset h}{\partial t} + \frac{\partial \emptyset Uh}{\partial x} = w_s (pE_s - \emptyset_b) \quad (3)$$

where h is the flow thickness, U is the layer-averaged velocity, $\emptyset$ is the layer-averaged suspended sediment concentration, $R = (\rho_s - \rho)/\rho$ is the submerged specific gravity, where ρ_s is the grain solid density and ρ the density of the ambient fluid, $S = tan\,\alpha$ is the bottom slope, g is the acceleration due to gravity, u_* is the shear velocity, E_w is the ambient fluid entrainment coefficient, E_s is the sediment entrainment coefficient, w_s is the settling velocity, $(1-p)$ is the porosity of the sediment and $\emptyset_b$ is the near-bed sediment concentration.

To solve the governing equations given above, closure relationships for the ambient fluid and sediment entrainment coefficients, shear velocity and near-bed sediment concentration must be specified. We use the fluid entrainment coefficient derived by Parker et al. (1987) from experimental data of turbidity currents and conservative saline currents:

$$E_w = \frac{0.0075}{\sqrt{1+718{Ri_b}^{2.4}}} \tag{4}$$

where Ri_b is the bulk Richardson number, which measures the stratification of the flow and is related to the densiometric Froude number (Fr_d) as it represents the ratio between the gravitational potential energy and the turbulent kinetic energy:

$$Ri_b = \frac{Rg\emptyset h}{U^2} = \frac{g\prime\emptyset h}{U^2} = \frac{1}{{Fr_d}^2} \tag{5}$$

The sediment entrainment coefficient is determined by the empirical relationship developed by Garcia and Parker (1991, 1993):

$$E_s = \frac{AZ_u^5}{1+\frac{A}{0.3}Z_u^5} \tag{6}$$

where $Z_u = \frac{u_*}{w_s}Re_p^{0.6}$, $u_* = \sqrt{\frac{\tau_b}{\rho}}$, $A = 1.3 \cdot 10^{-7}$ and $Re_p = \frac{\sqrt{RgD}D}{\nu}$ is the particle Reynolds number, where D is the particle diameter and ν is the kinematic viscosity.

Equations (1) and (3) are the fluid and sediment mass continuity equation, respectively, and equation (2) is the momentum equation. In the fluid continuity equation (1), the evolution of the current thickness is governed by the variations at the interface with the ambient fluid. The current thickness varies according to convergence or divergence of the current due to water entrainment (E_wU) and sediment settling (w_s). Water entrainment takes into account the turbulence effect at the interface between the ambient fluid and the turbidity current. The term E_wU represents the rate of increase of current thickness due to water entrainment. On the other hand, the settling velocity counteracts the effect of water entrainment as it favours the decrease of current thickness due to decantation. The settling velocity w_s in the model is function of the settling velocity in clear water. The settling velocity of sediment with grain diameter D is computed by the Zanke's formula (Zanke, 1977) that extends the Stokes' law for larger particles:

$$w_{s,w} = 10\frac{\nu}{D}\sqrt{1+\frac{0.01\left(\frac{\rho_S}{\rho}-1\right)gD^3}{\nu^2}} \tag{7}$$

The settling velocity also appears in equation (3) (i.e. balance of sediment mass). The term $w_s(pE_s - \emptyset_b)$ represents the net flux of sediment into the current due to erosion and deposition. Both erosion and deposition are expressed as empirical relationships depending on the settling velocity w_s of the sediment. E_s is the sediment entrainment coefficient, which is generally related to local bed shear stress and the settling velocity of particles. The inclusion of the porosity in the equation allows us to consider a possible consolidation of the sediment and thus a mobilization threshold. In our simulation we consider $\emptyset_b = \emptyset$.

The momentum equation (2) provides the energy equilibrium between the different forces acting on the current. The driving force is given by the projection of the reduced mass over the slope$RCghS$.

The hydrostatic pressure balance is established between the deviatory pressure and the excess of gravitational force provided by the sediment in the flow. The contribution of bed shear stress to motion is expressed by the quadratic formulation $\tau_b = \rho C_d U^2$, hence the shear velocity is: $u_*^2 = C_d U^2$ where C_d is the coefficient of bed friction. At equilibrium conditions (i.e. $\mathrm{Fr_d} = \frac{\mathrm{U}}{\sqrt{Rg\emptyset h}} = 1$) the driving force of the slope must be compensated by the bed shear. Hence, C_d is not constant and it may change as much as the forcing slope, with values ranging between 10^{-3} and 10^{-2} for turbulent flows as shown in Figure 3.4. The bed drag depends on the local properties of the flow: Reynolds number Re and relative roughness k_s/h, where k_s is the bed roughness associated to the grain sediment size and it is defined as $k_s = D$. Provided that the local flow properties may change at every time step and from one grid to another, C_d is calculated at every time step for every grid point. It includes the contribution of viscosity and turbulence to the bed shear stress, thus it is valid for all Reynolds numbers from laminar to fully turbulent. Figure 3.4 shows the evolution of C_d depending on Reynolds number for different relative roughness (k_s/h).

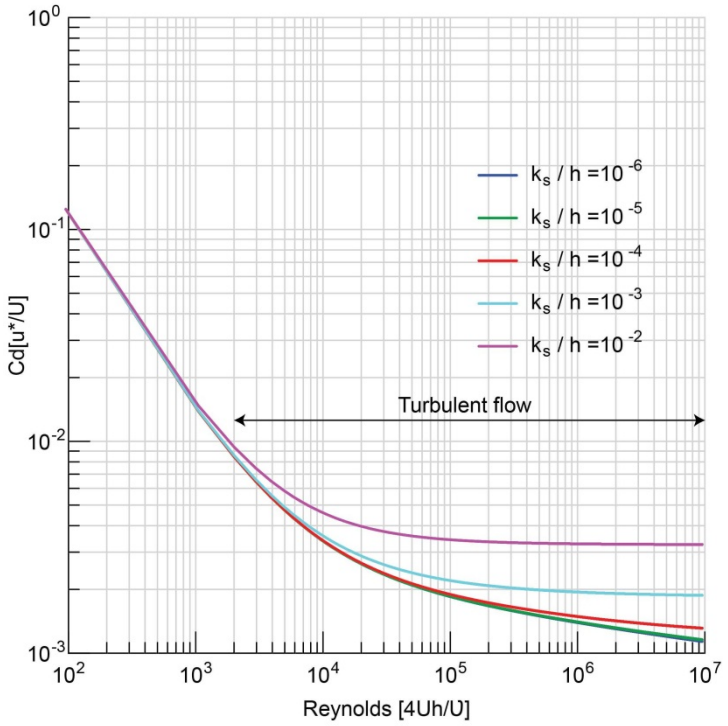

FIG. 3.4. BED FRICTION COEFFICIENT (C_D) AS A FUNCTION OF THE REYNOLDS NUMBER (Re) FOR DIFFERENT RELATIVE ROUGHNESS (K_S/H, WHERE K_S IS THE BED ROUGHNESS AND H THE CURRENT THICKNESS). THE RANGE OF VALUES CORRESPONDING TO TURBULENT FLOWS IS ALSO INDICATED.

3.2.2. Numerical scheme

The model is coded in Fortran. The Volume Finite Method permits evaluating the coupled system of nonlinear hyperbolic partial differential equations (Bradford and Katopodes, 1999). Source terms are calculated following an implicit scheme. The Riemann problem at each interface is solved following Roe (1981). The typical boundary condition of solid wall is used in the present study. The implementation of the boundary conditions is accomplished through the use of a ghost cell (outside the domain of interest) at the boundary. The reflection of the concentration, current thickness and velocities perpendicular and parallel to the wall are placed in the ghost cell (i.e. concentration, current thickness and perpendicular and horizontal velocity remain unchanged). These non-reflective

open outflow boundaries ensure that information can freely exit the computational domain without causing disturbances to the solution. The implicit numerical scheme ensures that numerical instability does not occur as implicit algorithms can cope with sharp changes in solution by using reduced time steps. The condition of stability is the Courant-Friedrichs-Levy (CFL) condition.

Inputs of the model are the orthogonal grid corresponding to the bathymetry of the canyon, sediment properties (i.e. grain size, fraction of a given sediment grain size and density) and initial deposit (i.e. volume concentration and porosity). The kinematic viscosity and density of water as well as the von Karman coefficient for the turbulence closure are also included in the parameters file. Initial and boundary conditions are provided to the model in terms of position, mass and volume of sediment remobilized (i.e. trawled area and remobilization due to trawling). Outputs of the model are the values of current thickness, current velocity (streamwise and transverse direction) and sediment concentration at each grid point. These variables allow the calculation of mass flux and instantaneous sediment transport, bed shear stress and horizontal distribution of sediment.

3.3. Methodology

Resuspension fluxes due to trawling are not fully understood. The assessment of trawling disturbances and trawling-induced resuspension requires quantifying the rate at which trawls inject sediment into the water column, the height of the plume generated by the trawl gear and the rate at which this plume fades (Durrieu de Madron et al., 2005).

Our methodology is based both on physical processes and inverse analysis of data at MGM. The methodology allows us to determine the three major unknowns related to the triggering mechanism of turbidity currents: area of influence, transfer function (i.e., response at MGM to different events over the fishing grounds previously defined) and resuspension (R_s) over the fishing grounds. The work flow is summarized as follows (Fig. 3.5): (i) we performed sensitivity tests for the area of influence of bottom trawling (section 3.3.1); (ii) we developed a transfer function for one event for MGM considering the area potentially affected by trawling (section 3.3.2); and (iii) we applied the inverse model based on the data measured at MGM in order to infer the resuspension (R_s) over the fishing grounds previously defined (section 3.3.3). In order to provide a spatial vision of sediment pathways due to trawling in the canyon, we include this estimated resuspension issued by the inverse modelling as forcing in the model (section 3.3.4).

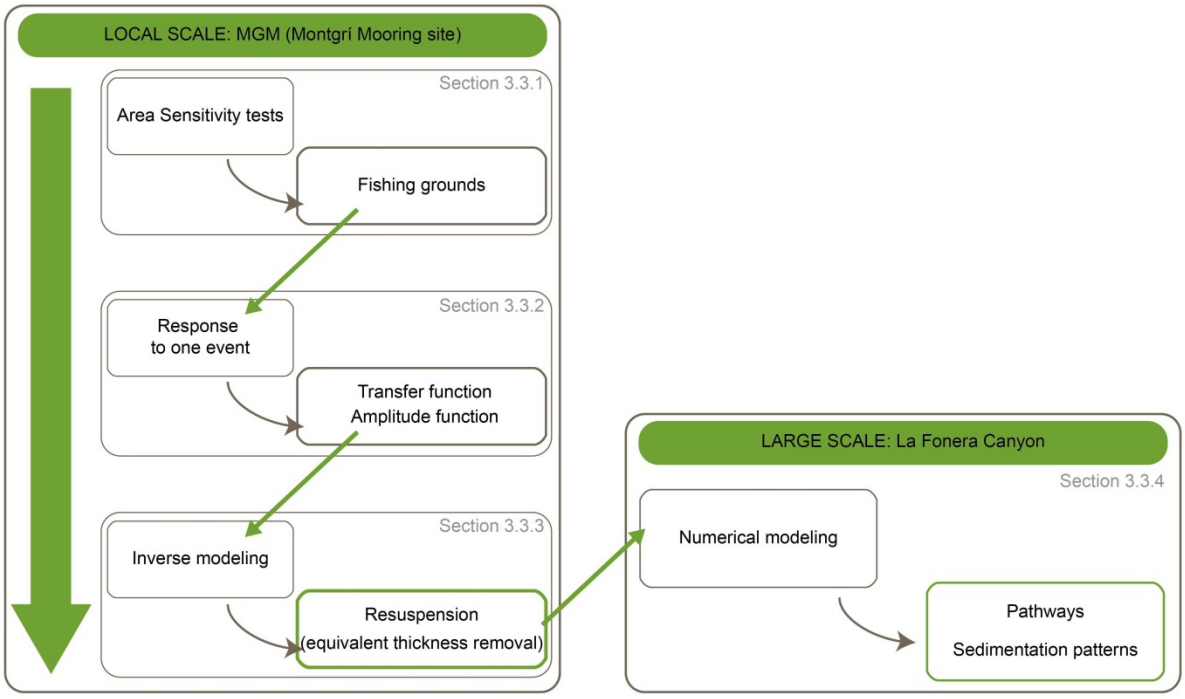

FIG. 3. 5. FLOW CHART SHOWING THE TWO DIFFERENT SPATIAL SCALES ANALYZED AND THE METHODOLOGY APPLIED IN EACH CASE. FOR EACH PHASE OF THE WORK FLOW, METHODS ARE SHOWN IN THE LEFT COLUMN AND OUTPUT ON THE RIGHT COLUMN.

Trawling activity is patchy both in time and space. The trawl gear ploughs furrows along the towpath leading to sediment remobilization. Seabed disturbance is simultaneous to sediment cloud release into the water column (Fig. 3.6a). However, the effective quantity of sediment resuspended by trawling in deep environments remains largely unknown. The parameters that allow the quantification of trawling impact over the fishing grounds show variation of one order of magnitude according to studies conducted in shallow environments. Trawling resuspension depends on the characteristics of the gear, the nature of the sediment and towing speed (Durrieu de Madron et al., 2005). The penetration depth (P_f) of the trawl in the sediment depends on the gear component and while the heavier parts, such as the otter doors that keep the net open, will penetrate down to several centimeters; others, such us the sweep lines, will only skim some millimeters of the seafloor surface (Schwinghamer et al., 1998; Dellapenna et al., 2006; O'Neill and Summerbell, 2011). The rate at which sediment plumes are released and fade depends on the sediment's clay content (Durrieu de Madron et al., 2005; Ivanović et al., 2011). The height (h) of sediment plumes after a trawler's passage on soft bottom sediments on continental shelves varies between 5 and 10 m (Churchill, 1989; Durrieu de Madron et al., 2005). The towing speed (V_T) also influences the sediment release and can vary during fishing hauls with common values between 2 and 5 knots (He and Winger, 2010). The amount of sediment remobilized by a trawler in fishing operation is given by the surface trawled per unit of time and the depth scraped (Fig. 3.6b). Since we lack information about the trawling resuspension fluxes over the fishing grounds and given the wide range of values and uncertainties in the variables involved, we consider a mean value of resuspension (R_s) spread over the whole fishing grounds under consideration. This approach averages the uncertainties while providing a more general picture of the sediment dynamics in the canyon. The resuspension is expressed in terms of equivalent remobilized sediment thickness and is considered to be instantaneously injected in the water column and uniformly resuspended over the first 10 m above the bottom in the water column (Churchill, 1989) (Fig. 3.6c). This initial height allows us to take into account the scale of turbulence, which is given by the fishing gear size. The volume concentration of the sediment plume released is calculated by means of mass conservation (equation (8)) between the sediment scraped from the

bed layer (i.e. left part of the equation) and the sediment injected into the water column (i.e. right part of the equation):

$$\emptyset_d \cdot R_s = \emptyset_s \cdot h \quad (8)$$

where $\emptyset_d$ is the volumetric concentration of the sediment in the bed, R_s is the sediment thickness remobilised, $\emptyset_s$ is the volumetric concentration of the sediment cloud and h is the height of the sediment cloud. In our simulations we consider a value of $\emptyset_d = 0.25$ (650 g/l).

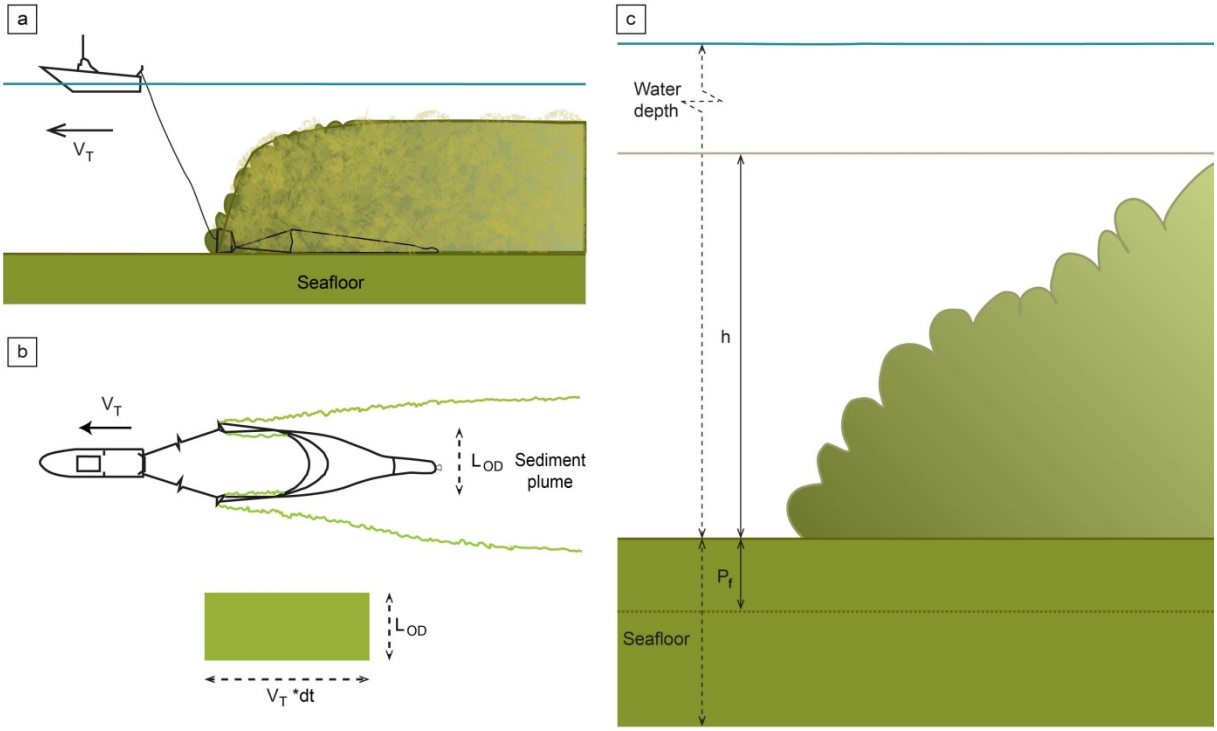

FIG. 3. 6. FISHING TRAWLERS CHARACTERISTICS AND PARAMETERS: SIDE (A) AND TOP (B) VIEWS OF A TRAWLER DURING FISHING OPERATION AT A TOWING SPEED OF V_T. THE SURFACE AREA OF SEDIMENT SCRAPED CAN BE ESTIMATED BY THE HORIZONTAL OPENING (L_{OD}) OF THE OTTER BOARDS MULTIPLIED BY THE DISTANCE $(V_T \cdot dt)$ TRAVELLED BY THE TRAWLER BY UNIT TIME $(L_{OD} \cdot V_T \cdot dt)$. (C) SKETCH OF THE INSTANTANEOUS RELEASE OF A SEDIMENT CLOUD OF h HEIGHT DUE TO THE SCRAPING OF SEDIMENT THICKNESS P_f BY THE TRAWLER.

3.3.1. Influence of the depth reached by trawlers in the sediment transport in MGM/Definition of the area of influence (i.e. critical depth) of the trawling fleet

A first set of simulations was performed to define the area of influence of the local trawling fleet and to determine the critical depth from which trawling-induced turbidity currents develop down the canyon reaching MGM. For all the simulations an initial homogeneous instantaneous remobilization is considered over the northern continental shelf, upper continental slope and canyon flank at an increasing range of depths. The shallower area considered reached the 200 m isobath, the second area increased the depth considered to 300 m and so on in 100 m increments until a depth of 800 m. (Fig. 3.2b). The 200 m isobath roughly corresponds to the canyon rim depth, thus restricting trawling to the continental shelf, whilst in the trawled area down to 800 m it covers both this part of the continental shelf and the canyon flank. The 800 m isobath defines the limit of actual trawling activity over the northern canyon flank. The initial sediment thickness considered is 1 cm, which is equivalent to a volumetric concentration of $\Phi_s = 2.5 \cdot 10^{-4}$ (0.65g/l).

3.3.2. Development of the transfer function

A second set of simulations for different initial events was carried out. Remobilization is imposed over the fishing grounds (Fig. 3.2a) defined on the basis of VMS data for the period 2007-2010. The resulting area is a conservative estimation of the potential area that can be bottom trawled. The remobilized thickness (R_s) ranges from 0.1 cm to 0.75 cm. These values correspond to resuspended sediment concentrations of 0.065 g/l and 0.4875 g/l respectively and trigger turbidity currents that, at the location of MGM, display values of instantaneous sediment transport of the same order of magnitude as those measured. Two functions are derived from this exercise: (i) a transfer function $f(t-\tau)$, and (ii) an amplitude function $A(R_s)$. The transfer function contains information about the response of the system at MGM to an event over the fishing grounds (i.e. temporal evolution and time scale). The transfer function is obtained by means of normalization of the responses at MGM for the different initial conditions. The application of a moving average filter with a window size of 600 s allows the removal of undesired noise associated with the combination of the different signals. The maximum window size applied is limited by the time lag between the first peak and the first valley and by the time lag of the arrival of the response at MGM, this is to say, 2100 s. The amplitude function contains information about the forcing imposed. The amplitude function relating amplitude at MGM and remobilization over the fishing grounds is found through spline fitting. The instantaneous transport ($M_{mp}(t)$) at MGM at a time t caused by a punctual remobilization R_s over the fishing grounds at a time τ_o is given by the product of both functions.

$$M_{mp}(t) = A(\tau_o) \cdot f(t-\tau_o) \quad (9)$$

3.3.3. Inverse analysis model

Our aim is to quantify the unknown sediment removal $R_s\,(t)$ along the fishing grounds that would cause turbidity events comparable to those measured in 2011 at MGM. To do so, we use an inverse analysis model, i.e. a model that calculates from a set of observations the causal factors that produce them. Our set of observations is the data measurements $M(t)$ at MGM, and the causal factor is the sediment remobilization over the fishing grounds $R_s\,(t)$. Our inverse model is based on the previously determined functions for a single event (i.e. transfer function $f(t-\tau)$ and amplitude function $A = f(R_s)$. The signal obtained at MGM is considered as linear superposition of n discrete instantaneous remobilization events over the fishing grounds (Fig. 3.7). Each one of these events condenses the remobilization associated to its 60 s window, implying that resuspension is expressed in terms of equivalent thickness removal per minute. The modelled instantaneous sediment ($M_m(t)$) transport at MGM is given by the convolution of the transfer function and the different different amplitudes.

$$M_m(t) = \int_0^t A(\tau) \cdot f(t-\tau) d\tau \quad (10)$$

By linearizing and discretizing the problem, we are able to relate the discrete data measurements ($M(t)$) at the mooring site to the discrete inverse model parameters (i.e. unknown amplitude of the different events $A(\tau)$). The comparison between measurements ($M(t)$) and inverse model output ($M_m(t)$) at MGM allows us to infer the amplitude $A(\tau)$ of the different events at MGM and due to the relationship $A_o \propto R_s$, we can infer the latter.

$$M(t) = M_m(t) \quad (11)$$

The left part of the previous expression $M(t)$ is the synthetic series of instantaneous sediment transport (kg/m^2) obtained from the dataset measured at MGM. The right part of the equation (11) $M_m(t)$ is the instantaneous sediment transport issued by the inverse model obtained through linear superposition of the different punctual events modelled.

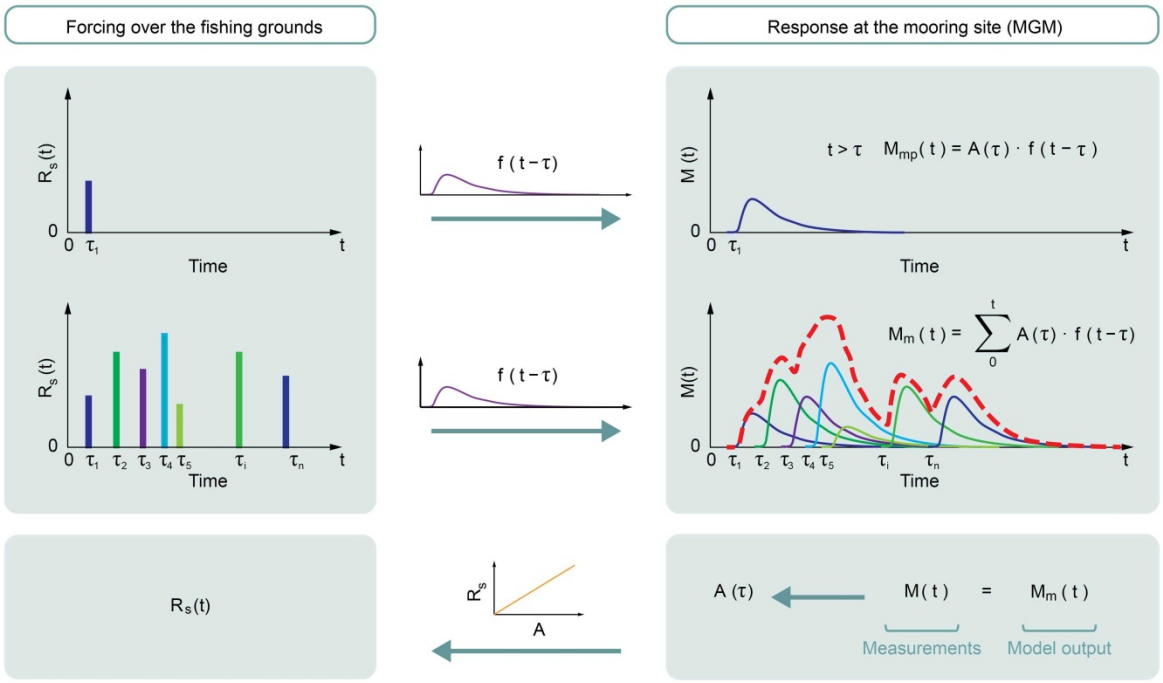

FIG. 3.7. BASIS OF THE INVERSE MODELLING APPLIED TO MGM DATA. THE BOXES ON THE LEFT CORRESPOND TO THE FORCING OVER THE FISHING GROUNDS THAT WE AIM TO DETERMINE. THE BOXES ON THE RIGHT CORRESPOND TO THE RESPONSE AT MGM TO THE FORCING THAT CAN BE OBTAINED BY THE CONVOLUTION OF AN AMPLITUDE FUNCTION $A(\tau)$ AND A TRANSFER FUNCTION $f(t-\tau)$. WE DISCRETIZE AND LINEARIZE THE PROBLEM BY CONSIDERING THE FORCING OVER THE FISHING GROUNDS AS A LINEAR SUPERPOSITION OF N DIFFERENT EVENTS WHOSE AMPLITUDE IS UNKNOWN. FROM THE COMPARISON BETWEEN MEASUREMENTS AT MGM $(M(t))$ AND RESULTS OF THE INVERSE MODEL $(M_m(t))$, THE AMPLITUDE $A(\tau)$ OF THE DIFFERENT EVENTS AT MGM CAN BE DETERMINED. THE RELATIONSHIP FOUND BETWEEN AMPLITUDE OF THE RESPONSE AT MGM AND THE FORCING OVER THE FISHING GROUNDS $(A_o \propto R_s)$ IS USED TO INFER THE LATTER.

The aim of the inverse modelling is to retrieve the amplitude $(A(\tau))$ of the n different events that will allow us to infer the forcing over the fishing grounds (R_s). However, $A(\tau)$ is largely unknown and multiple solutions are possible. In order to reduce the degrees of freedom of the system we follow two alternative approaches to determine the discrete inverse model parameters $A(\tau)$ and hence, infer the time series of resuspension $R_s(t)$ over the fishing grounds: Gaussian distribution and Autoregressive Moving Average Model (ARMA).

3.3.3.1. Gaussian distribution

A preliminary assessment of the impact of bottom trawling is explored by means of a Gaussian distribution of the fishing effort over the fishing grounds. This first simplified assessment is presented for illustration purposes and to evaluate the order of magnitude involved. A Gaussian distribution of the fishing effort over the two fishing grounds is considered. The relationship found between $A_o \propto R_s$ would suggest that, in a linear approach, if the fishing effort follows a Gaussian distribution, the amplitude of the events at MGM should also follow a Gaussian distribution.

Fishing activity over the flanks of the canyon takes place on working days, whilst on Saturday and Sunday there is no activity. Vessels head offshore at 6 a.m. and head back to port at about 3-4 p.m. (Martín et al., 2014b). We impose the following distribution for a working day:

$$A(t) = \gamma \cdot e^{-\frac{(t-t_0)^2}{2(dt)^2}} \qquad (12)$$

Where t_o=11 h so that the distribution is centered at 11 a.m. and its temporal window is dt^2=2. The coefficient γ is necessary so that the response of the inverse model and the measurements at MGM are of the same order of magnitude, and takes a value of $\gamma = 0.0091$. Once the time series of amplitude $A(t)$ at MGM of the different events considered is obtained, the remobilization R_s over the fishing grounds can be inferred from the relationship $A(R_s)$.

3.3.3.2. Autoregressive Moving Average Model

A more accurate assessment of the impact of bottom trawling over the fishing grounds can be determined by means of the Autoregressive Moving Average Model (ARMA) (Whittle, 1951; Box and Jenkins, 1976). The ARMA model allows splitting a signal in two parts: (i) an autoregressive part (M_{AR}) expressing the inherent behavior of the system itself, and (ii) a moving average part (M_{MA}) related to the external forcing of the system (i.e. the external forcing would be the time series of resuspension over the fishing grounds). The term $\varepsilon(t)$ corresponds to white noise error terms.

$$M(t) = M_{AR}(t) + M_{MA}(t) + \varepsilon(t) \quad (13)$$

$M_{AR}(t)$ explains the part of the signal due to the system itself as the output variable depends linearly on its own previous values. $M_{MA}(t)$ and $\varepsilon(t)$ explain the part of the signal due to the external forcing. One can isolate the part of the signal at MGM due exclusively to the external forcing by subtracting the autoregressive part (M_{AR}) as follows:

$$M_T(t) = M(t) - M_{AR}(t) \quad (14)$$

Thus, if we construct the time series of amplitude of events $A(t)$ as a function of $M_T(t)$, we will obtain the remobilization over the fishing grounds $R_s(t)$ solely associated to the external forcing (i.e. trawling).

$$A(t) = \gamma \cdot g(M_T(t)) \quad (15)$$

We propose the use of a quadratic expression $g\big(M_T(t)\big) = \alpha_1 M_T + \alpha_2 M_T^{\beta}$. This non-linear solution allows us to consider basal values and intensifies the value of the peaks.

The modelled response $M_m(t)$ at MGM is obtained by applying equation (11). The comparison of the measurements $M(t)$ and the inverse model $M_m(t)$ allows us to infer the time series of amplitudes $A(t)$. Best agreement between model outputs and measurements at MGM is found for $g\big(M_T(t)\big) = M_T^{1.3}$ and $\gamma = 0.3379$. Once $A(t)$ is determined, the time series of resuspension $R_s(t)$ is obtained through the relationship between the remobilization R_s along the fishing grounds and the amplitude A of the event at MGM.

3.3.4. Inclusion of trawling resuspension

The time series of resuspension $R_s(t)$ obtained through inverse modeling is used as forcing to model the sediment dynamics and sedimentation patterns due to trawling in the canyon. The resuspension is spread over the whole fishing grounds; hence the area considered is larger than the area actually trawled at a precise instant of time. The results provided by this approach might have a larger spatial distribution than in reality.

The resuspension is integrated in the model in terms of instantaneous sediment flux over the fishing grounds, allowing us to take into account the non-linearity inherent to turbidity currents. The sediment remobilized is equivalent to an additional volume concentration that is calculated at each grid point of the area affected by trawling, taking into account the instantaneous thickness of the sediment cloud at each time step. A height cloud threshold is imposed over the fishing grounds in order to take into account the scale of the turbulence provided by the fishing gears. Sensitivity tests were performed for this height threshold and best results were found for $h_{lim} = 1$ m. (Fig. 3.8)

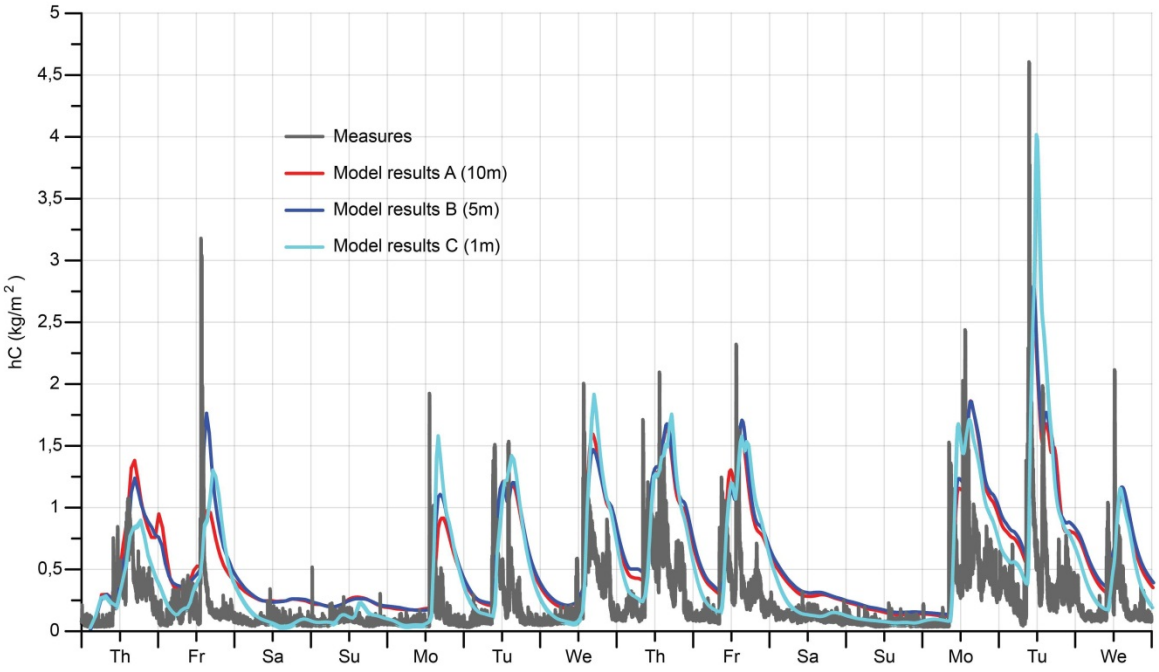

FIG. 3.8. SENSITIVITY TESTS PERFORMED FOR DIFFERENT HEIGHT CLOUD THRESHOLD OVER THE FISHING GROUNDS. OUTPUTS ARE PRESENTED AT MGM IN TERMS OF INSTANTANEOUS SEDIMENT TRANSPORT $hC\left(\frac{kg}{m^2}\right)$.

Sensitivity tests were performed for different sizes of sediment ranging from 1µm to 70µm and no significant differences were observed in terms of $hC(kg/m^2)$ at point P3 (see location in Fig. 3.1) for the range of values corresponding to silt (6-63 µm) (Fig. 3.9). The tests were performed for an initial event of sediment removal of 1cm over the fishing grounds instantaneously injected over 10 m of water column. This sediment removal is equivalent to an initial uniform volume concentration of $\Phi s = 2.5 \cdot 10^{-4}$ (0.65 g/l). A grain size of 63 µm is considered in order to take into account aggregates that would perform similarly to bigger particles.

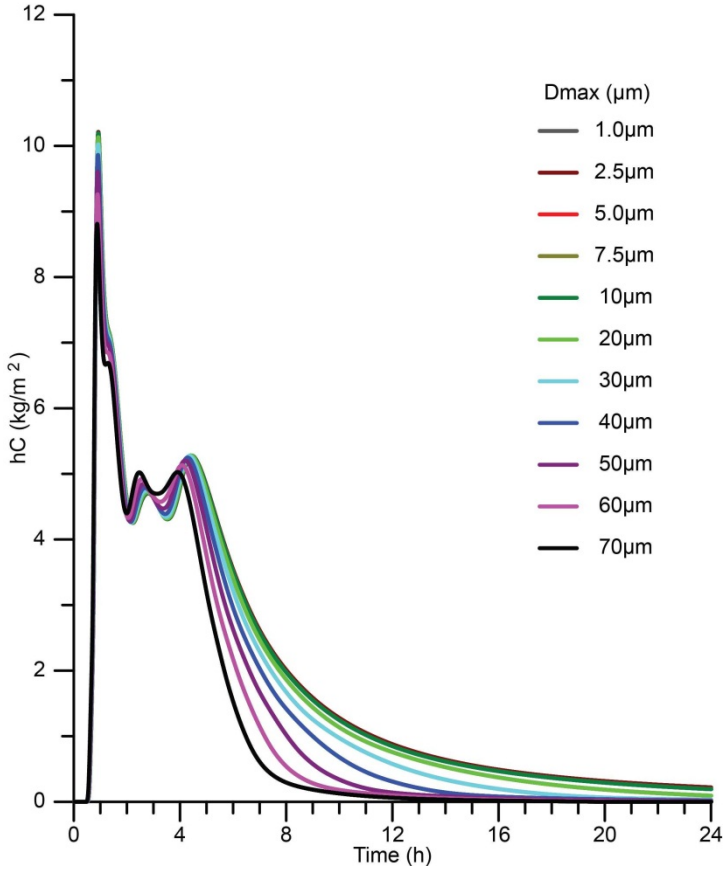

FIG. 3. 9. SENSITIVITY TESTS PERFORMED FOR DIFFERENT GRAIN SIZES IN THE RANGE OF SILT. RESULTS ARE PRESENTED IN THE FORM OF INSTANTANEOUS SEDIMENT TRANSPORT HC (KG/M2). OUTPUTS AT POINT P3 (LOCATION IN FIG 1) ARE SHOWN FOR AN INITIAL UNIFORM VOLUME CONCENTRATION OF $\Phi s = 2.5 \cdot 10^{-4}$ (0.65 G/L) OVER THE FISHING GROUNDS OF ROSTOLL, SANT SEBASTIÀ AND LLEVANT. THIS VALUE OF CONCENTRATION IS EQUIVALENT TO A SEDIMENT REMOVAL OF 1 CM OVER THE AREA CONSIDERED AND INSTANTANEOUSLY INJECTED OVER 10 M OF WATER COLUMN.

4. Results

4.1. At the local scale: mooring site

4.1.1. Bottom trawling influenced area

Turbidity currents do not reach the MGM mooring site when trawling is limited to the shelf at less than 200 m water depth. Shallower than this depth threshold, bottom trawling increases local turbidity without sediment laden flows developing down the continental slope due to the shelf low gradient (see Fig. 3.10).

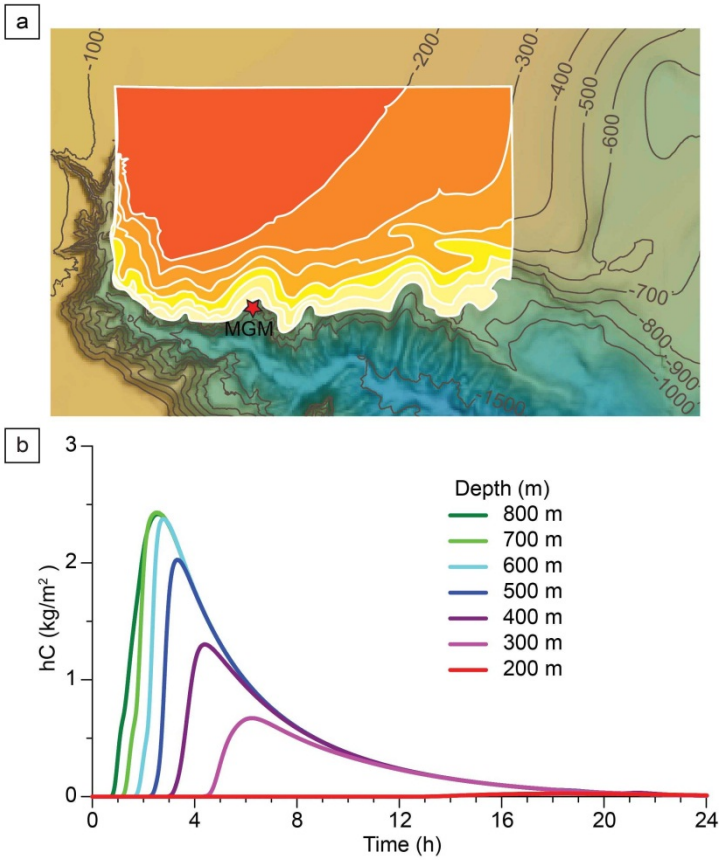

FIG. 3. 10. RESULTS FOR THE INFLUENCE AREA OF THE TRAWLING ACTIVITY. (A) THE FISHING GROUNDS CONSIDERED COVER PART OF THE CONTINENTAL SHELF AND EXTEND DOWN TO DIFFERENT DEPTHS (I.E. THE TRAWLED AREA CONSIDERED IS LARGER AS THE DEPTH INCREASES). THE STAR INDICATES THE POSITION OF THE MGM MOORING WHERE THE RESULTS ARE ANALYSED. (B) OUTPUTS OF THE MODEL IN TERMS OF INSTANTANEOUS SEDIMENT TRANSPORT (KG/M^2) AT MGM. THE DEPTHS REACHED BY THE FISHING GROUNDS ARE EXPRESSED IN THE LEGEND: 200 M DEPTH IMPLIES TRAWLING ACTION OVER PART OF THE CONTINENTAL SHELF AND DOWN TO 200 M WHILST 800 M DEPTH IMPLIES TRAWLING ACTION OVER PART OF THE CONTINENTAL SHELF AND DOWN 800 M.

4.1.2. Transfer function

Similar responses are obtained for different initial conditions over the fishing grounds considered (Fig. 3.11a). Each event of resuspension over the fishing grounds triggers a response at MGM that appears to last about 16 hours. There is a time lag of about 30' between the remobilization over the canyon flanks and arrival time at MGM. The peak of the event reaches MGM at about 90' after the remobilization. The similar responses obtained for each individual event in terms of time scale and the fact that response amplitudes are proportional to the forcing allow the decomposition of the signal into two functions: a quasi-linear relationship (Fig. 3.11b) between the remobilization (R_s) over the fishing grounds (i.e. forcing) and the amplitude (A) of the response at MGM, and a transfer function (Fig. 3.11c) containing the physical processes and time scales inherent to the system. By splitting the response of an event of resuspension into these two functions (i.e. transfer function and relationship $A \propto R_s$), we isolate the part of the response at MGM due to the system itself (i.e. transfer function) and the part of the response due to the external forcing (i.e. relationship $A \propto R_s$).

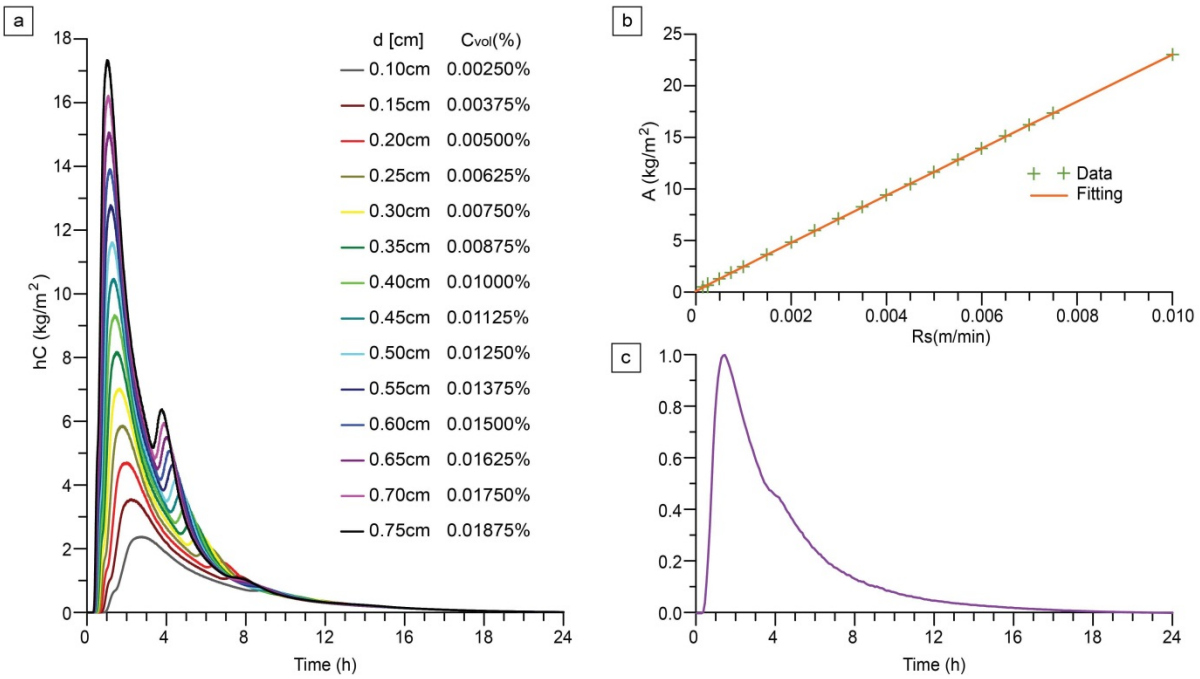

FIG. 3. 11. (A) RESULTS IN TERMS OF INSTANTANEOUS SEDIMENT TRANSPORT $hC\ (kg/m^2)$ AT MGM FOR THE DIFFERENT INITIAL CONDITIONS ANALYZED. (B) QUASI-LINEAR RELATIONSHIP FOUND BETWEEN THE FORCING (I.E. INITIAL CONDITIONS IN TERMS OF RESUSPENSION R_s) IMPOSED OVER THE FISHING GROUNDS AND THE AMPLITUDE A OF THE INSTANTANEOUS SEDIMENT TRANSPORT AT MGM. (C) TRANSFER FUNCTION OBTAINED FOR MGM.

4.1.3. Time series of resuspension due to trawling

Maximal resuspension values ($R_s(t)$) of $5\mu m/min$ over the fishing grounds are obtained through inverse modeling under the hypothesis of a Gaussian distribution of the fishing effort (Fig. 3.12). This maximal resuspension over the whole fishing grounds would be equivalent to the activity of the 22 vessels concerned by the La Fonera fisheries management plan (BOE Boletin Oficial del Estado, 2013) operating at a towing speed in the area between 2 and 3 knots scraping $3.8 \pm 0.7\ mm$ on average. Despite the incertitude in the variables involved in its calculation, these penetration depth values of the fishing gears are in the agreement with those found in the literature (Jones, 1992; Durrieu de Madron et al., 2005; Ivanović et al., 2011; O'Neill and Summerbell, 2011).

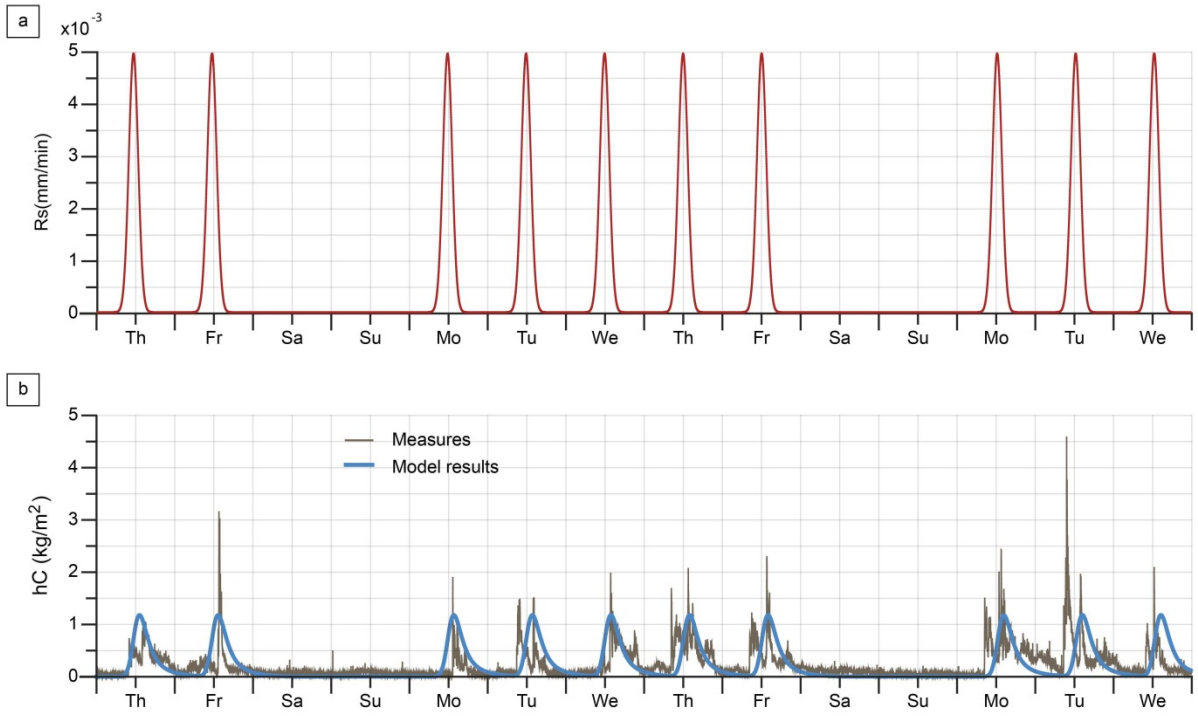

FIG. 3. 12. (A) TIME SERIES OF RESUSPENSION DUE TO TRAWLING OVER THE FISHING GROUNDS ISSUED BY THE INVERSE MODEL (GAUSSIAN APPROACH) FOR THE PERIOD 9TH TO 21ST JUNE 2011. (B) MEASURED (GREY LINE) AND INVERSE MODELED (BLUE LINE) INSTANTANEOUS SEDIMENT TRANSPORT AT MGM BETWEEN THE 9TH AND THE 21ST JUNE 2011.

A more accurate time series of trawling resuspension $R_s(t)$ over the fishing grounds considered is obtained through application of the inverse model and the ARMA model (Fig. 3.13) since in this alternative approach $A\ (t)$ is reconstructed as function of the forcing part ($M_{MA}(t)$) of the signal at MGM. Values of remobilized sediment thickness greater than 0.01 mm/min (Fig. 3.13a) over the fishing grounds trigger turbidity events capable of reaching MGM. This uniform resuspension over the whole area would correspond to the activity of 22 vessels on the area operating in the area at a towing speed between 2 and 3 knots and effectively scraping about 7.5$\pm$1mm of sediment and injecting it into the water column. Note the non-uniqueness of the solution, the amount of vessels could be less but would need a deeper effective erosion to create the same observed turbidity currents. The total amount of remobilized sediment due to trawling during the period analysed (i.e. fifteen days) is of about 1.27x10^{-3} km^3. Good agreement is found between the inverse model results and the measures at MGM (Fig. 3.13b). Pearson correlation coefficients between the re-suspension series $R_s(t)$ and the measurements $M(t)$ and between the results of the inverse model $M_m(t)$ and the measurements $M(t)$ are $r_{XY}\big(R_s(t),\ M(t)\big)$ = 0.0773 and $r_{XY}\big(M_m(t),\ M(t)\big)$ = 0.8381 respectively. These respective values evidence the fact that it is the transfer function which is integrating the physical processes and time scales of the system.

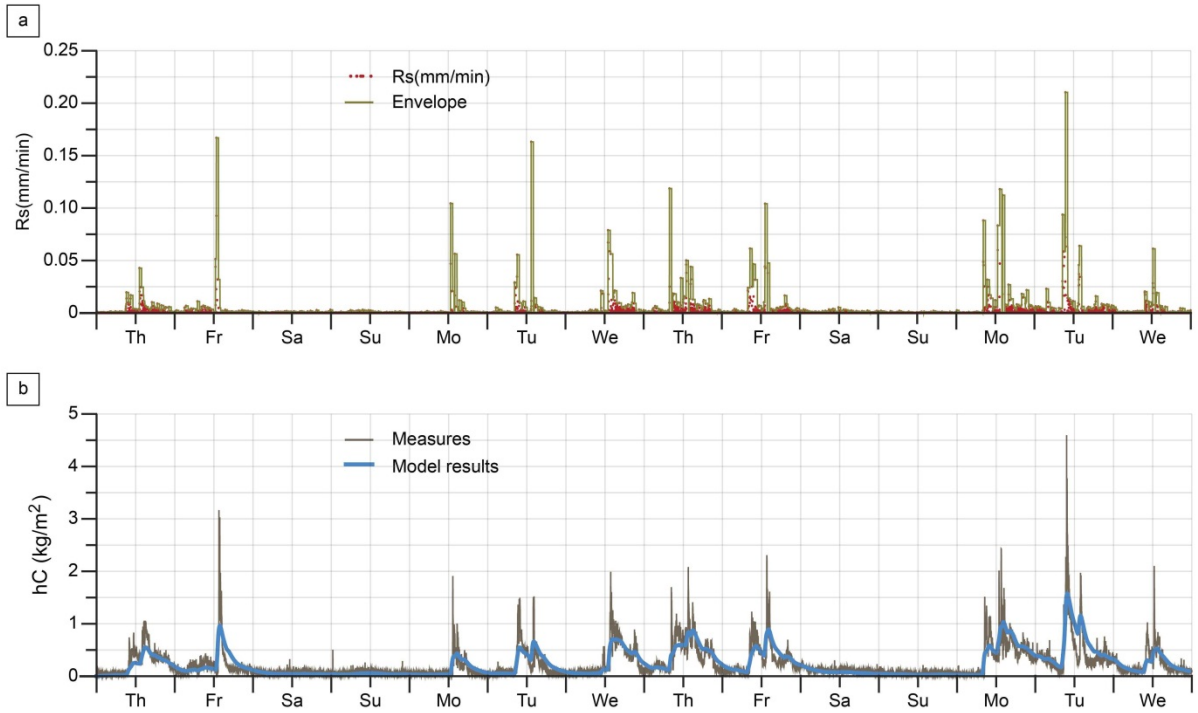

FIG. 3. 13. (A) TIME SERIES OF RESUSPENSION DUE TO TRAWLING OVER THE FISHING GROUNDS ISSUED OF THE INVERSE MODEL AND ARMA MODEL FOR THE PERIOD 9TH TO 21ST JUNE 2011. RED DOTS REPRESENT THE PUNCTUAL EVENTS CONSIDERED, IN ORDER TO EASE THE VISUALIZATION THE ENVELOPE OF THE REMOBILIZATION IS ALSO PLOTTED (GREEN LINE) (B) MEASURED (GREY LINE) AND INVERSE MODELED (BLUE LINE) INSTANTANEOUS SEDIMENT TRANSPORT AT MGM BETWEEN THE 9TH AND THE 21ST JUNE 2011.

4.2. The large scale view: down canyon and slope sediment transport and accumulation patterns

The time series of resuspension, issued by the ARMA modelling and the application of the inverse model, is used as forcing of the numerical model (section 2.3.4). This time series $R_s(t)$ spread over the whole fishing grounds triggers turbidity currents reaching MGM of the order of magnitude of those measured at MGM for the period analyzed between the 9th and the 21st June 2011 (Fig. 3.14). The model accurately reproduces both in time and magnitude the instantaneous sediment transport at MGM. The model is able to reproduce the sharp burst in sediment transport corresponding to the peak in the morning and the steady decay towards baseline values in the afternoon once the vessels head back to port.

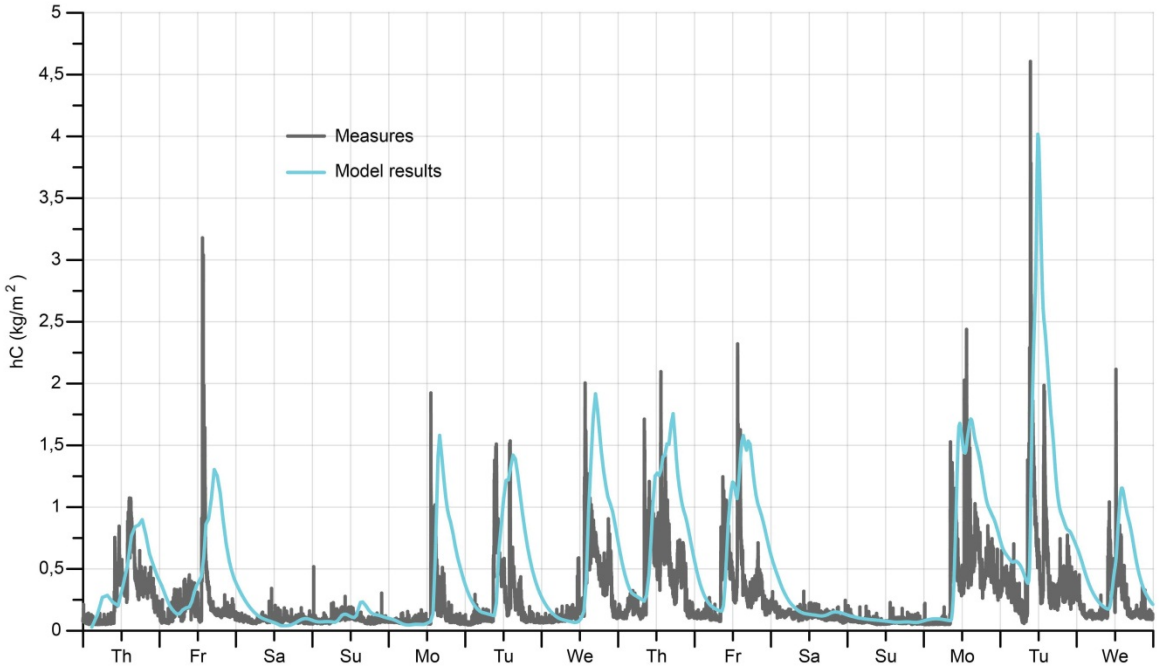

FIG. 3. 14. MEASURED AND MODELED INSTANTANEOUS SEDIMENT TRANSPORT AT MGM FOR THE PERIOD 9TH TO 21ST JUNE 2011. THE FORCING OF THE NUMERICAL MODEL IS THE RESUSPENSION TIME SERIES RS(T) OBTAINED THROUGH THE INVERSE MODEL UNDER THE ARMA APPROACH.

We identify potential propagation patterns of the resuspended sediment from the fishing grounds towards the canyon axis and beyond when we force Nixes-TC with the $R_s(t)$ issued by the inverse modeling (see Fig. 3.15). The results obtained depict an overall picture of pathways and areas indirectly affected by trawling. The spatial view of the canyon sediment dynamics may improve the definition of strategic locations for mooring arrays and cores. These additional data together with a better constraint of the forcing (i.e. quantification of the sediment resuspended by each vessel in fishing operation) would enable a more realistic simulation of trawling impact. For the forcing imposed, the flow is funnelled through gullies from the fishing grounds towards the canyon axis and beyond (Fig. 3.15 and Supplementary video MS1). A minor part of the remobilized sediment flows along the continental slope and joins the flow coming along the canyon axis at the glacis.

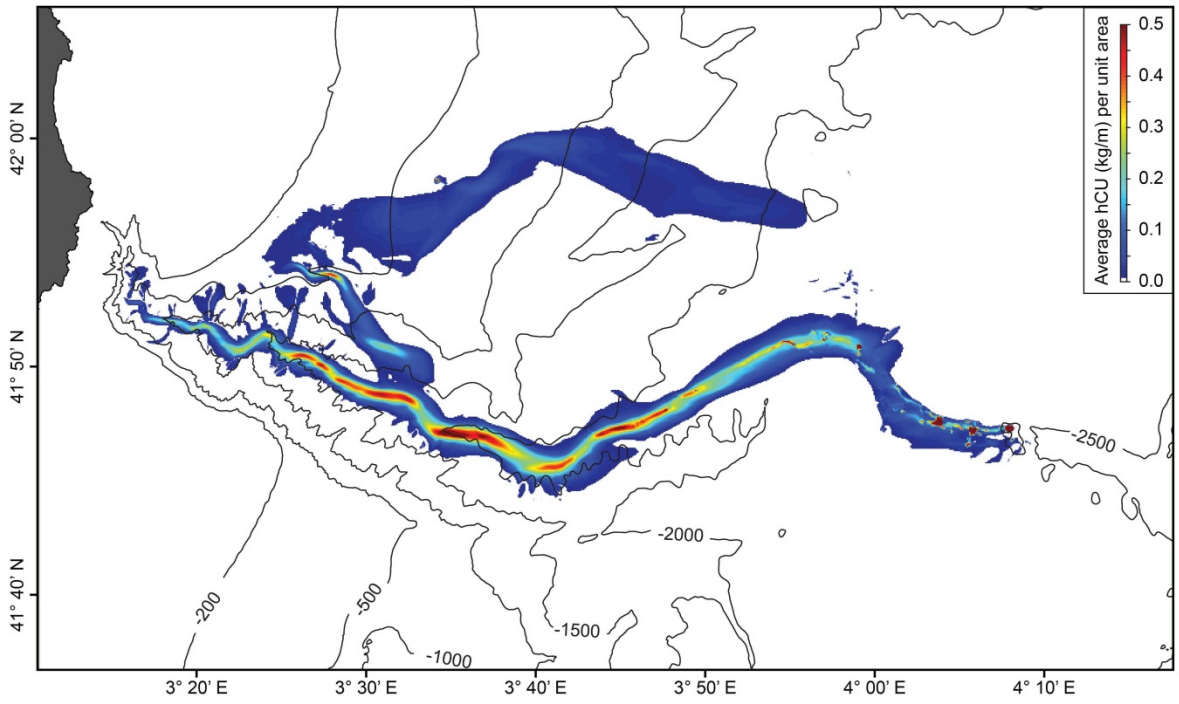

FIG. 3. 15. MODELLED AVERAGE SEDIMENT FLUX FOR THE TWO-WEEK PERIOD ANALYSED. THE FORCING IMPOSED TRIGGERS TURBIDITY CURRENTS REACHING MGM OF THE SAME ORDER OF MAGNITUDE THAN THOSE MEASURED AT MGM FOR PERIOD 9TH TO 21ST JUNE 2011. NOTE THAT THE RESULTS OBTAINED PROVIDE AN OVERALL PICTURE OF THE POTENTIAL DYNAMICS DUE TO TRAWLING IN THE LA FONERA SUBMARINE CANYON.

Mean current speed over the modelled two week-period goes up to 20 cm/s (Fig 3.16) with peak values reaching up to 50 cm/s (Fig. 3.17) along the canyon axis and gullies. The flow along the northern continental slope presents much lower values of current speed than those along the canyon axis and flanks. Maximum values of current speed along this northern branch of the flow go up to 25 cm/s whilst mean values reach 0.04 cm/s. Higher values are observed in the gullies of the northern flank and along the lower canyon axis where topographic constraints are at play. Once the flow reaches the continental rise, it spreads and lower values of mean velocity are obtained.

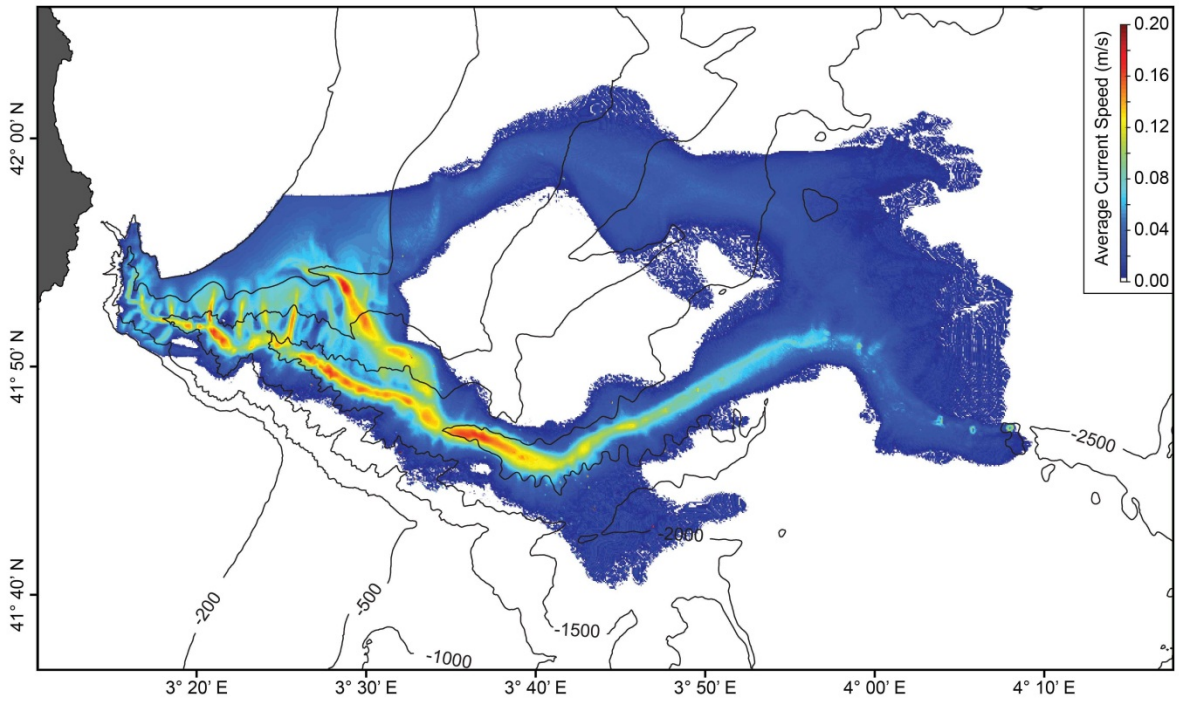

FIG. 3. 16. MODELLED AVERAGE CURRENT SPEED OVER THE TWO WEEK PERIOD CONSIDERED IN LA FONERA SUBMARINE CANYON. THE RESUSPENSION IMPOSED OVER THE FISHING GROUNDS PROVIDES VALUES OF INSTANTANEOUS SEDIMENT TRANSPORT AT MGM IN AGREEMENT WITH THOSE MEASURED FOR THE PERIOD 9TH TO 21ST JUNE 2011 AT MGM.

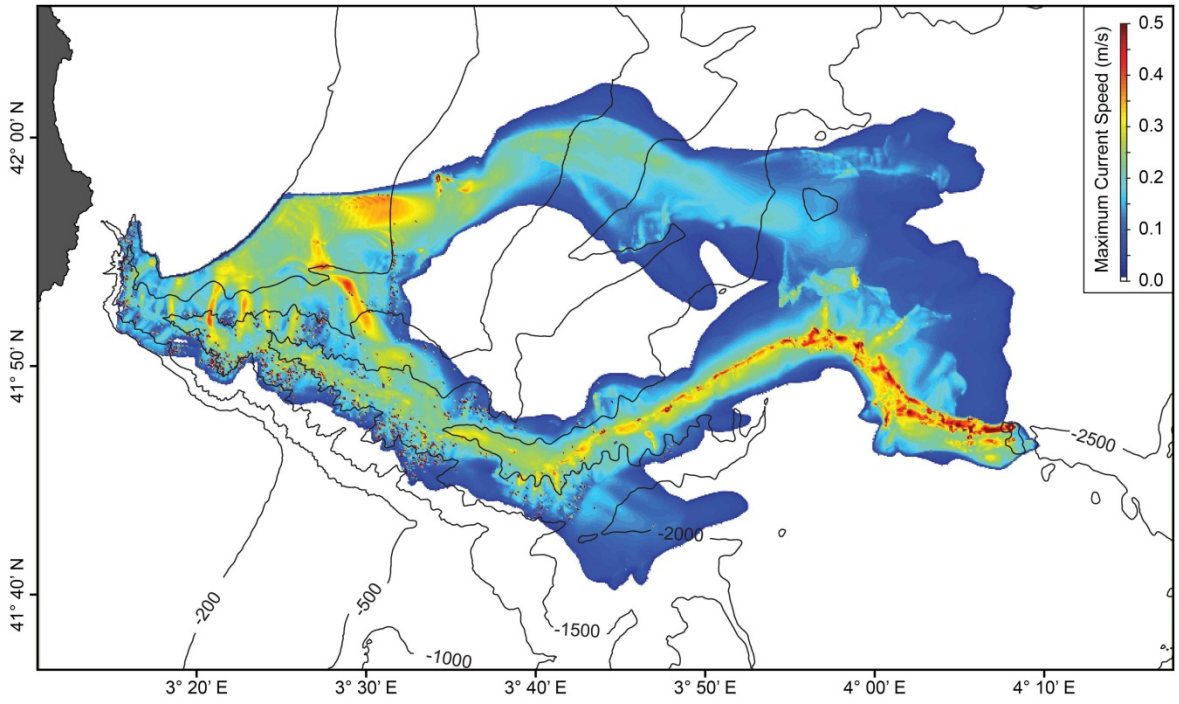

FIG. 3. 17. MODELLED MAXIMUM CURRENT SPEED FOR THE TWO WEEK PERIOD ANALYSED IN LA FONERA SUBMARINE CANYON. THE RESUSPENSION IMPOSED OVER THE FISHING GROUNDS PROVIDES VALUES OF INSTANTANEOUS SEDIMENT TRANSPORT AT MGM IN AGREEMENT WITH THOSE MEASURED FOR THE PERIOD 9TH TO 21ST JUNE 2011 AT MGM

Figure 3.18 shows the evolution of the flow at different locations along the LFC axis and northern canyon flank gullies (see Fig. 3.1c for P1 to P7 output points). There is no propagation of turbidity events associated with trawling at the point P1 at the canyon head (Fig. 3.18a). For other control

points, depending on their location, two different types of responses are identified. On one hand, the control points located inside gullies (MGM and P3) reproduce the forcing signal with well-defined working hours and holidays (Fig. 3.18b). On the other hand, along the canyon axis, transport seems to be continuous during the week only reaching natural baseline levels during the weekend (Fig. 3.18c and d). For these points along the canyon axis, there is an increasing trend in the values of instantaneous sediment transport through the week, with baselines levels on week days in the range of half of the peak value of the previous day. We observe a time lag in the signal along the canyon axis. Instantaneous sediment transport seems more intense in the mid-low canyon and in the monitored gully MGM compared to the upper canyon. The lower values of the points of cumulated sediment transport for the low canyon points are due to the time lag in the signal that prevents all the events from going through by the end of the analysed period. Table 1 summarizes the averaged and maximum instantaneous sediment transport (i.e. hC, Sup. Fig. 3.1); the averaged and maximum sediment transport (i.e. hCU) and the cumulated sediment transport after the 15 day period analyzed for the control points.

Control point	Position	Depth (m)	Averaged Instantaneous Sediment Transport $hC\ (kg/m^2)$	Maximum Instantaneous Sediment Transport $hC\ (kg/m^2)$	Averaged Sediment Transport $hCU\ \left(\frac{kg}{ms}\right)$	Maximum Sediment Transport $hCU\ \left(\frac{kg}{ms}\right)$	Cumulated Sediment Transport (15 days) $\int hCUdt\ \left(\frac{t}{m}\right)$
P1	Axis	470	0.0046	0.1572	0.0003	0.0223	0.5338
P2	Axis	1200	1.3538	4.4973	0.1980	0.6727	202.4391
MGM	Gully	998	0.5712	3.9959	0.1011	1.3878	99.0080
P3	Gully	1100	0.2047	1.7423	0.0343	0.4561	34.7561
P4	Axis	1700	2.7674	6.5637	0.44523	1.1986	471.1346
P5	Axis	1900	1.7890	5.7907	0.32583	1.3283	324.2193
P6	Axis	1900	2.2435	6.2130	0.3931	1.2091	395.2138
P7	Axis	2100	1.2363	5.8954	0.2497	1.1485	254.0664

TABLE 3. 1. AVERAGED AND MAXIMUM AND CUMULATED INSTANTANEOUS SEDIMENT TRANSPORT FOR THE CONTROL POINTS ANALYSED.

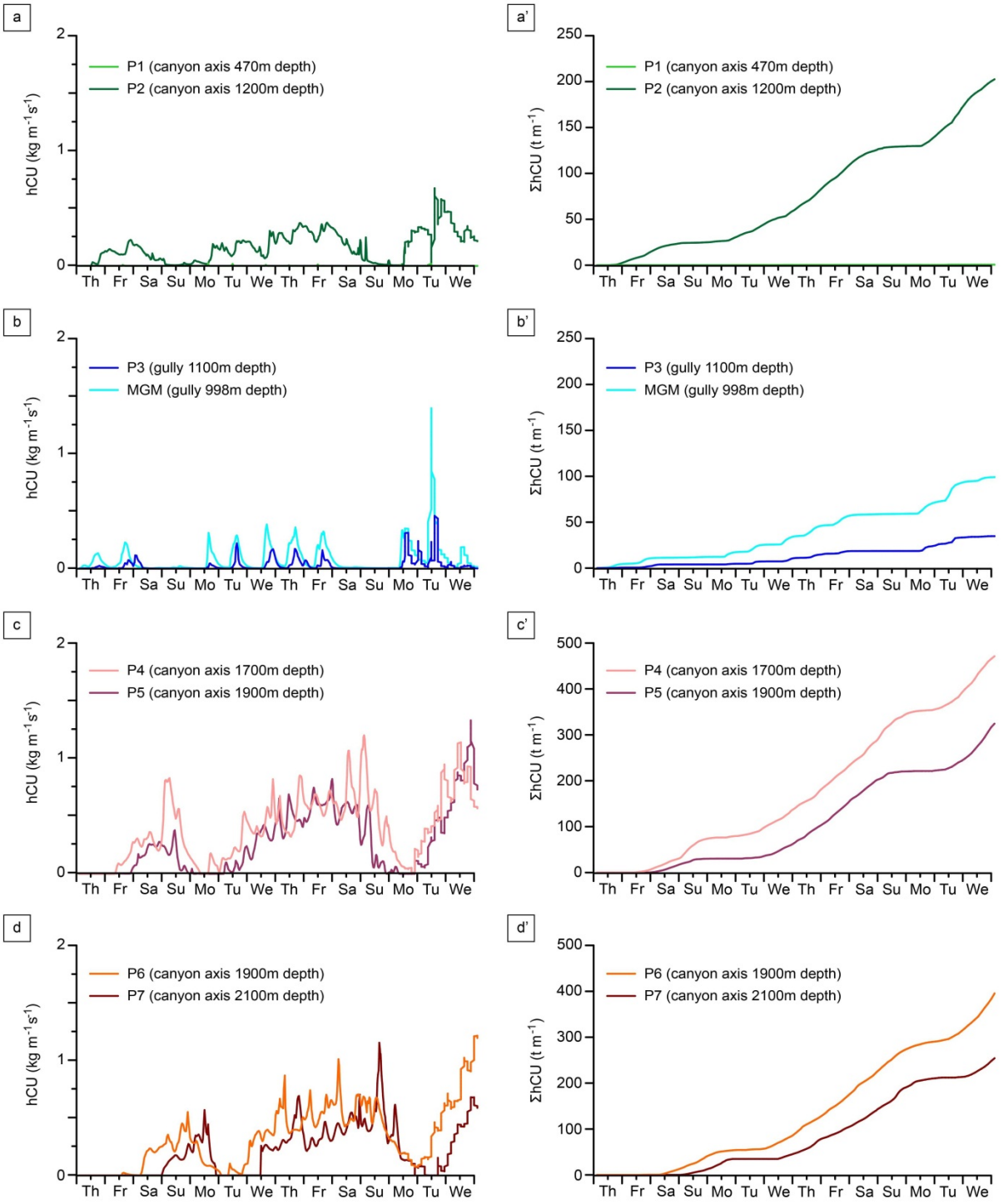

FIG. 3. 18. MODELLED SEDIMENT TRANSPORT AT DIFFERENT LOCATIONS ALONG THE CANYON AXIS AND NORTHERN CANYON FLANK GULLIES OF LA FONERA SUBMARINE CANYON FOR THE TWO-WEEK PERIOD ANALYSED. THE NUMERICAL MODEL IS FORCED WITH THE RESUSPENSION TIME SERIES RS(τ) OBTAINED THROUGH THE INVERSE MODEL UNDER THE ARMA APPROACH THAT TRIGGERS TURBIDITY CURRENTS REACHING MGM OF THE SAME ORDER OF MAGNITUDE THAN THOSE MEASURED AT MGM FOR THE PERIOD 9TH TO 21TH JUNE 2011. THE RESULTS ARE PRESENTED IN TERMS OF FLUX (hCU) AND CUMULATED FLUX ($\int hCUdt$) ON THE LEFT AND RIGHT COLUMN RESPECTIVELY.

The deposition thickness at the end of the study period is presented in Figure 3.19. Sediment gain on the lower part of southern canyon flank appears to be more important than on the northern wall. However these deposits and those along the canyon axis are probably ephemeral, at least in part, given the values of mean current speed. The deposition over the fishing grounds corresponds to the

decantation of part of the sediment injected to simulate trawling activity. An accumulation area develops at the canyon mouth, beyond the 2000 m isobath, due to sediment flows propagating through the canyon axis and also those coming from the continental slope. This depocentre is coherent with the loss of transport capacity of the flow observed and with the gradients of current speed obtained. Some deposition is observed in the southern lower canyon probably due to flow overbank.

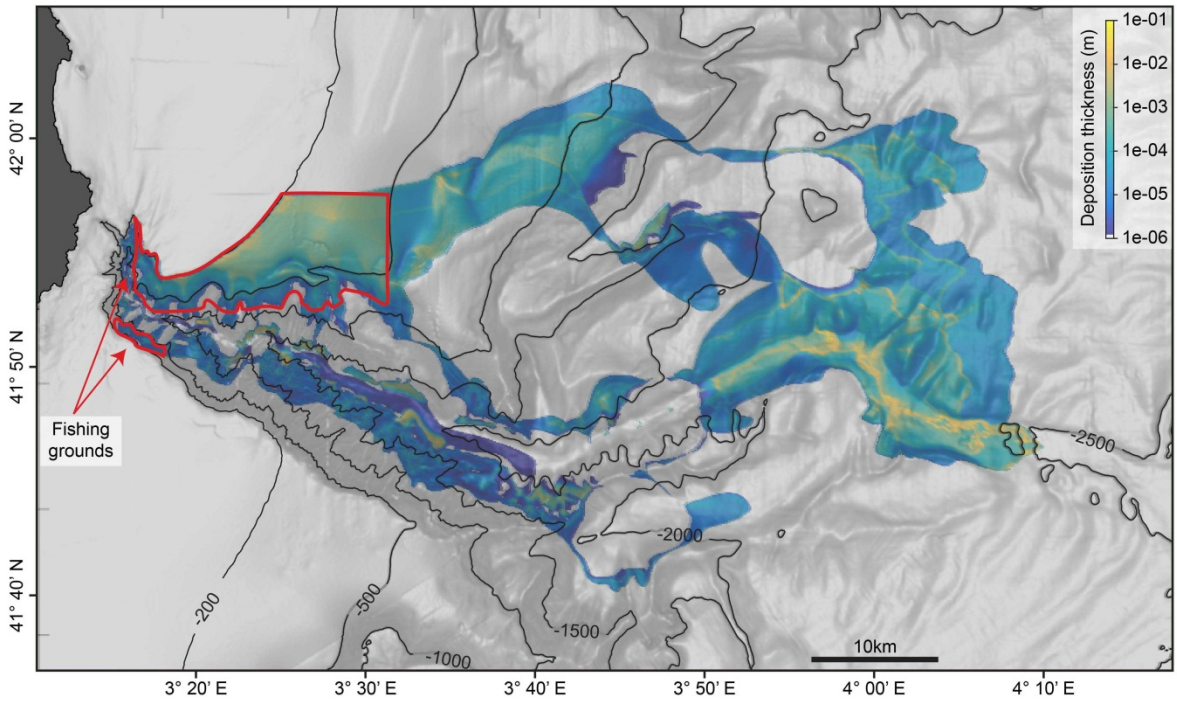

FIG. 3. 19. MAP OF MODELLED SEDIMENT THICKNESS ACCUMULATED FOR A TWO WEEK PERIOD OF TRAWLING ACTIVITY.

5. Discussion

By spreading resuspension over a potential area affected by trawling, we provide a wide picture of the trawling-induced dynamics in the canyon and show the value of numerical models in understanding deep-water processes associated with trawling. Turbidity currents can evolve significantly along their pathways. We show here that numerical models can provide insight into how fast these flows move, how far they can travel and how much sediment can be carried that are difficult to achieve by punctual measurements alone.

The results obtained in this study indicate notable differences between trawling shoreward and seaward of the 200 m isobath. Trawling over the flatter shallower areas can locally enhance turbidity in the water column, similarly to the observations of (Palanques et al. (2001) over the inner shelf off Barcelona; however, no sediment flows reach MGM. The results confirm previous observations in LFC (Palanques et al., 2006): it is only when fishing activity takes place on the steep slopes of the canyon flanks that trawling triggers turbidity currents. The high values of gradient slopes favor the ignition of sediment gravity flows that extend the impact of trawling beyond the fishing grounds.

We find similar responses for the different single event forcing scenarios evaluated. We separate physical processes and temporal evolution (i.e. transfer function), and intensity of the event (i.e. amplitude A_o, forcing). Our results suggest that for the identified trawled area, the intensity of the event at MGM (A_o) is strongly determined by the initial condition (R_s). The dynamics and temporal aspects of the flow are included in the transfer function that reproduces the behaviour of turbidity

currents discussed in literature (Middleton and Hampton, 1973; Kneller and Buckee, 2000) with a sharp waxing phase and a more gradual waning phase as sediment settles. Velocity and sediment concentration within the flow follow the same behaviour for a single turbidity current event. The transfer function and the quasilinear relationship between the modelled amplitude at MGM and its respective initial condition, R_s, allow the linearization of the problem and are the basis of the inverse modeling.

Inverse modelling strategies have been proposed to estimate flow speed from tsunami deposits (Jaffe et Gelfenbuam, 2007; Jaffe et al., 2011), for reconstruction of deposits from turbidity currents (Lesshafft et al., 2011), and to infer paleo-flow conditions from turbidites (Falcini et al., 2009). Here the objective is not to relate deposits and flow conditions, but to obtain a forcing (i.e. resuspension over the fishing grounds) capable of triggering events similar to those measured at MGM. The first approximation through a Gaussian distribution of the fishing effort provides a first validation of our approach since the equivalent estimated removal of $3.8 \pm 0.7\ mm$ by the fishing gears of the local trawling fleet falls in the range of values found in literature (Durrieu de Madron et al., 2005; Ivanović et al., 2011; O'Neill and Summerbell, 2011).

By using the ARMA model to isolate the part of the signal due to the external forcing M_{MA}, we were able to obtain a synthetic series of resuspension $R_s(t)$ due to trawling that triggers turbidity events reaching MGM comparable to those measured on June 2011. We observe a tight coupling between the temporal distribution of the resuspension $R_s(t)$ over the fishing grounds and the measured instantaneous sediment transport $M(t)$, and between the latter and the results of the inverse model $M_m(t)$. The inverse model accurately reproduces both phase and amplitude modulation of the instantaneous sediment transport at MGM showing an intensification of the sediment transport during the working hours of the local fishing fleet. The model presents accurate results, with a significant value of Pearson correlation coefficient of $r_{XY}\big(M_m(t), M(t)\big)$ = 83.81% between model outputs $M_m(t)$ and measurements $M\ (t)$. The time series $R_s(t)$ would be roughly equivalent to the activity of 22 vessels in the area towing at 2 and 3 knots and effectively scraping about 7.5$\pm$1mm, values that are coherent with those found in the bibliography (Durrieu de Madron et al., 2005; Ivanović et al., 2011; O'Neill and Summerbell, 2011). The accurate results obtained at MGM, together with the coherent equivalent value in terms of fishing effort and penetration of the fishing gears, validate our methodology.

The inclusion of trawling-induced resuspension as forcing in the numerical model allows the identification of transport patterns and accumulation areas. The outputs of the model for this given scenario show good agreement with the measurements at the validation point of MGM. At the canyon head (i.e. point P1, 470 m depth), model results show no influence of trawling, as other studies based on mooring data have already reported (Martín et al., 2007). Turbidity currents in the model seem to propagate further down than expected from previous studies (Palanques et al., 2005; Martín et al., 2006, 2007). We propose three possible explanations for this result. First, there is a lack of measurements beyond 1700 m along the canyon axis, and what happens in the canyon beyond that depth remains uncertain. Second, the model only includes the turbidity current dynamics but not the general pattern of circulation in the canyon. Measurements in 2001 showed periodical inversions up and down, with low mean values at different depths ranging between 2 and 3 cm/s and peaks reaching 20 to 40 cm/s, and net water mass flows close to the bottom directed upward (Palanques et al., 2005; Martín et al., 2006, 2007). These internal hydrodynamics of the canyon can interact with the turbidity flows and slow them down, limiting their propagation. In our model, gravity is the driving force; hence currents will always flow downslope. Third, different intensities of trawling impact can be expected since the data analysed in the present study is from a different time period to that used in previous studies. The mooring data used to infer the remobilization over the fishing grounds corresponds to measurements from 2011 whilst the mooring data in the other studies corresponds to 2001. Despite the slow reduction in the number of vessels in Palamós, the local fleet underwent a dramatic increase in the installed power at the beginning of the 21st century

(Puig et al., 2015). Since the installed power is a reliable proxy of the capacity of trawlers to resuspend bottom sediments (Martín et al., 2014a), the further propagation of turbidity currents in the model for 2011 could be reasonable.

Intensification of instantaneous sediment transport is concomitant with higher mean and maximal values of current speed. This would reflect the bathymetric control on the flows while funnelled through gullies. The canyon buffers transport similarly to river catchments; the signal is amplified along the canyon axis and week days do not imply a return to baselines values of sediment transport but to roughly half the values of the previous day. Part of the transfer of sediment from the fishing grounds to the deep takes place through the northern open continental slope following an alternative path for turbidity currents. This northern branch would interact with local along slope currents in the area with mean values of 2-4 cm/s and peaks reaching 20 cm/s (Palanques et al., 2005), presumably deflecting their path. Nevertheless, values of current speed and mean sediment flux are lower through this northern path that along the canyon axis indicating the canyon role as a preferential conduit of sediment transfer. Values of current speed (i.e. bed shear stress) along the canyon axis indicate that most of it acts as a bypass where ephemeral deposits could develop and might be reintegrated by the following flows. The thickness of the deposit after 15 days of activity along the deeper canyon axis region is coherent with the high sediment rates of 2.4 cm/yr measured for the last decade (Puig et al., 2015). The interaction of the turbidity currents with the hydrodynamics of the canyon axis can shift the accumulation areas further onshore than the results shown here. Previous studies (Martín et al., 2007; Puig et al., 2012) show a decreasing pattern in the sediment fluxes in the canyon for the spring and summer months which can be related to the higher availability of sediment on the external part of the continental shelf and the upper flanks after the winter storms. Since the time series analysed corresponds to the beginning of the fishing season, when more sediment is available, more heavily sediment laden currents can occur. The accumulation obtained over the fishing grounds, where erosion is expected (Martín et al., 2014c), is due to the decantation of the injected sediment over this area in order to simulate the source of sediment in the model. Due to lower gradients, the flow is slower over the fishing grounds implying that at the final stage of the simulation there is still sediment in the area which has not flowed downslope (Fig. 3.19).

The generalization of the area, defining it as the potential area of trawling, makes our approach more generally applicable and can be considered as an upper bound of the trawling process in the canyon. However, the reasonable orders of magnitude obtained for the different variables analyzed validate our methodology.

It has been claimed that the effects of trawling on bottom sediments are not limited to the fishing grounds but can propagate further and deeper from them (Martín et al., 2008, 2014b). Our results definitely support that view and provide a spatial vision of these long-range effects. The span of these trawling-induced flows highly depends on the area over which fishing activities take place. Our methodology can help in the definition of fishing grounds with lesser physical impacts at the scale of the canyon and of the continental margin. The global extent of bottom trawling gives further-reaching implications to our methodology beyond the local study of LFC.

VMS are deployed by several nations on large commercial fishing vessels (Molenaar and Tsamenyi, 2000). VMS are mandatory in the EU for vessels larger than 15 m and larger than 24 m in the USA. The application of the inverse model based on mooring data allowed us to obtain the value of resuspension over the fishing grounds defined on the basis of VMS data. Therefore, similar approaches could be followed in other regions were VMS data is available. Furthermore, the approach presented allows the definition of larger areas that could be affected by fishing activities taking into account the effects of bottom trawling on the sedimentary dynamics.

The application of the model provides a spatial vision of the sediment dynamics in the canyon. It enlarges the present understanding of trawling-induced sediment transfer from the fishing grounds

towards deeper areas. The results obtained in terms of sediment transport provide valuable information for the definition of future mooring/coring sites that should improve the insight and knowledge of the canyon dynamics and help both to better constrain the forcing we impose in the model and with its validation. Feedback loops between field measurements and modelling are needed for an improved knowledge of turbidity current processes in general.

6. Conclusion

We have developed a numerical methodology to calculate the trawling resuspension over the fishing grounds and its consequences in terms of sediment transport in canyons. This novel approach is based on the definition of an area susceptible to being trawled on the basis of VMS data, inverse analysis and numerical process modelling. The key variable in trawling impact on sediment dynamics, which is the sediment remobilized, is inferred from the inverse modelling over the area defined on the basis of VMS data. The numerical process based model validated against in situ mooring data has been used to study the sediment transfer due to trawling resuspension. The results obtained complete and enlarge the interpretations of the trawling impact on the sedimentary functioning of the canyon, since present knowledge is based on snapshots of field data limited in time and space. Our study allows the identification of the transfer patterns from the fishing grounds where resuspension is generated, towards the canyon axis and beyond and the associated trawling-induced accumulation areas. The canyon scale vision may help in the identification of strategic mooring and coring sites to further advance the state of our knowledge on sediment dynamics of the canyon and validate this model. The definition of trawling area based on VMS data allows identifying the potentially “damaging” and affected areas for sediment transport and would allow the identification of trawling areas with lesser impacts, with the aim of a management of fisheries not only based on the short term impact on individual species but with a more long term vision of ecosystem processes.

References

Alegret, J. L., and A. Garrido (2008), Historia del puerto pesquero de Palamós: migraciones, asociacionismo y desarrollo. AREAS, Rev. Int. Cienc. Soc., 27, 27-40.

Allen, S. E., and X. Durrieu de Madron (2009), A review of the role of submarine canyons in deep-ocean exchange with the shelf, *Ocean Sci.*, *5*(4), 607–620.

Amblas, D., M. Canals, R. Urgeles, G. Lastras, C. Liquete, J. E. Hughes-Clarke, J. L. Casamor, and A. M. Calafat (2006), Morphogenetic mesoscale analysis of the northeastern Iberian margin, NW Mediterranean Basin, *Mar. Geol.*, *234*(1–4), 3–20, doi:10.1016/j.margeo.2006.09.009.

BOE Boletin Oficial del Estado (2013), Orden AAA/923/2013, de 16 de mayo por la que se regula la pesca de gamba rosada (Aristeus antennatus) con arte de fondo en determinadas zonas marítimas próximas a Palamós,

Box, G. E. P., and G. M. Jenkins (1976), *Time series analysis: forecasting and control*, Holden-Day.

Bradford, S. F., and N. D. Katopodes (1999), Hydrodynamics of turbid underflows. I: Formulation and numerical analysis, *J. Hydraul. Eng.-Asce*, *125*(10), 1006–1015, doi:10.1061/(ASCE)0733-9429(1999)125:10(1006).

Churchill, J. H. (1989), The effect of commercial trawling on sediment resuspension and transport over the Middle Atlantic Bight continental shelf, *Cont. Shelf Res.*, *9*(9), 841–865, doi:10.1016/0278-4343(89)90016-2.

Company, J. B., P. Puig, F. Sardà, A. Palanques, M. Latasa, and R. Scharek (2008), Climate Influence on Deep Sea Populations, *PLoS ONE*, *3*(1), e1431, doi:10.1371/journal.pone.0001431.

Dellapenna, T. M., M. A. Allison, G. A. Gill, R. D. Lehman, and K. W. Warnken (2006), The impact of shrimp trawling and associated sediment resuspension in mud dominated, shallow estuaries, *Estuar. Coast. Shelf Sci.*, *69*(3–4), 519–530, doi:10.1016/j.ecss.2006.04.024.

Depestele, J., A. Ivanović, K. Degrendele, M. Esmaeili, H. Polet, M. Roche, K. Summerbell, L. R. Teal, B. Vanelslander, and F. G. O'Neill (2015), Measuring and assessing the physical impact of beam trawling, *ICES J. Mar. Sci. J. Cons.*, fsv056, doi:10.1093/icesjms/fsv056.

Diesing, M., D. Stephens, and J. Aldridge (2013), A proposed method for assessing the extent of the seabed significantly affected by demersal fishing in the Greater North Sea, *ICES J. Mar. Sci. J. Cons.*, *70*(6), 1085–1096, doi:10.1093/icesjms/fst066.

Durrieu de Madron, X., B. Ferré, G. Le Corre, C. Grenz, P. Conan, M. Pujo-Pay, R. Buscail, and O. Bodiot (2005), Trawling-induced resuspension and dispersal of muddy sediments and dissolved elements in the Gulf of Lion (NW Mediterranean), *Cont. Shelf Res.*, *25*(19–20), 2387–2409, doi:10.1016/j.csr.2005.08.002.

Dyerkjaer, S. M., J. K. Jensen, and E. Hoffmann (1995), *Mussel dredging and effects on the marine environment*, ICES CM 95/ E:13.

Eastwood, P. D., C. M. Mills, J. N. Aldridge, C. A. Houghton, and S. I. Rogers (2007), Human activities in UK offshore waters: an assessment of direct, physical pressure on the seabed, *ICES J. Mar. Sci. J. Cons.*, *64*(3), 453–463, doi:10.1093/icesjms/fsm001.

Esmaeili, M., and A. Ivanović (2014), Numerical modelling of bottom trawling ground gear element on the seabed, *Ocean Eng.*, *91*, 316–328, doi:10.1016/j.oceaneng.2014.08.014.

Falcini, F., M. Marini, S. Milli, and M. Moscatelli (2009), An inverse problem to infer paleoflow conditions from turbidites, *J. Geophys. Res. Oceans*, *114*(C10), C10019, doi:10.1029/2009JC005294.

Ferré, B., X. Durrieu de Madron, C. Estournel, C. Ulses, and G. Le Corre (2008), Impact of natural (waves and currents) and anthropogenic (trawl) resuspension on the export of particulate matter to the open ocean: Application to the Gulf of Lion (NW Mediterranean), *Cont. Shelf Res.*, *28*(15), 2071–2091, doi:10.1016/j.csr.2008.02.002.

Garcia, M., and G. Parker (1991), Entrainment of Bed Sediment into Suspension, *J. Hydraul. Eng.-Asce*, *117*(4), 414–435, doi:10.1061/(ASCE)0733-9429(1991)117:4(414).

Garcia, M., and G. Parker (1993), Experiments on the Entrainment of Sediment into Suspension by a Dense Bottom Current, *J. Geophys. Res.-Oceans*, *98*(C3), 4793–4807, doi:10.1029/92JC02404.

Haedrich, R. L., N. R. Merrett, and N. R. O'Dea (2001), Can ecological knowledge catch up with deep-water fishing? a North Atlantic perspective, *Fish. Res.*, *51*(2–3), 113–122, doi:10.1016/S0165-7836(01)00239-9.

He, P., and P. D. Winger (2010), Effect of Trawling on the Seabed and Mitigation Measures to Reduce Impact, in *Behavior of Marine Fishes*, edited by P. He, pp. 295–314, Wiley-Blackwell.

Ivanović, A., R. D. Neilson, and F. G. O'Neill (2011), Modelling the physical impact of trawl components on the seabed and comparison with sea trials, *Ocean Eng.*, *38*(7), 925–933, doi:10.1016/j.oceaneng.2010.09.011.

Jacinto, R. S., and D. Burel (2003), Modélisation du devenir à court terme des boues de dragage rejetées par clapage, *Rev. Fr. Génie Civ.*, *7*(9), 1151–1166, doi:10.1080/12795119.2003.9692539.

Jaffe, B., M. Buckley, B. Richmond, L. Strotz, S. Etienne, K. Clark, S. Watt, G. Gelfenbaum, and J. Goff (2011), Flow speed estimated by inverse modeling of sandy sediment deposited by the 29 September 2009 tsunami near Satitoa, east Upolu, Samoa, *Earth-Sci. Rev.*, *107*(1–2), 23–37, doi:10.1016/j.earscirev.2011.03.009.

Jaffe, B. E., and G. Gelfenbuam (2007), A simple model for calculating tsunami flow speed from tsunami deposits, *Sediment. Geol.*, *200*(3–4), 347–361, doi:10.1016/j.sedgeo.2007.01.013.

Jones, J. (1992), Environmental-Impact of Trawling on the Seabed - a Review, *N. Z. J. Mar. Freshw. Res.*, *26*(1), 59–67.

Jordi, A., A. Orfila, G. Basterretxea, and J. Tintoré (2005), Shelf-slope exchanges by frontal variability in a steep submarine canyon, *Prog. Oceanogr.*, *66*(2–4), 120–141, doi:10.1016/j.pocean.2004.07.009.

Kneller, B., and C. Buckee (2000), The structure and fluid mechanics of turbidity currents: a review of some recent studies and their geological implications, *Sedimentology*, *47*, 62–94, doi:10.1046/j.1365-3091.2000.047s1062.x.

Lastras, G. et al. (2011), Understanding sediment dynamics of two large submarine valleys from seafloor data: Blanes and La Fonera canyons, northwestern Mediterranean Sea, *Mar. Geol.*, *280*(1–4), 20–39, doi:10.1016/j.margeo.2010.11.005.

Lesshafft, L., E. Meiburg, B. Kneller, and A. Marsden (2011), Towards inverse modeling of turbidity currents: The inverse lock-exchange problem, *Comput. Geosci.*, *37*(4), 521–529, doi:10.1016/j.cageo.2010.09.015.

Martín, J., A. Palanques, and P. Puig (2006), Composition and variability of downward particulate matter fluxes in the Palamós submarine canyon (NW Mediterranean), *J. Mar. Syst.*, *60*(1–2), 75–97, doi:10.1016/j.jmarsys.2005.09.010.

Martín, J., A. Palanques, and P. Puig (2007), Near-bottom horizontal transfer of particulate matter in the Palamós Submarine Canyon (NW Mediterranean), *J. Mar. Res.*, *65*(2), 193–218.

Martín, J., P. Puig, A. Palanques, P. Masqué, and J. García-Orellana (2008), Effect of commercial trawling on the deep sedimentation in a Mediterranean submarine canyon, *Mar. Geol.*, *252*(3–4), 150–155, doi:10.1016/j.margeo.2008.03.012.

Martín, J., P. Puig, A. Palanques, and A. Giamportone (2014a), Commercial bottom trawling as a driver of sediment dynamics and deep seascape evolution in the Anthropocene, *Anthropocene*, *7*, 1–15, doi:10.1016/j.ancene.2015.01.002.

Martín, J., P. Puig, A. Palanques, and M. Ribó (2014b), Trawling-induced daily sediment resuspension in the flank of a Mediterranean submarine canyon, *Deep Sea Res. Part II Top. Stud. Oceanogr.*, *104*, 174–183, doi:10.1016/j.dsr2.2013.05.036.

Martín, J., P. Puig, P. Masqué, A. Palanques, and A. Sánchez-Gómez (2014c), Impact of Bottom Trawling on Deep-Sea Sediment Properties along the Flanks of a Submarine Canyon, *PLoS ONE*, *9*(8), e104536, doi:10.1371/journal.pone.0104536.

Middleton, G. V., and M. A. Hampton (1973), Part I. Sediment Gravity Flows: Mechanics of Flow and Deposition, , 1–38.

Millot, C. (1999), Circulation in the Western Mediterranean Sea, *J. Mar. Syst.*, *20*(1–4), 423–442, doi:10.1016/S0924-7963(98)00078-5.

Molenaar, E., and M. Tsamenyi (2000), *Satellite-based Vessel Monitoring Systems. International legal aspects and developments in state practice*, FAO United Nations.

Morato, T., R. Watson, T. J. Pitcher, and D. Pauly (2006), Fishing down the deep, *Fish Fish.*, *7*(1), 24–34, doi:10.1111/j.1467-2979.2006.00205.x.

O'Neill, F. G., and K. Summerbell (2011), The mobilisation of sediment by demersal otter trawls, *Mar. Pollut. Bull.*, *62*(5), 1088–1097, doi:10.1016/j.marpolbul.2011.01.038.

O'Neill, F. G., S. M. Simmons, D. R. Parsons, J. L. Best, P. J. Copland, F. Armstrong, M. Breen, and K. Summerbell (2013), Monitoring the generation and evolution of the sediment plume behind towed fishing gears using a multibeam echosounder, *ICES J. Mar. Sci. J. Cons.*, *70*(4), 892–903, doi:10.1093/icesjms/fst051.

Palanques, A., J. Guillén, and P. Puig (2001), Impact of bottom trawling on water turbidity and muddy sediment of an unfished continental shelf, *Limnol. Oceanogr.*, *46*(5), 1100–1110, doi:10.4319/lo.2001.46.5.1100.

Palanques, A. et al. (2005), General patterns of circulation, sediment fluxes and ecology of the Palamós (La Fonera) submarine canyon, northwestern Mediterranean, *Prog. Oceanogr.*, *66*(2–4), 89–119, doi:10.1016/j.pocean.2004.07.016.

Palanques, A., J. Martín, P. Puig, J. Guillén, J. B. Company, and F. Sardà (2006), Evidence of sediment gravity flows induced by trawling in the Palamós (Fonera) submarine canyon (northwestern Mediterranean), *Deep Sea Res. Part Oceanogr. Res. Pap.*, *53*(2), 201–214, doi:10.1016/j.dsr.2005.10.003.

Parker, G., Y. Fukushima, and H. M. Pantin (1986), Self-accelerating turbidity currents, *J. Fluid Mech.*, *171*, 145–181, doi:10.1017/S0022112086001404.

Parker, G., M. Garcia, Y. Fukushima, and W. Yu (1987), Experiments on turbidity currents over an erodible bed, *J. Hydraul. Res.*, *25*(1), 123–147, doi:10.1080/00221688709499292.

Prat, J., J. Antonijuan, A. Folch, A. Sala, A. Lucchetti, F. Sardà, and A. Manuel (2008), A simplified model of the interaction of the trawl warps, the otterboards and netting drag, *Fish. Res.*, *94*(1), 109–117, doi:10.1016/j.fishres.2008.07.007.

Puig, P., M. Canals, J. B. Company, J. Martín, D. Amblas, G. Lastras, A. Palanques, and A. M. Calafat (2012), Ploughing the deep sea floor, *Nature*, *489*(7415), 286–289, doi:10.1038/nature11410.

Puig, P., J. Martín, P. Masqué, and A. Palanques (2015), Increasing sediment accumulation rates in La Fonera (Palamós) submarine canyon axis and their relationship with bottom trawling activities, *Geophys. Res. Lett.*, *42*(19), 2015GL065052, doi:10.1002/2015GL065052.

Pusceddu, A., S. Bianchelli, J. Martín, P. Puig, A. Palanques, P. Masqué, and R. Danovaro (2014), Chronic and intensive bottom trawling impairs deep-sea biodiversity and ecosystem functioning, *Proc. Natl. Acad. Sci.*, 201405454, doi:10.1073/pnas.1405454111.

Ribó, M., P. Puig, A. Palanques, and C. Lo Iacono (2011), Dense shelf water cascades in the Cap de Creus and Palamós submarine canyons during winters 2007 and 2008, *Mar. Geol.*, *284*(1–4), 175–188, doi:10.1016/j.margeo.2011.04.001.

Roe, P. L. (1981), Approximate Riemann solvers, parameter vectors, and difference schemes, *J. Comput. Phys.*, *43*(2), 357–372, doi:10.1016/0021-9991(81)90128-5.

Sanchez-Vidal, A., et al. (2012), Impacts on the deep-sea ecosystem by a severe coastal storm, *PLOS ONE*, 7 (1), e30395, doi: 10.1371/journal.pone.0030395.

Sumaila, U. R., L. Teh, R. Watson, P. Tyedmers, and D. Pauly (2008), Fuel price increase, subsidies, overcapacity, and resource sustainability, *ICES J. Mar. Sci. J. Cons.*, *65*(6), 832–840, doi:10.1093/icesjms/fsn070.

Sumaila, U. R., A. Khan, L. Teh, R. Watson, P. Tyedmers, and D. Pauly (2010), Subsidies to high seas bottom trawl fleets and the sustainability of deep-sea demersal fish stocks, *Mar. Policy*, *34*(3), 495–497, doi:10.1016/j.marpol.2009.10.004.

Ulses, C., C. Estournel, P. Puig, X. Durrieu de Madron, and P. Marsaleix (2008), Dense shelf water cascading in the northwestern Mediterranean during the cold winter 2005: Quantification of the export through the Gulf of Lion and the Catalan margin, *Geophys. Res. Lett.*, *35*(7), n/a–n/a, doi:10.1029/2008GL033257.

Whittle, P. (1951), *Hypothesis testing in time series analysis.*, Almqvist & Wiksells boktr., Uppsala.

WRI (2001), *World Resources 2000-2001 | World Resources Institute*, World Resources Institute.

Zanke, U. (1977), *Berechnung der Sinkgeschindigkeiten von Sedimenten*, Mitt. des Franzius- Instituts für Wasserbau, Heft46, Seite 243, Technical University, Hannover, West Deutschland.

Supplementary information

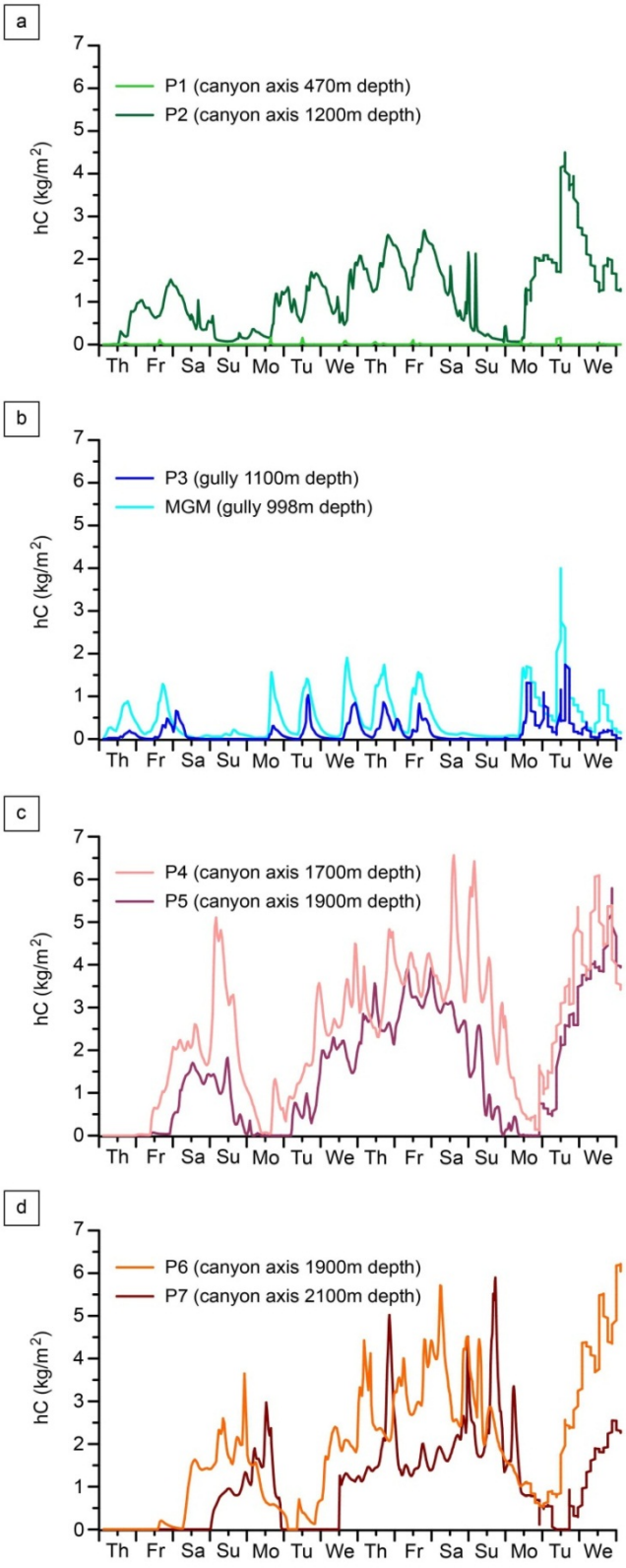

Supplementary Fig. 3.S1 Modeled sediment transport at different locations along the canyon axis and northern canyon flank gullies of La Fonera submarine canyon for the two-week period analyzed. The numerical model is forced with the resuspension time series Rs(t) obtained through the inverse model under the ARMA approach that triggers turbidity currents reaching MGM of the same order of magnitude than those measured at MGM for the period 9th to 21th June 2011. The results are presented in terms of instantaneous sediment transport (hC)

Influence of Coriolis forces on the TC evolution and sedimentation pattern

Coriolis forces are important when temporal and spatial scales of the flow are similar to those of the Earth rotation (See Chapter 2). This can be the case for TC with a duration of at least the same order of magnitude that the inertial period $T_{in} = 2\pi/f$ (see Chapter 2). In the case of La Fonera (i.e. at 41.5°N, then $f = 9.7057 \cdot 10^{-5}$), a current lasting ~18h would suffer Coriolis forces. As such, the turbidity current at the gully mooring site would not be *a priori* deflected by Coriolis forces, since the flow at this point lasts less than 18h. However, at more distal parts along the canyon axis and along the northern continental shelf the flow duration is superior to the inertial period, and hence it can be potentially deflected to the right by Coriolis forces. The scale at which Coriolis forces become important is expressed by the Rossby number $= U/(fL)$, where U is the depth integrated velocity, f the Coriolis parameter and L the length scale. Coriolis forces will dominate the TC when $Ro < 1$ (Nof, 1996). La Fonera submarine canyon sedimentary system extends for about 110km of which the canyon head occupies 28km (Lastras et al., 2011), as such, Coriolis forces would influence the trajectory of the TC for U<10.68m/s. For slower currents the length scale at which Coriolis forces become important will be smaller. When the flow is confined between the channel walls and in the gullys the transversal spatial scale (i.e. the width) might also play a role. If we consider that the threshold $Ro_w < 10$, with $Ro_w = U/(fW)$ (Cossu et al., 2015, 2010; Cossu and Wells, 2013), we can determinate whether or not Coriolis forces are at play. Hence in the case of the La Fonera with widths ranging between 400m and 1200m for the canyon floor along the canyon axis, velocity should be inferior to 0.39m/s and 1.16m/s respectively so that Coriolis forces were at play. Possible Rossby numbers are shown in Sup. Table 3.1 for different velocities. Considering the values of current speed of the TC triggered by trawling, Coriolis effects seem to have a minor influence in the mooring point whilst on the distal parts of the system and along the continental slope they may have a non-negligible influence.

Sup. Table 3. 1 Estimated Rossby numbers for La Fonera with f=2Ωsinφ ~1.0008×10^{-4} rads^{-1} at latitude 43.5N. Italic numbers indicate those combinations where Coriolis forces are at play. Spatial scales were retrieved from Lastras et al., (2011) and Canals et al., (2013),

	Spatial scale (m) Length (L)	Velocity U(m/s) 0.05	0.1	0.25	0.5
		$Ro = U/(fL)$			
System	110000	*0.005*	*0.009*	*0.023*	*0.047*
Canyon head	28000	*0.018*	*0.037*	*0.092*	*0.184*
Canyon – continental rise	70000	*0.007*	*0.015*	*0.039*	*0.074*
Gully	2000	*0.256*	*0.515*	1.288	2.586
	Spatial scale (m) Width (W)	Velocity U(m/s) 0.05	0.1	0.25	0.5
		$Ro_w = U/(fW)$			
Canyon floor at axis 1000m depth	500	*1.030*	*2.060*	*5.152*	*10.303*
Canyon floor at axis 1500m depth	400	*1.289*	*2.576*	*6.440*	*12.879*
Canyon floor at axis 2000m depth	1200	*0.429*	*0.858*	*2.146*	*4.293*
Gully	<200	*2.576*	*5.152*	12.879	25.758

Chapter 4:

HYPERPYCNAL FLOWS IN THE VAR TURBIDITE SYSTEM (NW MEDITERRANEAN SEA)

ABSTRACT

The Var Turbidite System, located in the French Riviera in the vicinity of Nice (northwest Mediterranean Sea), has been studied for over fifty years mainly on the basis of seismic profiles and cores. Two main triggering mechanisms of gravity flows have been identified in the canyon: those related to landslides and slope failures (e.g. Nice airport collapse) and those initiated by river floods of the Var River. The present study focuses on the second type of flows where the response of the Var system in terms of transport and deposition to the climatic variations during the Late Pleistocene-Holocene (50kyrs) is evaluated. The results of the implemented numerical modelling performed well in terms of intensity of the turbidity currents and associated deposition for the different analysed climatic periods. Larger magnitude currents and deposition was observed during the cold and arid periods of the stadials while lower magnitude flows and deposition was predicted during the warm and humid periods of the interstadials. However, although the numerical results at the core positions follow the observed trends in terms of sedimentary records, the differences between the considered periods are not as accentuated as those of the sedimentary records. The main reason for this might be the lack of accuracy of the initial conditions imposed at the river mouth. Moreover, the influence of Coriolis effects, usually neglected when studying and modelling turbidity currents, are explored and prove to be a key factor in the development of the Var Sedimentary Ridge.

RESUME

Le système turbiditique du Var, situé sur la Côte d'Azur à proximité de Nice (Méditerranée nord-occidentale) a fait l'objet de nombreuses études stratigraphiques basées sur des profils sismiques et des carottes sédimentaires. Deux mécanismes principaux à l'origine d'écoulements gravitaires ont été identifiés dans ce canyon : les glissements sous-marins et la déstabilisation des pentes (e.g. glissement de l'aéroport de Nice) et les courants hyperpycnaux liés aux crues du Var. Cette étude s'intéresse au deuxième type d'écoulement, ainsi l'activité turbiditique du Var, y compris le transport sédimentaire et les dépôts associés, au cours des différentes périodes climatiques du Pleistocene-Holocene (50ka) est évaluée. Les résultats du modèle en termes d'intensité de courant et de dépôt associé suivent la tendance enregistrée dans les sédiments. En effet, ces résultats montrent qu'au cours des stades froids et secs les courants et dépôts sont assez développés alors que pendant les interstades chauds et humides ils sont restreints. Bien que les résultats obtenus suivent la tendance observée à partir des carottes sédimentaires, la différence entre les 2 périodes climatiques étudiées n'est pas aussi marquée que l'enregistrement sédimentaire. Ceci doit être lié aux incertitudes sur les conditions initiales imposées à l'embouchure du Var. L'influence des forces de Coriolis que ne sont généralement pas prises en compte dans la plupart des études et modélisations de courants de turbidité, est mise en évidence dans ce travail. Ce chapitre montre ainsi le rôle majeur que les forces de Coriolis jouent dans la construction de la Ride Sédimentaire du Var.

1. Introduction

The Var Turbidite System is located in the French Riviera near to the city of Nice (northwest Mediterranean Sea). The system has been studied for over fifty years (Bourcart, 1962; Gennesseaux, 1962), the interest on the system was enhanced after the catastrophic submarine slide off Nice airport (Gennesseaux et al., 1980). Seismic profiles and cores have provided new data that has improved the understanding of the Var system and have specially focused on the construction of the Var Sedimentary Ridge (hereafter VSR), an asymmetric and hyper-developed levee on the right hand side (e.g. Savoye and Piper, 1991; Piper and Savoye, 1993; Savoye et al., 1993; Migeon, 2000; Migeon et al., 2001, 2006). Since then, works have focused on the two main triggering mechanisms of gravity flows in the canyon: those related to landslides and slope failures (e.g. Nice airport collapse) and those initiated by river floods. The analysis of sediment cores has evidenced the relationship between climatic changes on the drainage basin and sediment deposition on the sedimentary Var Ridge (Jorry et al., 2011; Bonneau et al., 2014). The present chapter focuses on the latter type of flows. To date, the dynamics of sediment transport and deposition have mainly been explored through the interpretation of turbidite deposits. Recent studies (Khripounoff et al., 2009, 2012; Mas et al., 2010) have shown that hyperpycnal flows are triggered in the Var Canyon with a frequency of up to 2.5 times per year. The response of the Var system in terms of transport and deposition to the climatic variations during the Late Pleistocene-Holocene (50 kyrs) is evaluated numerically as well as the influence of the Coriolis forces that are usually neglected when modelling and studying turbidite systems. The results of the implemented numerical modelling are compared to sediment cores recovered from the area.

2. Regional setting

2.1. Geological setting

The Var Turbidite system is located in the Northwest Mediterranean Sea and extends seaward off Nice (SE France) from the Var delta to the continental slope of Corsica at depths of 2700m (Fig. 4.1). The system covers approximately 16200 km^2 on the flat-floor basin developed during the Messinian Salinity crisis (Savoye et al., 1993). During the Messinian Salinity crisis, the Var paleo-canyon was cut in the slope (Savoye and Piper, 1991) and the Var deep sea fan began to form. The system continued its development during the Pliocene and Quaternary due to the progradation of the Var delta (Savoye et al., 1993). The continental slope is very steep with gradient values of up to 20-30° and average values of 13° (Mulder et al., 1994). The system is connected to the Var and the Paillon rivers by two deeply incised canyons, the Var and the Paillon canyons. The Var River is the main contributor to the Var turbidite system (Migeon et al., 2012) and the Paillon River is only a minor source of sediment (Klaucke et al., 2000). The nearby continental shelf is very narrow (2-3km) and even absent in the vicinity of the Var River mouth, this results in the direct connection between the river mouth and the deep basin during both highstand and lowstand conditions (Savoye et al., 1993). This effective connection explains the lack of sedimentation on the continental shelf and the high sedimentation rates recorded in the basin and in the VSR (Piper and Savoye, 1993).

The Var canyon extends along 25km from the Var river mouth to 1600m depth with a decreasing slope gradient from 11% to 4% and an increasing width from 300m to 1250m. The upper fan valley extends southeast for 12km from the confluence of the Var and Paillon canyons at 1650m down to water depths of 2000m at the base of the continental slope. The middle valley widens for 50km down to water depths of 2500m and showing a decreasing bottom slope of 2 to 0.3%. The middle valley is bounded by a small discontinuous levee on the northern side (left hand side); whilst the

southern side (right hand side) is limited by a well-developed levee (i.e. Var Sedimentary Ridge). The lower valley extends, from the southeast bend due to the Diapir wall, for 100km with a slope decreasing from 0.3% to 0.1% and feeds a sandy distal lobe at a water depth of 2700m (Piper and Savoye, 1993; Savoye et al., 1993).

The VSR is the distinct feature of the Var Turbidite System and it is the focus of the present study. It extends along the southern margin of the middle valley. Its cross section is highly asymmetrical with a steep and narrow northern flank and a flat and wide southern flank. The elevation of the Ridge decreases eastward (i.e. downcanyon) from about 400m to less than 30m, as such the boundary Ridge-valley is gradual in the eastern part whereas in the upstream part the levee shows steep walls (Migeon et al., 2000). In order to overflow the VSR currents must reach a thickness ranging between 300m and 30m depending on the part of the VSR (Migeon et al., 2012). The Ridge deposits are formed of sandy to muddy turbidites (Migeon et al., 2000; Jorry et al., 2011; Bonneau et al., 2014). At the western end of the Var Sedimentary Ridge a channel (i.e. Western Spillover Channel, hereafter WSC) leads to the south from a breach only a 200 m above the valley floor (Piper and Savoye, 1993).

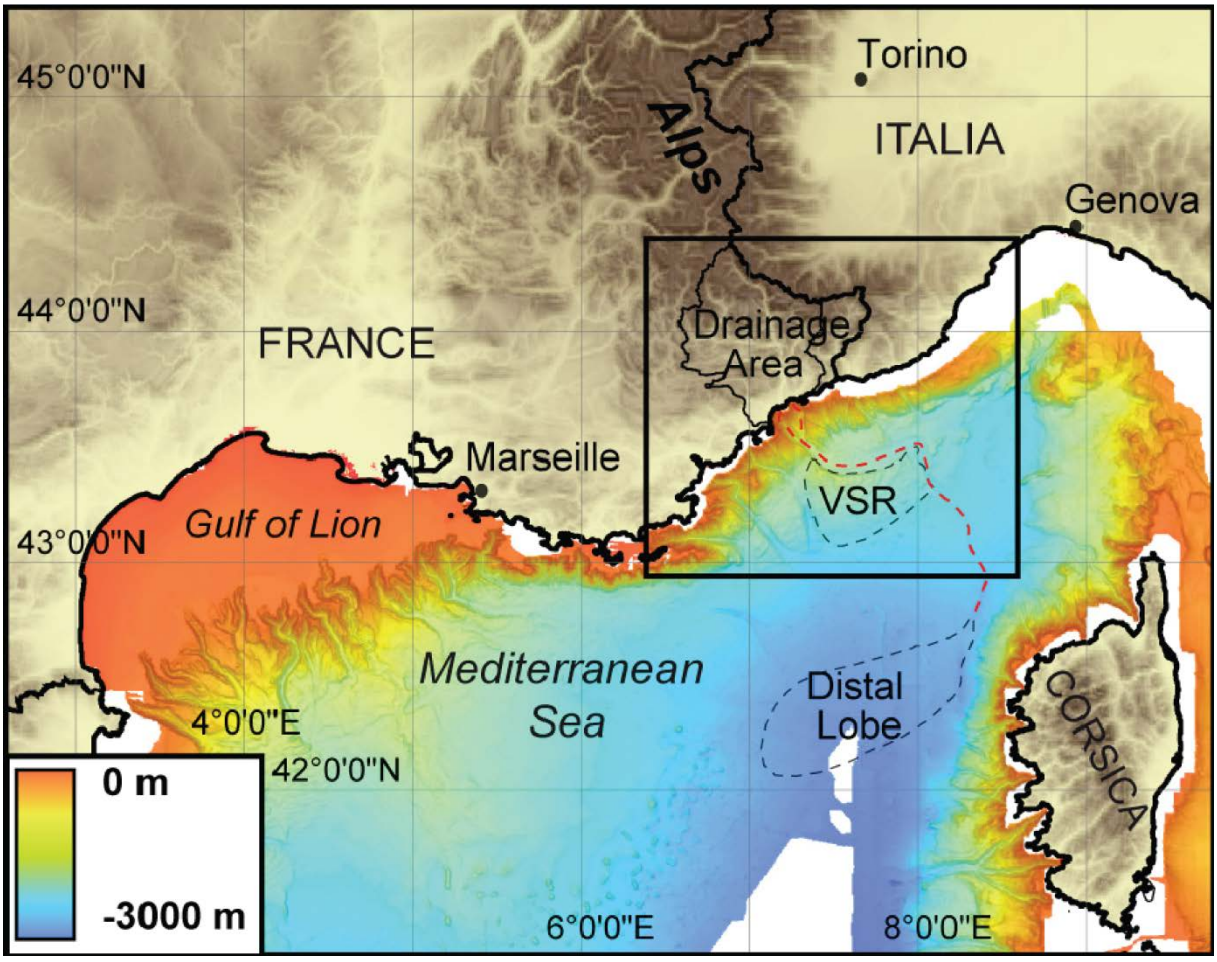

FIG. 4. 1 LOCATION OF THE VAR TURBIDITE SYSTEM IN THE NORTH-WESTERN MEDITERRANEAN SEA (FROM BONNEAU ET AL. (2014))

2.2.Hydrography-hydrological setting

The main contributor of the Var Turbidite System, the Var river, extends from the upper reaches of the Southern French Alps (up to 3000m) to Nice along 120km. The drainage area covers a surface of 2800km^2 and presents a steep slope (23°). The lithology of the drainage area is formed by igneous and metamorphic rocks in the upstream areas whilst the downstream part of the basin is formed by carbonate rocks (Bonneau et al., 2014). At present, the Var River presents a seasonal and torrential (bimodal distribution) regime discharge typical of the Mediterranean area with floods related to snow melting in spring and storms in autumn (Sage, 1976). The annual sediment discharge has been

estimated between 1.3 and 1.6 million t/yr and can be even higher if discharges after a long dry period are taken into account (Mulder et al., 1997a, 1998). High sediment discharge is mostly associated with flash floods that can increase the river liquid discharge from 20 m^3/s to 800m^3/s within hours (Dubar and Anthony, 1995). The average annual water discharge has been calculated in about 53m^3/s from collected data between 1968 and 1994 (Mulder et al., 1997a). Although exceptional floods can reach up to hundred times the mean annual liquid discharge, that is the case of the catastrophic flood of September 1994 (200 yr flood) with a peak discharge of 3770m^3/s (Mulder et al., 1997a, 1998). Due to the landfill for Nice Airport, land was reclaimed in the Var River mouth, and as such its width was reduced from 1 km to 350 m and its orientation was modified from NNW-SSE to NE-SW (Kelner et al., 2016).

2.3.Sediment supply

The Var canyon has been continuously active since the late Pleistocene (Piper and Savoye, 1993). The interpretation of the turbidite facies deposited along the canyon and on the Var sedimentary Ridge and field data from instrumented moorings indicate that 3 major triggering mechanisms are at play: 1) small size retroregressive shallow failures on recently deposited sediment on the upper steep slope, 2) large slope instabilities that evolve into surge-type currents (e.g Nice airport collapse 1979) and 3) hyperpycnal flows due to river floods (Piper and Savoye, 1993; Savoye et al., 1993; Mulder et al., 1997a; Dan et al., 2007; Khripounoff et al., 2009, 2012; Mas et al., 2010; Migeon et al., 2012;).

Flows that could produce a deposit thick and wide enough to be preserved in the sedimentary record of the Var sedimentary ridge correspond to the large slope instabilities and to hyperpycnal flows due to high magnitude floods since recent monitoring in the Var Canyon and the valley revealed that low magnitude hyperpycnal flows and small slide induced turbidity currents die in the canyon and upper valley (Khripounoff et al., 2009, 2012). The 1979 Nice airport collapse is considered representative of large Holocene events in the Var sedimentary system (Mulder et al., 1998). Traces of the turbidity current due to the 1979 event have been found in a terrace in the middle valley (Mulder et al., 2001b); however, the turbidity current did not overtop the VSR (Gennesseaux et al., 1980; Piper and Savoye, 1993; Mulder et al., 1997b).

Recent studies have analysed the link between inland climate changes and turbidite deposits due to hyperpycnal flows (Mulder et al., 2001b; Jorry et al., 2011; Bonneau et al., 2014;). Since the river-canyon connection is kept for high stands and low stands and the continental slope is very steep, the changes in sedimentation rates in the system seem controlled by variations in sediment supply and not by sea level changes (Piper and Savoye, 1993; Savoye et al., 1993). The preserved turbidity activity on the VSR seems to reflect changes in the magnitude of hyperpycnal flows (i.e. variations in the suspended sediment concentration during river flows) related to climatic variations inland (Bonneau et al., 2014). Turbidite frequency in the VSR shows strong correlation with the climatic variations at centennial-to millennial timescales (Jorry et al., 2011; Bonneau et al., 2014). The Pleistocene turbidite beds are associated with slow and thick currents, that can overflow the VSR, with a duration of days to weeks (Bonneau et al., 2014) and hence could be induced by floods in the Var River (i.e. hyperpycnal currents) (Piper and Savoye, 1993; Mulder et al., 2001a). As such, it was concluded that the variations in the frequency of overflows can reflect changes in the magnitude of the hyperpycnal flows and hence climatic variations inland (Bonneau et al., 2014) since the latter contains information about the prevailing climate conditions in the drainage area. Temporal changes in turbite deposits are recorded in the VSR; the turbidite deposition frequency seems to respond to the cycles of Dansgard Oeschgerd (hereafter D/O) following the pattern high activity/stadial and low activity/interstadial and also showing the highest activity during maximum glacial conditions and quickly decreasing during the last glacial-interglacial conditions (Fig. 4.2) (Bonneau et al., 2014).

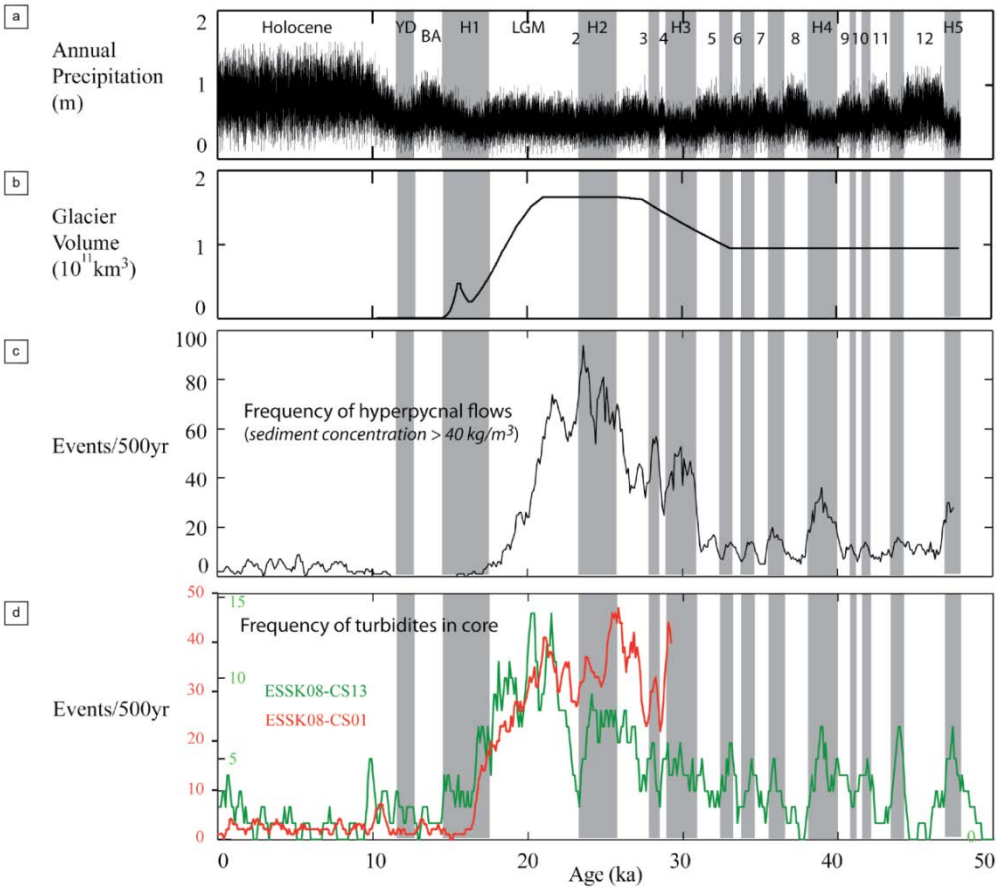

FIG. 4. 2 COMPARISON BETWEEN THE SIMULATED HYPERPYCNAL ACTIVITY (THRESHOLD FOR HYPERPYCNAL FLOWS 40KG/M^3) AND THE ACTIVITY OBSERVED IN THE CORES ESSK08-CS01 (DISTAL PART OF THE VAR SEDIMENTARY RIDGE) AND ESSK08-CS13 (SOUTHERN FLANK OF THE VAR SEDIMENTARY RIDGE). A) ANNUAL PRECIPITATION INPUT FOR HYDROTREND MODEL B) GLACIER VOLUME (INPUT FOR HYDROTREND MODEL). C) HYPERPYCNAL ACTIVITY OF THE VAR RIVER SIMULATED BY HYDROTREND. THE CONCENTRATION THRESHOLD HYPERPYCNAL FLOWS IS 40KG/M3. D) FREQUENCY OF TURBIDITES FOUND IN CORES. THE DIFFERENT CLIMATIC PERIODS ARE ALSO INDICATED: HOLOCENE, YOUNGER DRYAS (YD), BØLLING-ALLERØD (BA), LAST MAXIMUM GLACIATION (LGM), HEINRICH STADIAL (H), THE NUMBERS 1 TO 12 INDICATE THE INTERSTADIALS OF THE DANSGAARD-OESCHGER CYCLES. THE GREY BANDS INDICATE THE COLD STADIALS (HEINRICH STADIALS AND STADIALS OF THE DANSGAARD-OESCHGER CYCLES) AFTER (BONNEAU (2014).

Climatic variations have been shown to control sedimentary inputs and turbidity activity (Nakajima and Itaki, 2007; Covault et al., 2010). In the Var system climatic changes modify sediment supply in two ways: the availability of glacier derived sediment and the changes in erosion due to shifts in vegetation due to D/O cycles (Bonneau et al., 2014). The decrease in turbidite activity during the last Glaciar-Interglaciar period could be due to the retreat of glaciers and the lack of glacier derived sediment, in fact the high activity during the Pleistocene had already been related to high magnitude (i.e. high sediment load) hyperpycnal flows due to snow melting (Piper and Savoye, 1993). The D/O cycles induce changes in vegetation. During the warmer and wetter interstadials of the D/O cycles the vegetation cover is primarily forest, hence the catchment is less prone to erosion and, despite the flood liquid discharge being increased, the hyperpycnal activity is lower. On the other hand, during the cold and arid interstadials of the D/O cycles, the catchment is covered by steppe, and increased erosion along the hillslope leads to higher hyperpycnal activity (Bonneau, 2014). In the studies relating climatic changes inland to turbidite frequency in the marine record no distinction was made between hyperpycnites and “classic Bouma type turbidites” (Jorry et al., 2011; Bonneau et al., 2014). In fact, according to Migeon et al. (2012) only about 6% of the deposits in the VSR fit in the definition of hyperpycnite. Hyperpycnites are turbidite deposits due to hyperpycnal flows that present an inverse grading, climbing ripples and alocthonus fauna (Mulder and Alexander, 2001; Mulder et al., 2001a, 2003;).

Hyperpycnal flows are turbidity currents generated by the direct plunging of a dense sediment flow during floods (Mulder et al., 2001a). In theory, in the climatic setting (i.e. salinity and temperature) of the Var a sediment concentration of 42.5 kg/m^3 is needed so that a river flood triggers a hyperpycnal flow (Mulder et al., 2003). This value corresponds in present day conditions to a liquid discharge of 1250m^3/s (Mulder et al., 1997a). However, the instability processes at the river mouth are not completely understood and reconcentration processes, convective sedimentation and deposition from hypopycnal plume (Fig. 4.3)(Maxworthy, 1999) can reduce this critical threshold to as low as 5kg/m^3 (Parsons et al., 2001). In the Var this corresponds to about 300m^3/s that are reached 2.5 times per year (Mas, 2009; Bonneau, 2014). In fact weak hyperpycnal flows have been observed in the Var Canyon concomitant with flash floods of the Var River with a similar frequency per year (Mas, 2009; Khripounoff et al., 2009, 2012). In the following, we consider conservation of sediment mass and liquid discharge between the river flood and the turbidity current. As such, at the source point, the current sediment concentration and liquid discharge are those of the river discharge, meaning that the whole sedimentary charge and fluid plunge.

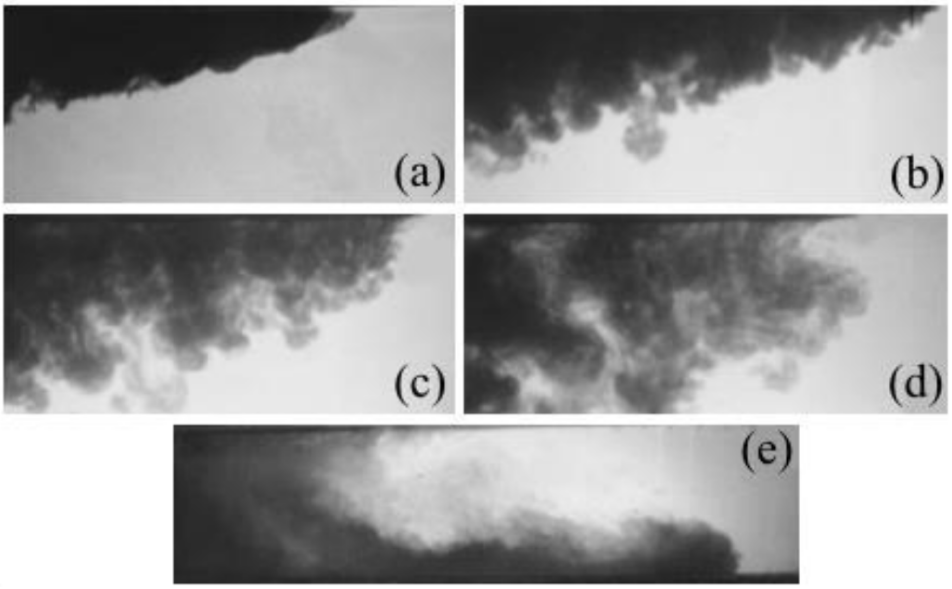

FIG. 4. 3 PHOTOGRAPHS OF THE TIME EVOLUTION OF AN EXPERIMENTAL SEDIMENTING CURRENT (G'=37.3). THE RECONCENTRATION AND SEDIMENTATION PROCESSES FROM A HYPOPYCNAL CURRENT (A) PROMOTE THE DEVELOPMENT OF A BOTTOM CURRENT (E). (MODIFIED FROM MAXWORTHY, 1999)

The capacity of a river to generate a hyperpycnal flow depends on the density contrast between the river and the seawater and hence it depends on the relationship between suspended sediment concentration and river discharge. Data on sediment concentration at the Var river mouth is scarce. Power laws for the Var based on field data have been proposed (Laurent, 1971; Mulder et al., 1997a) as well as on the basis of catchment modelling (Bonneau, 2014). The relationship between sediment concentration and river discharge have been shown to be highly dependent on climatic conditions (Mulder and Syvitski, 1995; Mulder et al., 1997a, 2001a, 2003). Hyperpycnal flows tend to mimic the dynamics of the river system they are associated to (Mulder et al., 2003). However, recent studies have shown that a single flood peak can generate a flow with multiple pulses (Khripounoff et al., 2012; Liu et al., 2012). Also fresh water organic matter that is used as a proxy for hyperpycnal deposits can be related to the failure of recently deposited flood sediment (Talling, 2014). As such, deposits that do not correspond to the theoretical definition of hyperpycnites might be the product of hyperpycnal flows.

2.4.Coriolis effects

Due to the low velocities of hyperpycnal flows and the size of the Var Sedimentary System, Coriolis forces may play an important role in the evolution of TC and in the final deposition pattern. Coriolis

forces influence has long been acknowledged in turbidity currents deposits but it is often neglected when studying and modelling turbidity currents. Piper and Savoye (1993) speculated about the potential role of centrifugal and Coriolis forces in the development of the VSR; however, this possibility has not been further explored. The influence of Coriolis becomes important when the spatial and temporal scales of Earth's rotation and of the flow are similar. As such, continuous and "slow" flows such as hyperpycnal flows in a system as large as the Var could potentially be driven at least partially by Coriolis forces.

3. Data & methods

3.1. Hydrology data

Sediment concentration data is scarce, as such, relationships solid charge-liquid discharge have been proposed for the Var following the classic power expression proposed by (Leopold and Maddock Jr, 1953).

$$C_s = a\,Q^b \qquad (4.1)$$

Where a and b are fitting coefficients for a given river and $C_s(kg/m^3)$ and $Q(m^3/s)$ are respectively the sediment concentration and the liquid discharge. This type of relationship is available for the Var River from present day measurements (instant values) (Laurent, 1971; Mulder et al., 1997a) and also for different climate periods from numerical modelling results from Hydrotrend (mean daily values, shown in Fig. 4.4)(Bonneau, 2014). Concentration values are underestimated by a 30-50% during flash floods when mean daily values are used since the peak of the discharge is smoothed (Mulder et al., 1997a); in order to cope with this underestimation the law proposed by Bonneau (2014) for present day conditions is increased by a 1.5 factor (i.e. the constant a is increased by a 1.5 factor, this simulated is named "Bonneau2"). The parameters a and b for the power laws are summarized in Table 4.1.

TABLE 4. 1 POWER LAWS RELATING SEDIMENT CONCENTRATION (KG/M3) AND LIQUID DISCHARGE AT THE RIVER MOUTH OF THE VAR FOR THE DIFFERENT PERIODS ANALYSED.

Age	Reference	a	b
Modern	Laurent (1971), Mulder et al. (1997a)	$7.67 \cdot 10^{-4}$	1.534
Modern	Mulder et al. (1997a)	$7.67 \cdot 10^{-4}$	1.700
Modern	Bonneau (2014)	0.0102	0.916
Modern	Bonneau (2014)-Present study (Bonneau2)	1.5x0.0102	0.916
LGM	Bonneau (2014)	0.0397	1.006
InterStadial 8	Bonneau (2014)	0.0227	0.954
Stadial 8	Bonneau (2014)	0.0271	1.019
HS4	Bonneau (2014)	0.0356	1.038

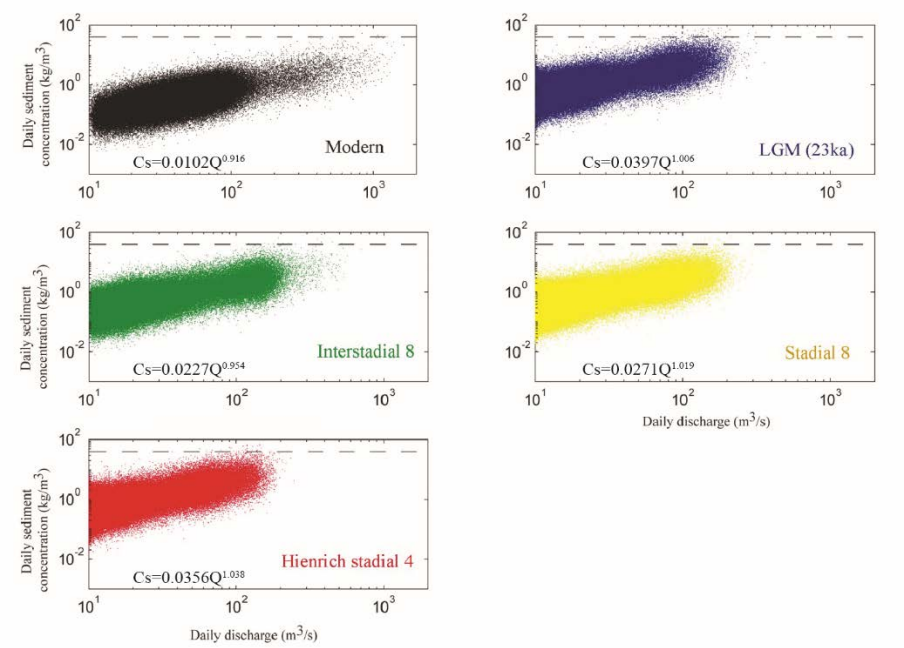

FIG. 4. 4 LIQUID DISCHARGE (M3/S) AND SEDIMENT CONCENTRATION (KG/M3) FOR THE DIFFERENT CLIMATIC PERIODS ANALYZED: MODERN (PRESENT DAY), LAST MAXIMUM GLACIATION (LGM), INTERSTADIAL 8, STADIAL 8 AND HEINRICH STADIAL 4. THE POWER LAWS FOR EACH CLIMATIC PERIOD ARE ALSO SHOWN. THE DOTTED LINE INDICATES THE THEORETICAL THRESHOLD FOR HYPERPYCNAL FLOWS. (AFTER (BONNEAU, 2014)).

In the following, the 2008 flash flood allows assessing the performance of the different laws in reproducing present day conditions at the river mouth that would trigger TC. Due to the lack of information on the duration of flash floods, the Dec 2008 flash flood is used as temporal pattern of the flood at the river mouth for the simulations at other climatic periods. Snow-melting floods supposedly would present a longer temporal pattern, however since this parameter is largely unknown, for all the simulations performed the duration and temporal evolution is that of the 2008 event. The peak liquid discharge is defined from the daily discharge of recurrence interval of 10 and 100 years modelled by Bonneau (2014) and shown in Fig. 4.5. The temporal evolution of the discharge is obtained by similarity from the temporal pattern of the 2008 flash flood.

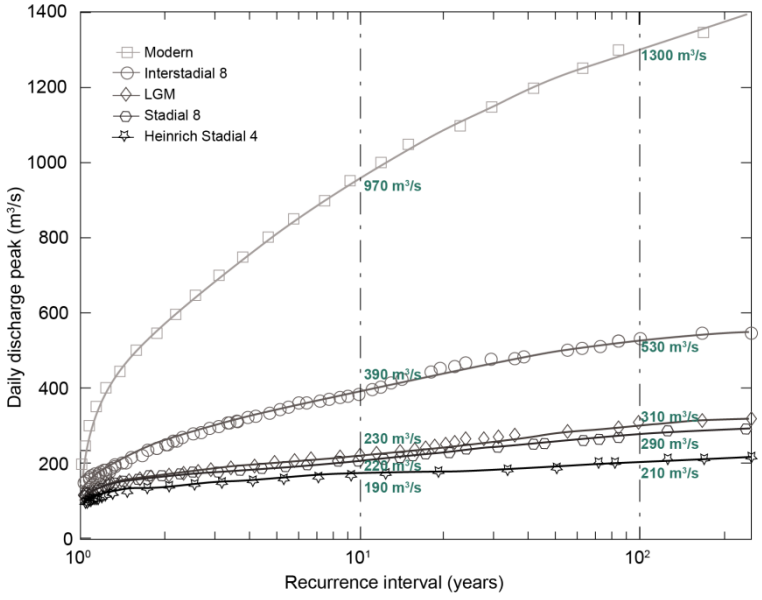

FIG. 4. 5 RECURRENCE INTERVAL OF THE FLASH FLOODS IN THE VAR ISSUED FROM HYDROTREND : MODERN (PRESENT DAY), LAST MAXIMUM GLACIATION (LGM), STADIAL 8, INTERSTADIAL 8, HEINRICH STADIAL 4. MODIFIED FROM BONNEAU (2014). THE LIQUID DISCHARGE OF RECURRENCE INTERVAL OF 10 YEARS AND 100 YEARS ARE ALSO INDICATED FOR EACH ONE OF THE CLIMATIC PERIODS.

As such the peak liquid discharge values, corresponding peak sediment concentration and sediment load according to the power laws shown in Fig. 4.5 and Table 4.1 are shown in Table 4.2.

TABLE 4. 2 PEAK LIQUID DISCHARGE (Q) AND ASSOCIATED PEAK SEDIMENT CONCENTRATION (C_s) GIVEN BY THE POWER LAWS FOR EACH ONE OF THE CLIMATIC PERIODS ANALYSED: LAST MAXIMUM GLACIATION (LGM), INTERSTADIAL 8 (I8), STADIAL 8 (S8) AND HEINRICH STADIAL 4 (HS4). THE SEDIMENT LOAD $q_s = QC_s$ IS ALSO EXPRESSED.

	$Q(m^3/s)$	$C(kg/m^3)$	$q_s\ (kg/s)$
LGM T10	230	9,43	2169,78
LGM T100	310	12,74	3948,77
I8 T10	390	6,73	2624,01
I8 T100	530	9,02	4778,16
S8 T10	220	6,61	1453,18
S8 T100	290	8,75	2538,35
HS4 T10	190	8,26	1568,75
HS4 T100	210	9,16	1923,68

However these values of concentration shown in Table 4.2 correspond to the "mean" value given by the fitting laws and are shown to be potentially reached at least a couple of times per year when analysing the recurrence interval for the peaks of sediment concentration as shown in Fig. 4.6. In fact, the daily sediment concentration values for the recurrence intervals of interest are one order of magnitude (i.e. between 3.8 and 6.5 times) larger than those values given by the exponential laws (Table 4.2). The values given by the laws correspond to the central part of the distribution of points in all the cases the peak concentration is above the threshold of $C_s > 5kg/m^3$ for hyperpycnal flows provided by Parsons et al., (2001). In the following, the simulations which forcing correspond to the original laws given by Bonneau (2014) are referred to as "**Base simulations**". The upper bound of the cloud of points in Fig 4.4 can be considered by establishing the ratio ($k = C_{RI}/C_s$) between the concentration (C_s) given by the laws and the value that shows the same recurrence interval (C_{RI}) in Fig 4.6. By increasing the power laws by the factor k, one would consider the upper bound of concentrations for a given recurrence interval. The sediment load for the peak of the floods of the increased laws $q_{s_{hyper}}$ is also shown in Table 4.3. For example, for the flash floods of recurrence interval of 10 years during the LGM, the power law gives a value of $C_s \sim 9.4\ kg/m^3$ for the 10yr liquid discharge $= 230m^3/s$. This concentration represents a mean value of concentration for this liquid discharge. However, the 10yr concentration shows a value of $C_{RI} \sim 42.5kg/m^3$ (Fig. 4.6) since it corresponds to the upper bounds of the data in Fig. 4.4 given a recurrence interval of 10yrs. As such, the ratio $k = C_{RI}/C_s$ for a 10yr recurrence interval is $k \sim 4.5$ as shown in Table 4.3.

TABLE 4. 3 PEAK LIQUID DISCHARGE (Q) AND ASSOCIATED PEAK SEDIMENT CONCENTRATION (C_s) ACCORDING TO THE POWER LAWS. PEAK SEDIMENT CONCENTRATION FOR THE RECURRENCE INTERVALS CONSIDERED (C_{RI}). RATIO BETWEEN THE SEDIMENT CONCENTRATION OF A GIVEN RECURRENCE INTERVAL AND THE SEDIMENT CONCENTRATION GIVEN BY THE POWER LAW (k) THE SEDIMENT LOAD $q_s = QC_s$ IS ALSO EXPRESSED.

	$Q(m^3/s)$	$C_s\ (kg/m^3)$	$C_{RI}\ (kg/m^3)$	$k = C_{RI}/C_s$	$q_{s_{hyper}}(kg/s)$
LGM T10	230	9,433844	42,5	4,505056	9775
LGM T100	310	12,73797	75	5,887906	23250
I8 T10	390	6,728240	26	3,864309	10140
I8 T100	530	9,015401	48	5,324223	25440
S8 T10	220	6,605383	29	4,390359	6380
S8 T100	290	8,752918	53	6,055124	15370
HS4 T10	190	8,256505	33	3,996849	6270
HS4 T100	210	9,160383	60	6,549945	12600

One can remark that classical hyperpycnal conditions ($C > 40\ kg/m^3$) are reached for the LGM conditions of recurrence interval T=100 yrs and for all the climatic periods considered (i.e. LGM, Interstadial 8, Stadial 8 and Heinrich Stadial 4), these cases will be simulated in the following and are hereafter referred to as "**Hyperpycnal simulations**".

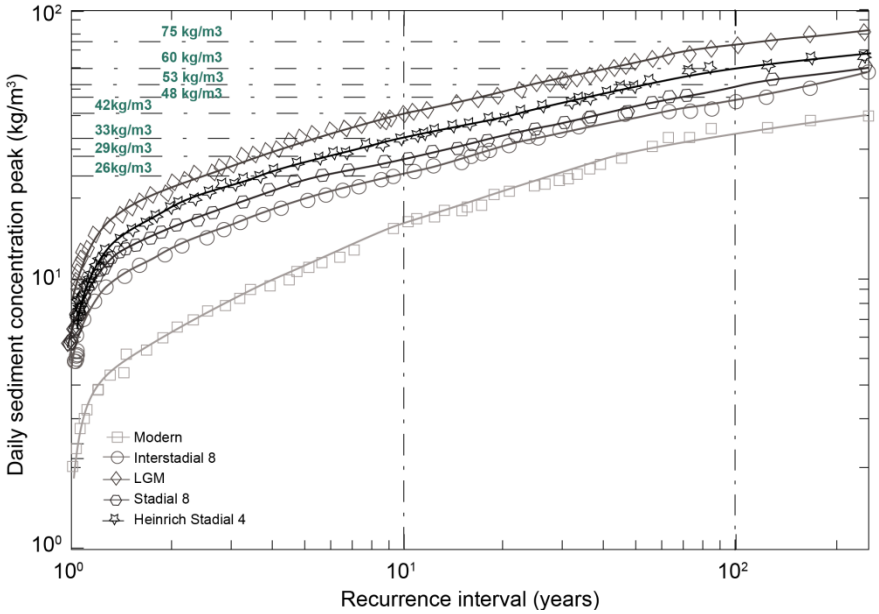

FIG. 4. 6 RECURRENCE INTERVAL FOR THE PEAKS OF SEDIMENT CONCENTRATION FOR THE DIFFERENT CLIMATIC PERIODS ANALYSED: MODERN (PRESENT DAY), LAST MAXIMUM GLACIATION (LGM), INTERSTADIAL 8, STADIAL 8 AND HEINRICH STADIAL 8. THE SEDIMENT CONCENTRATION FOR THE RECURRENCE INTERVAL OF 10 YEARS AND 100 YEARS ARE ALSO INDICATED FOR EACH ONE OF THE CLIMATIC PERIODS.

3.2. Field data

Bathymetric data is derived from a compilation of several datasets from multiple cruises from French institutions including Ifremer. A 125m resolution bathymetric grid (879x879 cells) was generated from this compilation and has been included in the model (Fig. 4.7). The modelled results are compared to mooring data in the Var canyon and to cores along the Var Sedimentary Ridge (Fig 4.7). Three moorings were deployed from December 2008 to March 2009 at three stations along the axis of the canyon (Khripounoff et al., 2012). The shallower mooring (VE) was located at 510m depth, the second (VV) at 1280m depth and the third (VA) at 1575m depth the confluence of the Var and Paillon canyons. Four piston cores are used in the present study (Table 4.4). One Kullenberg piston core (KNI22) collected during the 1993 NICASAR cruise on board R/V Le Suroît (IFREMER) and three Callypso cores (ESSK08-CS01, ESSK08-CS05 and ESSK08-CS13) collected during the 2008 ESSDIV cruise on board the R/V Pourquoi Pas? (IFREMER). Sediment cores KNI22, ESSK08-CS01 and ESSK08-CS05 were collected along the levee crest; sediment core ESSK08-CS13 is located on the south-western flank of the Var Sedimentary Ridge.

TABLE 4. 4 LOCATION, BATHYMETRY AND LENGTH OF THE SEDIMENT CORES. THE CORES ARE INDICATED FROM WEST TO EAST.

Core	Cruise	R/V	Latitude	Longitude	Water depth (m)	Length (cm)
ESSK08-CS05	ESSDIV	Pourquoi Pas?	43° 23'.60N	07° 25.190'E	1694	2878
KNI22	NICASAR	Le Suroît	43° 21.75'N	07° 32.630'E	1900	849
ESSK08-CS01	ESSDIV	Pourquoi Pas?	43° 23.24'N	07° 44.181'E	2130	1052
ESSK08-CS13	ESSDIV	Pourquoi Pas?	43° 23'.22N	07° 47.817'E	2473	2450

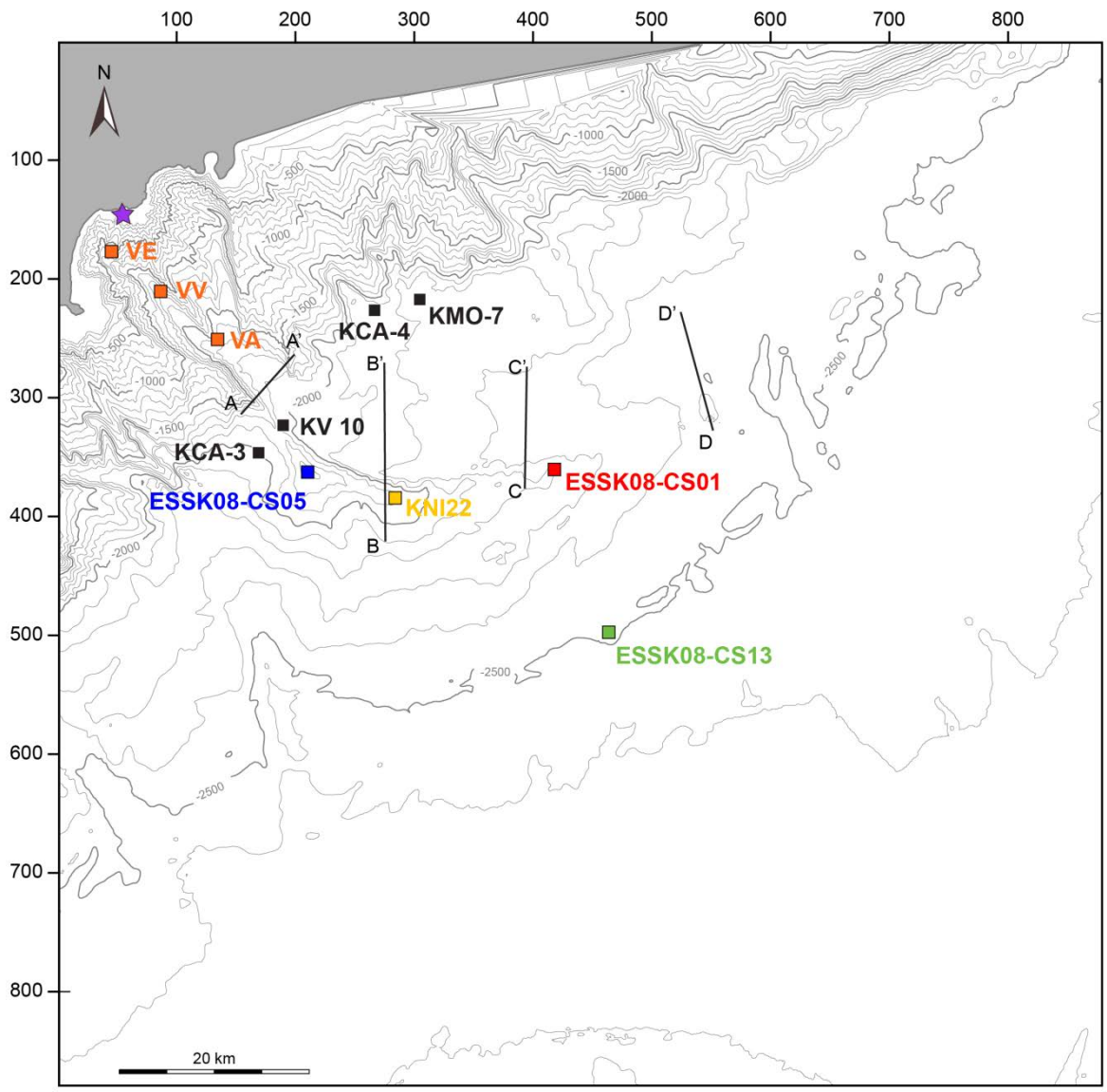

FIG. 4. 7 BATHYMETRY OF THE VAR SEDIMENTARY SYSTEM (CONTOUR INTERVALS IN METRES) USED FOR NUMERICAL MODELLING. PURPLE STAR REPRESENTS THE RIVER MOUTH (SOURCE OF HYPERPYCNAL FLOWS). THE MAP ALSO SHOWS THE POSITION OF THE INSTRUMENTED MOORING (VE, VV AND VA) AND OF THE SEDIMENT CORES (KNI22, ESSK08-CS01, ESSK08-CS05 AND ESSK08-CS13) USED FOR VALIDATION OF MODEL RESULTS. THE POSITION OF THE CORES KCA-3, KCA-4 AND KMO-7 (PIPER AND SAVOYE, 1993) AND KV-10 (MULDER ET AL., 2001B; MAS ET AL., 2010) THAT WOULD BE USED IN THE DISCUSSION IS ALSO INDICATED. ALSO SHOWN THE POSITION OF THE PROFILES USED IN TABLE 4.6. ISOBATHS FOR 100M INTERVALS ARE PRESENTED.

Core descriptions are available for the four cores used in the present study (Migeon et al., 2000; Jorry et al., 2011; Bonneau, 2014). The sediment distribution along the Var Sedimentary Ridge changes western to eastern: deposits are coarser eastward and there is a change from interbedded laminated mud and silt and laminated mud with a basal silt or sand layer to centimetric fine-sand turbidites and well-developed medium sand turbidites (Migeon et al., 2001). Sedimentation rates also increase eastward, with values of about 17cm/ky in the western part of the Ridge since the last glacial period whilst on the eastern part the rate is up to 4 times higher (Piper and Savoye, 1993). In the following a short description of the different cores from west to east is provided. The synthetic lithology logs are shown in Fig. 4.8.

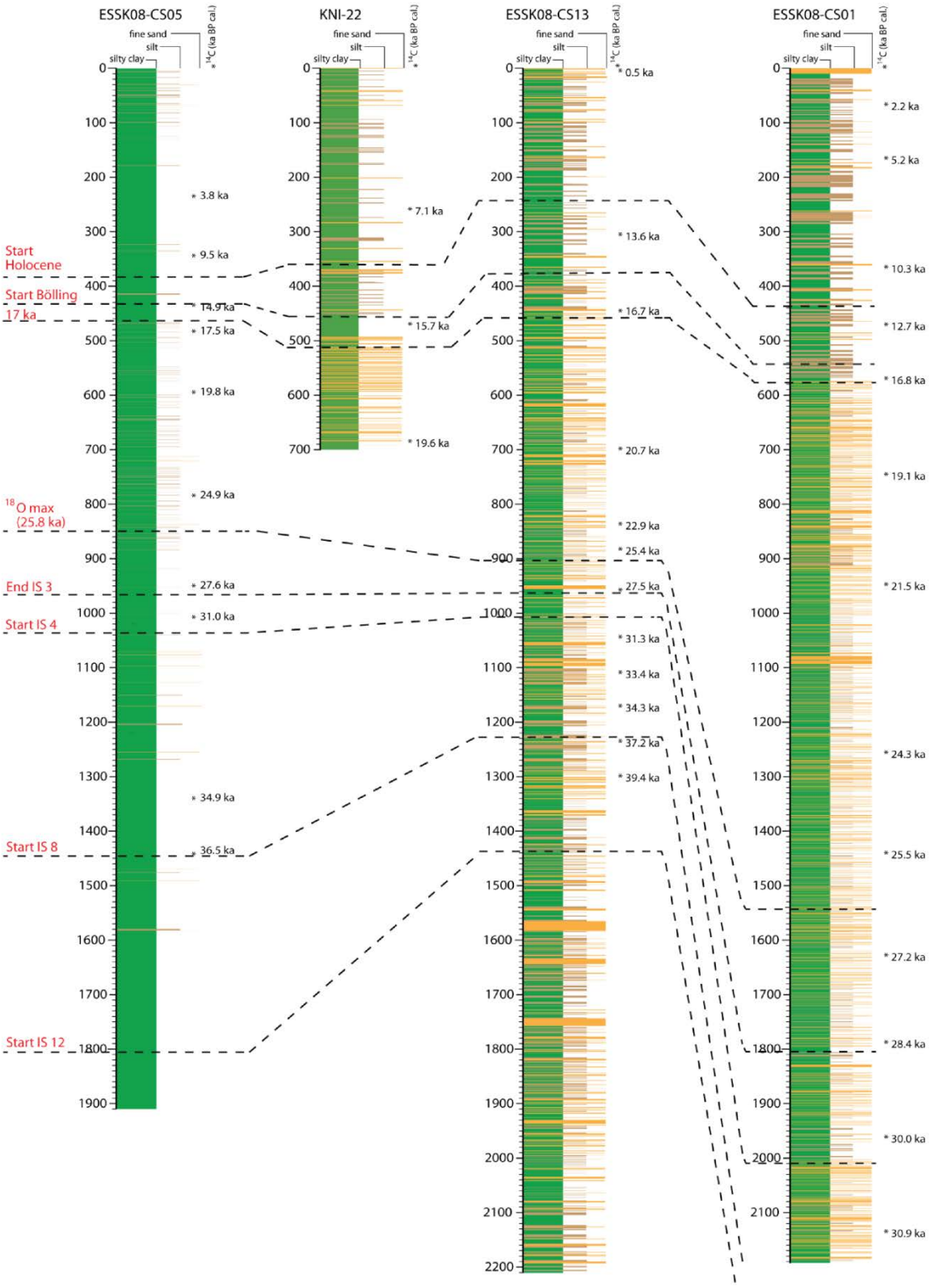

FIG. 4. 8 LITHOLOGICAL LOGS AND 14C DATES (CAL KA BP) FOR THE CORES ESSK08-CS05, KNI22, ESSK08-CS13 AND ESSK08-CS01. AFTER BONNEAU (2014).

Core **ESSK08-CS05** was collected from the uppermost part of the Var Sedimentary Ridge at about 350m above the valley floor (see Fig 4.7 for location). The core is mainly composed of hemipelagic muds and very scarce milimetric silty turbidite beds. The thin turbidites are present between 0 and 100cmbsf (cm below sea floor) and between 450 and 850cmbsf (Jorry et al., 2011; Bonneau, 2014;).

Core **KNI22** was collected along the crest of the Var Sedimentary Ridge at about 260m above the valley floor about 10km eastward than ESSK08-CS05 (see Fig 4.7 for location). The upper 5 m are composed of hemipelagic facies with some thin fine grained turbidites (Fig. 4.8). Below 5m, turbidites become thicker and sandier downwards. The thickness of the turbidites ranges between some mm and 2cm. Hemipelagic deposits between turbidite layers are well developed (Migeon et al., 2000).

Core **ESSK08-CS01** was collected along the distal part of the crest of the Var Sedimentary Ridge at about 130m above the valley floor (see Fig 4.7 for location) and contains the highest number of turbidites (Fig 4.8). Hemipelagic facies dominate the upper 5m although some fine grained turbidites are present. Below that depth, sandy turbidites are very frequent and show a thickness inferior to 4cm. The sequence of turbidites shows no hemipelagic deposit in between probably. Since the base of the turbidites is mostly non erosive, a high frequency of turbidity currents could explain the no preservation of hemipelagic sedimentation in the sedimentary record. Two intervals at the base of the core, between 1800 and 1840cmbsf and between 1940 and 2000cmbsf, show a scarce number of turbidite deposits (Bonneau, 2014).

Core **ESSK08-CS13** was collected on the southeastern flank of the Var Sedimentary Ridge about 20km from the valley (see Fig 4.7 for location). It is characterized by sandy turbidites interbedded with hemipelagic layers (Fig 4.8). The thickness of the hemipelagic deposits indicates that turbidity currents are spaced in time so that hemipelagic sedimentation can be preserved in the sedimentary record. The frequency of sandy turbidites increases downward the core and turbidite beds can reach thickness of several cm (Jorry et al., 2011; Bonneau, 2014).

The analysis of the different cores has evidenced the heterogeneous deposition and preservation of turbidites that highly depends on the position along the VSR (Jorry et al., 2011; Bonneau et al., 2014, Fig. 4.9). Higher sedimentation rates (about 70cm/ky) are found in the core ESSK08-CS01 located in the distal part of the VSR whilst the lower sedimentation rates (about 30cm/ky) are recorded in the core ESSK08-CS13 in the southern flank of the VSR (Bonneau et al., 2014). The presence of sandy turbidites is negligible in the core ESSK08-CS05 on the uppermost part of the VSR and increases towards the distal part of the VSR being maximal in the core ESSK08-CS 01 (40% of the total). Sedimentation rates are higher during the LGM and during the cold stadials of the cycles D/O and HS and lower during the interstadials of the cycles of D/O. However the relationship between turbidite frequency and sedimentation rate is complex, for example core ESSK08-CS01 presents the higher sedimentation rates and a large turbidite frequency. On the other hand, the core ESSK08-CS13 shows a higher turbidity frequency than the core ESSK08-CS05 but a lower sedimentation rate. The climatic influence is clearer for the turbidite frequency (Fig. 4.10) with higher activity during the LGM and an evolution of the frequency related to the cycles of D/O with low activity during the warm interstadials and high activity during the cold stadials and HS. The variation in the frequency of overflows recorded in the cores is attributed to changes in the magnitude of hyperpycnal flows of Var River floods related to climatic periods (Bonneau et al., 2014).

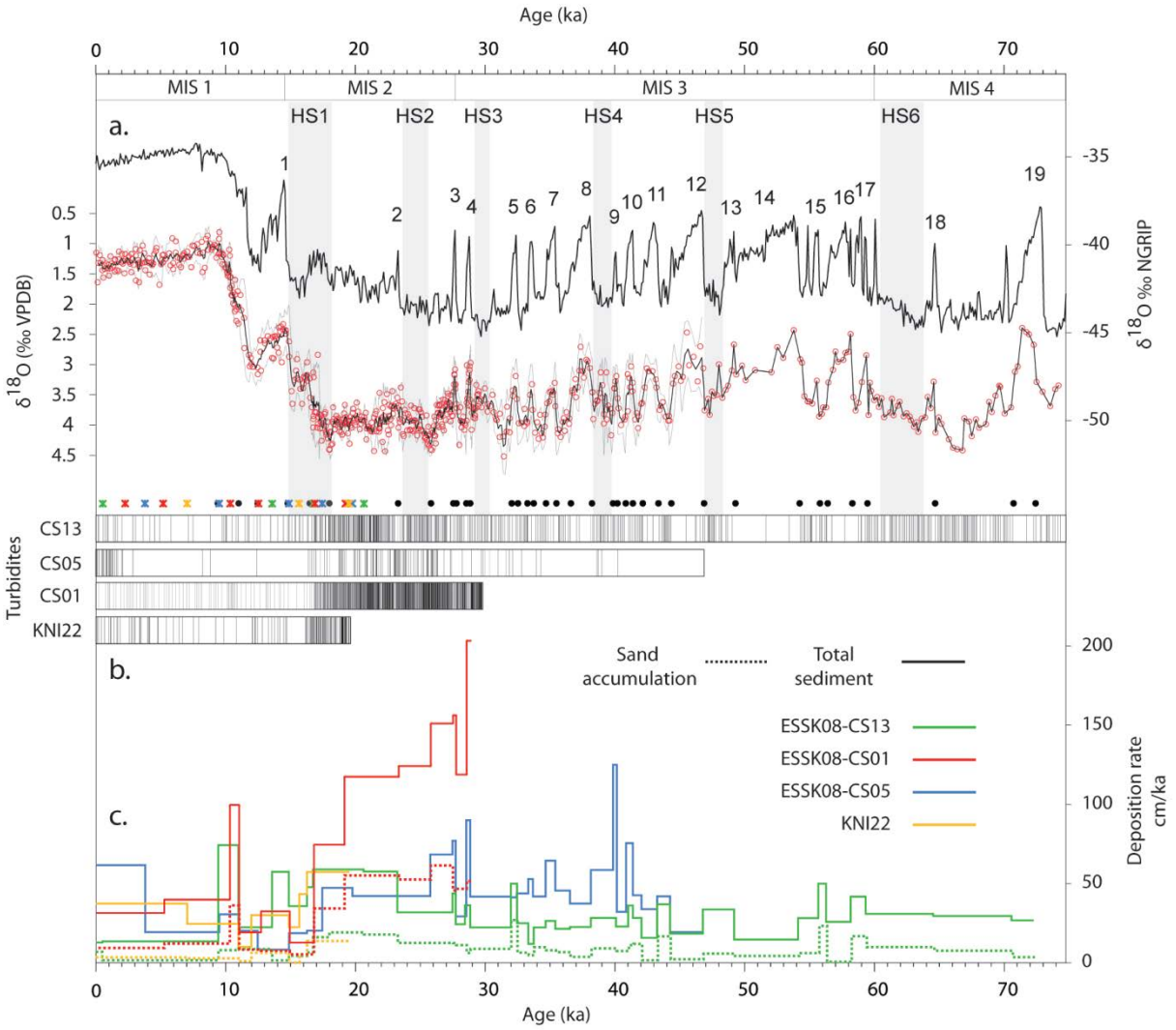

FIG. 4. 9 A) COMPOSITE $\delta^{18}O$ CURVE OF *GLOBIGERINA BULLOIDES*, DERIVED FROM THE STACK OF DATA OBTAINED IN ALL CORES (CIRCLES OF LOWER LINE; LEFT-HAND SCALE) THE CORE MODEL IS ANCHORED BY ^{14}C ACCELERATOR MASS SPECTROMETRY DATES (ASTERISKS IN BOTTOM PANEL) ANDHAS BEEN REFINED USING THE TUNING OF THE *GLOBIGERINA BULLOIDES* $\delta^{18}O$ CURVES WITH THE $\delta^{18}O$ RECORD FROM THE NORTH GREENLAND ICE CORE PROJECT (NGRIP) ICE CORE ISOTOPES CURVE (GREENLAND ICE CORE CHRONOLOGY 2005 [GICC05] UP TO 60 KYR AGO [KA], NGRIP THEREAFTER; NGRIP MEMBERS 2004;RASMUSSEN ET AL. 2006; SVENSSON ET AL. 2008). TIE POINTS ARE REPRESENTED BY FILLED CIRCLES AT THE BOTTOM OF THE PANEL; THE OPEN CIRCLES CORRESPOND TO TIE POINTS USED IN THE 0–20KA CHRONOSTRATIGRAPHY PREVIOUSLY ESTABLISHED BY JORRY ET AL. (2011). B) INTERPOLATED AGES OF TURBIDITE SEQUENCES FOR THE FOUR SEDIMENT CORES. C) SEDIMENTATION RATES (SOLID LINES) AND SAND ACCUMULATION (DOTTED LINES, EXCEPT FOR ESSK08-CS05 WHERE SAND CONTENT IS NEGLIGIBLE). FROM BONNEAU ET AL., 2014.

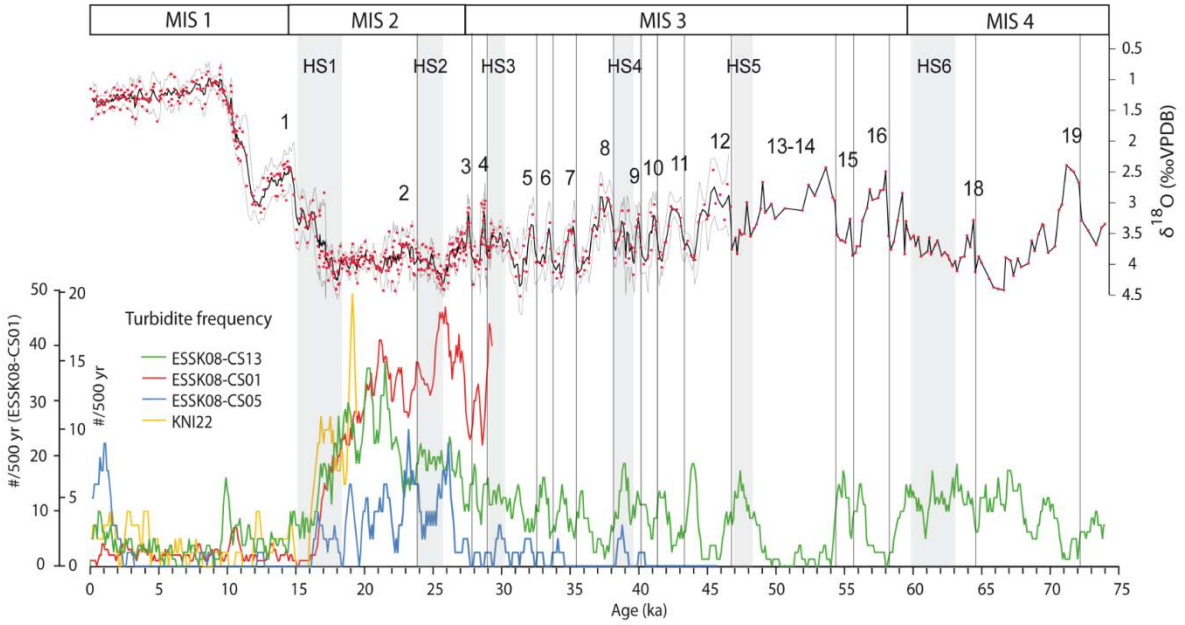

FIG. 4. 10 EVOLUTION OF THE TURBIDITE FREQUENCY (NUMBER OF TURBITES PER 500YRS) FOR THE REFERENCE CORES. NOTE THAT THE LEFT-HAND SCALE CONCERNS THE CORE ESSK08-CS01 WHEREAS RIGHT HAND SCALE CONCERNS THE OTHER CORES. FROM BONNEAU (2014).

3.3.Numerical modelling

The process-based model Nixes-TC (Jacinto and Burel, 2003) is implemented to the Var Sedimentary System. The model simulates the spatial development of an unsteady TC flowing in deep ambient fluid and provides the deposition pattern produced by the simulated TC. The equations of the model are the depth integrated fluid, momentum and sediment conservation equations (Equations 4.2 to 4.5). Equations are reminded here:

$$\frac{\partial h}{\partial t} + \frac{\partial U_x h}{\partial x} + \frac{\partial U_y h}{\partial y} = e_w U - w_s \quad (4.2)$$

$$\frac{\partial U_x h}{\partial t} + \frac{\partial (U_x{}^2\, h)}{\partial x} + \frac{\partial (U_x U_y\, h)}{\partial y} = -\frac{1}{2} Rg \frac{\partial \emptyset h^2}{\partial x} + R\emptyset g h S_x - (u_{*x})^2 + f h U_y \quad (4.3)$$

$$\frac{\partial U_y h}{\partial t} + \frac{\partial (U_x U_y\, h)}{\partial x} + \frac{\partial (U_x{}^2\, h)}{\partial y} = -\frac{1}{2} Rg \frac{\partial \emptyset h^2}{\partial y} + R\emptyset g h S_y - \left(u_{*y}\right)^2 - f h U_x \quad (4.4)$$

$$\frac{\partial \emptyset h}{\partial t} + \frac{\partial \emptyset U h}{\partial x} = w_s (p E_s - \emptyset_b) \quad (4.5)$$

A full description of the model can be found in Chapter 2. Inputs of the model are the regular orthogonal grid of the bathymetry, sediment properties (i.e. grain size and density) and initial deposit (i.e. volume concentration and porosity). Sensitivity tests were performed for grain sizes in the range of silt and fine sand since larger grain sizes would be a priori transported as bedload. The results of the grain sensitivity tests can be found in the Supplementary information at the end of the present chapter. In the following, a single grain size of 50 µm was chosen for the simulations. Initial and boundary conditions are provided to the model in terms of values of volume concentration (Ø), current thickness (h), and velocity (U_x and U_y) at the river mouth. Since the position and width of the river mouth changed with the landfill for the airport of Nice, sensitivity tests were performed and can also be found in the Supplementary information of the present chapter. Present day simulations are run considering present width and orientation (i.e. width 350m and orientation NE-SW) whilst for the climatic simulations the river mouth considered is that prior to 1946 (i.e. width 1km and orientation NNW-SSW). The laws expressing the relationship between liquid discharge and sediment

concentration are those given in Table 4.1. No ambient current is considered in any of the simulations performed.

Three different sets of simulations are performed: present day conditions (i.e. December 2008 flash flood) in order to assess the performance of the model and the different laws proposed in literature, influence of Coriolis in the construction of the VSR, for which present day conditions are applied, and finally reconstruction of hyperpycnal flows at different climatic periods.

3.4. Influence of Coriolis forces on the TC evolution and sedimentation pattern

Coriolis forces are important when temporal and spatial scales of the flow are similar to those of the Earth rotation. This can be the case for TC with a duration of at least the same order of magnitude as the inertial period $T_{in} = 2\pi/f$ (see Chapter 2). In the case of Nice (i.e. at 43.5°N, then $f = 1.0008 \cdot 10^{-4}$), a current lasting 17h30' would suffer Coriolis forces. The scale at which Coriolis forces become important is expressed by the Rossby number $= U/(fL)$, where U is the depth integrated velocity, f the Coriolis parameter and L the length scale. Coriolis forces will dominate the TC when $Ro < 1$ (Nof, 1996). The Var sedimentary system extends for about 180km, as such, Coriolis forces would influence the trajectory of the TC for U<18m/s. For slower currents the length scale at which Coriolis forces become important will be smaller. Channel asymmetry may be potentially caused by Coriolis forces, the effect of Coriolis on the asymmetry of a channel can be estimated by using a Rossby number based on channel width (W) $Ro_w = U/(fW)$ (Cossu and Wells, 2013; Cossu et al., 2015, 2010). Coriolis forces are important in channel asymmetry when $Ro_w < 10$. Hence in the case of the Var where channel width ranges between 4000m in the upper valley and 12000m in the mid valley, velocity should be inferior to 4m/s and 12m/s respectively so that Coriolis forces were at play. Possible Rossby numbers are shown in Table 4.6 for different velocities.

TABLE 4. 5 ESTIMATED ROSSBY NUMBERS FOR THE VAR SEDIMENTARY SYSTEM WITH F=2ΩSINΦ ~1.0008×10^{-4} RADS^{-1} AT LATITUDE 43.5N. ITALIC NUMBERS INDICATE THOSE COMBINATIONS WHERE CORIOLIS FORCES ARE AT PLAY. SPATIAL SCALES WERE RETRIEVED FROM MIGEON ET AL., (2012) (CHANNEL WIDTHS) AND SAVOYE ET AL., (1993) (SYSTEM), THE POSITION OF THE PROFILES AA', BB', CC' AND DD' IS SHOWN IN FIG. 4.7.

	Spatial scale (m)	Velocity U(m/s)				
	Length (L)	20	10	5	1	0.5
		$Ro = U/(fL)$				
System	180000	1.10	0.55	0.28	*0.06*	*0.03*
	Spatial scale (m)	Velocity U(m/s)				
	Width (W)	20	10	5	1	0.5
		$Ro_w = U/(fW)$				
Channel Upper valley (AA')	4000	49.60	24.80	12.40	*2.48*	*1.24*
Channel mid valley (BB')	12000	16.53	*8.27*	*4.13*	*0.83*	*0.41*
Channel mid valley (CC')	9000	22.05	11.02	*5.51*	*1.10*	*0.55*
Channel mid valley (DD')	6000	16.53	16.53	*8.27*	*1.65*	*0.83*

As a first estimate of the importance of Coriolis forces, one can consider the landslide of 1979 for which estimates of velocity on the basis of cable breaks are 7m/s (Gennesseaux et al., 1980) and hence Earth rotation might be at paly at least in the lower part of the system (distal part of the Ridge). In fact the TC due to the 1979 did not overtop the VSR (Gennesseaux et al., 1980; Piper and Savoye, 1993; Mulder et al., 1997b). Estimations of velocity of hyperpycnal flows on the basis of sediment waves (Piper and Savoye, 1993) provide a value of 0.35m/s, as such, hyperpycnal flows would be prone to suffer Coriolis forces.

4. Results

4.1. December 2008 flash flood

4.1.1. Without Coriolis forces

The liquid discharge for the December 2008 is available from measurements whilst the sediment concentration is obtained from published power laws (see Table 4.1). The peak conditions for liquid discharge, sediment concentration and sediment load are summarized in Table 4.5:

TABLE 4. 6 PEAK LIQUID DISCHARGE (Q) AND ASSOCIATED PEAK SEDIMENT CONCENTRATION (C_s) GIVEN FOR PRESENT DAY CONDITIONS BY THE POWER LAWS AVAILABLE IN THE LITERATURE. ADDITIONALLY THE SEDIMENT LOAD (q_s) IS ALSO EXPRESSED.

	Q(m^3/s)	C(kg/m^3)	Sediment load (kg/s)
Laurent	625	14,91679	9322,992
Mulder	625	43,43016	27143,85
Bonneau	625	3,712156	2320,098
Bonneau2	625	5,568235	3480,147

The modelling results in terms of current speed $U(m/s)$ are shown at the mooring locations VE (Fig. 4.11. a and b), VV (Fig. 4.11. a' and b') and VA (Fig. 4.11. a'' and b''). Data obtained from ADCP current meters (30mab) at the locations of VE and VV is shown for comparison (Khripounoff et al., 2012). No data is available for this event at the location of VA..

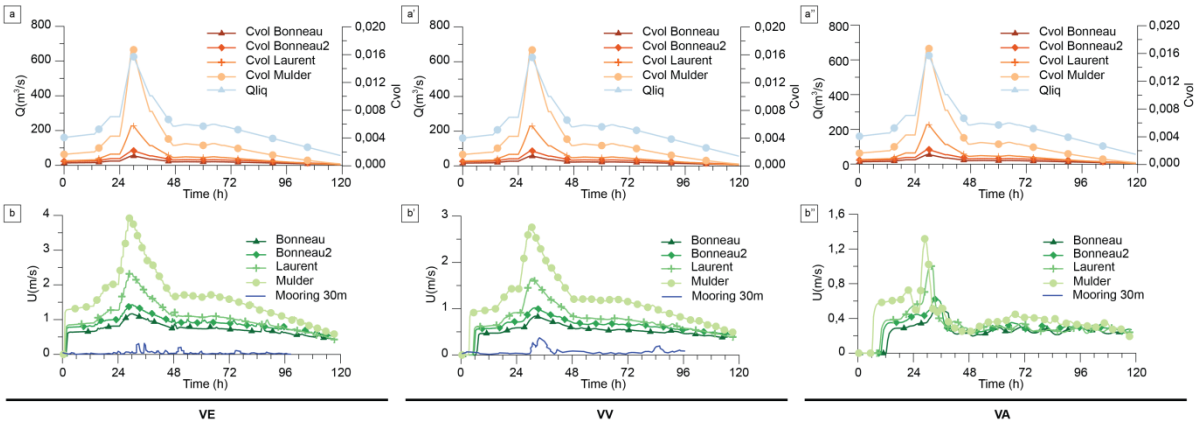

FIG. 4. 11 MODELLING RESULTS FOR THE FLASH FLOOD OF DECEMBER 2008 FOR THE POINTS VE (A, B, C, D, E), VV(A', B', C', D', E') AND VA (A'', B'', C'', D'', E'') IN THE VAR CANYON. A), A') & A'') LIQUID DISCHARGE (M3/S) AND VOLUMETRIC CONCENTRATION. B), B') & B'') DEPTH INTEGRATED CURRENT SPEED FOR THE MODEL RESULTS AND MEASURED CURRENT SPEED AT 30MAB. THE VALUES OF CONCENTRATION ARE CALCULATED WITH THE POWER LAWS FOR PRESENT DAY (MODERN) CONDITIONS GIVEN IN TABLE 4.1: MULDER, LAURENT, BONNEAU AND BONNEAU2. THE PEAK VALUES OF THE FORCING CONDITIONS Q AND CS ARE SUMMARIZED IN TABLE 4.6.

Values of velocity and instantaneous sediment transport obtained for the relationship given by Mulder et al. (1997a) and Laurent (1971) are respectively up to ~3.5 and up to 2 times bigger than those obtained for the relationship proposed by Bonneau (2014). For example, peak velocity values obtained for the mooring point VE for the relationship given by Mulder et al. (1997a) shows a value of ~4m/s whilst for the relationship proposed by Bonneau (2014), the value obtained is of ~1m/s.

For the point VA (Fig. 4.12), the instantaneous sediment transport obtained for the relationship proposed by Bonneau (2014) is inferior to 100 kg/m^2 whilst for the relationships given by Laurent (1971) and Mulder et al. (1997a) are of ~200 kg/m^2 and 700 kg/m^2 respectively. The time arrival of the TC to the points VE and VV as well as the current thickness is similar for the different laws analysed. For the point VA the more charged TC produced by the laws of Laurent (1971) and Mulder

et al. (1997a) arrive earlier and present larger values of current thickness than those obtained on the basis of the law given by Bonneau (2014).

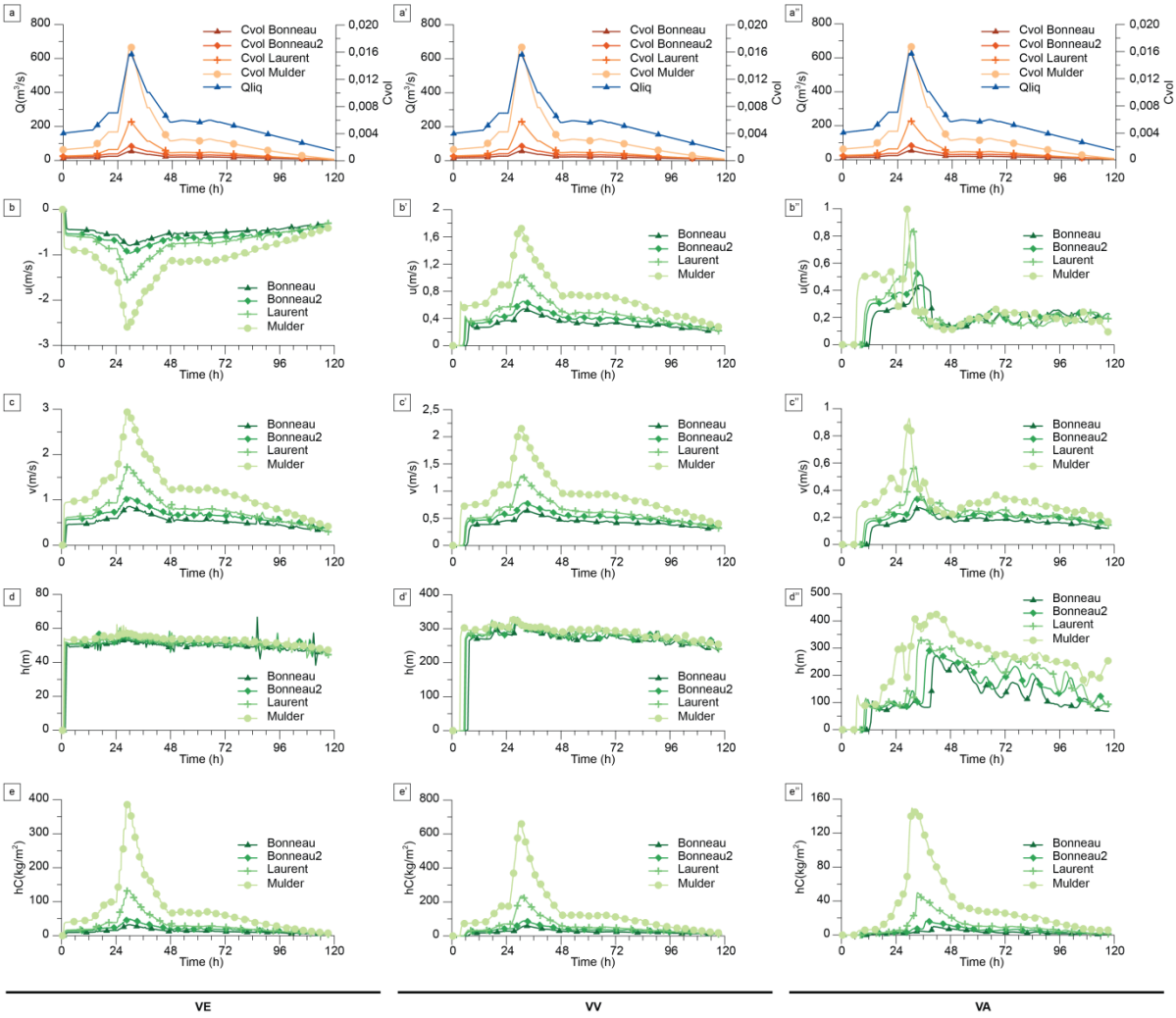

FIG. 4. 12 MODELLING RESULTS FOR THE FLASH FLOOD OF DECEMBER 2008 FOR THE POINTS VE (A, B, C, D, E), VV(A', B', C', D', E') AND VA (A'', B'', C'', D'', E'') IN THE VAR CANYON. A), A') & A'') LIQUID DISCHARGE (M3/S) AND VOLUMETRIC CONCENTRATION. B), B') & B'') DEPTH INTEGRATED CURRENT SPEED (X DIRECTION). C), C') & C'') DEPTH INTEGRATED CURRENT SPEED (Y DIRECTION). D), D') & D'') CURRENT THICKNESS (M). E), E') & E'') INSTANTANEOUS SEDIMENT TRANSPORT HC (KG/M^2). THE VALUES OF CONCENTRATION ARE CALCULATED WITH THE POWER LAWS FOR PRESENT DAY (MODERN) CONDITIONS GIVEN IN TABLE 4.1: MULDER, LAURENT, BONNEAU AND BONNEAU2. THE PEAK VALUES OF THE FORCING CONDITIONS Q AND CS ARE SUMMARIZED IN TABLE 4.5.

4.1.2. With Coriolis forces

The effects of Coriolis are evaluated for the flash flood of December 2008 (i.e. $Q_p \sim 600 m3/s$). The sediment charge is calculated from the power relationship given for present day (Table 4.1). Results of the model runs are shown (Fig. 4.13) for the point VV, located in the Var canyon, and the core ESSK08-CS05, located on the uppermost part of the Var Sedimentary Ridge (positions of the points are shown in Fig. 4.7).

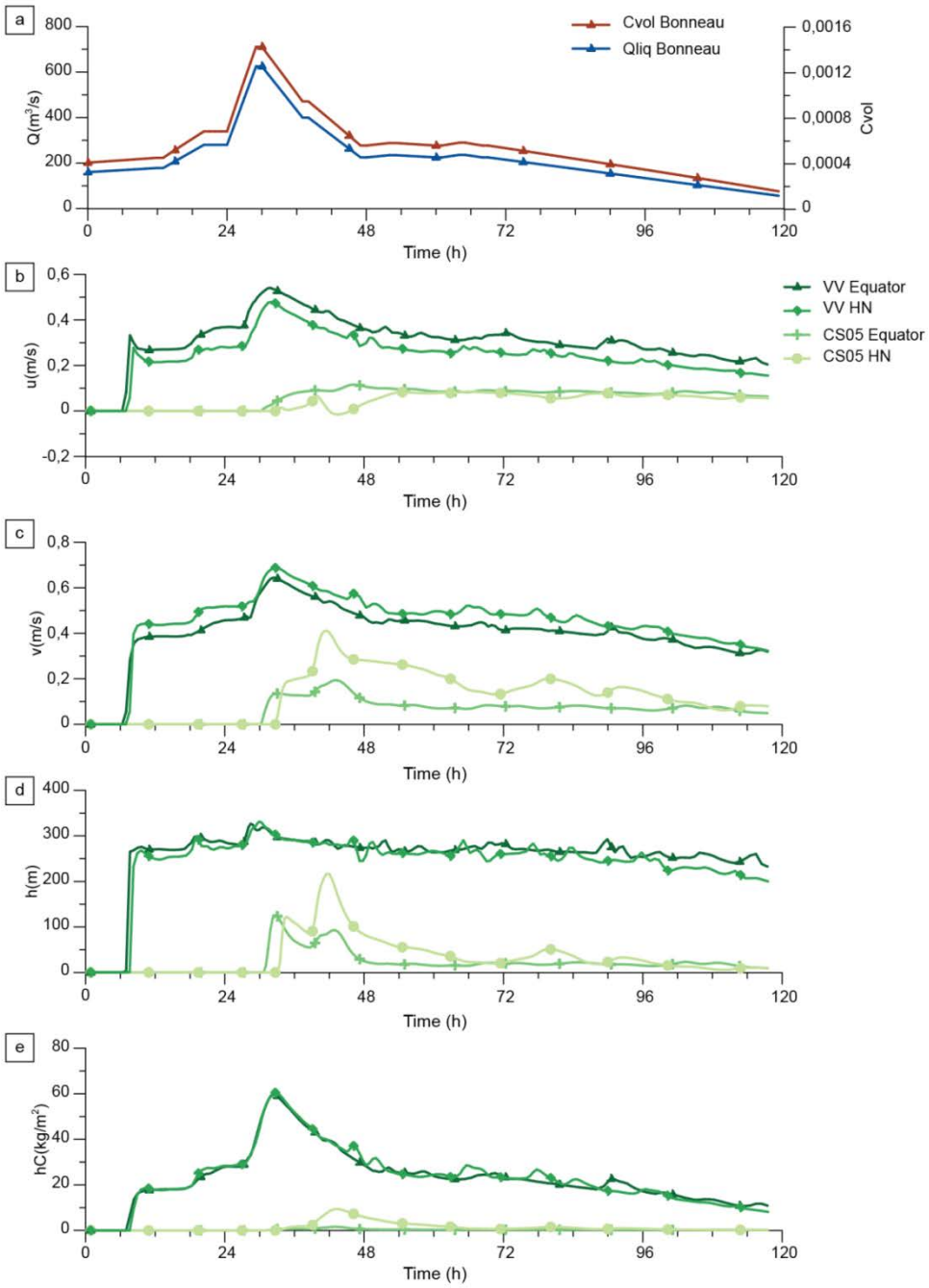

FIG. 4. 13 MODELLING RESULTS FOR THE FLASH FLOOD OF DECEMBER 2008 FOR THE POINT VV IN THE VAR CANYON AND THE CORE POSITION CS05 AT THE UPPERMOST PART OF THE VAR SEDIMENTARY RIDGE. RESULTS ARE SHOWN FOR THE RUNS INCLUDING CORIOLIS FORCES (HN) AND NOT INCLUDING CORIOLIS FORCES (EQUATOR). A) LIQUID DISCHARGE (M3/S) AND VOLUMETRIC CONCENTRATION. B) DEPTH INTEGRATED CURRENT SPEED (X DIRECTION). C) DEPTH INTEGRATED CURRENT SPEED (Y DIRECTION). D) CURRENT THICKNESS (M). E) INSTANTANEOUS SEDIMENT TRANSPORT HC (KG/M2).

The modelling results show that Coriolis forces have a negligible influence in the Var Canyon whilst in the Var Sedimentary Ridge the values can differ up to double when considering Coriolis forces. The influence of Coriolis forces is not limited to the magnitude of the different variables of the current but also its trajectory and deposition patterns as shown in Fig 4.14. When Coriolis forces are not included the trajectory of the TC and its deposition pattern is strictly controlled by the bathymetry, as such, the current spreads once it reaches the low gradient slopes of the mid valley. On the other hand, when Coriolis forces are included, the TC bends to the right hand side. Once the TC exits the Var Canyon, part of the TC leads to the south east through the WSC (i.e. western part of the VSR) that is only a 200m above the valley floor, and part continues along the VSR.

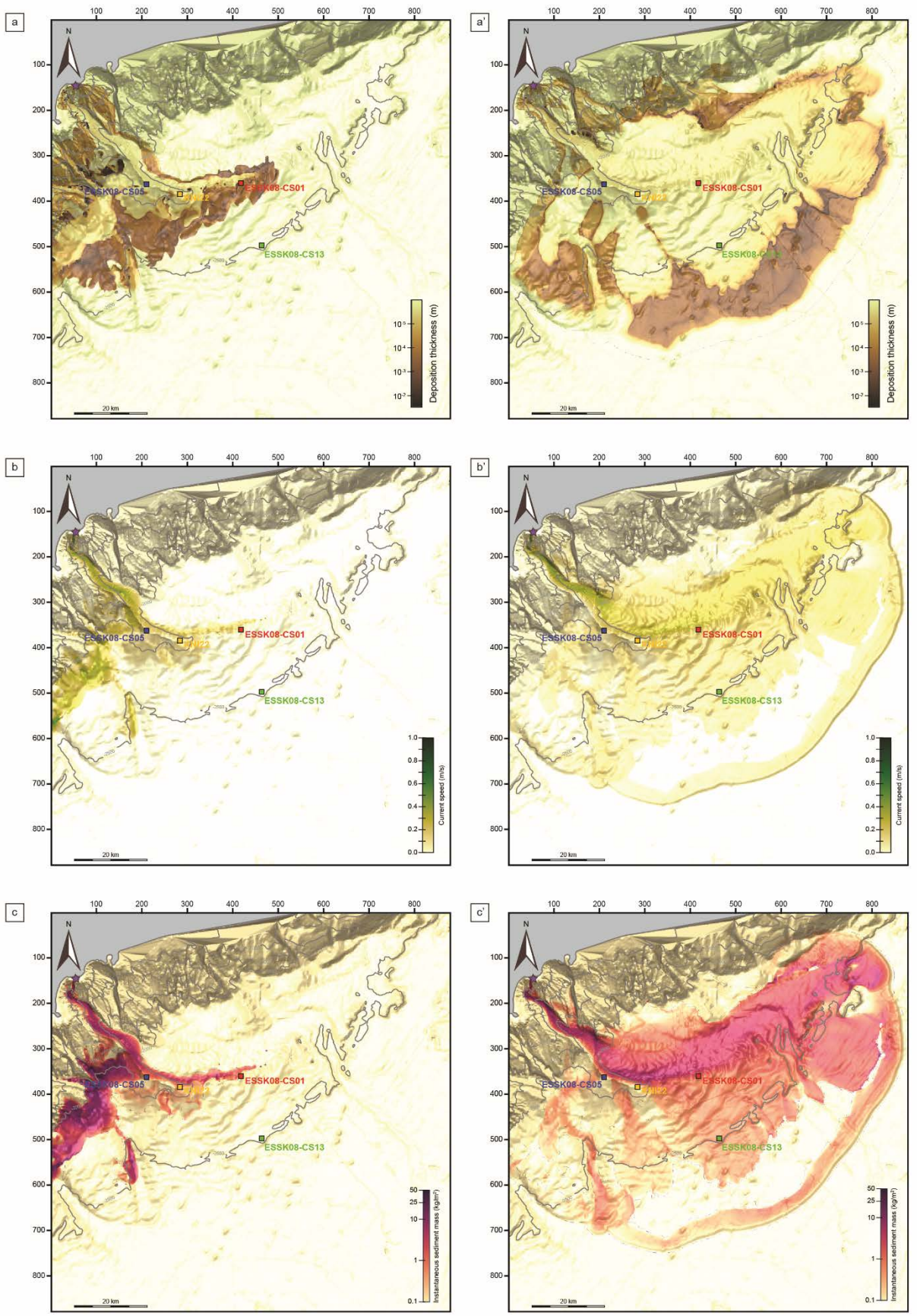

FIG. 4. 14 MODELLING RESULTS FOR THE FINAL STAGE (T=118H) FOR THE 2008 FLASH FLOOD. FIGURES ON THE LEFT (A,B,C) CORRESPOND TO SIMULATIONS WHERE CORIOLIS FORCES WHERE INCLUDED WHILST FOR THE SIMULATIONS ON THE RIGHT (A',B',C') CORIOLIS FORCES WERE NOT INCLUDED. A) & A') FINAL DEPOSITION THICKNESS (M) CONSIDERING A VOLUMETRIC DENSITY OF 0.25 AND A SEDIMENT DENSITY OF 2600KG/M3.

THE SCALE IS LOGARITHMIC. B) & B') CURRENT SPEED AT THE FINAL STAGE OF THE SIMULATION (T=118H). C) & C') INSTANTANEOUS SEDIMENT MASS HC(KG/M2) AT THE FINAL STAGE OF THE SIMULATION (T=118H). THE SCALE IS LOGARITHMIC.

4.2. Hyperpycnal flows at different climatic periods

Flash floods of recurrence interval T=10 years (Q_{T10}) and T=100 years (Q_{T100}) are evaluated for the different climatic periods considered (i.e. LGM, Interstadial 8, Stadial 8 and Hiernich Stadial 4). The temporal pattern of the flash floods follows the one of the December 2008 flood for which data is available. Modelling results for Base simulations and Hyperpycnal simulations are presented in the following.

4.2.1. Base simulations

The results are shown for the points corresponding to the core positions CS05 (Fig. 4.15), KNI22 (Fig. 4.16) and CS01 (Fig. 4.17) (i.e. from west to east). The TC didn't reach the point CS13 in any case and hence no results figure is presented for this point.

A general pattern is observed from the modelling results for both recurrence intervals: TC present decreasing intensity for LGM, HS4, S8 and I8. The peak liquid discharge, sediment concentration and sediment loading at the source for each one of the climatic periods analysed are given in Table 4.7. One can remark that none of the sediment concentration overcomes the classic threshold of 42.5kg/m^3 for hyperpycnal flows.

TABLE 4. 7 PEAK LIQUID DISCHARGE AND ASSOCIATED PEAK SEDIMENT CONCENTRATION FOR EACH ONE OF THE CLIMATIC PERIODS ANALYSED: LAST MAXIMUM GLACIATION (LGM), INTERSTADIAL 8 (I8), STADIAL 8 (S8) AND HEINRICH STADIAL 4 (HS4).

	Q(m^3/s)	C(kg/m^3)	Sediment load (kg/s)
LGM T10	230	9,43	2169,78
LGM T100	310	12,74	3948,77
I8 T10	390	6,73	2624,01
I8 T100	530	9,02	4778,16
S8 T10	220	6,61	1453,18
S8 T100	290	8,75	2538,35
HS4 T10	190	8,26	1568,75
HS4 T100	210	9,16	1923,68

At **CS05** (uppermost core position on the VSR), the TC arrives earlier for LGM, then for HS4, then for S8 and finally for I8. Values of horizontal velocity u (in the W-E direction, Fig. 4.15b) show the pattern $u_{LGM} < u_{HS4} < u_{S8} < u_{I8}$ whilst the horizontal velocity v (in the N-S direction, Fig. 4.15c) show the pattern $v_{LGM} > v_{HS4} > v_{S8} > v_{I8}$. The same temporal pattern can be observed for all the 4 periods with a first peak in current thickness (Fig. 4.15d) corresponding to the arrival to the front of the current between 18h and 24h since the beginning of the simulation. The magnitude of the first peak follows the pattern $h_{LGM} > h_{HS4} > h_{S8} > h_{I8}$. A second peak arrives at the same moment for all the climatic periods corresponding to the peak in the river discharge. This second peak shows the same value for all the simulations with a current thickness of about 350m for a T=10yrs and h= 375 for T=100yrs. In terms of instantaneous sediment transport hC (Fig. 4.15e) the temporal evolution show a peak at about 6 hours after the peak of the river discharge concomitant with the second peak in current speed. The climatic pattern of hC is similar to that of h, this is to say $hC_{LGM} > hC_{HS4} > hC_{S8} > hC_{I8}$. Once the peak of intensity has passed the differences between the currents HS4, S8 and I8 are almost negligible.

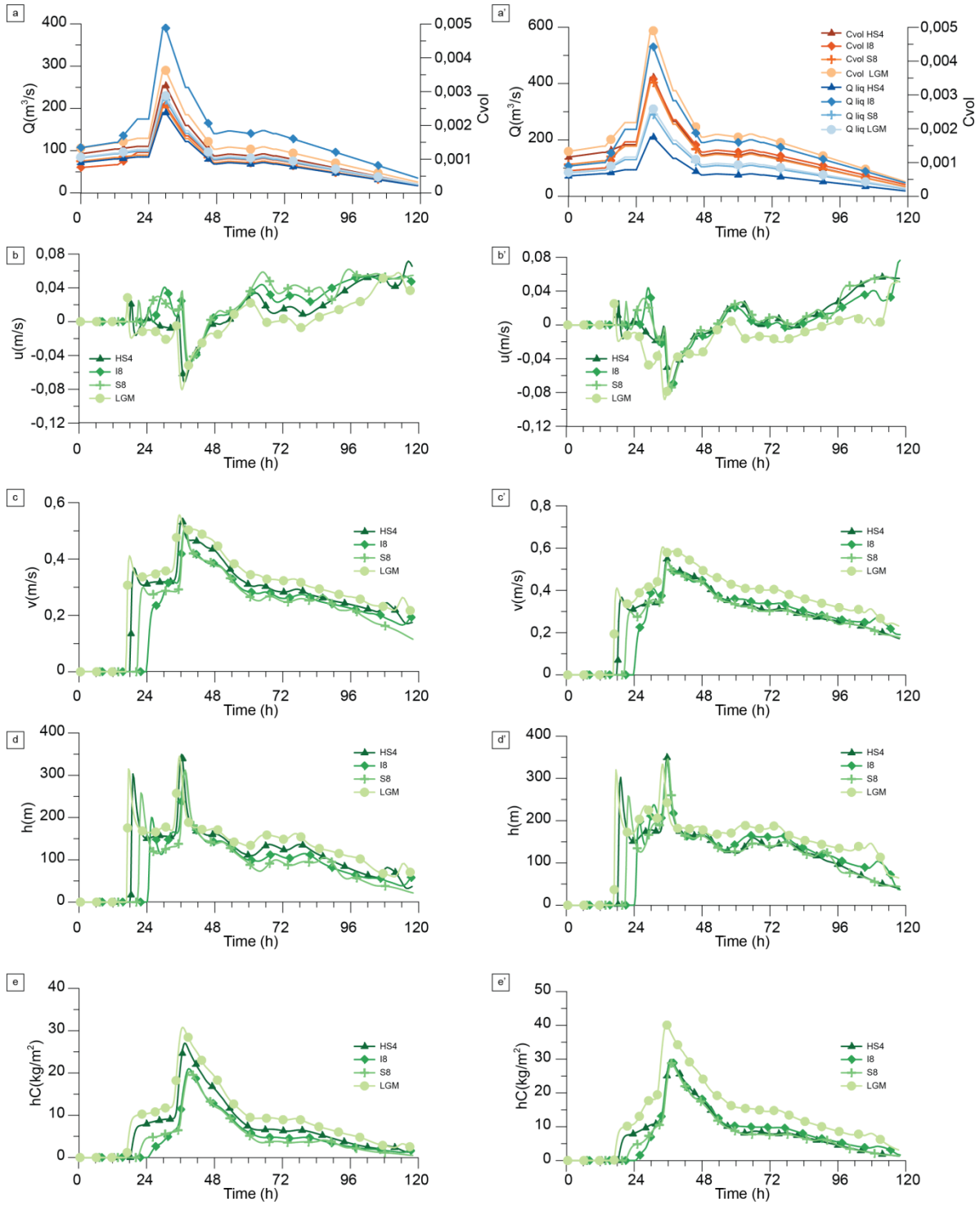

FIG. 4. 15 MODELLING RESULTS AT THE POSITION OF THE CORE **ESSK08-CS05** FOR THE FLASH FLOODS OF RECURRENCE INTERVAL **T= 10** YRS (A, B, C, D, E) **T=100**YRS (A', B', C', D') FOR THE DIFFERENT CLIMATIC PERIODS ANALYSED: LAST MAXIMUM GLACIATION (LGM), INTERSTADIAL 8 (I8), STADIAL 8 (S8) AND HIERNICH STADIAL 4 (HS4). RESULTS ARE SHOWN FOR THE RUNS INCLUDING CORIOLIS FORCES (HN) AND FOR A GRAIN SIZE OF D=50µM. A) & A') LIQUID DISCHARGE (M^3/S) AND VOLUMETRIC CONCENTRATION. B) & B') DEPTH INTEGRATED CURRENT SPEED (X DIRECTION). C) & C') DEPTH INTEGRATED CURRENT SPEED (Y DIRECTION). D) & D') CURRENT THICKNESS (M). E) & E') INSTANTANEOUS SEDIMENT TRANSPORT HC (KG/M^2).

At **KNI22**, the TC arrives earlier for LGM, then for HS4, then for S8 and finally for I8. Values of horizontal velocity u (in the W-E direction, Fig. 4.16b) show the pattern $u_{LGM} > u_{HS4} > u_{S8} > u_{I8}$ whilst the horizontal velocity v (in the N-S direction, Fig. 4.16c) show the pattern $v_{LGM} > v_{HS4} > v_{S8} > v_{I8}$. The same temporal pattern can be observed for all the 4 periods with a first peak in

current thickness (Fig. 4.16d) corresponding to the arrival to the front of the current between 24h and 48h since the beginning of the simulation. The magnitude of the first peak follows the pattern $h_{LGM} > h_{HS4} > h_{S8} > h_{I8}$. Differences in arrival time of the second peak are smaller between the different periods, with 6h delay between LGM's second peak and I8's second peak. This second peak shows the same value for all the simulations with a current thickness of about 250m for a T=10yrs and h= 300m for T=100yrs and it corresponds to the peak in the river discharge.. In terms of instantaneous sediment transport hC (Fig. 4.16e) the temporal evolution show a peak at about 6 hours after the peak of the river discharge concomitant with the second peak in current speed. The climatic pattern of hC is similar to that of h, this is to say $hC_{LGM} > hC_{HS4} > hC_{S8} > hC_{I8}$. Once the peak of intensity has passed the differences between the currents HS4, S8 and I8 are almost negligible.

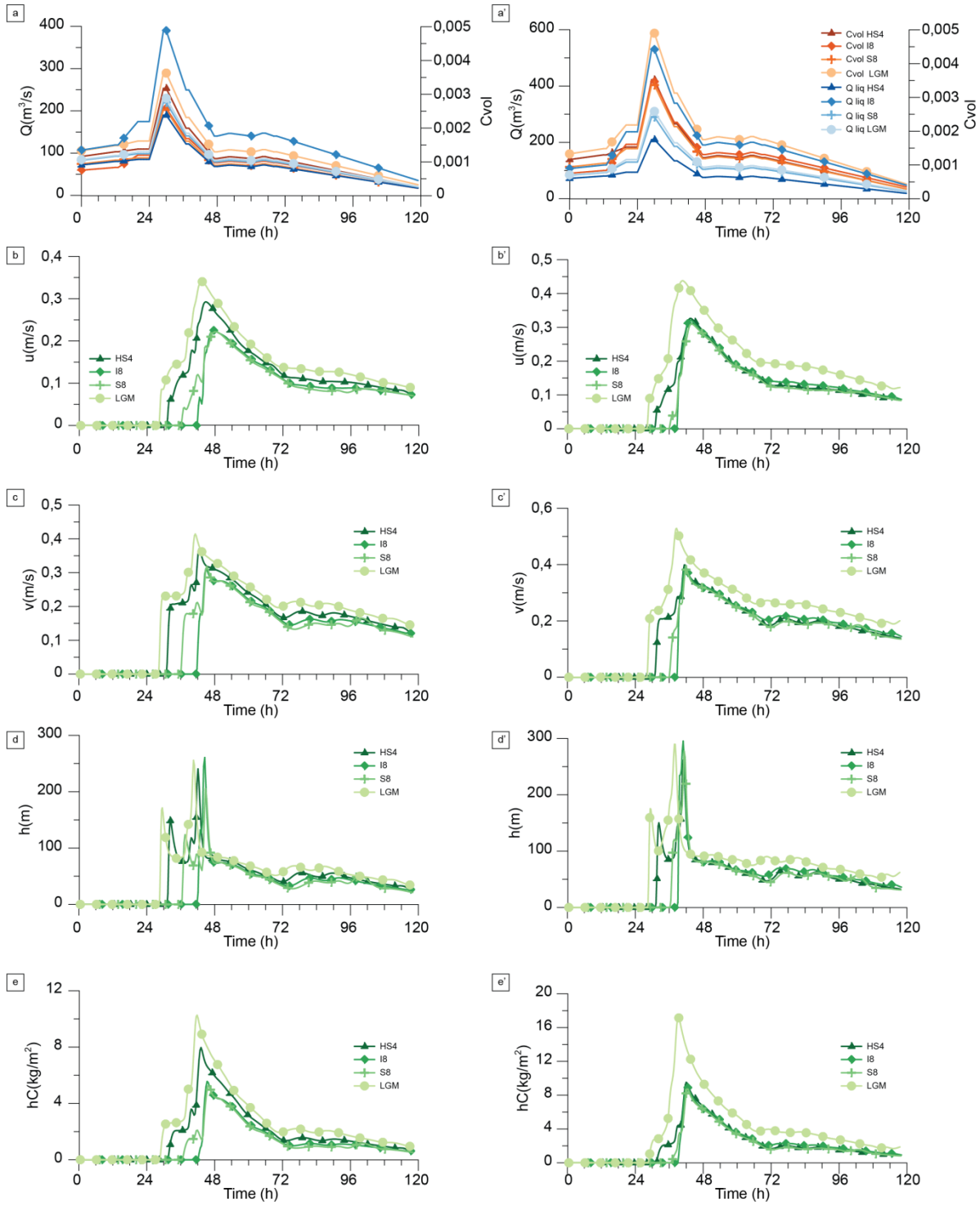

FIG. 4. 16 MODELLING RESULTS AT THE POSITION OF THE CORE KNI22 FOR THE FLASH FLOODS OF RECURRENCE INTERVAL T= 10 YRS (A, B, C, D, E) T=100YRS (A', B', C', D') FOR THE DIFFERENT CLIMATIC PERIODS ANALYSED: LAST MAXIMUM GLACIATION (LGM), INTERSTADIAL 8 (I8), STADIAL 8 (S8) AND HIERNICH STADIAL 4 (HS4). RESULTS ARE SHOWN FOR THE RUNS INCLUDING CORIOLIS FORCES (HN) AND FOR A GRAIN SIZE OF D=50µM. A) & A')LIQUID DISCHARGE (M3/S) AND VOLUMETRIC CONCENTRATION. B) & B') DEPTH INTEGRATED CURRENT SPEED (X DIRECTION). C) & C') DEPTH INTEGRATED CURRENT SPEED (Y DIRECTION). D) & D') CURRENT THICKNESS (M). E) & E') INSTANTANEOUS SEDIMENT TRANSPORT HC (KG/M2).

At **CS01** (distal part of the VSR), the TC arrives earlier for LGM, then for HS4, then for S8 and finally for I8. Values of horizontal velocity u (in the W-E direction, Fig. 4.17b) show the pattern $u_{LGM} > u_{HS4} > u_{S8} > u_{I8}$ whilst the horizontal velocity v (in the N-S direction, Fig. 4.17c) show the pattern $v_{LGM} > v_{HS4} > v_{S8} > v_{I8}$. The time lag differences in the arrival of the event are more evident in this core located in the distal part of the VSR. A single peak is registered for the current thickness

(Fig. 4.17d) corresponding to the arrival to the front of the current between 60h and 78h since the beginning of the simulation for T=10yrs and between 50 and 66h in the cases for T=100yrs. The magnitude of peak follows the pattern $h_{LGM} > h_{HS4} > h_{S8} \sim h_{I8}$. For the cases T=100yrs the differences between HS4, I8 and S8 are negligible as well as between I8 and S8 for T=10yrs. In terms of instantaneous sediment transport hC (Fig. 4.17e) the temporal evolution shows a peak at about 36h for T=10yrs and at about 30h for LGM and 38h for the rest of climatic cases for T=100yrs hours after the peak of the river discharge. The maximum values in hC are concomitant with those of the current thickness. The climatic pattern of hC is similar to that of h, this is to say $hC_{LGM} > hC_{HS4} > hC_{S8} > hC_{I8}$.

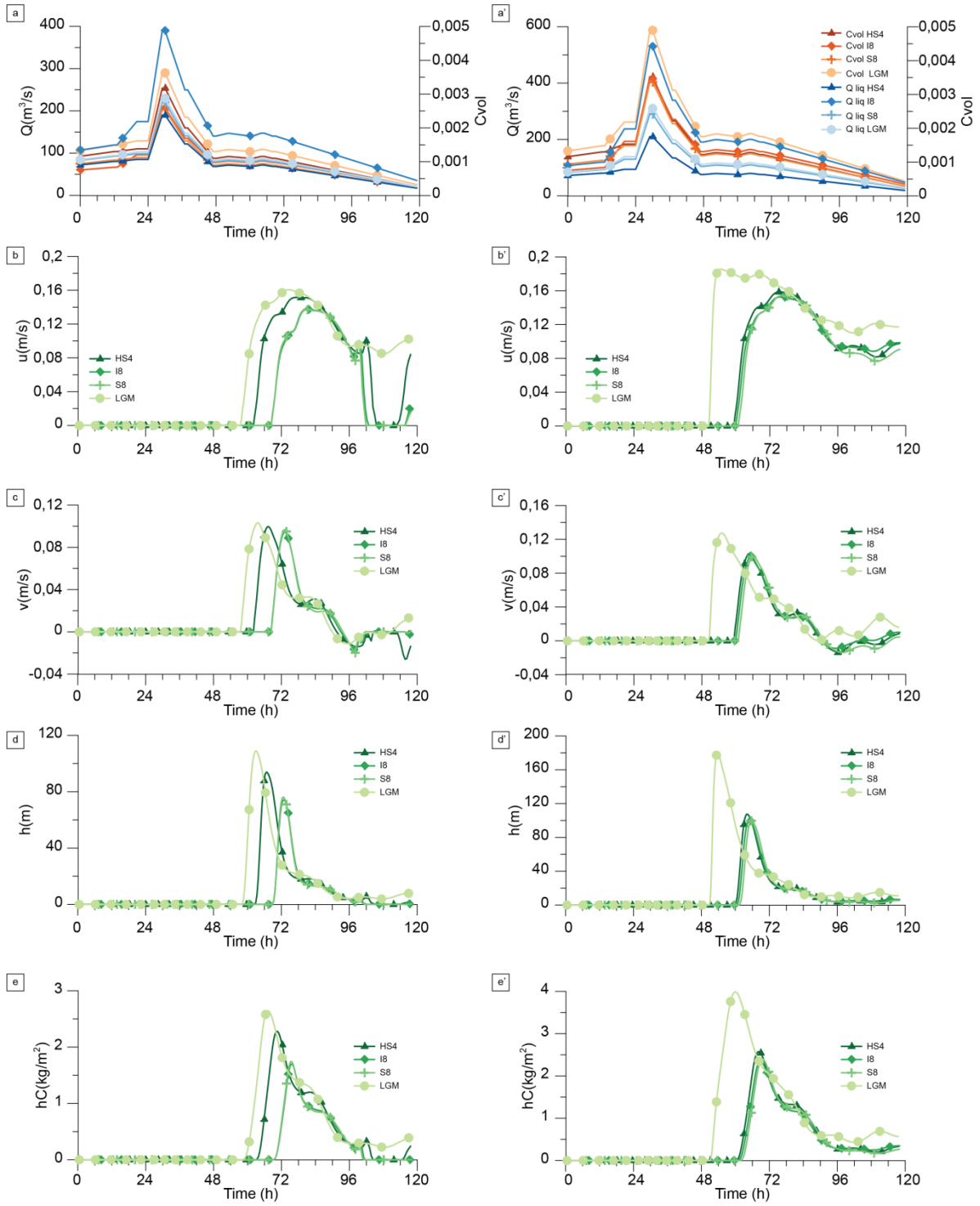

FIG. 4. 17 MODELLING RESULTS AT THE POSITION OF THE CORE ESSK08-CS01 (DISTAL PART OF THE VSR) FOR THE FLASH FLOODS OF RECURRENCE INTERVAL T= 10 YRS (A, B, C, D, E) & T=100YRS (A', B', C', D') FOR THE DIFFERENT CLIMATIC PERIODS ANALYSED: LAST MAXIMUM GLACIATION (LGM), INTERSTADIAL 8 (I8), STADIAL 8 (S8) AND HIERNICH STADIAL 4 (HS4). RESULTS ARE SHOWN FOR THE RUNS INCLUDING CORIOLIS FORCES (HN) AND FOR A GRAIN SIZE OF D=50µM. A) & A')LIQUID DISCHARGE (M3/S) AND VOLUMETRIC CONCENTRATION. B) & B') DEPTH INTEGRATED CURRENT SPEED (X DIRECTION). C) & C') DEPTH INTEGRATED CURRENT SPEED (Y DIRECTION). D) & D') CURRENT THICKNESS (M). E) & E') INSTANTANEOUS SEDIMENT TRANSPORT HC (KG/M2).

4.2.2. Hyperpycnal cases

The results are shown for the points corresponding to the core positions ESSK08-CS05 (Fig. 4.18), KNI22 (Fig. 4.18), ESSK08-CS01 (Fig. 4.19) and ESSK08-CS13 (Fig. 4.19). The results are only presented for the cases when theoretical hyperpycnal flow conditions are reached for T=100yrs. Despite

hyperpycnal conditions being reached at the LGM for T=10yrs, the results are not shown here in order to prevent cluttering since the aim is to compare different climatic periods. The peak liquid discharge, sediment concentration and sediment loading at the source for each one of the climatic periods analysed are given in Table 4.9.

TABLE 4. 8 PEAK LIQUID DISCHARGE (Q) AND PEAK SEDIMENT CONCENTRATION FOR THE RECURRENCE INTERVALS CONSIDERED (C_{RI}). THE SEDIMENT LOAD $q_s = QC_s$ IS ALSO EXPRESSED.

	$Q(m^3/s)$	$C_{RI}\ (kg/m^3)$	$q_{s_{hyper}}(kg/s)$
LGM T10	230	42,5	9775
LGM T100	310	75	23250
I8 T100	530	48	25440
S8 T100	290	53	15370
HS4 T100	210	60	12600

The general pattern observed from the hyperpycnal modelling results is similar to the one found for the base cases: TC present decreasing intensity for LGM, HS4, S8 and I8. In these second set of simulations, current intensity is amplified however the ratio of amplification in the different current values differ to the ratio between the peak concentrations of base and hyperpycnal simulations (i.e. parameter $K = C_{RI}/C_s$ in Table 4.3) due to the non-linear nature of TC. The time lags between the arrival of the event to the different points analysed are reduced since current velocity is greater than in the base cases.

At **CS05** (uppermost core position on the VSR, Fig. 4.18 a, b, c, d, e), and **KNI-22** (middle point along the crest of the VSR, Fig. 4.18 a', b', c', d', e') the TC arrives earlier for LGM, then for HS4, then for S8 and finally for I8. Values of horizontal velocity u (in the W-E direction, Fig. 4.18 b & b') and v (in the N-S direction, Fig. 4.18 c & c') show the pattern $u_{LGM} > u_{HS4} > u_{S8} > u_{I8}$. The same temporal pattern can be observed for all the 4 periods with a sharp first peak in current thickness (Fig. 4.18 d & d') corresponding to the arrival to the front of the current between 6h and 12h since the beginning of the simulation. The magnitude of the first peak follows the pattern $h_{LGM} > h_{HS4} > h_{S8} > h_{I8}$. A second peak arrives at the same moment for all the climatic periods corresponding to the peak in the river discharge. This second peak shows the same value for all the simulations with a current thickness of about 260m for the point CS05 (Fig. 4.18 d) and h= 320m for KNI-22 (Fig. 4.18 d'). In terms of instantaneous sediment transport hC (Fig. 4.18e) the temporal evolution show a peak at about 4 hours after the peak of the river discharge concomitant with the second peak in current speed. The climatic pattern of hC is similar to that of h, this is to say $hC_{LGM} > hC_{HS4} > hC_{S8} > hC_{I8}$. Once the peak of intensity has passed the differences between the currents HS4, S8 and I8 are almost negligible.

At **CS01** (distal part of the VSR, (Fig. 4.19 a, b, c, d, e), and **CS13** (southern flank of the VSR, Fig. 4.19 a',b',c',d',e') the TC arrives earlier for LGM, then for HS4, then for S8 and finally for I8. Values of horizontal velocity u (in the W-E direction, Fig. 4.19 b) and v (in the N-s direction, Fig. 4.19 c) show the pattern $u_{LGM} > u_{HS4} > u_{S8} > u_{I8}$. The same temporal pattern can be observed for all the 4 periods at CS01 with a first peak in current thickness (Fig. 4.19 d) corresponding to the arrival to the front of the current between 18h and 32h since the beginning of the simulation. The magnitude of the first peak follows the pattern $h_{LGM} > h_{HS4} > h_{S8}$. However at the point CS01, the magnitude of the first peak due to the arrival of the TC is less important than that of the base simulations (Fig. 4.17). And in some cases is even inexistent as for the I8. A second peak arrives at the same moment for all the climatic periods at CS01 corresponding to the peak in the river discharge. This second peak shows the same value for all the simulations with a current thickness of about 560m for the point CS01. In terms of instantaneous sediment transport hC (Fig. 4.19 e) the temporal evolution show a peak at about 3 hours after the peak of the river discharge concomitant with the second peak in current speed. The climatic pattern of hC is similar to that of h, this is to say $hC_{LGM} > hC_{HS4} >$

$hC_{S8} > hC_{I8}$. Once the peak of intensity has passed the differences between the currents HS4, S8 and I8 are almost negligible. TC at CS13 (Fig. 4.19 a', b', c', d', e') follow the general trend of less intense currents for interstadials and more important currents for stadials, then HS4 and then LGM. However the temporal evolution at CS13 is radically different since the different variables analysed show a periodicity according to the modelling results. Current thickness (Fig. 4.19 d') reaches values of up to 550m for the LGM and HS4 whilst for the I8 current thickness is lower than 100m. Values of instantaneous sediment transport (Fig. 4.19 e') for the LGM are about 4 times those of the HS4.

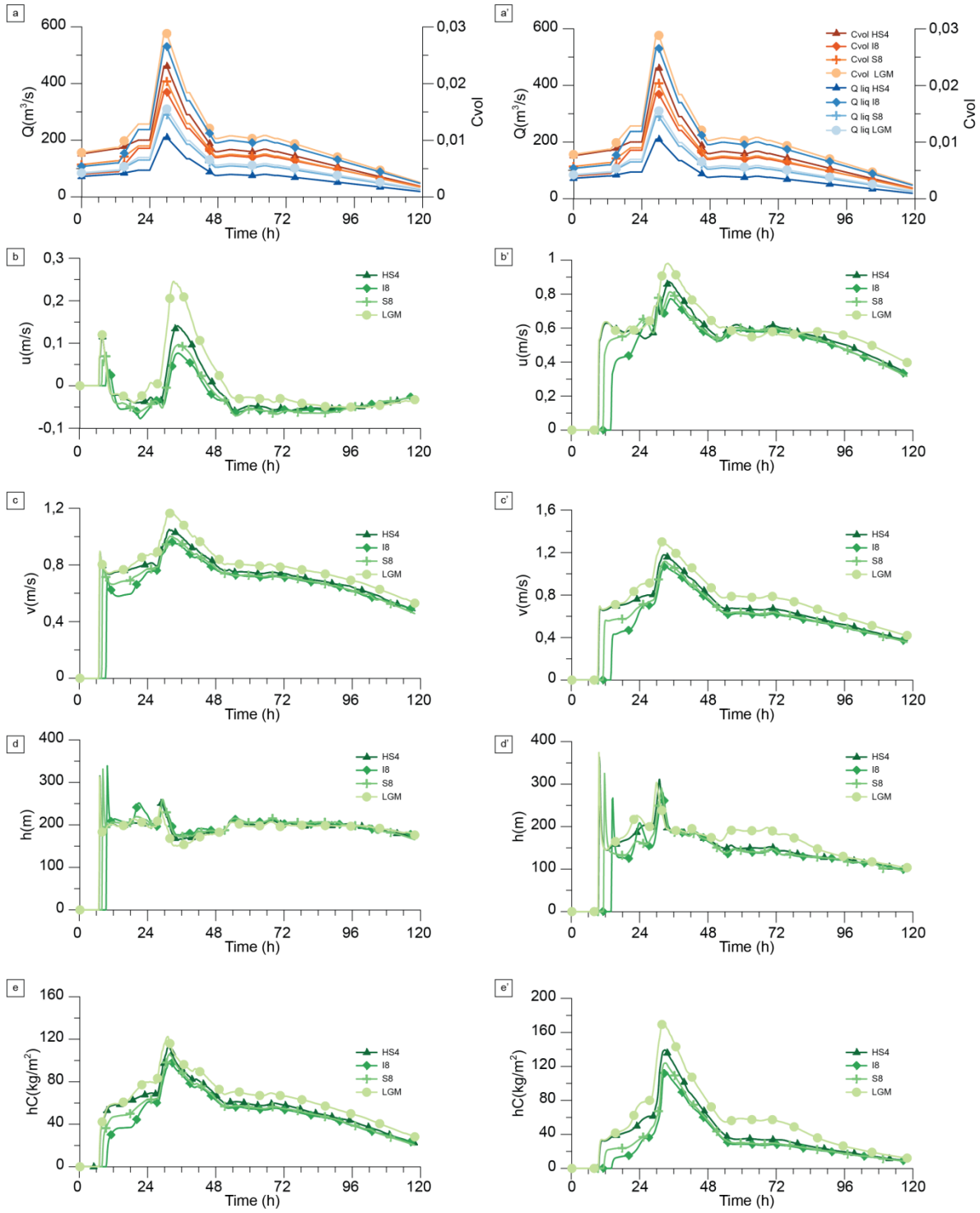

FIG. 4. 18 MODELLING RESULTS FOR THE FLASH FLOODS OF RECURRENCE INTERVAL T=100YRS AT THE CORE POSITIONS ESSK08-CS05 (UPPERMOST PART OF THE VSR) (A, B, C, D, E) & KNI22 (MIDDLE POSITION ALONG THE VSR CREST) (A', B', C', D') FOR THE DIFFERENT CLIMATIC PERIODS ANALYSED: LAST MAXIMUM GLACIATION (LGM), INTERSTADIAL 8 (I8), STADIAL 8 (S8) AND HEINRICH STADIAL 4 (HS4). RESULTS ARE SHOWN FOR THE RUNS INCLUDING CORIOLIS FORCES (HN) AND FOR A GRAIN SIZE OF D=50μM. A) & A')LIQUID DISCHARGE (M3/S) AND VOLUMETRIC CONCENTRATION. B) & B') DEPTH INTEGRATED CURRENT SPEED (X DIRECTION). C) & C') DEPTH INTEGRATED CURRENT SPEED (Y DIRECTION). D) & D') CURRENT THICKNESS (M). E) & E') INSTANTANEOUS SEDIMENT TRANSPORT HC (KG/M2).

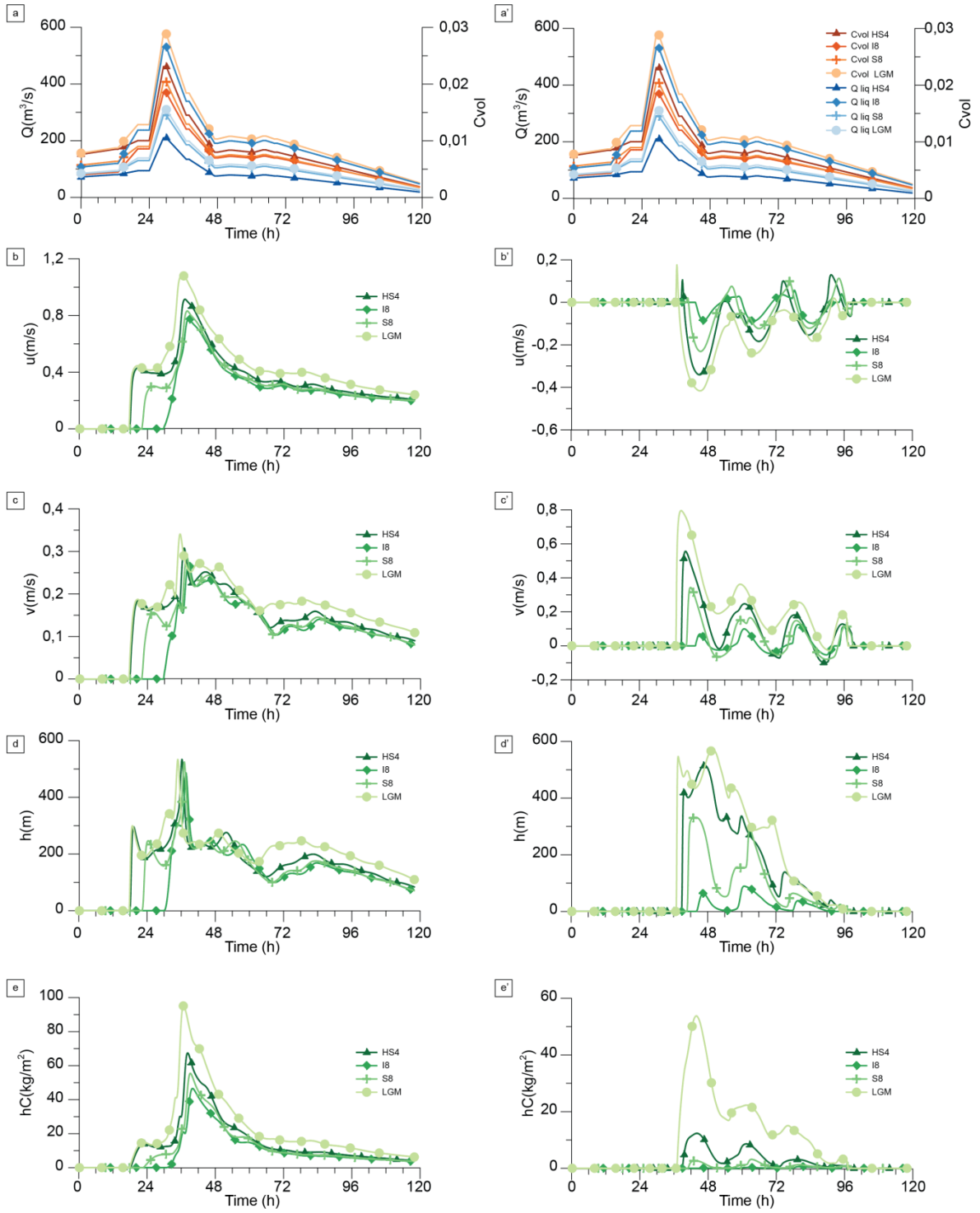

FIG. 4. 19 MODELLING RESULTS FOR THE FLASH FLOODS OF RECURRENCE INTERVALT=100YRS AT THE CORE POSITIONS ESSK08-CS01 (DISTAL PART OF THE VSR) (A, B, C, D, E) & ESSK08-CS13 (SOUTHERN FLANK OF THE VSR) (A', B', C', D') FOR THE DIFFERENT CLIMATIC PERIODS ANALYSED: LAST MAXIMUM GLACIATION (LGM), INTERSTADIAL 8 (I8), STADIAL 8 (S8) AND HEINRICH STADIAL 4 (HS4). RESULTS ARE SHOWN FOR THE RUNS INCLUDING CORIOLIS FORCES (HN) AND FOR A GRAIN SIZE OF D=50μM. A) & A')LIQUID DISCHARGE (M3/S) AND VOLUMETRIC CONCENTRATION. B) & B') DEPTH INTEGRATED CURRENT SPEED (X DIRECTION). C) & C') DEPTH INTEGRATED CURRENT SPEED (Y DIRECTION). D) & D') CURRENT THICKNESS (M). E) & E') INSTANTANEOUS SEDIMENT TRANSPORT HC (KG/M2).

The previous results are summarised in the boxplot of Fig. 4.20. with whiskers with maximum 1.5 interquartile range for the current thickness and for the sediment transport. For a given climatic period, the range of variation for the mean and between maximum and minimum period is smaller for the cores ESSK08-CS05 and KNI-22. On the other hand, the cores ESSK08-CS01 and ESSK08-CS13

present a larger range of variation for the current thickness, as the length of the segments shows. The model results show a light climatic modulation for the mean values with more intense currents for the LGM and HS4.

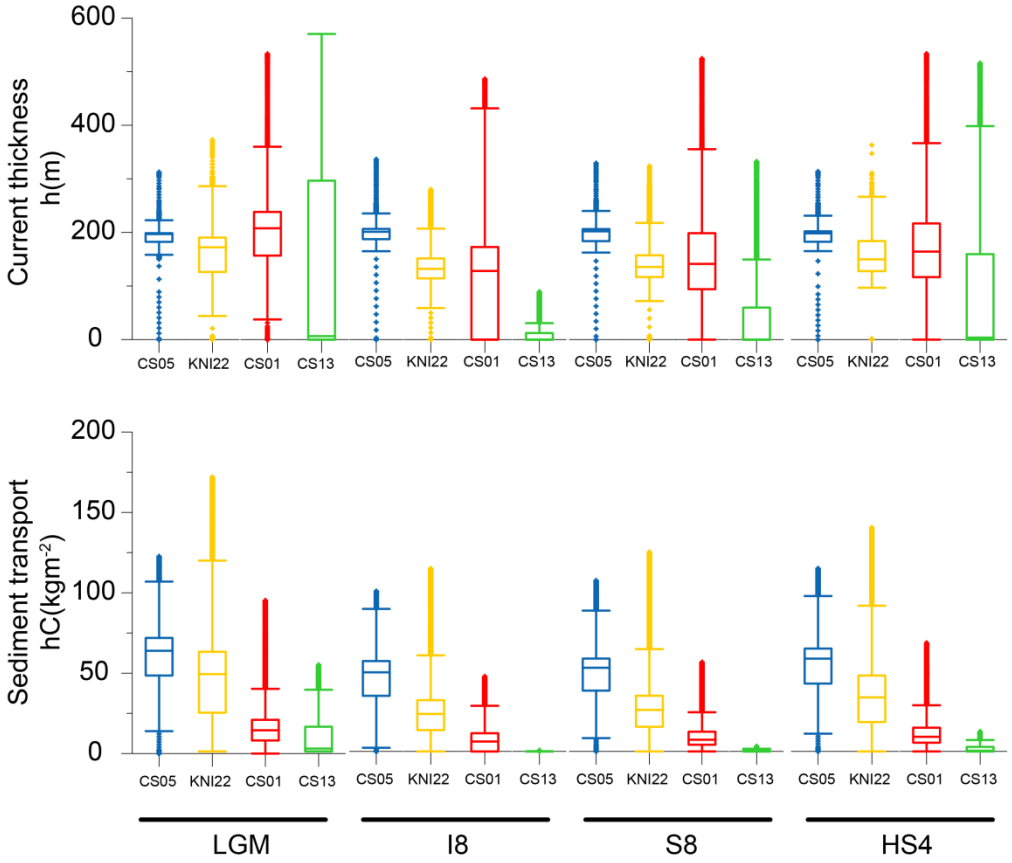

FIG. 4. 20 BOXPLOTS SUMMARIZING THE MODEL RESULTS IN TERMS OF CURRENT SPEED, CURRENT THICKNESS AND INSTANTANEOUS SEDIMENT TRANSPORT FOR THE CLIMATIC PERIODS ANALYSED AT THE CORE POSITIONS ESSK08-CS05, KNI22, ESSK08-CS01 AND ESSK08-CS13. LGM: LAST MAXIMUM GLACIATION, S8: STADIAL 8, I8: INTERSTADIAL 8 AND HS4: HEINRICH STADIAL 4.

The temporal evolution of the sediment flux $hCU(kgm^{-1}\ s^{-1})$ for the flood LGM QT100 is shown in Fig. 4.21. A minor part of the TC flows through the WSC at the first stages of the simulation. Most of the TC continues its path along the VSR. The TC overflows the VSR initially at the distal part where the height of the VSR is lowest. In later stages, the TC would overflow the VSR along its entire length. On the southern flank three preferential paths can be identified (Fig. 21. c & d). The TC bends to the right (south-west) at the most distal part of the VSR.

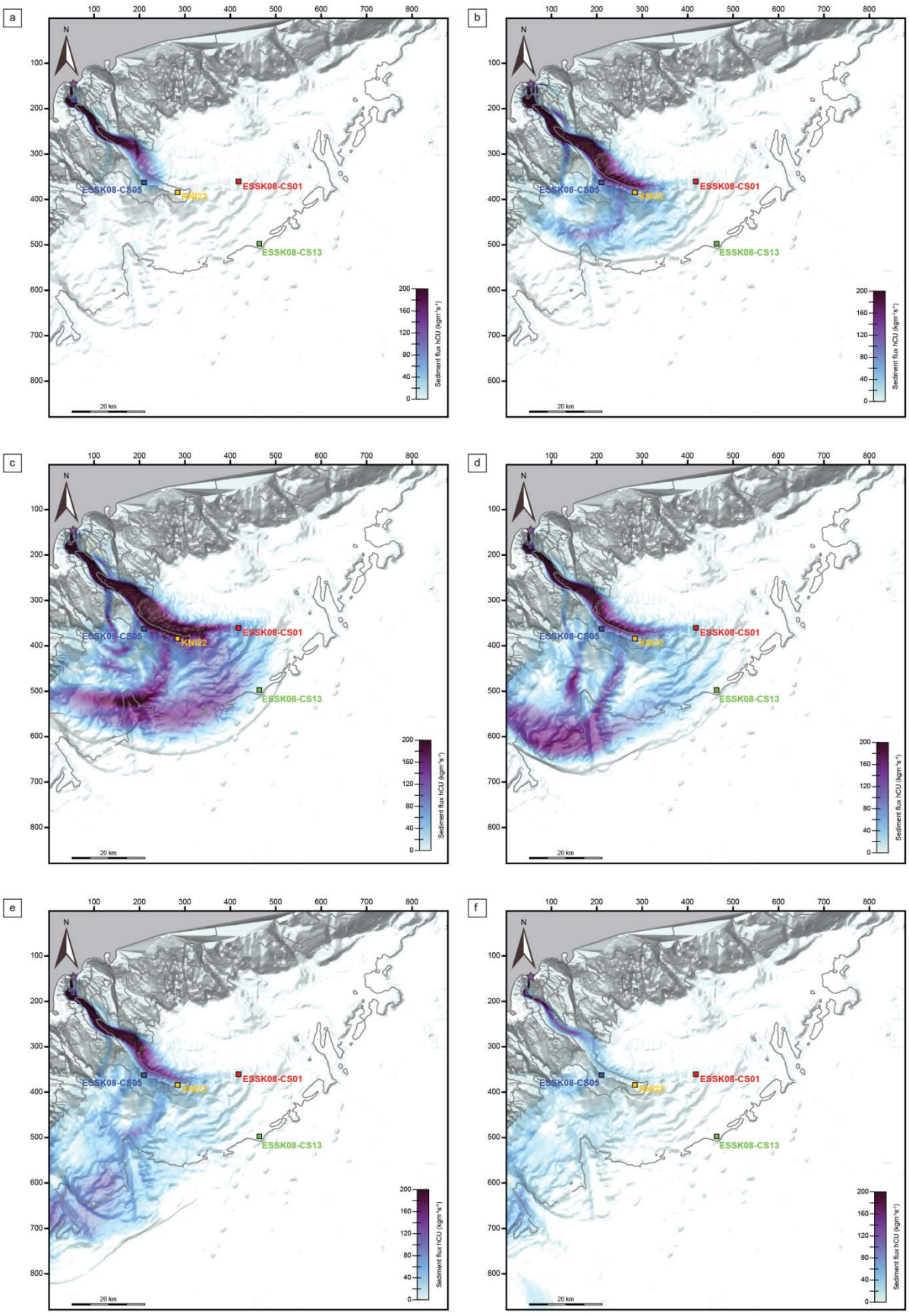

FIG. 4. 21 MODEL RESULTS IN TERMS OF SEDIMENT FLUX $hCU(kgm^{-1}\,s^{-1})$ FOR THE FLASH FLOOD OF RECURRENCE INTERVAL 100YRS AT THE LGM (LAST GLACIAL MAXIMUM). SUCCESSIVE PANELS REPRESENT MODEL RESULTS FOR: A) $t = 8h$; B) $t = 26h$; C) $t = 40h$; D) $t = 49h$; E)$t = 67h$ & F) $t = 111h$.

5. Discussion

5.1. 2008 flood

5.1.1. Without Coriolis

Modelling results at the mooring points are largely influenced by the sediment load provided by the different laws. The non-linear nature of TC is evidenced by the absence of a linear relationship between the input forcing and the results obtained at the different points. The modelling results obtained for different laws (i.e. Mulder, Laurent, Bonneau and Bonneau2) can differ up to ~10 times, whilst the ratio between the different laws is of about 4, however the different power laws perform similarly in terms of temporal evolution. The best estimation of the current values is the one obtained for the input conditions provided by Bonneau (2014) (see Fig. 4.11). Estimated maximum current speed and current thickness from field mooring data (Khripounoff et al., 2012) considering quasi-stationary conditions provide values that are half the value of the ones obtained here (h~150 vs. h=326m and U=0.37m/s vs. U~1m/s). The time scale of the current and the sediment concentration (C~0.5g/l) seems accurate. To date, best modelling results are found for the most recent relationship proposed by (Bonneau, 2014). In the present simulations, the sediment concentration input is obtained from the best fitting law. However, the relationship between sediment concentration and liquid discharge (see Fig. 4.4) shows that for single value of liquid discharge the possible values of sediment concentration can vary by up to four orders of magnitude. Given the results obtained, the 2008 event might correspond to the lower bound of the data shown in Fig. 4.4. Part of the observed discrepancy can be caused by not considering Coriolis effects in the simulations presented in Fig. 4.12 that might be at play given the low velocity values obtained.

5.1.2. With Coriolis effects

Coriolis seem to play a major role in the construction of the VSR since it deflects the flow to the right (i.e. to the west) contributing together with the centrifugal forces and the overflow of the VSR. The influence of Coriolis forces has been acknowledged for long time in the system (Piper and Savoye, 1993; Jorry et al., 2011) however its implications have not been studied yet. Simulations performed without Coriolis (latitude= 0°) show a spatial pattern of evolution of the TC that is quasi-symmetric. Once the mid valley is reached the current spreads and its propagation is mainly controlled by the bathymetry (i.e. slope). On the other hand, when Coriolis effects are considered, the flow is deflected to the right (i.e. west) by both centrifugal and Coriolis forces. Both forces contribute to the lateral tilt of the interface of the TC and to the overflow on the right hand side and hence to the construction of the VSR. Part of the flow is drained through the WSC. The core KV10 (Mulder et al., 2001b) located on a terrace in the inner part of the upper middle valley that opens to the WSC (Fig. 4.7) registers frequent hyperpycnal activity at present day (Mulder et al., 2001b; Mas et al., 2010). The low magnitude, high frequency (yearly) hyperpycnal currents do not seem to have a strong control on the sediment deposition or canyon morphology (Mas et al., 2010), since they didn't propagate down the VSR. According to the modelling results obtained here, these very low magnitude flows may be strongly influenced by Coriolis due to their low velocity and be deflected to the right through the WSC. In fact, a core located in the WSC (i.e. core KCA-3 in Piper and Savoye (1993), see Fig. 4.7. for location) presents very thin silty and sandy laminae corresponding to Holocene records.

Simulations not considering Coriolis show an even spatial distribution of sediment deposition. Cores located on the continuation of the north eastern slope (i.e. cores KM07 and KCA-04 in Piper and Savoye (1993), Fig. 4.7) challenge the even distribution of sediment that is suggested by simulations without Coriolis. Holocene turbidites are missing and the distribution of the existent sandy turbidites suggests an origin linked to the eastern part of the continental shelf. The effect of Coriolis and centrifugal forces on the construction of the VSR would be eventually favoured by the thermohaline circulation flowing westward that is not considered in the present study simulations. The results

obtained indicate that at mid-latitudes a TC can potentially propagate along the lower part of the continental slope exclusively due to Coriolis forces without interaction with contour currents.

The effects of Coriolis forces seem to have a minor effect on the upper part of the canyon (i.e. mooring locations). The discrepancy observed between the model results and the measurements is more likely to be due to the input conditions imposed at the river mouth.

5.2.Hyperpycnal flows at different climatic periods

The TC triggered by the conditions imposed at the source reproduces, for both base and hyperpycnal cases, a trend coherent to the one registered in the sedimentary record: larger magnitude currents are present at LGM, HS4, S8 and I8 according to the same trend in the sediment concentration for the different climatic periods. The very thin deposits issued by the base cases would potentially be eroded by larger magnitude flows and hence wouldn't leave a trace in the sedimentary record. As such, focus is given to the outputs from the hyperpycnal cases; however, the climatic magnitude pattern is similar for base and hyperpycnal cases. For all the cores (except for ESSK08-CS13) larger depositions are found for the LGM, followed by the HS4 and S8 and lower values are found for the I8. The O(10) μm sediment thickness that is deposited falls within the order of magnitude needed for the sedimentation rates found in the cores. For a single climatic period the depositions obtained at the different cores do not seem to follow the same spatial pattern as the sedimentation rates. This is due to the difficulty in relating a single event with the sedimentation rate for a whole climatic period.

The simulations performed correspond to the mean relationship for a given period provided by the laws of (Bonneau, 2014). The scattering of the distribution is not taken into account in those laws. An attempt was made in order to consider the upper bound of the distribution by applying those same laws at the source but increased by a factor including the relationship between the concentration given by the base laws and the peak concentration for a given recurrence interval (i.e. hyper simulations). The results in terms of trends are similar to those of the base cases however the thickness deposited is more accurate. A more precise analysis of the outputs of Hydrotrend may establish more accurate conditions at the river mouth and could solve at least partly the inaccuracies found.

The conditions at the river mouth are largely unknown not only in terms of Q-Cs but also in terms of temporal evolution and duration of flash flood events. Hyperpycnal flows tend to mimic the rising and falling phase of the hydrographs of the river discharge (Mulder et al., 2003). The results of the present study and other recent studies (Khripounoff et al., 2012; Liu et al., 2012) show that a single flood peak can generate a flow with multiple pulses. However at the uppermost part of the system the TC highly correlates with the shape of the hydrograph. As such, I suppose that at the uppermost part of the system the shape of the hydrograph largely influences the TC whilst on the distal part of the system its influence is completely unknown. The shape of the hydrograph depends on the catchment and on the duration and intensity of the rain. Whilst the catchment is well known the two latter are not well defined and are largely unknown for ancient times. The duration of the flash flood may play an important role in terms of deposition along the VSR. Snow-melting floods would *a priori* show a longer duration than autumn floods, however this parameter is largely unknown. The sensitivity tests performed suggest that the duration of the flood has no influence on the magnitude of the different variables since they seem to reach a threshold; however, it can have an effect on the final deposition since the total quantity of sediment transported is larger.

The unknowns for the source are not limited to the conditions at the river mouth. The processes at the interface river mouth / TC are highly non-linear and not completely understood. The boundary conditions imposed were established on the basis of conservation of sediment load ($Q \cdot C_s$) between the river mouth and the TC, that is to say, the discharge and concentration at the TC source point are those of the river. Settling processes, which will largely depend on the grain size (i.e. settling velocity), can modify the combination of values of liquid discharge and sediment concentration, modifying the sediment load, and hence trigger TC that would potentially have a different behaviour.

6. Conclusion

The present study presents the first attempt to simulate the evolution and deposition of hyperpycnal flows in the Var Sedimentary System. The influence of Coriolis in spatial evolution of TC and hence in the construction of the VSR is evidenced for the first time. The simulations performed well in terms of intensity of the TC for the different climatic periods with high intensity TC during the LGM and the stadials of the D/O and HS and lower intensity during the interstadials of the D/O. However the differences shown by the numerical results between the different climatic periods are not as accentuated as those of the sedimentary record. The main reason for this fact might be the input conditions imposed at the source. The relationships $Q - C_s$ used in the present study provide a "mean" value of concentration for a given liquid discharge. A detailed statistical analysis could improve the conditions inland. At the interface river mouth/TC the processes are not fully understood. As such, the conditions at the source, both inland and the interface, demand further research. For the different cases analysed the model results reproduce qualitatively the sedimentation trends. The results cannot be considered of predictive quality mainly because forcing conditions demand further research both in terms of physical processes at the interface river/TC and of statistical analysis for the determination of sediment concentration at the river mouth. The numerical model proves to be a valuable tool to test hypotheses of functioning based on field evidence, such as the major role played by Coriolis forces in the development of the VSR.

References

Bonneau, L., 2014. Impact des oscillations climatiques rapides du dernier cycle glaciaire sur l'érosion et les transferts sédimentaires dans le sud des Alpes (SE France). Paris 6.

Bonneau, L., Jorry, S.J., Toucanne, S., Jacinto, R.S., Emmanuel, L., 2014. Millennial-scale response of a western Mediterranean river to late quaternary climate changes: A view from the deep sea. J. Geol. 122, 687–703. doi:10.1086/677844

Bourcart, J., 1962. La Méditerranée et la révolution du Pliocène. Livre À Mém. Profr. P FALLOT 1, 103–116.

Cossu, R., Wells, M.G., Wåhlin, A.K., 2010. Influence of the Coriolis force on the velocity structure of gravity currents in straight submarine channel systems. J. Geophys. Res. Oceans 115, C11016. doi:10.1029/2010JC006208

Cossu, R., Wells, M.G., 2013. The evolution of submarine channels under the influence of Coriolis forces: experimental observations of flow structures. Terra Nova 25, 65–71. doi:10.1111/ter.12006

Cossu, R., Wells, M.G., Peakall, J., 2015. Latitudinal variations in submarine channel sedimentation patterns: the role of Coriolis forces. J. Geol. Soc. 172, 161–174. doi:10.1144/jgs2014-043

Covault, J.A., Romans, B.W., Fildani, A., McGann, M., Graham, S.A., 2010. Rapid climatic signal propagation from source to sink in a southern California sediment-routing system. J. Geol. 118, 247–259. doi:10.1086/651539

Dan, G., Sultan, N., Savoye, B., 2007. The 1979 Nice harbour catastrophe revisited: Trigger mechanism inferred from geotechnical measurements and numerical modelling. Mar. Geol. 245, 40–64. doi:10.1016/j.margeo.2007.06.011

Dubar, M., Anthony, E.J., 1995. Holocene environmental change and river-mouth sedimentation in the Baie des Anges, French Riviera. Quat. Res. 43, 329–343. doi:10.1006/qres.1995.1039

Gennesseaux, M., 1962. Les canyons de la Baie des Anges, leur remplissage sedimentaire et leur role dans la sedimentation profonde. Comptes Rendus Hebd. Seances Acad. Sci. Serie D 254, 2409.

Gennesseaux, M., Mauffret, A., Pautot, G., 1980. Les glissements sous-marins de la pente continentale niçoise et la rupture des câbles en mer Ligure (Méditerranée occidentale). C R Acad Sci Paris Série D, 959–962.

Jacinto, R.S., Burel, D., 2003. Modélisation du devenir à court terme des boues de dragage rejetées par clapage. Rev. Fr. Génie Civ. 7, 1151–1166. doi:10.1080/12795119.2003.9692539

Jorry, S.J., Jégou, I., Emmanuel, L., Silva Jacinto, R., Savoye, B., 2011. Turbiditic levee deposition in response to climate changes: The Var Sedimentary Ridge (Ligurian Sea). Mar. Geol. 279, 148–161. doi:10.1016/j.margeo.2010.10.021

Kelner, M., Migeon, S., Tric, E., Couboulex, F., Dano, A., Lebourg, T., Taboada, A., 2016. Frequency and triggering of small-scale submarine landslides on decadal timescales: Analysis of 4D bathymetric data from the continental slope offshore Nice (France). Mar. Geol. 379, 281–297. doi:10.1016/j.margeo.2016.06.009

Khripounoff, A., Vangriesheim, A., Crassous, P., Etoubleau, J., 2009. High frequency of sediment gravity flow events in the Var submarine canyon (Mediterranean Sea). Mar. Geol. 263, 1–6. doi:10.1016/j.margeo.2009.03.014

Khripounoff, A., Crassous, P., Lo Bue, N., Dennielou, B., Silva Jacinto, R., 2012. Different types of sediment gravity flows detected in the Var submarine canyon (northwestern Mediterranean Sea). Prog. Oceanogr. 106, 138–153. doi:10.1016/j.pocean.2012.09.001

Klaucke, I., Savoye, B., Cochonat, P., 2000. Patterns and processes of sediment dispersal on the continental slope off Nice, SE France. Mar. Geol. 162, 405–422. doi:10.1016/S0025-3227(99)00063-8

Laurent, R., 1971. Charge solide en suspension et géochimie dans une fleuve côtier méditerranéen. le Var (Alpes- Maritimes) (Thèse troisième cycle de sédimentologie). Nice.

Leopold, L.B., Maddock Jr, T., 1953. The hydraulic geometry of stream channels and some physiographic implications.

Liu, J.T., Wang, Y.-H., Yang, R.J., Hsu, R.T., Kao, S.-J., Lin, H.-L., Kuo, F.H., 2012. Cyclone-induced hyperpycnal turbidity currents in a submarine canyon. J. Geophys. Res. Oceans 117, C04033. doi:10.1029/2011JC007630

Mas, V., 2009. Caractérisation de l'activité hydrosédimentaire dans le système turbiditique du Var (NO Méditerranée) et de son enregistrement dans l'archive sédimentaire. Bordeaux 1.

Mas, V., Mulder, T., Dennielou, B., Schmidt, S., Khripounoff, A., Savoye, B., 2010. Multiscale spatio-temporal variability of sedimentary deposits in the Var turbidite system (North-Western Mediterranean Sea). Mar. Geol. 275, 37–52. doi:10.1016/j.margeo.2010.04.006

Maxworthy, T., 1999. The dynamics of sedimenting surface gravity currents. J. Fluid Mech. 392, 27–44. doi:10.1017/S002211209900556X

Migeon, S., 2000. Dunes géantes et levées sédimentaires en domaine marin profond : Approches morphologique, sismique et sédimentologique. (Ph.D. Thesis). Univ. Bordeaux 1. doi:10.1016/j.margBordeaux 1.

Migeon, S., Savoye, B., Faugeres, J.-C., 2000. Quaternary development of migrating sediment waves in the Var deep-sea fan: Distribution, growth pattern, and implication for levee evolution. Sediment. Geol. 133, 265–293. doi:10.1016/S0037-0738(00)00043-9

Migeon, S., Savoye, B., Zanella, E., Mulder, T., Faugères, J.-C., Weber, O., 2001. Detailed seismic-reflection and sedimentary study of turbidite sediment waves on the Var Sedimentary Ridge (SE France): Significance for sediment transport and deposition and for the mechanisms of sediment-wave construction. Mar. Pet. Geol. 18, 179–208. doi:10.1016/S0264-8172(00)00060-X

Migeon, S., Mulder, T., Savoye, B., Sage, F., 2006. The Var turbidite system (Ligurian Sea, northwestern Mediterranean) - morphology, sediment supply, construction of turbidite levee and sediment waves: Implications for hydrocarbon reservoirs. Geo-Mar. Lett. 26, 361–371. doi:10.1007/s00367-006-0047-x

Migeon, S., Mulder, T., Savoye, B., Sage, F., 2012. Hydrodynamic processes, velocity structure and stratification in natural turbidity currents: Results inferred from field data in the Var Turbidite System. Sediment. Geol. 245–246, 48–62. doi:10.1016/j.sedgeo.2011.12.007

Mulder, T., Alexander, J., 2001. The physical character of subaqueous sedimentary density flows and their deposits. Sedimentology 48, 269–299. doi:10.1046/j.1365-3091.2001.00360.x

Mulder, T., Tisot, J.-P., Cochonat, P., Bourillet, J.-F., 1994. Regional assessment of mass failure events in the Baie des Anges, Mediterranean Sea. Mar. Geol. 122, 29–45. doi:10.1016/0025-3227(94)90203-8

Mulder, T., Syvitski, J.P.M., 1995. Turbidity currents generated at river mouths during exceptional discharges to the world oceans. J. Geol. 103, 285–299.

Mulder, T., Savoye, B., Syvitski, J., Parize, O., 1997a. Des courants de turbidité hyperpycnaux dans la tête du canyon du Var ? Données hydrologiques et observations de terrain. Ocean. Acta 20, 607–626.

Mulder, T., Savoye, B., Syvitski, J.P.M., 1997b. Numerical modelling of a mid-sized gravity flow: the 1979 Nice turbidity current (dynamics, processes, sediment budget and seafloor impact). Sedimentology 44, 305–326. doi:10.1111/j.1365-3091.1997.tb01526.x

Mulder, T., Savoye, B., Piper, D.J.W., Syvitski, J.P.M., 1998. The Var submarine sedimentary system: understanding Holocene sediment delivery processes and their importance to the geological record. Geol. Soc. Lond. Spec. Publ. 129, 145–166. doi:10.1144/GSL.SP.1998.129.01.10

Mulder, T., Migeon, S., Savoye, B., Faugères, J.-C., 2001a. Inversely graded turbidite sequences in the deep Mediterranean: a record of deposits from flood-generated turbidity currents? Geo-Mar. Lett. 21, 86–93. doi:10.1007/s003670100071

Mulder, T., Migeon, S., Savoye, B., Jouanneau, J.-M., 2001b. Twentieth century floods recorded in the deep Mediterranean sediments. Geology 29, 1011–1014. doi:10.1130/0091-7613(2001)029<1011:TCFRIT>2.0.CO;2

Mulder, T., Syvitski, J.P.M., Migeon, S., Faugères, J.-C., Savoye, B., 2003. Marine hyperpycnal flows: Initiation, behavior and related deposits. A review. Mar. Pet. Geol. 20, 861–882. doi:10.1016/j.marpetgeo.2003.01.003

Nakajima, T., Itaki, T., 2007. Late Quaternary terrestrial climatic variability recorded in deep-sea turbidites along the Toyama Deep-Sea Channel, central Japan Sea. Palaeogeogr. Palaeoclimatol. Palaeoecol. 247, 162–179. doi:10.1016/j.palaeo.2006.11.028

Nof, D., 1996. Rotational turbidity flows and the 1929 Grand Banks earthquake. Deep-Sea Res. Part 1 Oceanogr. Res. Pap. 43, 1143–1163.

Parsons, J.D., Bush, J.W.M., Syvitski, J.P.M., 2001. Hyperpycnal plume formation from riverine outflows with small sediment concentrations. Sedimentology 48, 465–478. doi:10.1046/j.1365-3091.2001.00384.x

Piper, D.J.W., Savoye, B., 1993. Processes of late Quaternary turbidity current flow and deposition on the Var deep-sea fan, north-west Mediterranean Sea. Sedimentology 40, 557–582. doi:10.1111/j.1365-3091.1993.tb01350.x

Sage, L., 1976. La sédimentation à l'embouchure d'un fleuve côtier méditerranéen: le Var (Ph.D. Thesis). Université de Nice, Nice.

Savoye, B., Piper, D.J.W., 1991. The Messinian event on the margin of the Mediterranean Sea in the Nice area, southern France. Mar. Geol. 97, 279–304. doi:10.1016/0025-3227(91)90121-J

Savoye, B., Piper, D.J.W., Droz, L., 1993. Plio-Pleistocene evolution of the Var deep-sea fan off the French Riviera. Mar. Pet. Geol. 10, 550–571. doi:10.1016/0264-8172(93)90059-2

Talling, P.J., 2014. On the triggers, resulting flow types and frequencies of subaqueous sediment density flows in different settings. Mar. Geol. 352, 155–182. doi:10.1016/j.margeo.2014.02.006

Supplementary information

Grain size sensitivity tests

Grain size sensitivity tests are performed covering the range of grain size of silts and fine sand (i.e. sediment susceptible of being transported in suspension since larger sand is supposed to be transported as bedload). No Coriolis influence was taken into account for the grain size sensitivity tests. The outputs of the grain sensitivity tests are presented for the points corresponding to the instrumented moorings (i.e. VE, VV and VA) and for three of the core positions (ESSK08-CS05, ESSK08-CS01 and ESSK08-CS13) analysed in the present study and are shown in Sup. Fig. 4.1 (points VE and VV), Fig. 4.2 (points VA and ESSK08-CS05) and Sup. Fig 4.3. (points ESSK08-CS01 and ESSK08-CS13). The grain size influence is more important in the distal parts of the current, TC with larger grain sizes are slower and less intense than those with finer grain size. The grain size chosen for the analysis of the influence of climatic periods on TC is 50µm since it can represent an average behaviour of the current.

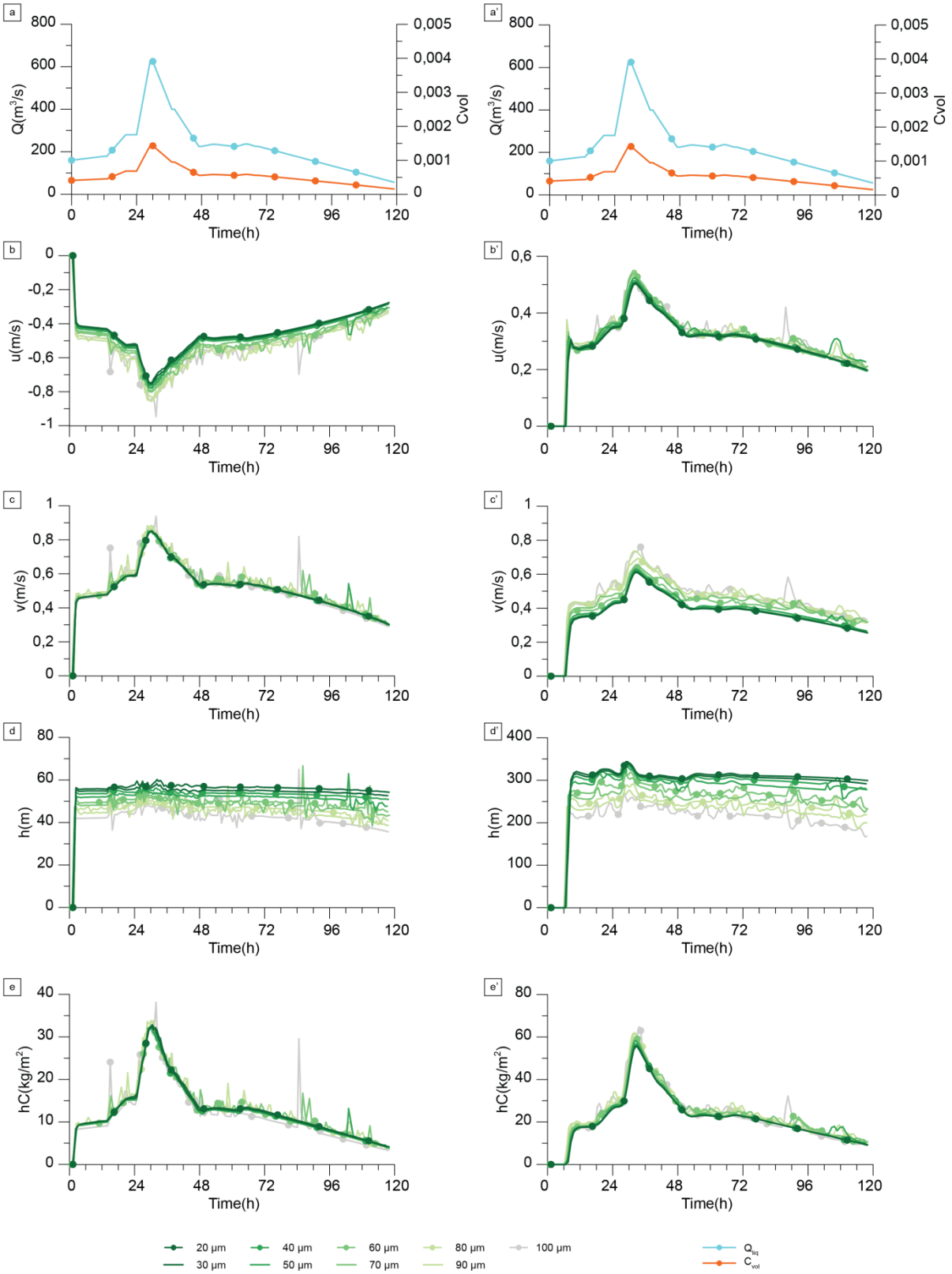

SUP. FIG. 4. 1 SENSITIVITY TESTS FOR THE GRAIN SIZE. MODELLING RESULTS AT THE POSITIONS OF THE MOORINGS VE (A, B, C, D, E) AND VV (A', B', C', D', E'), BOTH OF THEM LOCATED IN THE VAR CANYON. THE FLOOD CONSIDERED IS THE DECEMBER 2008 THAT PRESENTS A PEAK OF RIVER DISCHARGE OF 625M3/S, THE VOLUMETRIC CONCENTRATION CONSIDERED IS GIVEN BY THE RELATIONSHIP FOR PRESENT DAY GIVEN BY (BONNEAU, 2014). RESULTS ARE SHOWN FOR THE RUNS WITHOUT INCLUSION OF CORIOLIS FORCES (EQUATOR). A) & A')LIQUID DISCHARGE (M3/S) AND VOLUMETRIC CONCENTRATION. B) & B') DEPTH INTEGRATED CURRENT SPEED (X DIRECTION). C) & C') DEPTH INTEGRATED CURRENT SPEED (Y DIRECTION). D) & D') CURRENT THICKNESS (M). E) & E') INSTANTANEOUS SEDIMENT TRANSPORT HC (KG/M2).

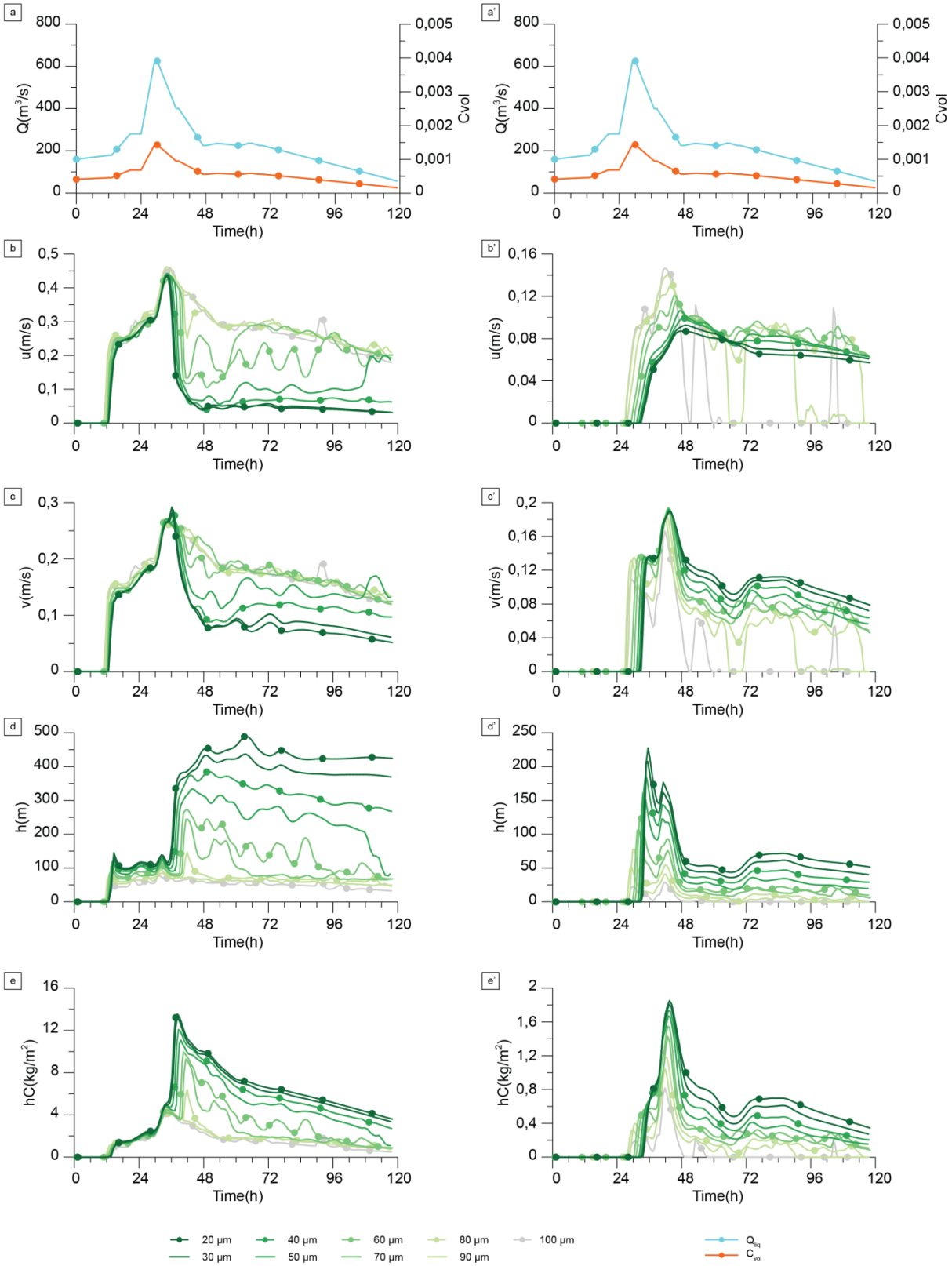

SUP. FIG. 4. 2 SENSITIVITY TESTS FOR THE GRAIN SIZE. MODELLING RESULTS AT THE POSITION OF THE MOORING VA (A, B, C, D, E) IN THE VAR CANYON AND THE POSITION OF THE CORE ESSK08-CS05 (A', B', C', D', E')ON THE UPPERMOST PART OF THE VSR. THE FLOOD CONSIDERED IS THE DECEMBER 2008 THAT PRESENTS A PEAK OF RIVER DISCHARGE OF 625M3/S, THE VOLUMETRIC CONCENTRATION CONSIDERED IS GIVEN BY THE RELATIONSHIP FOR PRESENT DAY GIVEN BY (BONNEAU, 2014). RESULTS ARE SHOWN FOR THE RUNS WITHOUT INCLUSION OF CORIOLIS FORCES (EQUATOR). A) & A')LIQUID DISCHARGE (M3/S) AND VOLUMETRIC CONCENTRATION. B) & B') DEPTH INTEGRATED CURRENT SPEED (X DIRECTION). C) & C') DEPTH INTEGRATED CURRENT SPEED (Y DIRECTION). D) & D') CURRENT THICKNESS (M). E) & E') INSTANTANEOUS SEDIMENT TRANSPORT HC (KG/M2).

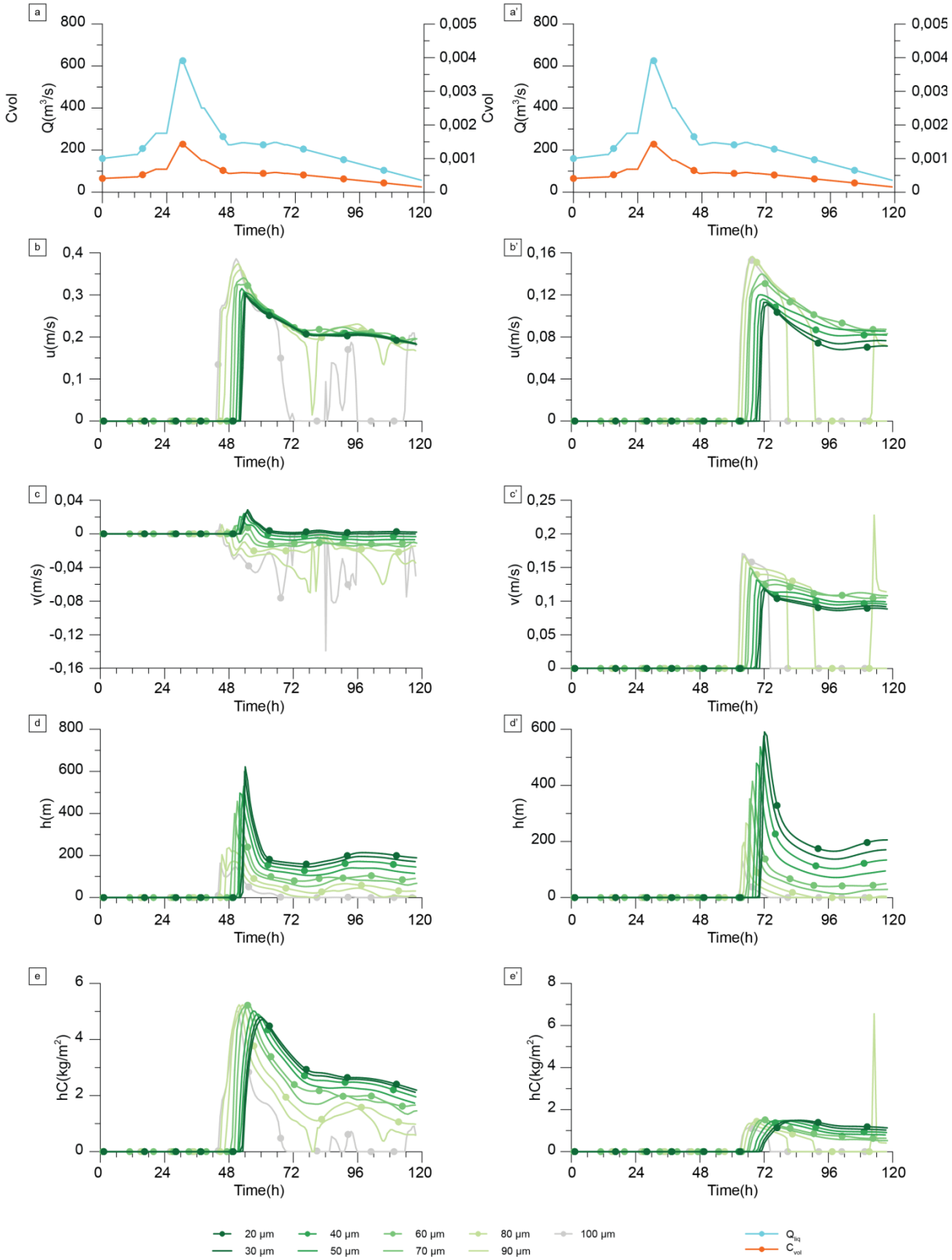

SUP. FIG. 4. 3 SENSITIVITY TESTS FOR THE GRAIN SIZE. MODELLING RESULTS AT THE POSITION CORE POSITION ESSK08-CS01 (A, B, C, D, E) ON THE DISTAL PART OF THE VSR AND AT THE POSITION OF THE CORE ESSK08-CS13 (A', B', C', D', E') ON THE SOUTHERN FLANK OF THE VSR. THE FLOOD CONSIDERED IS THE DECEMBER 2008 THAT PRESENTS A PEAK OF RIVER DISCHARGE OF 625M3/S, THE VOLUMETRIC CONCENTRATION CONSIDERED IS GIVEN BY THE RELATIONSHIP FOR PRESENT DAY GIVEN BY (BONNEAU, 2014). RESULTS ARE SHOWN FOR THE RUNS WITHOUT INCLUSION OF CORIOLIS FORCES (EQUATOR). A) & A')LIQUID DISCHARGE (M3/S) AND VOLUMETRIC CONCENTRATION. B) & B') DEPTH INTEGRATED CURRENT SPEED (X DIRECTION). C) & C') DEPTH INTEGRATED CURRENT SPEED (Y DIRECTION). D) & D') CURRENT THICKNESS (M). E) & E') INSTANTANEOUS SEDIMENT TRANSPORT HC (KG/M2).

Sensitivity tests for the river mouth

Sensitivity test for the river mouth width and orientation are performed (Fig. 4.4). The sensitivity tests are performed for a constant river discharge of 4000 m^3/s. The associated volume concentration is given by the power expression for present day $C = 0.0102Q^{0.916}$ (Bonneau, 2014). No Coriolis influence is considered for the sensitivity tests for the river mouth. The river mouth conditions analysed are 1 km and orientation NNW-SSE (i.e. conditions prior to 1946) and 350 m width and orientation NE-SW (i.e. present day conditions). In both cases, the grain size considered is 63µm. Sensitivity test results are presented for two points in the Var canyon (VV and VA) and for the uppermost point (CS05) and the most distal point (CS01) along the crest of the VSR. Values differ less than 10% except for the current thickness and the instantaneous sediment transport where differences can reach 25%.

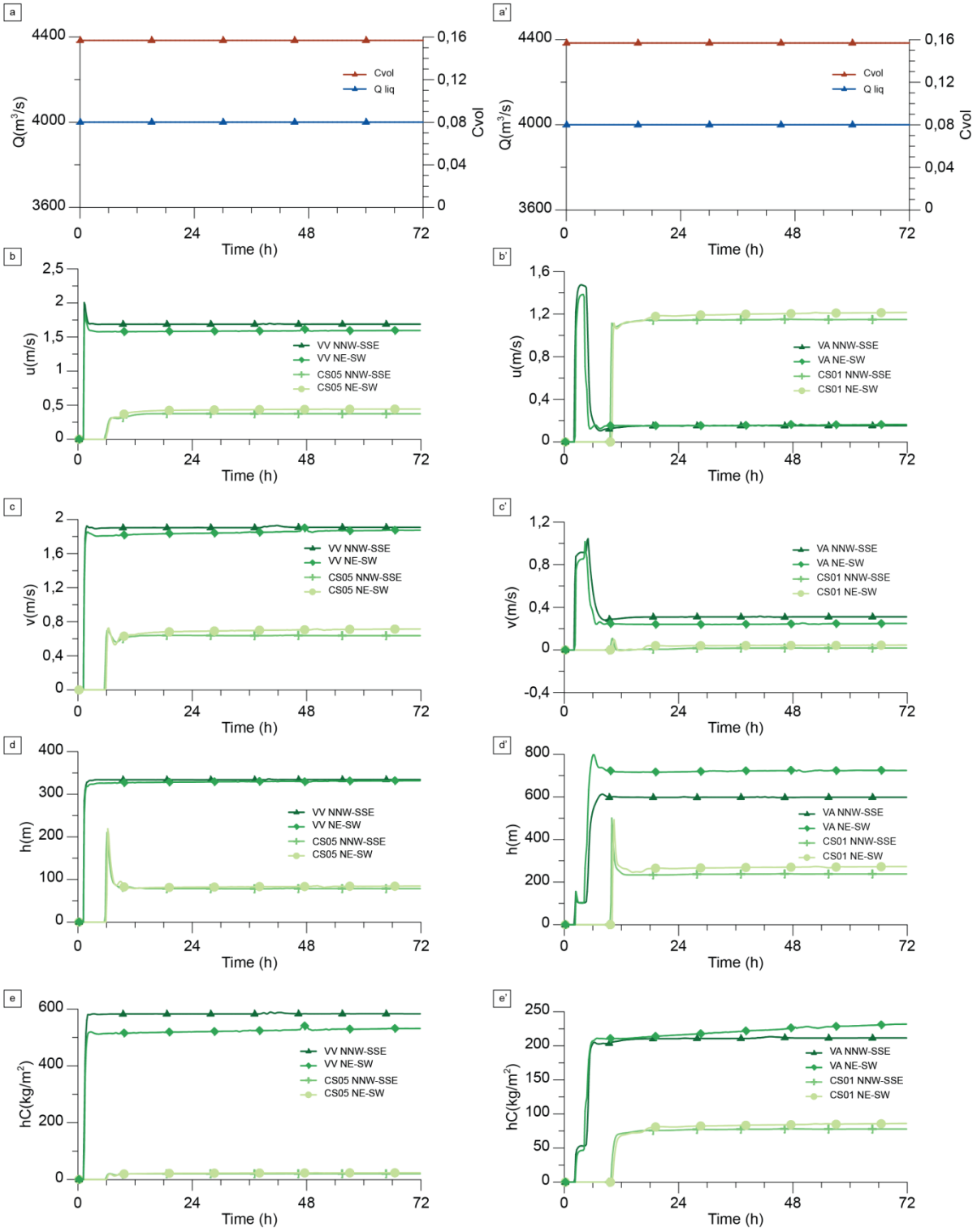

SUP. FIG. 4. 4 SENSITIVITY TESTS FOR THE ORIENTATION AND WIDTH OF THE RIVER MOUTH. MODELLING RESULTS AT THE POSITIONS OF THE MOORING VV AND CORE ESSK08-CS05 (A, B, C, D, E) AND FOR THE MOORING VA AND THE CORE ESSK08-CS01 (A', B', C', D', E'). THE FOOD CONSIDERED PRESENTS 4000M3/S OF RIVER DISCHARGE, THE VOLUMETRIC CONCENTRATION CONSIDERED IS GIVEN BY THE RELATIONSHIP FOR PRESENT DAY GIVEN BY (BONNEAU, 2014). RESULTS ARE SHOWN FOR THE RUNS WITHOUT INCLUSION OF CORIOLIS FORCES (HN) AND FOR A GRAIN SIZE OF D=63µM. A) & A')LIQUID DISCHARGE (M3/S) AND VOLUMETRIC CONCENTRATION. B) & B') DEPTH INTEGRATED CURRENT SPEED (X DIRECTION). C) & C') DEPTH INTEGRATED CURRENT SPEED (Y DIRECTION). D) & D') CURRENT THICKNESS (M). E) & E') INSTANTANEOUS SEDIMENT TRANSPORT HC (KG/M2).

Chapter 5 (English):

CONCLUSIONS AND PERSPECTIVES

1. Overview

This PhD thesis aims to apply a 2DH process-based model to simulate large scale turbidity currents (hereafter TC) of real-life modern and ancient turbiditic systems. The reliability of Nixes-TC to consistently reproduce sediment transport and sedimentation patterns is assessed by comparing the model results with field observations, coring and existing functioning models of the studied canyons. In this chapter the main conclusions of the work are summarized and responses to the questions raised in the Introduction chapter are provided. Suggested improvements and future work are proposed at the end of the chapter.

2. Concluding remarks

The modelling results show that Nixes-TC can simulate the hydrodynamic behaviour, current evolution and sedimentation of TC, and is a valuable tool and complementary approach to laboratory experiments and field data. Using a numerical model has several advantages: flow parameters can be determined "continuously", different case scenarios (e.g. density, bathymetry, grain size and volume) can be evaluated, as can the system's reaction to those parameters. Numerical model results provide a spatial vision of the system and overcome the fixed temporal frame since they solve the temporal evolution of the turbidity current. Surge type currents (e.g. La Fonera) and more continuous-like currents (e.g. Var sedimentary system) can be simulated. The model has proven to provide coherent results for both confined (i.e. inside the canyon) and unconfined flows (i.e. once the glacis is reached). The present knowledge of the different systems was used to validate the Nixes-TC model but this knowledge was also enlarged and improved by numerical modelling.

2.1. General conclusion about the modelling approach

The hydrodynamics of TC are difficult to study in natural environments. Laboratory experiments are time consuming and measurement of flow properties and relationships between flow structure and transport and deposition remain difficult to establish. Numerical modelling can cope with some of the limitations of field data and experimental modelling; nonetheless the three different approaches are complementary and form an interlinked feedback system.

2DH models are preferred since they can produce accurate predictions of current evolution and deposit characteristics of large scale flows with affordable computing resources. Among the 2DH models available, the use of Nixes-TC is justified given the key improvements of this model: the inclusion of a non-linear sedimentation model (settling velocity) in the equation of flux conservation, the development of a non-linear flow-dependent shear stress coefficient valid for all Re from laminar to fully turbulent flows, the inclusion of Coriolis effects, the treatment of the head and the existence of equilibrium solutions. The existence of equilibrium solutions is of major importance: the current thickness is provided by the balance between the water entrainment and the sedimentation model, contrary to classical models of turbidity currents in which the current thickness is exclusively determined by the water entrainment. This means that the TC is self-accelerated and can grow its thickness continuously, resulting in flows that grow to physically unrealistic proportions. Since the shear stress coefficient is dependent on the flow characteristics, the flow is not preconditioned, which is usually the case in other modelling approaches. At the equilibrium, the gravity forces are counteracted by the shear stress and the slope. By considering a constant value of shear stress, as is the case in most models, one would also impose the flow conditions, since C_d is related to Ri and hence to Fr. The approach followed by the model takes into account the non-linearities inherent to

TC and allows the current to propagate over long distances once the low gradient slopes of the glacis are reached, before finally waning and depositing.

The results of the two case studies show that the simulated hydrodynamic behaviour and geometry of the deposits are reasonably similar to those shown by the scarce field data that is available for the analysed systems. For the case studies the model reproduces qualitatively the sedimentation trends and patterns and the orders of magnitude are comparable to those provided by field data. The evolution of the hydrodynamic behaviour is coherent with observations and field data when those are available.

2.2.Conclusions on the study cases

Three questions arose at the beginning of this thesis in the study case of **La Fonera**: 1) Can we model turbidity currents on the basis of Vessel Monitoring System? 2) What are the TC pathways and sedimentation patterns due to trawling-induced turbidity currents? And 3) How can this study help to define areas of bottom trawling less destructive and more environment friendly?

We have developed a numerical methodology to calculate the trawling resuspension over the fishing grounds and its consequences in terms of sediment transport in canyons. This novel approach is based on the definition of an area susceptible to being trawled on the basis of VMS data, inverse analysis and numerical process modelling. The key variable in trawling impact on sediment dynamics, which is the sediment remobilized, is inferred from the inverse modelling over the area defined on the basis of VMS data. The numerical process based model validated against in situ mooring data has been used to study the sediment transfer due to trawling resuspension.

The results obtained complete and enlarge the interpretations of the trawling impact on the sedimentary functioning of the canyon, since present knowledge is based on snapshots of field data limited in time and space. The study allows the identification of the transfer patterns from the fishing grounds where resuspension is generated, towards the canyon axis and beyond and the associated trawling-induced accumulation areas (Fig. 5.1).

The canyon scale vision may help in the identification of strategic mooring and coring sites to further advance the state of our knowledge on sediment dynamics of the canyon and validate this model. The definition of trawling area based on VMS data allows identifying the potentially “damaging” and affected areas for sediment transport and would allow the identification of trawling areas with lesser impacts, with the aim of a management of fisheries not only based on the short term impact on individual species but with a more long term vision of ecosystem processes. The same methodology could be applied in other canyons and continental slopes where trawling is active.

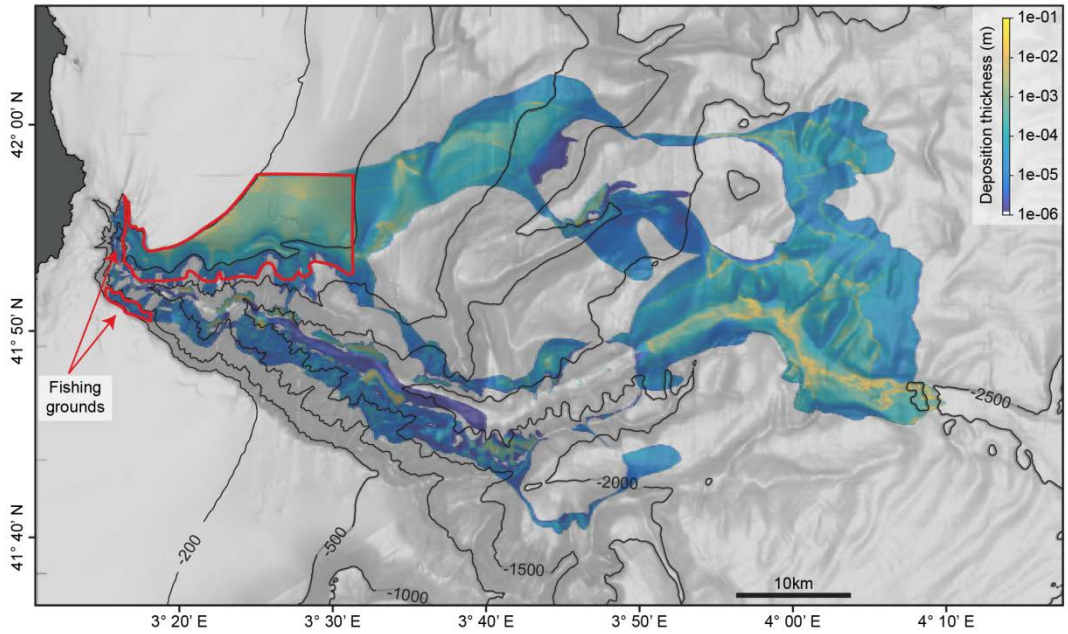

FIG.5. 1 MODELLED SEDIMENT THICKNESS ACCUMULATED FOR A TWO WEEK PERIOD OF TRAWLING ACTIVITY.

In the case of **the Var**, two questions were posed: 1) How are hyperpycnal flows triggered, and do they have a climatic control? And 2) Do Coriolis forces play a significant role in the construction of the Var Sedimentary Ridge?

This study presents the first attempt to simulate the evolution and deposition of hyperpycnal flows in the Var Sedimentary System. The influence of Coriolis forces on the spatial evolution of TC and hence in the construction of the Var Sedimentary Ridge (VSR) is evidenced and supported for the first time. The simulations in which Coriolis is not taken into account show a quasi-symmetric pattern of spreading and sedimentation of the TC which is only partially constrained by the VSR. When Coriolis is taken into account the TC is deflected to the right once the confinement of the canyon walls is lost. Part of the TC flows through the Western Spillover Channel (WSC) and part continues along the VSR, contributing to its development (Fig. 5.2). If the flow does not reach the thickness needed to overspill the WSC the flow continues along the VSR. Coriolis forces can also help to explain the higher sedimentation rates observed in the distal part of the VSR.

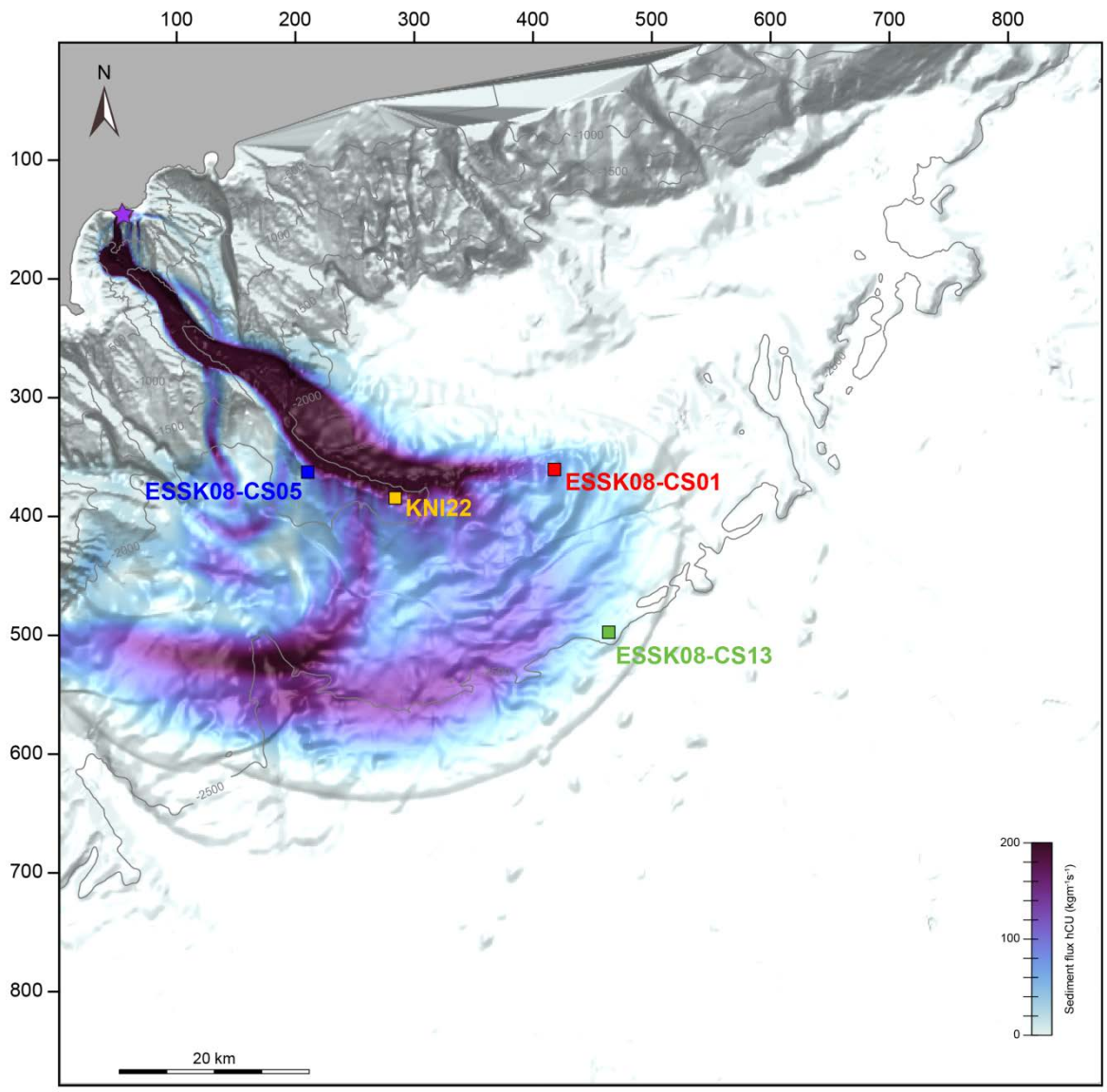

FIG.5. 2 SEDIMENT FLUX (hCU) IN KGM-1S-1 AT T=40H SINCE THE BEGINNING OF THE SIMULATION FOR THE HYPERPYCNAL CASE AT THE LGM AND RECURRENCE INTERVAL OF 100 YEARS. THE LOCATION OF THE REFERENCE CORES USED FOR VALIDATION IS SHOWN (ESSK08-CS05, KNI22, ESSK08-CS01 AND ESSK08-CS13). THE SOURCE POINT IS INDICATED WITH A PURPLE STAR.

The model results reproduce qualitatively well the sedimentation patterns inferred from the sedimentary cores. The simulations performed well in terms of intensity of the TC for the different climatic periods, with high intensity TC during the LGM and the stadials of the D/O and HS, and lower intensity during the interstadials of the D/O. However, although the results at the core positions follow the trend observed in the sedimentary record, they do not show differences between the climatic periods that are as accentuated as those of the sedimentary record. The main reason for this fact might be the input conditions imposed at the river mouth. The different power laws $Q - C_s$ imposed at the source correspond to the best fitting for a set of modelling results of Hydrotrend; a detailed statistical analysis of this data could improve the conditions inland. In the present study, in order to reduce the degrees of freedom, all the flash floods that were analysed follow the temporal pattern and evolution of the December 2008 flood, whilst in reality the temporal patterns of the floods of different recurrence interval can differ and are unknown for the cases analysed. The hydrograph of a flood depends on the characteristics of the catchment and on the duration of the rain fall. Different temporal patterns of the flash flood at the river mouth can imply different total sediment load and hence different TC evolution and final sedimentation pattern and deposit thickness. The processes at the river mouth/TC interface are highly non-linear and not completely

understood. The threshold for the triggering of hyperpycnal flows is established in sediment concentrations as low as 5kg/m^3 for the river outflow (Parsons et al., 2001); however, how this concentration and the river liquid discharge evolve into a TC is not fully understood. The boundary conditions were established on the basis of conservation of sediment load ($Q \cdot C_s$) between the river mouth and the TC, that is to say, the discharge and concentration at the TC source point are those of the river. Settling processes, which will largely depend on the grain size (i.e. settling velocity), can modify the combination of values of liquid discharge and sediment concentration, and hence trigger TC that would potentially have a different behaviour.

For the cases studied the model results reproduce qualitatively the sedimentation trends, and the orders of magnitude are comparable. The modelling results cannot be considered of predictive quality mainly because the forcing conditions are not known. The application of a 2DH process based model proves to be an affordable method to explore the hydrodynamics of turbidity currents, their evolution, their response to different topographies and the final sedimentation patterns. The model can be applied to both present day short scale processes and to geological time scales; providing in both cases insight into the system and enlarging the present understanding. In addition to this, the modelling methodology proves to be a helpful tool in the determination of suitable and interesting mooring and core positions.

The two cases studied represent two different modelling approaches. In the case of La Fonera, the area, timing and sediment involved in the TC can be considered as known since they are inferred from the inverse model. The modelling results can be validated at the mooring site and allow the assessment of the unknown trawling impacts in terms of deposition patterns and sediment accumulation. As such this first approach can be considered as forward modelling. On the contrary, in the case of the Var, the source is unknown whilst the information available is that of the sedimentary record (i.e. turbidite frequency, accumulation areas and VSR construction). The current evolution can be validated at present day conditions by the 2008 event; however, at the different climatic periods the validation of the currents modelled can only be achieved by comparison with the available sedimentary cores. As such, this second case can be considered to some extent as a backward calculation. The model behaves qualitatively well, providing results comparable with those of the data available, and proves to be a useful tool in both approaches from source to impact or result and conversely from impact or result to source.

3. Future work

Parameterization of the sediment transport and ambient fluid entrainment is based on relationships established by experiments. Those relationships are valid for the specific conditions on which the experiments were run, i.e. steady-state simulations; in reality turbidity currents are highly unsteady. The water entrainment rate (e_w) is expressed as a function of the bulk Richardson number (Ri_b) (Parker et al., 1987); however, this relationship is based on experimental data that shows a scatter of up to an order of magnitude in e_w for a given Ri_b (Fig. 5.3). These differences might imply significant differences in the behaviour of the modelled turbidity current. If the rate of water entrainment is overestimated, the current would be artificially more diluted; thus the density of the TC would be lower, resulting in loss of potential energy and hence less energy available to be transformed into kinetic energy to compensate the shear. The flow would potentially decelerate and sediment fall out. As such, a current with an overestimated water entrainment rate would potentially see its run-out limited and present more localized deposition areas. On the contrary, a current with underestimated water entrainment rate would be denser; it would have potentially higher velocities, and hence more kinetic energy would be available in order to balance the shear stress, allowing the current to have longer run-outs and even an erosive character.

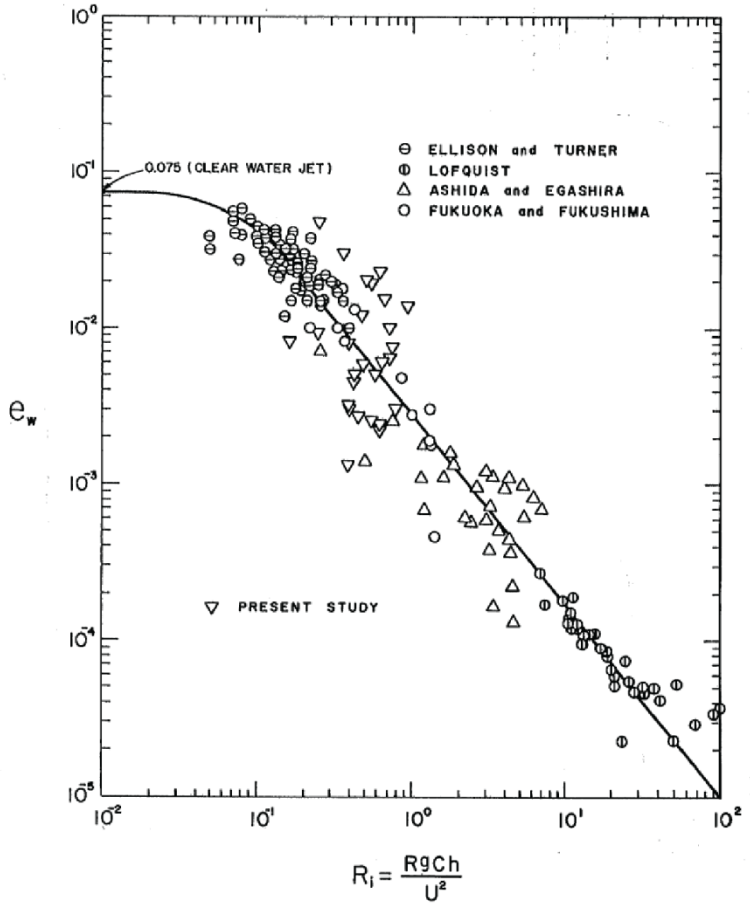

FIG.5. 3 WATER ENTRAINMENT COEFFICIENT e_w VERSUS RICHARDSON NUMBER Ri (FROM PARKER ET AL. 1987). THE POINTS REPRESENT THE DIFFERENT EXPERIMENTAL DATA. THE LINE IS THAT OF THE BEST FITTING FOUND BY PARKER ET AL. (1987) AND USED IN THE PRESENT STUDY.

The sediment entrainment rate E_s is established in the model through the balance between sedimentation and entrainment fluxes (Garcia and Parker, 1993), and represents the entrainment of bed sediment into suspension due to turbulence. While others formulations are available for erosion, based on a threshold for initiation of movement, the major issue is the lack of a physical theory of erosion that would allow overcoming empirical formulations.

The case studies analysed can be considered as a first attempt of modelling a real-life system; as such, they bring out exciting challenges for future research. In both cases the data available for the boundary conditions were scarce; however, despite this limitation, numerical modelling proves to be a useful tool to enlarge the insight in the dynamics of the canyon.

In the case of La Fonera, the modelling results allow the determination of new mooring sites that could provide data to improve the inverse model, and hence the resuspension imposed over the fishing grounds. The TCs reaching the mooring site are more important in spring and summer time when there is sediment available over the fishing ground after the winter storms. TC lose intensity towards the end of the summer and autumn, it would be therefore be interesting to take into account how the availability of sediment over the fishing grounds varies throughout the year and how the successive fishing activity depletes it. The Coriolis forces were not taken into account in the simulations presented in Chapter 3. At the position of the mooring site, the effects of Coriolis are likely to be negligible, since the TC is confined and the spatial scales are small. On the contrary, they might have an influence in the propagation of the current once the glacis is reached and on the open continental slope since these zones have lower Rossby numbers (Ro). Numerical simulations considering the influence of Coriolis forces are in progress.

The Var Sedimentary System clearly reflects how the issues related to the source remain crucial for future research of TC. Statistical time series analysis of historic records of flash flood and modelling results would enable a better constraining of the boundary conditions in terms of liquid discharge and sediment concentration. Analysis of historical datasets of liquid discharge at the river mouth would allow establishing "ideal" hydrographs for different interval recurrence floods. These hydrographs would largely depend on climatic conditions such as precipitation duration and intensity, and snow melting. Further research is needed in how hyperpycnal flows are triggered for concentration thresholds as low as 5kg/m^3; while the threshold is well established the highly non-linear processes at the river mouth/TC interface are not fully understood. Another possible improvement of the model that could have relevance in the case of the Var would be the inclusion of bed load transport, since the sandy turbidites are supposed to be transported by bed load in this system. This could be achieved by developing a 2 layer model, the upper layer being the one containing the suspended sediment; and the lower one containing the sediment transported due to bed load transport.

Future work could include the exploration of the morphodynamic capabilities of the model. The inclusion of a bed continuity equation is the starting point for morphodynamics and stratigraphic models. The stratigraphic long term evolution can be achieved by the development of a morphodynamic strategy and the simulation of multiple flows. Stratigraphic modelling might be achieved through upscaling of morphodynamics and the use of Morphological Acceleration Factor (MORFAC), a concept that is already used in coastal environments. The use of MORFAC would enable to bridge the gap between short-term hydrodynamics varying from hours to days and morphological changes taking place over much longer periods.

References

Garcia, M., Parker, G., 1993. Experiments on the entrainment of sediment into suspension by a dense bottom current. J. Geophys. Res. Oceans 98, 4793–4807. doi:10.1029/92JC02404

Parker, G., Garcia, M., Fukushima, Y., Yu, W., 1987. Experiments on turbidity currents over an erodible bed. J. Hydraul. Res. 25, 123–147. doi:10.1080/00221688709499292

Parsons, J.D., Bush, J.W.M., Syvitski, J.P.M., 2001. Hyperpycnal plume formation from riverine outflows with small sediment concentrations. Sedimentology 48, 465–478. doi:10.1046/j.1365-3091.2001.00384.x

Chapitre 5 (Français):

CONCLUSIONS ET PERSPECTIVES

1. Rappel: problématique, objectifs et méthodes

Ce projet de thèse vise à appliquer la modélisation numérique des courants de turbidité (ci-après dénommés TC), sur la base des processus physiques à des systèmes turbiditiques modernes et anciens. L'ensemble de données disponibles (bathymétrie, couverture sédimentaire, carottages, sismiques, mouillages hydrosédimentaires) ainsi que les modèles de fonctionnement existants permettront d'évaluer la capacité de Nixes-TC de reproduire la dynamique de transfert sédimentaire dans les canyons étudiés. Ce chapitre résumera les principales conclusions de ce travail et répondra aux questions posées en introduction de la thèse. Les améliorations futures à mener ainsi que les perspectives découlant de ce travail sont présentes à la fin du chapitre.

2. Conclusions

Les résultats du modèle montrent la capacité de Nixes-TC de simuler le comportement hydrodynamique, l'évolution du courant et la dynamique sédimentaire des TC. L'application d'un outil de simulation numérique présente des avantages : les paramètres de l'écoulement peuvent être déterminés en continu, différents scenarii (e.g. densité, bathymétrie, taille de grain, volume initial) peuvent être analysés, tout comme la sensibilité du système à chacun de ces paramètres. Les résultats de la modélisation numérique permettent d'obtenir une vision spatiale du transport et des dépôts associés aux courants, ainsi qu'une vision de son évolution au cours du temps. Nixes-TC permet de modéliser des courants type *surge* (e.g. La Fonera) ainsi que des écoulements *continuous-like* (e.g. Var). Les résultats du modèle sont cohérents pour des écoulements confinés (i.e. dans les canyons sous-marins) ainsi que pour des écoulements non-confinés (i.e. en aval de l'embouchure du canyon). La connaissance actuelle des différents systèmes est utilisée pour valider le modèle Nixes-TC, mais cette connaissance peut être aussi élargie et améliorée par la modélisation numérique.

2.1. Modélisation numérique

L'hydrodynamique des TC est difficile d'étudier dans leur milieu naturel. Les modèles analogiques s'avèrent chronophages et les propriétés de l'écoulement sont difficiles de mesurer. Les relations entre la structure de l'écoulement, le transport et le dépôt sont toujours difficiles d'établir. La modélisation numérique peut faire face à certaines des limitations des études basées sur des données terrain éparses et de la modélisation analogique; cependant, les trois approches sont complémentaires et souvent déterminants.

Les modèles 2DH basés sur des processus physiques sont plus précis puisqu'ils fournissent des résultats en termes d'évolution de l'écoulement et des dépôts associés réalistes tout en mobilisant des moyens raisonnables en temps de calcul et en mémoire. Nixes-TC apporte des améliorations clés par rapport à d'autres modèles 2DH existants, ce qui justifie son utilisation comme outil de simulation dans le cadre de cette thèse. Parmi ces améliorations, on peut citer l'inclusion d'un modèle de sédimentation (vitesse de chute) dans l'équation de conservation du flux sédimentaire, le développement d'un coefficient de frottement non-linéaire valide pour des écoulements laminaires et turbulents, l'incorporation des forces de Coriolis, le traitement de la tête de l'écoulement et l'existence de solutions à l'équilibre. L'existence de solutions à l'équilibre a une importance majeure : l'épaisseur de courant est déterminée par la balance entre l'entrainement d'eau et le modèle de décantation. Par contre, les modèles classiques de TC, l'épaisseur est déterminée exclusivement par l'entrainement d'eau. C'est-à-dire, le courant est *self-accelerated* et peut voir croitre son épaisseur jusqu'à des valeurs physiquement non réalistes. Le coefficient de frottement sur le fond (C_d) du modèle dépend des caractéristiques de l'écoulement, ainsi l'écoulement n'est pas pré-conditionné

comme c'est le cas dans la plupart des modèles. A l'équilibre, la pesanteur est compensée par le frottement et la pente. L'approche suivie prend en compte les non-linéarités inhérentes aux TC et permet au courant de se propager sur des longues distances lorsque les faibles gradients du glacis continental sont atteints, avant de décélérer et déposer sa charge sédimentaire.
Les résultats obtenus pour les deux cas d'étude en termes de comportement hydrodynamique et géométrie des dépôts reproduisent raisonnablement les données observées. Dans le deux cas, le modèle reproduit qualitativement les tendances de sédimentation et de géométrie du dépôt et les ordres de magnitude sont comparables à ceux de la donnée terrain. L'évolution hydrodynamique est cohérente avec les observations et la donnée du terrain, quand celle-ci est disponible.

2.2.Les cas d'étude.

Trois questions ont été posées au début de cette thèse pour le cas d'étude de **La Fonera** : 1) Est-ce que les courants de turbidité peuvent être modélisés sur la base des données du « Vessel Monitoring System » (VMS)? 2) Quels sont les chemins préférentiels ainsi que les zones de dépôt des courants de turbidité liés au chalutage ? et 3) Cette étude peut-elle aider dans la définition des zones de pêche au chalut avec un moindre impact ?

Nous avons développé une méthodologie numérique qui permet de calculer la remise en suspension sur les zones de pêche au chalut et ses conséquences en termes de transport sédimentaire dans les canyons sous-marins. Cette approche novatrice est axée sur la définition d'une zone susceptible d'être soumise au chalutage à partir des données VMS, l'application d'un modèle inverse et la modélisation numérique. Le sédiment remobilisé dans la zone de chalutage, définie en se basant sur les données VMS, a été quantifié par analyse inverse afin d'obtenir des évènements turbiditiques comparables à ceux enregistrés au point de mouillage et de mesure.

L'application du modèle numérique basé sur des processus physiques a permis de prédire la réponse du système en termes de courants de turbidité et a fourni une vision spatiale et globale des impacts potentiels du chalutage sur la dynamique sédimentaire du canyon. Les écoulements se propagent à partir des zones de chalutage vers l'axe du canyon en prenant les ravines comme chemins préférentiels. Cependant une partie de l'écoulement atteint le glacis continental par la pente continentale orientale. Les écoulements gravitaires liés au chalutage favorisent l'accumulation sédimentaire au-delà de l'embouchure du canyon, ainsi l'action du chalutage n'est pas restreinte aux zones mitoyennes de cette activité (Fig. 5.1).

La vision à l'échelle du canyon peut permettre de mieux préparer des cibles lors des campagnes à la mer (mouillages et carottes sédimentaires). Cela permettra d'améliorer l'état des connaissances de la dynamique sédimentaire de ce canyon et d'avoir une meilleure validation du modèle. La définition de la zone de chalutage sur la base des données VMS permet l'identification des zones avec un moindre impact afin d'avoir une gestion de pêche non plus basée sur l'impact à court terme sur des espèces concrètes mais sur une vision à plus long terme focalisée sur la préservation des écosystèmes. Cette méthodologie appliquée au cas concret de La Fonera peut être appliquée dans d'autres canyons sous-marins ou pentes continentales où le chalutage est actif.

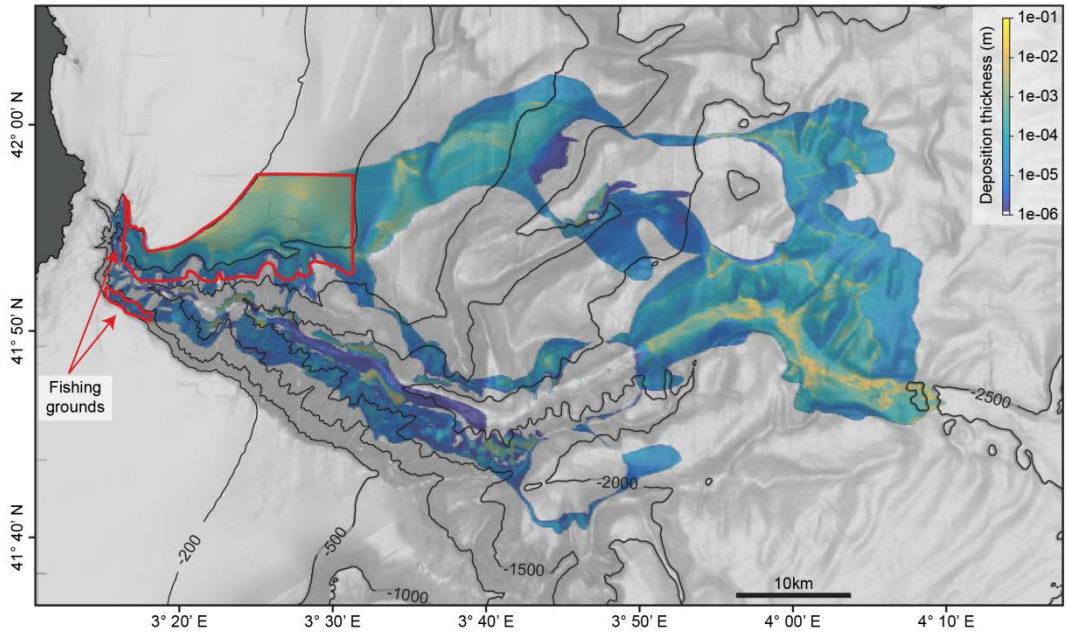

FIG.5. 4 RESULTATS DU MODELE EN TERMES DE EPAISSEUR DE DEPOT SUITE A L'ACTIVITE DU CHALUTAGE PENDANT DEUX SEMAINES.

Pour le cas d'étude du **Var**, deux questions se sont posées: 1) Comment sont déclenchés les courants hyperpycnaux et ont-ils un control climatique ? et 2) est-ce que les forces de Coriolis jouent un rôle important dans la construction de la Ride Sédimentaire du Var ?
Cette étude représente le premier effort de simulation de la dynamique sédimentaire et dépôt des courants hyperpycnaux dans le système sédimentaire du Var. L'influence des forces de Coriolis sur l'évolution spatiale des TC et sur la construction de la Ride du Var (VSR) est mise en évidence et attestée pour la première fois. Les résultats des simulations pour lesquelles les effets de Coriolis n'ont pas été pris en compte montrent une étendue spatiale du courant quasi-symétrique, n'étant confiné que partialement par la VSR. Au contraire, quand les effets des forces de Coriolis sont pris en compte, l'écoulement est dévié vers la droite en aval de l'embouchure du canyon. Une partie du courant est déviée et emprunte le Chenal de débordement occidental (WSC), tandis qu'une autre partie longe la VSR et contribue ainsi à sa construction (Fig. 5.2). Les forces de Coriolis peuvent être aussi à l'origine des taux de sédimentation plus élevés dans la partie distal de la VSR.

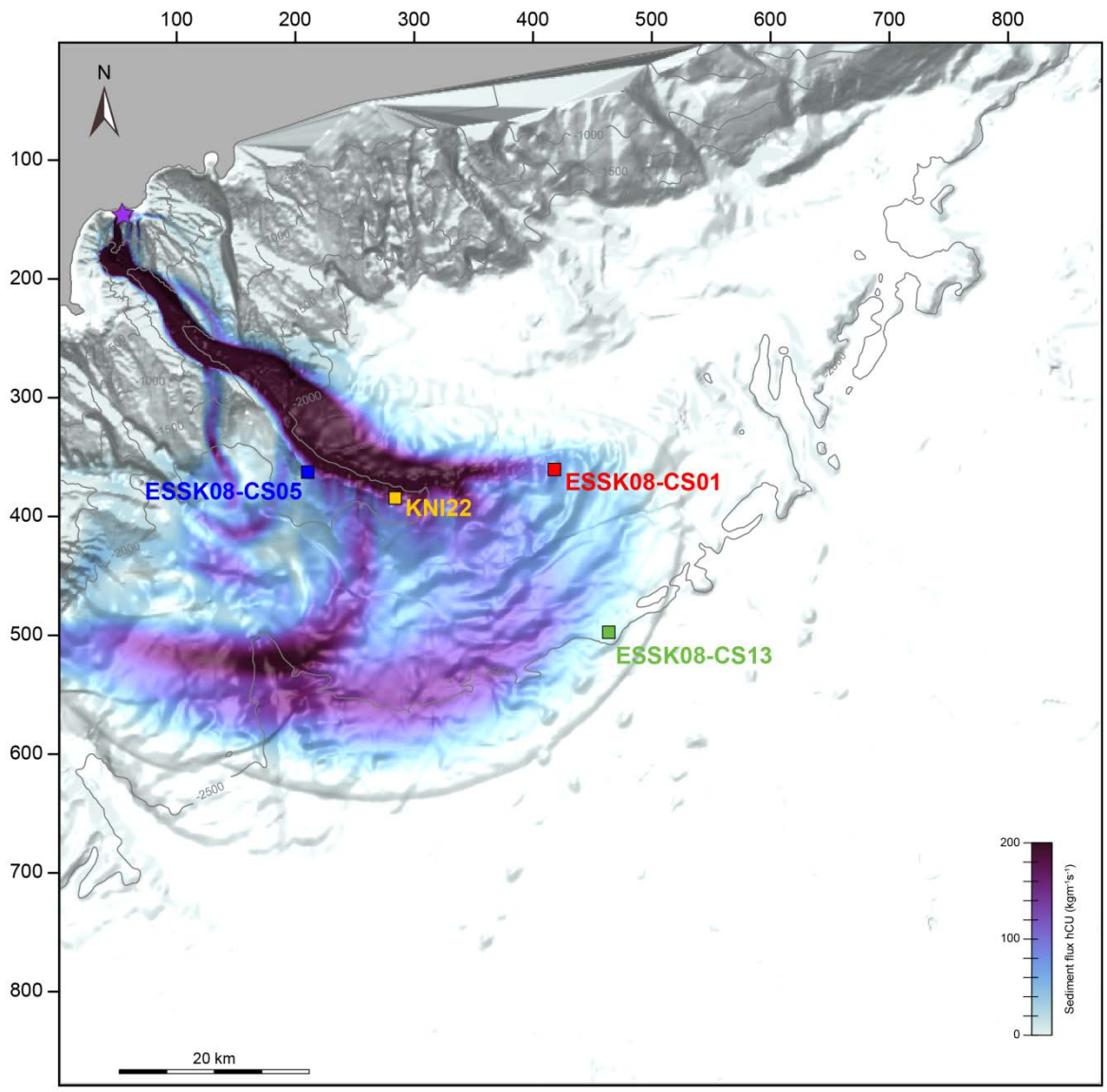

FIG.5. 5 FLUX DE SEDIMENT $hCU\ (kgm^{-1}s^{-1})$ 40H APRES LE DEBUT DE LA SIMULATION POUR LE CAS HYPERPYCNAL AU COURS DE LGM AVEC UNE PERIODE DE RETOUR DE 100 ANS. LA LOCALISATION DES CAROTTES SEDIMENTAIRES UTILISEE DANS LA VALIDATION DU MODELE EST AUSSI INDIQUEE (ESSK08-CS05, KNI22, ESSK08-CS01 AND ESSK08-CS13). LE POINT SOURCE EST INDIQUE PAR L'ETOILE VIOLET.

Les résultats du modèle en termes d'intensité de courant et de dépôt associé suivent la tendance enregistrée dans les sédiments. En effet, ces résultats montrent qu'au cours des stades froids et secs (stades des D/O et HS) les courants et dépôts sont assez développés alors que pendant les interstades chauds et humides (interstades des D/O) ils sont restreints. Bien que les résultats obtenus suivent la tendance observée à partir des carottes sédimentaires, la différence entre les 2 périodes climatiques étudiées n'est pas aussi marquée que l'enregistrement sédimentaire. Ceci doit être lié aux incertitudes sur les conditions initiales imposées à l'embouchure du Var.

Les conditions à la source sont imposées sur la base des relations Q-Cs issues de l'ajustement à partir des résultats de modélisation de Hydrotrend. Une analyse statistique de ces résultats pourrait améliorer les conditions imposées à l'embouchure. Au cours de cette étude et pour mieux contraindre les degrés de liberté, nous avons considéré pour toutes les crues modélisées, ont une même durée et une même évolution temporelle que la crue soudaine de Décembre 2008. En réalité ces deux valeurs (durée et évolution temporelle) peuvent varier considérablement et sont méconnues pour les cas d'étude. L'hydrogramme d'un écoulement dépend des caractéristiques du bassin versant et de la durée des précipitations associées. Différentes évolutions temporelles du

débit à l'embouchure du fleuve peuvent engendrer des charges sédimentaires totalement différentes et donc différentes évolutions temporelles des courants de turbidité et différentes géométries et épaisseur de dépôt.Les processus à l'interface embouchure/courant de turbidité sont fortement non linéaires et ne sont pas encore parfaitement compris. Le seuil de déclenchement des courants hyperpycnaux a été établi pour des concentrations aussi faibles que 5kg/m^3 à l'embouchure (Parsons et al., 2001); cependant la façon dont une si faible concentration de crue peut se transformer en courants hyperpycnaux n'est pas encore complètement élucidé. Le forçage a été établi en considérant la conservation de la charge sédimentaire ($Q \cdot C_s$) entre l'embouchure et le courant, c'est-à-dire au point source le débit et la concentration sont ceux du fleuve. Des processus de décantation, dépendant largement de la taille de grain (i.e. vitesse de chute), peuvent modifier le ratio décharge liquide et concentration sédimentaire, et de ce fait déclencher des TC présentant un comportement différent.

Les résultats du modèle en termes d'évolution de l'écoulement et des dépôts associés sont réalistes dans la mesure où les ordres de magnitude sont comparables à ceux de la donnée terrain. La modélisation numérique des courants de turbidité ne peut pas fournir à présent des résultats de qualité prédictive du fait de la quantité limitée d'information disponible pour établir les conditions initiales de l'écoulement. Malgré ce fait, la modélisation numérique 2DH basée sur des processus physiques est essentielle car elle permet d'élargir les interprétations du fonctionnement sédimentaire des canyons étudiés, d'identifier les chemins empruntés par les écoulements et leur dépôt final, tout en mobilisant des moyens raisonnables en temps de calcul et en mémoire. La spatialisation du transport et du dépôt permet de mieux sélectionner les zones cibles (mouillages et carottage) lors des campagnes à la mer.

Les deux cas d'étude représentent deux approches de modélisation contrastées. Dans le cas de La Fonera, la zone source, la période d'activités et le sédiment remobilisé ont été identifiés à partir des données VMS et l'application d'un modèle inverse. Les résultats obtenus sont validés au point de mouillage et fournissent une vision spatiale et globale des impacts potentiels du chalutage sur la dynamique sédimentaire du canyon jusqu'à présent méconnus. A l'opposé, dans le cas du Var, l'inconnue est la source tandis que l'information disponible est celle de l'enregistrement sédimentaire (fréquence des turbidites, zones d'accumulation et construction de la Ride). L'évolution du courant a pu être validée pour les conditions de l'événement de 2008 ; cependant pour les autres périodes climatiques étudiées, cette validation n'a pu être réalisée que partiellement que par une comparaison avec les carottes sédimentaires disponibles.

3. Perspectives

La paramétrisation du transport sédimentaire et de l'entrainement du fluide ambiant est basée sur des relations établies en laboratoire. Ces relations sont valides pour la gamme de conditions de l'expérience, i.e des conditions stationnaires alors qu'en réalité, les écoulements sont fortement transitoires. L'entrainement du fluide ambiant (e_w) est fonction du nombre global de Richardson (Ri_b) (Parker et al., 1987); cependant, la relation est établie sur des données expérimentales qui montrent un écart de plus d'un ordre de magnitude dans les valeurs de e_w pour une valeur de Ri_b donnée (Fig.5.3). Ces différences peuvent modifier fondamentalement le comportement de l'écoulement. Si la quantité d'entrainement d'eau ambiante est surestimée, le courant sera plus dilué ; ainsi le TC aura une densité moindre ce qui résulte en énergie potentielle plus faible disponible pour être transformée en énergie cinétique. L'écoulement décélère et perd sa charge sédimentaire par dépôt. Ainsi un écoulement avec un entrainement d'eau ambiante surestimé peut voir son parcours limité et peut ainsi présenter des zones de dépôt plus localisées. A l'opposé, un écoulement avec un entrainement d'eau ambiante sous-estimé peut générer des vitesses de courant

plus importantes, et donc une d'énergie cinétique disponible plus élevée pour compenser les pertes par frottement. L'écoulement aura ainsi un parcours plus étendu et même un caractère érosif.

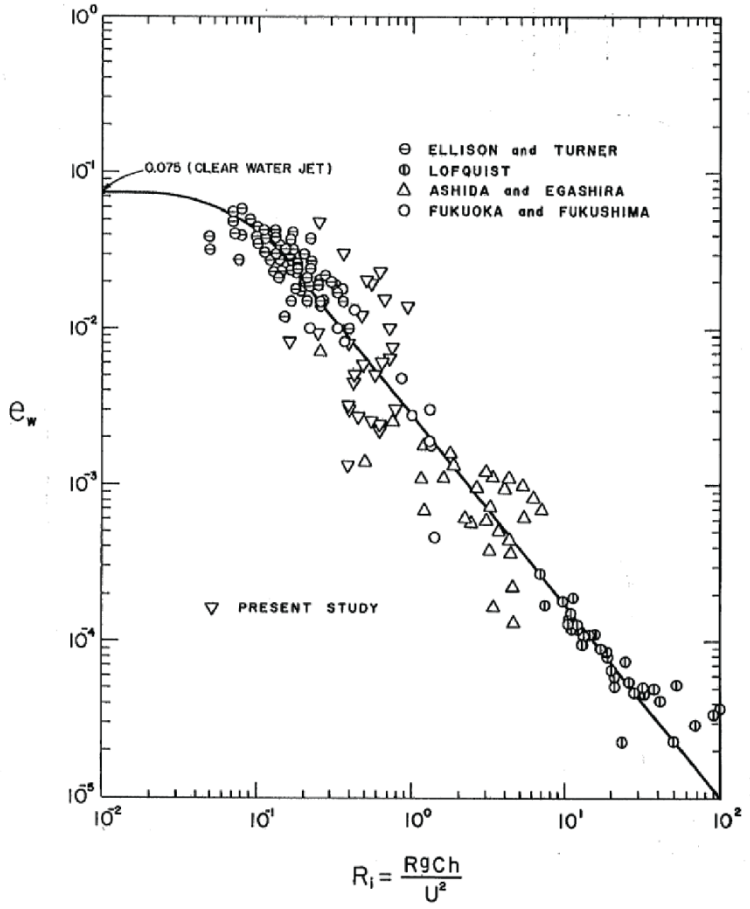

FIG.5. 6 ENTRAINEMENT D'EAU e_w VERSUS NOMBRE DE RICHARDSON Ri (PARKER ET AL. 1987). LES POINTS REPRESENTENT DIFFERENTS SETS DE DONNEES EXPERIMENTALES. LA LIGNE CONTINUE MONTRE LA RELATION DE PARKER ET AL. (1987) UTILISEE DANS LE MOELE.

Le coefficient d'érosion E_S est établi par la balance entre les flux d'érosion et le dépôt (Garcia and Parker, 1993), et représente le taux de sédiment en suspension lié à la turbulence. D'autres formulations empiriques sont disponibles pour l'érosion, basées sur de valeurs critiques de mise en mouvement.

Les cas d'étude de cette thèse peuvent être considérés comme une première démarche vers la modélisation des systèmes réels. Dans les deux cas les données disponibles pour établir le forçage sont éparses ; malgré cette limitation, la modélisation numérique permet d'élargir l'état des connaissances des canyons étudiés.

Dans le cas de **La Fonera**, les résultats du modèle permettent d'identifier des cibles possibles pour des mouillages, ce qui pourrait permettre d'améliorer le modèle inverse et donc l'estimation de la quantité de sédiment remobilisé sur les zones de pêche. Les tempêtes de l'automne et hiver augmentent le sédiment disponible sur les zones de chalutage, ce qui peut expliquer des écoulements plus importants enregistrés au point de mouillage pendant le printemps et l'été. Les écoulements sont par contre moins importants à la fin de l'été et pendant l'automne. Il est peut être intéressant de prendre en compte cette variabilité annuelle du budget de sédiment disponible sur les zones de chalutage et de considérer l'activité continue des bateaux qui réduit la disponibilité du sédiment mobilisable. L'effet des forces de Coriolis n'a pas été pris en compte pour les simulations présentées dans le chapitre 3. Ces effets son potentiellement négligeables à la position du point du mouillage du fait du confinement de l'écoulement et la petite échelle spatiale du système. Par contre le talus continental et le glacis présentent des valeurs de nombre de Rossby plus réduites du fait de

la perte de confinement de l'écoulement. Ainsi dans la partie plus distale et ouverte du système, les effets de Coriolis peuvent influencer la propagation de l'écoulement. Des simulations numériques sont en cours afin de vérifier cet aspect.

Le système sédimentaire du **Var** montre clairement l'importance de la définition des conditions de forçage pour les travaux futurs dans le domaine des TC. Une analyse statistique des séries historiques de données des crues soudaines du Var à l'embouchure pourrait permettre une meilleure définition des conditions de forçage en termes de débit liquide et solide. L'analyse des bases de données historiques de débit liquide à l'embouchure peut permettre de définir un hydrographe idéal pour les différentes périodes de retour. Ces hydrographes dépendent largement des conditions climatiques telles que la durée et l'intensité de précipitation et la fonte des neiges. Une perspective de recherche est constituée pour l'amélioration de l'état de l'art en ce qui concerne les courants hyperpycnaux déclenchés pour des concentrations aussi basses que 5kg/m^3. Tandis que cette valeur est bien établie, les processus associés sont fortement non linéaires et méconnus. Une autre amélioration qui peut avoir une certaine importance dans le cas du Var est l'inclusion du transport par charriage, car c'est par charriage qu'ont été transportées les turbidites sableuses présentes sur la Ride. L'inclusion du charriage pourrait être effectuée par le développement d'un modèle à deux couches, la plus éloignée du fond contenant le transport en suspension, tandis que celle plus proche du fond contenant le transport par charriage.

Des travaux futurs peuvent permettre d'évaluer la capacité du modèle à reproduire des évolutions morphodynamiques. L'équation d'évolution du fond est le point de départ pour les modèles morphodynamiques et stratigraphiques. Une stratégie de modélisation morphodynamique et la simulation des plusieurs écoulements successifs s'avèrent nécessaires afin d'atteindre cet objectif. La modélisation stratigraphique peut être explorée avec l'amplification des changements morphodynamiques et l'application d'un *Morphological Acceleration Factor* (MORFAC), un concept qui est déjà utilisé dans la modélisation côtière. L'utilisation de ce type de facteur pourrait combler le fossé entre les processus hydrodynamiques de courte échelle de temps (heures voire jours) et les changements morphologiques avec des échelles de temps plus longues.

Références

Garcia, M., Parker, G., 1993. Experiments on the entrainment of sediment into suspension by a dense bottom current. J. Geophys. Res. Oceans 98, 4793–4807. doi:10.1029/92JC02404

Parker, G., Garcia, M., Fukushima, Y., Yu, W., 1987. Experiments on turbidity currents over an erodible bed. J. Hydraul. Res. 25, 123–147. doi:10.1080/00221688709499292

Parsons, J.D., Bush, J.W.M., Syvitski, J.P.M., 2001. Hyperpycnal plume formation from riverine outflows with small sediment concentrations. Sedimentology 48, 465–478. doi:10.1046/j.1365-3091.2001.00384.x

Modélisation du transport sédimentaire et des interactions morphodynamiques par les courants de turbidité dans les canyons sous-marins. Application à la Méditerranée Occidentale

Marta PAYO PAYO, 2016

Les courants de turbidité dans les canyons sous-marins contribuent largement au transfert sédimentaire à travers des marges continentales. L'étude géologique des canyons sous-marins et des systèmes turbiditiques associés a permis des avancées fondamentales dans la compréhension de l'évolution des courants de turbidité. Ces études sont cependant limitées à des interprétations a posteriori, basées sur la répartition des dépôts et des évidences morphologiques. Cette thèse vise à l'application de la modélisation numérique des courants de turbidité, sur la base des processus physiques, à deux canyons sous-marins de la côte Méditerranée Occidentale.

Des courants de turbidité liés au chalutage de fond sont modélisés dans le canyon de La Fonera. Les résultats du modèle permettent de spatialiser ce transport; ainsi le modèle peut être un point de départ pour l'identification de zones de pêche au chalut avec un moindre impact. L'absence d'un plateau continental au niveau de Nice a permis une alimentation continue du système turbiditique du Var indépendamment des variations du niveau marin. Ainsi ce système s'avère un laboratoire naturel pour l'étude du control climatique sur l'activité turbiditique. L'influence des forces de Coriolis dans l'évolution spatiale des courants de turbidité et dans la construction de la Ride sédimentaire du Var est modélisée et mise en évidence pour la première fois.

La modélisation numérique des courants de turbidité ne peut pas fournir à présent des résultats de qualité prédictive du fait de la quantité limitée d'information disponible pour établir les conditions initiales de l'écoulement qui impactent largement son évolution et dépôts. Malgré ce fait, la modélisation numérique permet d'élargir les interprétations du fonctionnement sédimentaire des canyons étudiés, d'identifier les chemins empruntés par les écoulements et leur dépôt final et de mieux préparer des cibles (mouillages et carottage) lors des campagnes à la mer.

Mots-clés canyons sous-marins, chalutage, courants de turbidité, forces de Coriolis, hydrodynamique, modélisation, sédimentologie

Modelling sediment transport and morphodynamical interactions by turbidity currents in submarine canyons. Implementation to western Mediterranean canyons

Marta PAYO PAYO, 2016

Turbidity currents in submarine canyons are the main contribution for sediment transfer across the continental margins. Geological studies of submarine canyons and associated turbiditic systems for more than 30 years led to an extraordinary breakthrough in the understanding of how turbidite systems evolve. However, these studies remain limited to a posteriori interpretations, based on the distribution of deposits and morphological evidences. The overarching aim of this thesis is to apply a 2DH process-based model to simulate large-scale turbidity currents on two different submarine canyons in the western Mediterranean coast.

The work in La Fonera canyon, in the Catalan margin, focuses on the modelling of sediment transport and accumulation resulting from trawling activities on the canyon flanks. The numerical process-based provides a 3D visualization of potential trawling impacts on sediment dynamics. The study represents a starting point for the assessment of the sedimentary impact of bottom trawling in deep continental margins. The present work can help in the identification of trawling areas with lesser impacts. The Var Sedimentary System, located in the vicinity of Nice (France), is connected to the Var River during both low and high-stands and it can be considered as a natural laboratory for the study of the climatic control on the turbiditic activity. The influence of Coriolis forces on the spatial evolution of the hyperpycnal flows and hence in the construction of the Var Sedimentary Ridge (VSR) is evidenced and supported for the first time.

The major drawback is the limited amount of information for the necessary initial and boundary conditions; hence modelling results might not be of predictive quality. However, modelling results provide a full-scale vision of the system allowing the identification of sediment pathways and deposition areas on the basis of physical processes and enlarge the present knowledge of the canyons studied. The results obtained may help in the identification of strategic mooring and coring sites to further advance the state of our knowledge on sediment dynamics of the different cases studies.

Keywords Coriolis forces, modelling, hydrodynamics, sedimentology, submarine canyons, trawling, turbidity current